Preflight Summary Report for: ClassicThesis-pdfA.pdf

Profile: Convert to PDF/A-2u (Processed pages 1 to 251)

Processed by Honza Blažek, Date: 30/06/2018 08:56

Fixups

- Discard all actions that are not compliant with PDF/A (1086 objects)
- Prepare annotations for PDF/A-2 (1269 objects)
- Discard image interpolation flag (86 objects)
- Convert to PDF/A-2u (1 object)
- Set blend color space to sRGB if missing (15 objects)
- Downsample/compress color images (1 object)
- Downsample/compress grayscale images (1 object)
- Downsample/compress monochrome images (1 object)
- Flatten transparency (1 object)
- Discard all comments and form fields (1 object)
- Discard all form submission, import and reset actions (1 object)
- Discard all JavaScript actions (1 object)
- Discard all external cross references (1 object)
- Discard all alternate images (1 object)
- Discard embedded thumbnails (1 object)
- Discard private data from other applications (1 object)
- Discard document structure (1 object)
- Discard hidden layer content and flatten visible layers (1 object)
- Convert smooth lines to curves (1 object)
- Detect and merge image fragments (1 object)
- Remove, apply or adjust object compression (1 object)
- Compress all uncompressed objects using lossless ZIP compression (1 object)
- Recompress LZW as ZIP (1 object)
- Remove invalid bookmarks (1 object)
- Remove invalid links (1 object)
- Remove unreferenced named destinations (1 object)
- Optimize the PDF for fast web view (1 object)
- Fix glyph width information (1 object)
- Adjust colors for PDF based ISO standards (1 object)
- Fix font encoding (CIDToGIDMap) (2 objects)
- Add missing SPACE glyphs (245 objects)
- Set Overprint Mode for ICCbased CMYK object to 0 (851 objects)
- Make document XMP Metadata compliant with PDF/A-2 (1 object)
- Remove CharSet if incomplete (430 objects)
- Repair invalid bookmark hierarchies (1 object)
- Repair invalid ToUnicode CMap information in fonts (156 objects)
- Convert page content into image (30 objects)
- Remove Differences array from TrueType fonts for PDF/A-2 (285 objects)

Results (Summary)

Error

- Character references .notdef glyph (4280 matches on 91 pages) - 17, 21, 28, 30, 33, 35, 38, 39, 40, 41, 42, 43, 44, 45, 46, 47, 48, 50, 51, 53, 58, 63, 65, 73, 75...
- Glyphs missing in embedded font (4280 matches on 91 pages) - 17, 21, 28, 30, 33, 35, 38, 39, 40, 41, 42, 43, 44, 45, 46, 47, 48, 50, 51, 53, 58, 63, 65, 73, 75...
- Missing Extended graphic state "pgf@CA.8" (785 matches on 1 page) - 43
- Missing Extended graphic state "pgf@CA0.1" (1 match on 1 page) - 77
- Missing Extended graphic state "pgf@CA0.5" (3 matches on 1 page) - 27
- Missing Extended graphic state "pgf@CA0.7" (5 matches on 1 page) - 27
- Missing Extended graphic state "pgf@CA0.9" (46 matches on 1 page) - 25
- Missing Extended graphic state "pgf@ca.8" (785 matches on 1 page) - 43
- Missing Extended graphic state "pgf@ca0.1" (1 match on 1 page) - 77
- Missing Extended graphic state "pgf@ca0.5" (3 matches on 1 page) - 27
- Missing Extended graphic state "pgf@ca0.7" (5 matches on 1 page) - 27
- Missing Extended graphic state "pgf@ca0.9" (46 matches on 1 page) - 25
- Text cannot be mapped to Unicode (4389 matches on 101 pages) - 17, 19, 20, 21, 28, 30, 33, 34, 35, 38, 39, 40, 41, 42, 43, 44, 45, 46, 47, 48, 50, 51, 53, 58...
- Width information for rendered glyphs is inconsistent (31498 matches on 69 pages) - 118, 123, 128, 136, 137, 138, 139, 140, 141, 142, 143, 144, 145, 146...

Document information

File name: "ClassicThesis-pdfA.pdf"
Path: "/Users/gimli/Qsync/phd-thesis"
PDF version number: "1.6"
File size (MB): 101.6
Title: "Multimodal Image Processing in Art Investigation"
Author: "Jan Blažek"
Creator: "LaTeX with hyperref package"

Preflight Summary Report for: ClassicThesis-pdfA.pdf

Profile: Convert to PDF/A-2u (Processed pages 1 to 251)

Processed by Honza Blažek, Date: 30/06/2018 08:56

Producer: "pdfTeX"

Created: "30/06/2018 01:13"

Modified: "30/06/2018 01:19"

Subject: "Art investigation and digital image processing demarcate an interdisciplinary field of the presented thesis. Over the past 8 years we have published thirteen papers belonging to this field of research. This thesis presents the current state of the art and puts these papers into context. Our research is focused on modalities in the visible and near-infrared parts of the spectrum and affects various tasks of art investigation. For studying the spectral response of paint materials, we suggest a low-cost mobile multi-band acquisition system and a calibration method extended by a light source with an adjustable wavelength. We created the m3art database of the spectral responses of pigments, available for comparison and public use. The central point of our research is underdrawing detection and visualization. For this purpose we have developed: acquisition guidelines based on optical properties of the topmost non-transparent layer, a visualization technique for comparison of modalities, and a signal separation technique based on spectral extrapolation. The limits and performance of the separation method were demonstrated."

Trapping: "False"

Additional actions

Page open action
Type: Go to page in current document
Page open action
Type: Go to page in current document
Page open action
Type: Go to page in current document

Preflight Summary Report for: ClassicThesis-pdfA.pdf

Profile: Convert to PDF/A-2u (Processed pages 1 to 251)

Processed by Honza Blažek, Date: 30/06/2018 08:56

Type: Go to page in current document
Page open action
Type: Go to page in current document
Page open action
Type: Go to page in current document
Page open action

Preflight Summary Report for: ClassicThesis-pdfA.pdf

Profile: Convert to PDF/A-2u (Processed pages 1 to 251)

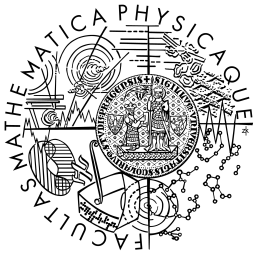
Processed by Honza Blažek, Date: 30/06/2018 08:56

Type: Go to page in current document
Page open action
Type: Go to page in current document
Page open action
Type: Go to page in current document
Page open action
Type: Go to page in current document
Page open action
Type: Go to page in current document
Page open action
Type: Go to page in current document
Page open action
Type: Go to page in current document
Page open action
Type: Go to page in current document
Page open action
Type: Go to page in current document
Page open action
Type: Go to page in current document
Page open action
Type: Go to page in current document
Page open action
Type: Go to page in current document
Page open action
Type: Go to page in current document
Page open action
Type: Go to page in current document
Page open action
Type: Go to page in current document
Page open action
Type: Go to page in current document
Page open action
Type: Go to page in current document
Page open action
Type: Go to page in current document
Page open action
Type: Go to page in current document
Page open action
Type: Go to page in current document
Number of plates: 4
Names of plates: "(Cyan) (Magenta) (Yellow) (Black) "

Environment

Preflight, 18.2.0 (201)
Acrobat version: 18.110
Operating system: Mac OS X 10.13.5

All problems according to Preflight profile
Convert to PDF/A-2u



FACULTY
OF MATHEMATICS
AND PHYSICS
Charles University

DOCTORAL THESIS

JAN BLAŽEK

MULTIMODAL IMAGE PROCESSING IN ART INVESTIGATION

Insitute of Information Theory and Automation of the CAS,
dep. of Digital Image Processing

Supervisor:	RNDr. Barbara Zitová PhD.
Study program:	Computer Science
Study branch:	Computer Graphics and Image Analysis

Prague 2017

All problems according to Preflight profile
Convert to PDF/A-2u

Jan Blažek: *Multimodal Image Processing in Art Investigation,* © July 2017

All problems according to Preflight profile
Convert to PDF/A-2u

ACKNOWLEDGMENTS

Writing my thesis has taken a really long time, but finally all the words are on the paper. Here, it is my pleasure to express my tremendous gratitude to all the people who have stood by me and helped me to extend my knowledge and understanding.

First of all, I am enormously grateful to my supervisor RNDr. Barbara Zitová, PhD., and I thank her for her professional feedback and help during my work. I would also like to thank RNDr. Janka Hradilová, who introduced me to the problem of art investigation, from the perspective of an art expert. Many thanks belong to Anna Pelagotti, who was the gray eminence of my PhD. study. She has overseen me from my first conference, invisibly guiding me in my study visit in Florence as well as contributing with her knowledge to my research. Finally, in the research field, I need to thank Jana Striová, who helped me to fulfill my demands during and after the Florence study visit.

I am much obliged to the Institute of Archaeology of the Academy of Sciences of the Czech Republic, the Academy of Fine Arts in Prague, and Opificio delle Pietre Dure for providing us with materials necessary for this work.

The majority of this thesis was created with the support of the Czech Science Foundation (project no. P103/12/2211).

Last, but not least, there were the people who suffered on account of my studies but supported me without hesitation in my effort: my wife, my sons and my parents.

All problems according to Preflight profile
Convert to PDF/A-2u

All problems according to Preflight profile
Convert to PDF/A-2u

DECLARATION

I declare that I carried out this doctoral thesis independently, and only with the cited sources and literature, and other professional sources.

I understand that my work relates to the rights and obligations under the Act No. 121/2000 Coll., the Copyright Act, as amended, in particular the fact that Charles University in Prague has the right to conclude a license agreement on the use of this work as a school work pursuant to Section 60 paragraph 1 of the Copyright Act.

Prague, July 2017

Jan Blažek

All problems according to Preflight profile
Convert to PDF/A-2u

All problems according to Preflight profile
Convert to PDF/A-2u

ABSTRACT

TITLE: Multimodal Image Processing in Art Investigation

AUTHOR: Jan Blažek

DEPARTMENT: Department of Image Processing, IITA of the CAS

SUPERVISOR: RNDr. Barbara Zitová PhD., Institute of Information Theory and Automation

SUPERVISOR'S E-MAIL ADDRESS: zitova@utia.cas.cz

ABSTRACT: Art investigation and digital image processing demarcate an interdisciplinary field of the presented thesis. Over the past 8 years we have published thirteen papers belonging to this field of research. This thesis presents the current state of the art and puts these papers into context. Our research is focused on modalities in the visible and near-infrared parts of the spectrum and affects various tasks of art investigation. For studying the spectral response of paint materials, we suggest a low-cost mobile multi-band acquisition system and a calibration method extended by a light source with an adjustable wavelength. We created the m3art database of the spectral responses of pigments, available for comparison and public use. The central point of our research is underdrawing detection and visualization. For this purpose we have developed: acquisition guidelines based on optical properties of the topmost non-transparent layer, a visualization technique for comparison of modalities, and a signal separation technique based on spectral extrapolation. The limits and performance of the separation method were demonstrated.

KEYWORDS: multimodal dataset, spectral response, paint material, information gain, difference visualization, NIR acquisition

All problems according to Preflight profile
Convert to PDF/A-2u

CONTENTS

I MOTIVATION: MULTIMODAL DATASET IN ART INVESTIGATION 1
1 Modalities, their meaning and limitations 5
2 Image processing approaches to art investigation tasks 9

II SIGNAL PROCESSING IN ART INVESTIGATION 11
3 Data acquisition and interpretation 16
3.1 Scanners . . . 16
3.2 Physical models . . . 17
3.2.1 Calibration . . . 17
3.2.2 Optical properties of materials . . . 18
3.2.3 Multi-layer model . . . 19
3.2.4 Two-layer model . . . 20
3.2.5 Pigment-mixture model . . . 20
4 Building of databases 21
4.1 Fibre optic reflectance spectroscopy and colorimetry . . . 21
4.2 Database of the XRF spectra of pigments . . . 22
5 Expert knowledge 23
5.1 Painting techniques . . . 23
5.2 Pigment descriptors . . . 24
5.3 Artwork context . . . 25
6 Computational analysis and image processing 26
6.1 Preprocessing . . . 27
6.1.1 Transillumination artifacts removal . . . 28
6.1.2 Registration . . . 29
6.2 Information content analysis . . . 31
6.2.1 Dimensionality reduction . . . 32
6.2.2 Decomposition techniques . . . 33
6.3 Pixel descriptors . . . 36
6.3.1 Artifact descriptors . . . 37
6.3.2 Pigment descriptors . . . 38
6.3.3 Descriptors for region of interest (ROI) . . . 39
6.4 Classification . . . 40
6.4.1 Pigment identification . . . 40
6.5 Scene modeling . . . 43
6.6 Visualization . . . 44
6.6.1 False colors . . . 45
7 Virtual restoration and lacuna filling 46
7.1 Color restoration . . . 46
7.2 Crack removal . . . 47
7.2.1 Rough crack map . . . 47

All problems according to Preflight profile
Convert to PDF/A-2u

7.2.2 Elimination of brush strokes from crack maps . . 48
7.2.3 Reconstruction 49
7.3 Lacuna filling 50
8 Open problems 51
9 Research without an impact on artwork itself 53
9.1 Painting style 53
9.2 Authorship 54
9.3 Metadata-based image retrieval 55

III OUTLINE: MY CONTRIBUTION TO THE STATE OF THE ART 57
10 Outline 61
10.1 Fresco restoration: digital image processing approach . . 61
10.2 Removing the Artifacts from Artwork Cross-section Images 62
10.3 Image fusion for art analysis 62
10.4 Detection of Copies Using Mathematical Processing of Images II: Story of a Painting on Canvas of a Boy Petting a Bird 62
10.5 Detection of Copies Using Mathematical Processing of Images I: Theoretical Basis and Methodology 63
10.6 Image Fusion for Difference Visualization in Art Analysis 64
10.7 LEDs in an 8-by-8 matrix - technical report 65
10.8 Low-cost mobile system for multispectral cultural heritage data acquisition 65
10.9 M3art: A Database of Models of Canvas Paintings . . . 67
10.10Optical properties of historical paint pigments under near-infrared radiation 67
10.11Statistical evaluation of color change 68
10.12Improvement of the visibility of concealed features in artwork NIR reflectograms by information separation . 68

IV SUMMARY AND OUTLOOK 71
11 Conclusion 73
11.1 Contribution 73
11.2 Our outlook and future work 74

V BIBLIOGRAPHY 77

VI APPENDIX 103
12 Appendix 105
12.1 Improved visualization of concealed features - the context of the state of the art 232

All problems according to Preflight profile
Convert to PDF/A-2u

LIST OF FIGURES

Figure 1 Current state of the art timeline 3
Figure 2 Empirical vs. analytical 10
Figure 3 Digital image processing pipeline 13
Figure 4 Digital image processing task classification . . . 15
Figure 5 Certified color target x-rite ColorChecker Digital SG 18
Figure 7 Similarity measure: cross-correlation 31
Figure 8 Demonstration of the penetrative ability of particular modalities. 34
Figure 9 Attributed to Leonardo da Vinci and another artist: *Madonna with Yarnwinder*, oil on panel. $50.2cm \times 34.6cm$. Private collection, United States. 36
Figure 12 Johannes Vermeer: *Girl with a Pearl Earring*, 1665, oil on canvas. $44.5cm \times 39cm$. Mauritshuis, The Hague, Netherlands. 43
Figure 13 Jan van Eyck: *Arnolfini Portrait*, 1434, oil on wood. $82.2cm \times 60cm$. National Gallery, London. 44
Figure 16 Fusion of ultraviolet fluorescence (UVF) and visible (VIS) modality in false colors. A fresco from a church in Kostoľány pod Tríbečom, Slovakia. . . 45
Figure 17 Empirical and analytical context to our research 60
Figure 18 Computation of La*b* maximal saturation . . . 65
Figure 20 LEDs in an 8-by-8 matrix 65
Figure 21 LEDs spectral intensity 66
Figure 23 Fruit Festoon by Tomáš Tichý 67
Figure 25 Gothic samples - m3art 67
Figure 26 Fluorite in macro image 68
Figure 28 Where extrapolation succeeds 236
Figure 29 Where extrapolation fails 237

All problems according to Preflight profile
Convert to PDF/A-2u

ACRONYMS

ANN	artificial neural network
BSS	blind source separation
CEM	constrained energy minimization
DIP	digital image processing
DSLR	digital single lens reflex camera
EM	expectation-maximization
FIR	far infrared
FORS	fibre optics reflectance spectroscopy
FOTS	fibre optics transmittance spectroscopy
ICA	independent component analysis
ICF	infrared cut-off filter
ICM	matrix of corresponding intensities
IITA	Institute of Information Theory and Automation
INO	Instituto Nationale di Ottica
IR	infrared
KM	Kubelka-Munk
LBP	local binary patterns
LED	light-emitting diodes
LSMA	linear spectral mixture analysis
LWIR	long-wave infrared
MCA	morphological component analysis
MNF	maximum noise fraction
MWIR	mid-wave infrared
NIR	near infrared
OCT	optical coherent tomography
PCA	principal component analysis
ROI	region of interest
SAM	spectral angle mapper
SCM	spectral correlation mapper
SID	spectral information divergence
SNR	signal-to-noise ratio
SP	signal processing
SWIR	short-wave infrared
THz	terahertz radiation
UV	ultraviolet
UVF	ultraviolet fluorescence
VIS	visible
XRF	X-ray fluorescence

All problems according to Preflight profile
Convert to PDF/A-2u

All problems according to Preflight profile
Convert to PDF/A-2u

Part I

MOTIVATION: MULTIMODAL DATASET IN ART INVESTIGATION

An identification of art investigation targets, short overview of available modalities for noninvasive artwork screening, and categorization of contemporary usage of digital image processing.

All problems according to Preflight profile
Convert to PDF/A-2u

All problems according to Preflight profile
Convert to PDF/A-2u

Targets of art investigation, overview of available modalities, categorization of DIP

Over the last 100 years, art investigation has developed various radiometric acquisition techniques for non-invasive artwork screening [1, 2], see figure 1. Each modality (from a radiometric dataset) is a piece of the puzzle in the art investigation task and contains different information about an artwork, helping to uncover the artist's technique, materials used or history of interventions in the artwork itself (restoration, repainting, degradation of materials, etc.).

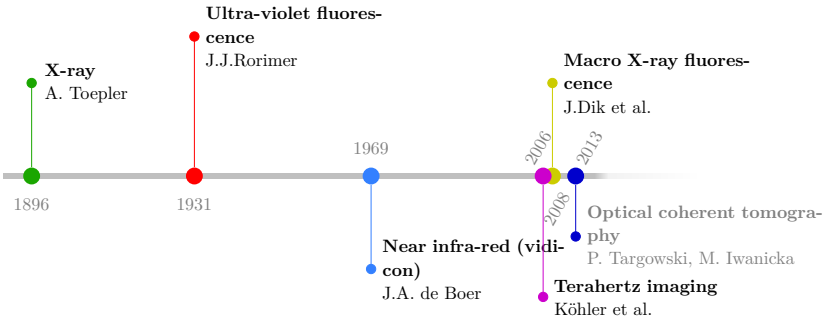


Figure 1: Timeline showing development of non-invasive screening principles (implementation of the first screenings)

The levels of modality knowledge and its application in DIP

After a scanning principle is introduced, knowledge of modality capabilities arises. At the first level, scanning limitations are investigated, namely what it is possible to see in the collected data and what would be possible to see if the scanner had better parameters. A rough definition of the classes distinguishable in the modality under consideration is an output. At the second level this rough description is refined. A database of recognized classes for modal behavior is created. Here, as a class we understand: which paint material was used (i.e. a mixture of pigment, binding media, filler and other compounds), defect type, layer, layer combinations or other things. Qualitative and quantitative analysis of modality and screening outputs is the final level. This highest level is usable for development of an automatic classification algorithm and interpretation without the need for an expert.

Achievement of these levels depends mainly on scanner price and scanner availability. In the field of art investigation, however, the research is directed by available technology instead of by greed for the best achievable dataset and results. Usage of VIS, near infrared (NIR) or UVF modalities is more common than usage of other modalities (terahertz radiation (THz), mid-wave infrared (MWIR), X-ray fluorescence (XRF), X-ray). Sometimes database creation can be quickly achieved by reusing data from different fields of research (optical properties of materials, XRF peaks in the spectra of chemical elements). Reusing data that has already been collected helps ensure faster development and application of scanning techniques.

In this thesis we will talk only about radiometric techniques that produce images, in spite of other modalities, where just a point (or small areas) can be measured (e.g. optical coherent tomography (OCT),

All problems according to Preflight profile
Convert to PDF/A-2u

Raman spectroscopy, etc.). I would like to present multimodal images, their informational content and modality-based uncertainties.

All problems according to Preflight profile
Convert to PDF/A-2u

MODALITIES, THEIR MEANING AND LIMITATIONS

Description of currently available modalities, what they show and their common problems.

In the following paragraphs I would like to present a very brief survey of contemporary modal screening methods that produce images. All these (and only these) modalities will be taken into account later in this thesis. For a deeper knowledge of modality usage do not hesitate to look in other publications, e.g.: [1, 2, 3, 4].

SCREENING IN THE VISIBLE PART OF SPECTRA is the oldest method, used mainly for the purpose of documenting the state of the artwork. Nowadays, images achieving the best quality have pixels measured in the color space La*b* [5, 6] or as a relative reflectance spectrum in very narrow bands. The spatial resolution of collected images is almost needlessly high (the best cameras have more than 50 Mpx nowadays). By using calibrated devices (and after registration), the aging process of the artwork can be documented by a periodic screening [7]. The monitored parameters are: changes in color, craquelure, or other degradation. VIS modality is the cornerstone of modal image comparison and the most important source of information for non-invasive paint material identification. VIS screening also functions as documentation of the restorer's steps and of the state of the artwork before an intervention. VIS analysis and comparative techniques are commonly used without any published scientific impact.

Screening is achievable by a digital single lens reflex camera (DSLR) capturing images in RGB color space or by VIS-NIR multispectral [5] and hyperspectral scanners [8, 9] providing pixel full spectral response.

ULTRAVIOLET FLUORESCENCE was first published in 1931 [10] not as a screening technique, but as a visualization technique. The main application of UVF is for localization of retouches and varnish layers or for other analysis of the topmost (often transparent) layers of the artwork (an extensive description can be found in [11], Chapter 8). The significant parameters are pixel intensity (ratio between the source radiation and reflectance radiation) and pixel color (a shift in wavelength).

Old resins have low intensity concentrated around green wavelength, while young varnishes have high intensity concentrated around blue wavelength [4]. Automatic determination of varnish age is still impossible, because a quantitative description of the aging of paint materials is missing. Usage of UVF is therefore limited to expert evaluation. An approach to the creation of a reference UVF database is presented in [12], but an extension with more paint reference materials is neces-

All problems according to Preflight profile
Convert to PDF/A-2u

sary for generalization and wider applicability. Scanners used for UVF are the same as for VIS and NIR because wavelengths are shifted due to the fluorescence effect into VIS and NIR. A system for acquisition of 7 UVF bands was presented in [13]. The main improvement of this system is the possibility for quantitative analysis of UVF modality.

X-RAY screening encapsulates many different methods using very short wavelengths. *"Alan Burroughs became interested in X-rays in 1923 after a request from the Director of the Minneapolis Institute of Arts to examine a painted ornament on the outside of a mummy case. After purchasing X-ray equipment, Burroughs made X-radiographs of paintings from the Fogg Museum of Art in Cambridge, Massachusetts, and the Metropolitan Museum of Art in New York, and sent two 'expeditions' to Europe (in 1926 and 1927) to 'collect shadowgraphs of famous pictures'. These expeditions coincided with renewed interest in the use of X-radiography in a number of European museums, particularly in Austria, Germany and the Netherlands."*[14]. The first attempts at artwork screening using X-rays was in 1896 [15].

The significant parameters of X-ray screening are:

- Whether transmission or reflectance images were captured (reflectance is a relatively newer technique) [1]
- Sensor pixel density
- Recognized X-ray energy levels

Transmission and reflection determine the information and artifacts contained in the image. The sensor construction (pixel density and energy levels) affects the details obtained.

From the point of view of DIP, information content and artifacts are more important, because they determine the algorithms used for further processing. From the point of view of art analysis, a level of detail is highly important for defining what is and is not possible to see in radiograms.

X-ray screening is very useful but does have limitations. The limits range from the immobility of the majority of scanning devices to the related costs of such screening. This is the reason why radiograms are not so common in practice. On the contrary, only short wavelengths, high energy photons and neutrons, have the ability to go through all layers of a painting and should be used for the study of very complex artwork stratigraphy [1]. Contemporary devices are able not only to capture a radiogram, but also to map the distribution of chemical elements in an artwork [16, 17]. For the purpose of material identification as well as in the case of XRF, existing databases of the X-Ray responses of chemical elements were reused (see Table 1).

X-RAY FLUORESCENCE screening has been used for art investigation since 1992, but (macro-XRF) detectors producing images of larger

All problems according to Preflight profile
Convert to PDF/A-2u

areas were first presented in [18, 19] (2008 and 2013). In spite of its late appearance in the field of non-invasive screening techniques, the XRF method profits from the existence of databases of chemical elements XRF. The produced images can therefore be automatically processed into maps of elements used on an artwork. The last scanner developed for XRF, Maia [20], eliminates the problem through a time-consuming scanning process. The measurement of one point has been sped up from a few seconds up to several milliseconds. The main disadvantage of macro-XRF is the need for a synchrotron X-ray source and thus limited device mobility, as well as a high price for a scanning device [1]. Impressive case studies using this modality have recently been published (see Section 6.4.1).

INFRARED the spectral sub-band is often subdivided into five sections: NIR, short-wave infrared (SWIR), MWIR, long-wave infrared (LWIR) and far infrared (FIR). A detailed description of individual sub-bands is given in the paragraphs that follow. In the context of art investigation, the most important and most studied is NIR $\langle 700; 1400\rangle nm$, with part of SWIR $\langle 1400; 3000\rangle nm$ jointly described in the paragraph *Near infrared*. The abilities of MWIR $\langle 3000nm; 8\mu m\rangle$ to classify paint materials were described in [21, 22]. Pigment molecule identification in the surface of an artwork by MWIR was studied in [23, 24]. This ability is similar to XRF screening, but unlike for XRF, a pigment behavior description database for comparison or material identification was still lacking for the MWIR modality. The availability of MWIR scanners, especially those with sufficient spatial resolution, is also problematic. MWIR is therefore on the edge of its applicability and is very rarely used. LWIR covers the wavelengths $\langle 3\mu m; 8\mu m\rangle$, but its application in art screening is rare. Recently, there have been experiments to use it for defect detection [25] in combination with wavelet decomposition. The furthermost part of FIR, namely terahertz radiation, is described in its own paragraph as well.

NEAR INFRARED screening has the ability to penetrate most pigment layers. Painting materials become transparent for wavelengths in the range $\langle 700; 2200\rangle nm$, but materials used for underpainting (bone black, carbon, etc.) absorb these wavelengths. Therefore, black underdrawings are often visible in this spectral band. For the purpose of underpainting detection, NIR was first used in 1969 [26] and its usage continues [27, 5, 28, 29, 30, 31, 32, 23]. The major advantage of NIR modality is very inexpensive sensors. In common practice, standard DSLR is adjusted by simply removing the infrared cut-off filter (ICF) for wavelengths up to $1050nm$. More distant NIR up to $2500nm$ must be captured by more expensive InGaAs sensors. Higher spectral density is reached by diffraction [8, 9] or spectral filters [5]. A major disadvantage of NIR modality is insufficient database coverage of paint materials

All problems according to Preflight profile
Convert to PDF/A-2u

MODALITY	acquaintance	DB OF CLASSES	quantitative analysis
XRF	yes	yes	yes
X-ray	partial	partial	partial
UVF	partial	some	no
VIS	yes	partial	partial
NIR	partial	some	no
MWIR	no	no	no
THz	partial	no	no

Table 1: Contemporary level of knowledge of imaging modalities used for art investigation. Columns from left to right correspond to levels of knowledge. The first level is a rough description of a modality acquaintance, the second level requires a database of recognized classes (paint materials and their behavior) and the final level requires quantitative analysis of the scanned data, which enables automatic processing.

(see Section 4.1). Some approaches to database creation can be found in [33, 34, 35]. In spite of the existence of a database, the correct interpretation of scans is still uncertain and often needs to be supplied with a database related to paint material samples. Unlike X-ray or UVF modality, a high correlation with VIS modality is typical for NIR images.

Major research in the THz domain is summarized in Kaori Fukunaga's monograph [38].

TERAHERTZ scanning is relatively new. The THz imaging technique was first published in 1995 [36] and was applied in art investigation in 2006 by Köhler et al. [37]. THz combines the ability of X-rays to penetrate (up to a depth of $1mm$ under a painting's surface) and the softness of NIR [39, 1]. For THz modality, we understand the radiation range to be between $[15\mu m; 3mm]$. A particular ability of THz modality can be seen in a number of recent publications [38]. Adam et al. [40] explore its ability to visualize hidden layers of umber. Fukunaga and Picollo [41] document the "fingerprints" of paint materials in the THz domain. Abraham et al. [42] have studied the ability of THz to visualize graphite sketches. In [43, 44, 45], case studies are described, along with the ability of THz to identify compounds of a multi-layer painting. Since radiograms are a relatively new scanning technique, there is a lack of a deeper description of what information can be extracted from them. The development of the THz screening technique is quickly reaching the level of necessary knowledge for practical usage. For screening in this modality, industrial scanners like T-Ray™4000 by Picometrix [41] are used.

All problems according to Preflight profile
Convert to PDF/A-2u

IMAGE PROCESSING APPROACHES TO ART INVESTIGATION TASKS

For art investigation, there are tasks like dating an artwork, identification of provinenance, identification of paint materials used, localization of repaintings and retouches, underdrawings and pentimenti, etc. In the following text we look at these tasks from the perspective of applied DIP and interpret them as a target for classification. In the case of dating there will be classes defined by centuries or years; in the case of layer description we classify each pixel according to its layer content. We will define classes of paint materials, and meaningful classes can also be created for painting techniques, etc. This is a very non-specific generalization that will be particularized in subsequent paragraphs (a similar generalization was made in [46]). A successful classification is often the source of a story about an artwork, a background for effective restoration and conservation or, finally, an extension of contemporary historical knowledge.

There are two types of DIP methods: the supporting restorer and the independent expert.

All classifications are made by human experts nowadays, mainly because a broad context for the targets of an investigation is necessary (see dark-gray part on Figure 2). We understand the context to include knowledge of painting techniques, pigment sources available in the century of creation, chemical processes of paint material degradation, biography of an author, historical context, and more. The need for context is the reason why the majority of automated processes (such as the DIP of scanned images) are used merely for data arrangement and not for classification itself.

There exist rare cases when expert knowledge was not necessary for analysis.

In the last two decades, there have been few papers that reduced the necessary context to a minimum, allowing for automatic classification through algorithmic, context-based rules (these papers belong at the intersection of the blue stripes and gray area in Figure 2). For the development of such rules, it was necessary to have quantified knowledge of the spectral responses of paint materials [47, 48, 49] as well as the geometric rules of perspective projection, applied to the creation of paintings [50, 51]. These approaches lead to precise mathematical models and to the development of classification algorithms.

For the purpose of my thesis, I recognize two types of art investigation tasks. For the first type, it is not possible to reduce the classification context to a mathematical model or classification algorithm, and expert knowledge is required. For the final decision, usage of DIP algorithms is limited to data arrangement and visualization only. In the second type of investigation task, a reduction of the necessary context to the level of a mathematical model is possible. If such a model is created,

All problems according to Preflight profile
Convert to PDF/A-2u

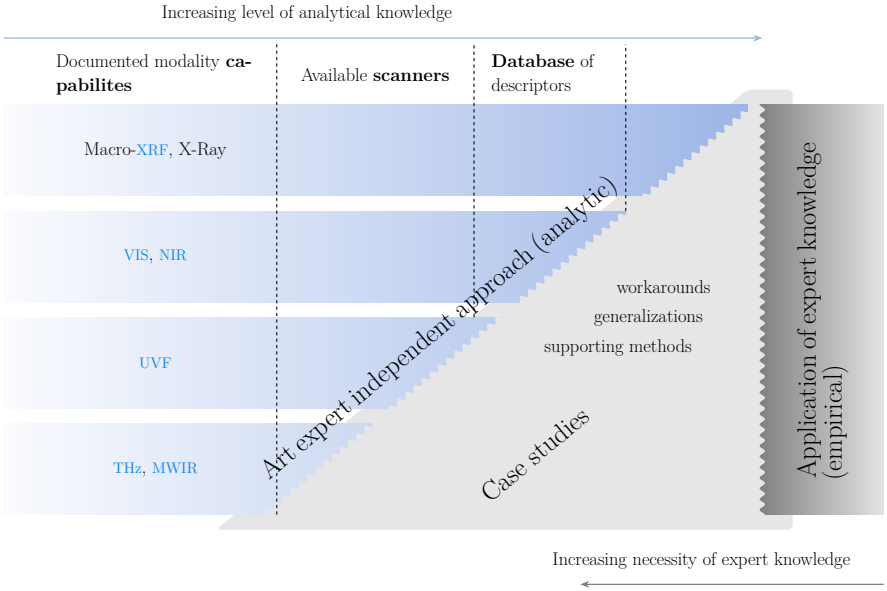


Figure 2: Current state of the art with respect to an analytic approach. The dark gray area corresponds to a blind analysis without a precise description of scanned data requiring expert knowledge. The blue stripes represent research based on reproducibility of results and a priori knowledge. To the light gray area belong publications focused on case studies combining both types of knowledge.

it is possible to process data automatically up to a final classification. Unlike in expert analysis, such results are easily reproducible.

DIP algorithms are made to measure for an art analysis task.

If we make the distinction between these two groups more fuzzy, we can establish a group of tasks in between them , where some context reduction is possible (*case studies* part of Figure 2). Such a reduction should improve the results of DIP by eliminating some uncertainties (e.g. diminish the set of possible classes, reduce the size of an area to be processed, etc.). Expert knowledge is used here not only for the final decision, but above all for the elimination of irrelevant configurations of DIP algorithms.

The group of algorithms based on blind analysis, which contains low-level algorithms such as denoising, contrast enhancement, color space conversions or fusion will not be part of my thesis (and are also missing in Figure 2). These algorithms are cornerstones of DIP, well-described in other publications [52], and have a nonexistent or weak linkage to art investigation.

In my thesis I would like to document how the specialized DIP algorithms for art investigation were developed. The focus of the work spans from acquisition and measurement, through database building, to DIP development and refinement.

All problems according to Preflight profile
Convert to PDF/A-2u

Part II

SIGNAL PROCESSING IN ART INVESTIGATION

An overview of digital image processing in art investigation and its requirements: calibration, data acquisition, preprocessing, database creation, and algorithm construction and refinement. Presentation of the current state of the art.

All problems according to Preflight profile
Convert to PDF/A-2u

All problems according to Preflight profile
Convert to PDF/A-2u

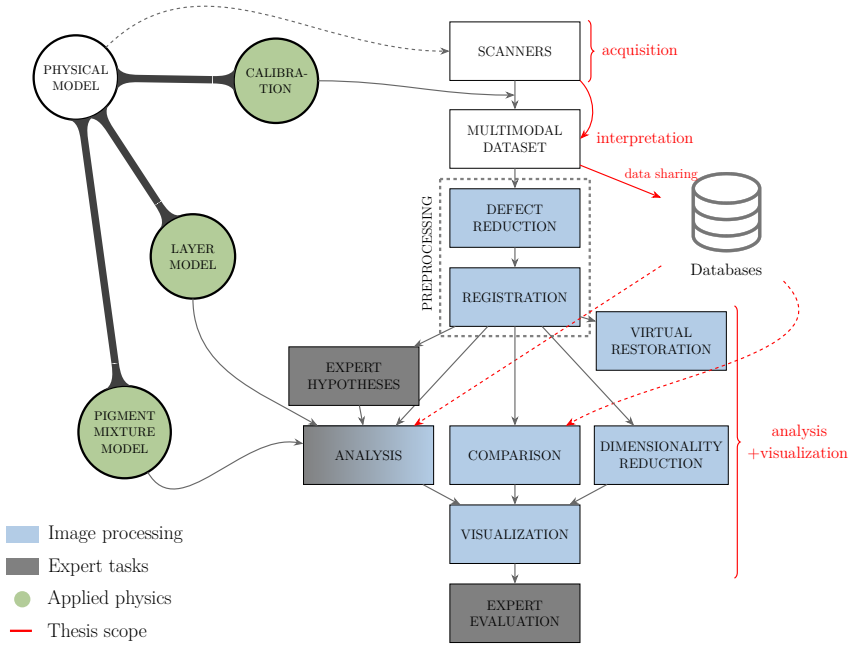


Figure 3: Art investigation generalized pipeline from the perspective of DIP and this thesis (red lines and comments).

In the scientific papers referred to in this part, many case studies have been documented. The following chapters correspond to subtasks solved in the referred papers and summarize the current state of the art in the interdisciplinary field of DIP and art investigation. For a better understanding of the "big picture" look at Figure 3, where I visualize the general flow of DIP in the context of physics (circles) and art analysis (gray color). A case study typically starts with data acquisition and interpretation, as described in Chapter 3. Construction of databases of pigments and paint materials, which are crucial for material analysis and comparison, is tracked in Chapter 4. How to employ the context of the artwork and expert knowledge to DIP and signal processing (SP) provides the subject matter for chapter 5. All these elements of an art investigation precede DIP, which I split into two chapters: Computational analysis and image processing and Virtual restoration and lacuna filling

Research focusing on a single subtask includes construction of scanners and building of databases, in contrast to case studies, where a whole pipeline is often constructed.

From the point of view of the presented pipeline (see Figure 3) the flow has three main stages:

1. Acquisition and data normalization (Chapter 3)
2. Preprocessing (Section 6.1)
3. Various analyses and visualizations

The first two (acquisition and preprocessing) are well-defined tasks as well as visualization techniques (Section 6.6). In contrast, it is hard to

All problems according to Preflight profile
Convert to PDF/A-2u

define common principles or targets for various analyses, and they require finer sorting. In Figure 4 such a sorting is proposed. According to our experience we define two dimensions: the target of analyses (targets correspond to blue rows) and the types of algorithms used for data processing (represented by columns). Moreover, Figure 4 puts other data sources into this context as well: expert knowledge and databases of paint materials.

We identify the following as the roles of DIP in the art investigation process:

- Evaluation of expert hypotheses
- Visualization of concealed features

When the expert hypothesis is given, descriptors are calculated and visualized or automatically evaluated. Algorithms belonging here follow tasks represented by the *expert hypothesis* box (see Figure 3) and are covered by boxes labeled *analysis* (gray part) and *visualization*.

The second role, visualization of concealed features and ROI identification, is represented by the boxes labeled *dimensionality reduction*, *comparison*, *analysis* (blue part) and *visualization*. However, it is always followed by *expert evaluation*.

All boxes from the presented figures (3, 4) will be described in subsequent chapters and sections with appropriate references. Please do not hesitate to return to figures 3 and 4 when necessary.

All problems according to Preflight profile
Convert to PDF/A-2u

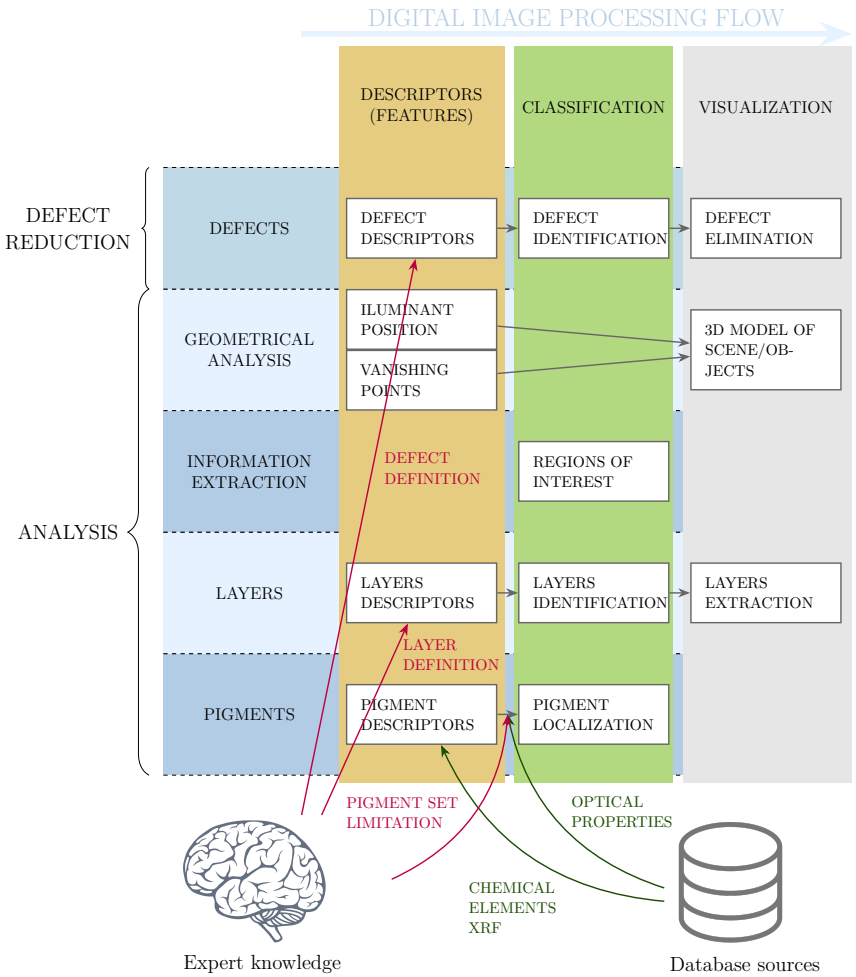


Figure 4: Visualization of DIP pipelines for various targets. Algorithms in each pipeline are grouped according to their principle (descriptors/-classifiers). Other data sources (expert knowledge and databases of paint materials) and their application are shown as colored arrows. Black arrow connections visualize the flow of the data (from the knowledge base or as a result of a previous DIP task in the pipeline). On a more general level, we distinguish *extraction of features*, *classification* and *visualization*, which are represented by vertical color stripes.

All problems according to Preflight profile
Convert to PDF/A-2u

The quality of various datasets is very different.

Art investigation starts with measurement and interpretation of obtained values. Data acquisition is an expensive process, which creates pressure for a good ratio between the quality of the acquired dataset and its price. The highest-quality dataset is achievable in just a few laboratories all over the world, while datasets of common quality, containing spatially misaligned images from a very limited number of modalities, are widespread.

The motivations for data normalization are reproducibility and comparability.

The acquisition must fulfill physical model requirements and is followed by data transformation and normalization according to calibration parameters. The output should be a suitable description of the artwork. Interpretation and comparison of the measured values is possible only if calibration parameters are properly estimated. Estimation of calibration parameters as well as setup preparation for an ideal and controlled acquisition (e.g. *in situ*) is quite problematic for some devices [53] . For this reason, the dataset is not properly normalized in most cases and measurements are not comparable; this step is simply skipped, with implications for the subsequent data processing. The main reasons for the normalization are measurement reproducibility and production of images and point descriptors, which are comprehensible for art experts or convenient for computer-based processing.

Here I split the workflow of acquisition and calibration methodology into the following sections about 3.1 Scanners and 3.2 Physical models.

3.1 SCANNERS

Scanning techniques are closely watched and periodically reviewed. To get a good notion about the state of the art, I recommend some recent review articles from 2014 [54] and 2013 [2], which can be complemented with a high-resolution X-ray article [55], a monograph about the THz domain [38] and a report about the new hyperspectral scanner HySCAP, working in the range $\langle 370; 1100 \rangle nm$ [56]. A short overview can also be found in [57] (Table 1).

In short, CCD sensors are widely used in common restorer practice (due to their price and mobility). Adjusted DSLR with proper illumination is able to provide UVF, VIS and NIR modalities, while the number of sub-bands and their density depends on the photographic filters used. I refer to other scanners as "scientific", because their availability is limited to equipped laboratories. To this group belong medical X-ray devices, X-ray laminography [58], XRF scanners [18, 20], multispectral and hyperspectral single-point scanners operating in ultraviolet (UV), VIS, and

All problems according to Preflight profile
Convert to PDF/A-2u

NIR [5, 32, 56], THz scanners [41] and mid-infrared (IR) scanners [21]. Naturally, these scanners provide datasets of higher quality than those commonly available, with all necessary calibration and normalization. 'Scientific' scanners create the basis for a commercial solution of acquisition system for art investigation, and their output datasets are used as a sandbox for the development of suitable algorithms.

3.2 PHYSICAL MODELS

The description of optical properties and their connection with measured values by means of the materials used, and the degradation of those materials, is done in three steps. The first step is measurement (in our case multimodal and non-invasive). The second step is a physical model for converting numbers to a spectral response or quantified material descriptors. And the third step is a database of descriptors, which are necessary for final mapping and classification of materials. It is advantageous to use a physical model that is simple, robust and precise. The physical model reflects the modality and scanner principle used.

In the following sections I will skip the model used for XRF, which is well-known and widely used in industry for the identification of heavy elements. Instead, I will focus on other modalities where the lack of a useful model should be demonstrated.

Successful application of the XRF model was already demonstrated in [18, 48] and [49].

3.2.1 *Calibration*

First of all, every scanner must be calibrated to produce reproducible and comparable measurements. For each wavelength in the measured spectra, it is necessary to know

Light sources as well as sensors must be monitored for temperature and age.

- **Intensity of light source**: All light sources change spectral characteristics with their own temperature and age. For this reason each light source has its reference spectra measured after heating (reaching its maximal temperature), and its lifespan is limited.
- **Permeability of optical system**: Absorbance and refraction of band-pass filters, lenses and gratings vary across measured spectra. Permeability of each static optical element must be determined or estimated.
- **Sensitivity of sensor**: Sensor response is not necessarily linear with regard to intensity of illumination, and the dynamic range is limited. Above all, for CCD cameras non-linearity is an advantage that allows for a higher dynamic range to be reached, but it is a disadvantage for scientific measurements. A second problem is sensor heating. Higher temperature produces noise in the collected data.

All problems according to Preflight profile
Convert to PDF/A-2u

Light source intensity, permeability of the optical system, sensor response function and operating temperature must be known and controlled. Moreover, it is necessary to compensate for inhomogeneity of the artwork illumination. How to handle a calibration process and the subsequent data acquisition can be found in [59] for DSLR; in [60] the authors describe calibration of a CRISATEL multispectral camera for reaching a higher dynamic range, and in [61] chromatic calibration for color reproduction is described. Finally, in [62] we described the estimation of calibration parameters.

A calibration equation with relevant parameters can look like this:

$$I_{x,y,\lambda} \quad s\ Id\ \ r\ x,y,\lambda\ p\ \lambda\ \ , \tag{1}$$

where

x, y	-	spatial coordinates of the measured pixel,
λ	-	measured modality wavelength,
$I_{x,y,\lambda}$	-	measured intensity for a pixel and wavelength
I	-	intensity of the illuminating light source,
d	-	size of pixel as a solid angle with center in illuminant,
$r\ x,y,\lambda$	-	reflectance factor at position x,y for wavelength λ,
$p\ \lambda$	-	permeability of optical system for wavelength λ,
s	-	sensor response function.

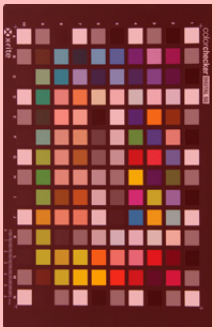


Figure 5: Certified color target x-rite ColorChecker Digital SG

A similar model can be found in [63], where a linear sensor response is expected and therefore the sensor response function s is missing. However, Ribés et. al. incorporate additive noise in their formula, whereas we omit the noise in equation 1, because no noise estimation follows in the data processing pipeline. Noise is therefore distributed into every subformula.

In practice, a calibration process consists of the measurement of certified targets (with known spectral response [59, 60, 61, 5]) under the same illumination as the scanned artwork. Example of such target shows Figure 5. This simplification is possible if the mentioned parameters are stable and known for the acquisition setting used.

3.2.2 *Optical properties of materials*

The dataset representation used in most cases for measured values is an n-dimensional vector of wavelength-dependent reflectance or transmittance. This vector is used as a per-pixel spectral "fingerprint".

The optical properties of paint materials, such as indices of refraction, absorption and fluorescence, which are used in optics, determine the appearance of the paint material under illumination (see Chapter 6

All problems according to Preflight profile
Convert to PDF/A-2u

in [64]). These properties can be derived from measurements of single-layered samples [34] or pigment particles [65], but in the referenced papers refraction and absorption are rarely used. Only the fluorescence of various materials was measured and applied for material identification by A. Pelagotti in [12, 13, 66]. Computation of optical properties is still an open problem with uncertain applicability. The problem is in the reproducibility of measured paint materials. In theory, the index of refraction as well as absorption depends on the ratios of mixed compounds, size of particles in a mixture, paint material homogeneity and surface roughness of a layer. Reference measurements of optical properties is problematic due to the variability of a receipt used for paint material preparation.

An example of paint material complexity can be demonstrated in the handling of opacity.

Introduction to the paint material opacity effect.

As a demonstration of paint material complexity, we describe the handling of opacity, where optical characteristics can be found in the domain of expert knowledge. In [67]: Indices of refraction of the pigment and binder determine paint material opacity. A growing difference between the indices increases the opacity of a material. According to expert knowledge, aging of organic substances can change the material index of refraction. This effect is observable as increasing transparency (e.g. of oil layers, egg tempera) in paint materials that are mixtures of compounds with very different indices of refraction. When such paint material is mixed, a low ratio of pigment/binder is necessary to attain opacity. Highier ratio of binder/pigment will increase the effect of growing transparency.

3.2.3 *Multi-layer model*

Optically homogeneous layers and painted colors often blend in terminology (e.g.: [70, 31]).

A common model of a painting simplifies it to a multi-layer system, e.g. in: [68, 40, 19, 69]. This model assumes that a painting is a composition of several layers of homogeneous materials, where homogeneous is understood in the sense of optical properties (see Section 3.2.2). The basic idea of color layers is a cornerstone for the development of material descriptors (these descriptors will be described in Chapter 4). Nevertheless, this idea is only applied in the form of expert knowledge, according to which assumptions are generated. There is currently a lack of useful mathematical formulas for the interpretation of measured values in the form of layer descriptors.

An individual color layer, composed of a pigment, binder and filling in a homogeneous mixture, is represented by (per wavelength) reflectance, transmittance, absorption, index of refraction and layer thickness. But experiments have shown that the effect of scattering between layers deserves a more parametric model (i.e. the layer-crossing geometry should be included [24]). Additional necessary parameters are hard to influence or measure. A descriptive model becomes too complex to be applied here.

All problems according to Preflight profile
Convert to PDF/A-2u

3.2.4 *Two-layer model*

An alternative to the previous multi-layer model is a new perspective, defining modality content. This approach is relatively new and its terminology has not yet settled. In [71] the authors name the second layer: *"... what appears to have been a substantially finished portrait before it was painted over"*. In subsequent publications the authors reduce multi-layer complexity by speaking about modality *"innovation component"* [72], *"hidden painting"* [48], *"visually significant regions"* [73] and modality *"information gain"* [74]. In all articles the authors do not work with color layers but rather with the information content of a modality (especially X-ray and NIR). This approach significantly decreases the complexity of a multi-layer model. The layer identification problem, which is ill posed, is transformed into an information separation task and a signal decorrelation, which are mathematically approachable. Various solutions of decomposition are listed in appendix Section 12.1, where the referenced articles are described in more detail.

The outputs of the mentioned articles were in all cases simply presented as visualizations designated for expert analysis (see Section 6.6).

3.2.5 *Pigment-mixture model*

The third model, used for pigment mixtures, is the Kubelka-Munk (KM) theory [75, 76]. This theory allows estimation of the optical properties of a mixture from the known properties of its compounds: *"A limiting assumption is that the particles making up the layer must be much smaller than the total thickness. Both absorbing and scattering media must be uniformly distributed through the sheet. Ideally, illumination should be with diffuse monochromatic light and observation should be of the diffuse reflectance of the paper. The theory works best for optically thick materials where* $> 50\%$ *of light is reflected and* $< 20\%$ *is transmitted"* [75]. KM theory requires precise calibration and provides an estimate of the spectral response of a pigment mixture. Its limitations are discussed in [77, 78].

Application of KM theory to the identification of pigment mixtures was successfully tested in [79]. In [80] KM theory extends the discriminative power of the suggested pipeline for material identification. Finally, [29] uses the KM model for comparison of a pigment mixture used in artwork with prepared paint material mock-ups, possibly used in a mixture.

All problems according to Preflight profile
Convert to PDF/A-2u

The research of materials is crucial and constitutes the largest part of art investigation research (in terms of number of publications). Non-invasive techniques, including multimodal screening, uncover the identity of materials [12, 18, 81, 35, 34] and their origin [82], and they help with identification of the degradation level of a painting [83]. Transparency in IR modality was discovered in 1969 [26], and since then more modalities and more materials have been studied. There have been many attempts to entangle materials and their spectral responses, e.g. in [84, 65, 85, 86, 34], more or less covering the UV-NIR range. However, the complexity of available paint materials is so huge that the usability of material databases is very limited. The application of multispectral screening of prepared color samples was presented in several case studies (e.g.: [87, 88, 81, 66, 86]) where a set of necessary color mixtures was tested and compared with the studied painting.

The mentioned research in the field of material spectroscopy is far from DIP, but without any a priori knowledge, the applicability of DIP and classification of algorithms is very limited. Here, I would also like to list databases from other modalities (MWIR and THz), but as far as I know, such databases have not yet been published.

4.1 FIBRE OPTIC REFLECTANCE SPECTROSCOPY AND COLORIMETRY

In the past decade, publicly available FORS databases of pigments have begun to appear. The oldest database, [33], which follows the research of applied fibre optics reflectance spectroscopy (FORS) in art investigation [89, 90, 88], was created by the Restoration Laboratory of the Opificio delle Pietre Dure and the Applied Spectroscopy Laboratory of the Institute of Applied Physics "Nello Carrara" of the Italian National Research Council. This database contains spectral responses in the range $\langle 380, 1700 \rangle nm$ from 440 samples prepared for this purpose. This set is available online at [91].

The second database was created by our team as part of the project m3art. Our database contains 634 samples scanned in the range $\langle 428, 1050 \rangle nm$, where each sample was created by combining the underdrawings and covering layer. For each sample, several measurements of reflected spectra as well as transmitted spectra are available. The database is available online at [92] and was created in the years 2012-2014.

All problems according to Preflight profile
Convert to PDF/A-2u

The third database was created by Antonino Cosentino in 2015 and contains 324 samples created by a combination of one of 54 pigments with 6 types of binders. Samples were scanned in the range $\langle 360, 1000 \rangle nm$. The database is available as a zip file downloadable at [93].

These datasets are sufficient from the perspective of colorimetry. Spectra measured by FORS in the range $\langle 400, 700 \rangle nm$ can be directly converted to XYZ color space values according to CIE specification.[1]. Conversions to other color spaces have been well described, e.g. in [94].

4.2 DATABASE OF THE XRF SPECTRA OF PIGMENTS

Research presented in the field of pigment identification and localization based on material spectroscopy and macro-XRF studies is very promising [48, 71, 49]. The advantage of XRF modality in pigment identification over UV-NIR FORS lies in the possibility to extrapolate the behavior of chemical elements to the entire paint material mixture. According to [95], most of the pigments owe their color to their own chemical composition. The interaction of electrons with X-rays, and the excitation of these electrons, creates peaks in the XRF spectrum. According to the measured peaks (their energy levels or wavelength), chemical elements are distinguishable. A database of the X-ray energy levels of chemical elements has existed since 1960 and is accessible, e.g. in [96]. These tables have been successfully used in industry for the creation of element maps.

A map of chemical elements is useful for identification of a pigment. The pigment represents a class with a certain chemical element weight ratio. The measured content of a pixel is mapped to these classes. However, this step must tackle the same problems as pigment identification by FORS, in that a huge set of classes (possible paint material compositions) must be taken into account. A reduction of this set is necessary and is constructed according to expert knowledge. The set of possible paint materials is reduced according to an artwork's era of creation, origin and paint material color. The papers referenced above demonstrate that a reasonable cardinality of the set can be obtained in this way.

The third part is color reconstruction. This problem is not yet fully solved: *"This is a very difficult problem as the mechanisms by which many disparate pigments, not all of which are sensed by the X-ray fluorescence technique, come together to form a single color are very complex" [48].* Authors therefore attach a color to a chemical element [71] (i.e. Hg for red, Co for blue) and shadings are reconstructed through the alpha mixing of attached colors [48], in [49] by using special mixing software that takes into account the measured elements ratio.

"... the colours flowed in as appropriate." [71]

1 Details in: ISO 11664-1:2007(E)/CIE S 014-1/E:2006

All problems according to Preflight profile
Convert to PDF/A-2u

EXPERT KNOWLEDGE

We understand expert knowledge to mean generalized experience gained from various case studies in the practice of a conservator or restorer. The context of an artwork is hard to describe analytically. However, it can imply relevant assumptions and limits applicable during an investigation.

In my experience we can talk about the following contexts: painting techniques, usage of pigments across ages and localities, and knowledge of the restoration process. Expert knowledge in papers is hard to track, primarily because often only its projection into assumptions can be noticed in the referenced papers and parts thereof cited below. Therefore, the following sections, rather than describing the current state of the art, document how expert knowledge has been effectively applied in the form of hypotheses or evaluations in various case studies.

5.1 PAINTING TECHNIQUES

Painting techniques vary across ages, among authors and also among author's eras. These variations can be used for applying effective limitations to art investigation, especially to DIP.

Determination of underdrawing visibility from artwork painting technique

First of all, work *in situ* can be accelerated by suitable estimates of ROI. For example, we can expect to find visible underdrawings in an NIR reflectogram for gothic paintings because white was most common color of support and egg tempera were the most common binder. On the other hand, baroque paintings typical have earth support, where the contrast of underdrawings in the DSLR sensitivity range is almost useless. Effective usage of DSLR can therefore be evaluated by one or two probe images identifying ROIs. In this way, time spent on *in situ* measurements can be saved.

Identification of uncertain structures in noise images

The typical painting technique of a certain author, along with his or her era, can be evaluated in a case study. A hypothesis can be proven (or rejected) according to sketches and their position, materials used, or typical composition and how it changes during creation of an artwork. Descriptors for such a case study are created according to knowledge of an artist's biography. This procedure was used, e.g. in [97], where the authors tracked the painting technique used in portraits by Fridrich von Amerling.

In [73] the authors interpreted a concealed still life in X-rays. According to expert knowledge of painting technique and knowledge of the basics of still-life composition, it is possible to interpret the cap-

All problems according to Preflight profile
Convert to PDF/A-2u

turd transmission of X-rays as *"underlying composition of a still-life with flowers"*.

Identification of a drawing tool

Knowledge of painting technique can also be used for determination of underdrawing/underpainting descriptors: *"In (Bomford, 2002) a detailed description of individual fluid drawing media and dry drawing media is given. To briefly summarize, when the paint or ink is very fluid, the lines appear smooth and continuous, have some variations in width and density and often show a droplet at the end of a stroke. In addition, the appearance of a fluid stroke depends on the drawing tool (brush or pen). Dry materials like charcoal, chalk, graphite or metal point, on the other hand, are less varying in width, less smooth and have a more granular appearance."* This formulation is from [98], where the authors use this expert knowledge for classification of material used for primary sketches.

5.2 PIGMENT DESCRIPTORS

Boles and earth pigments tell us about an artwork's origin and the author's sphere of activity.

Red earth and boles pigments are typically from the same location where the artwork that used them was created. This general claim arises from the price of these pigments and the numerous local producers documented at that time. Distribution of these pigments over long distances would not be economical. According to this claim, art experts are able to recognize an artwork's origin and the artist's sphere of activity. Knowledge of pigment compounds and element weight ratios is helpful here. Useful modalities for their analysis are documented in [99, 100]. A case study in which expert knowledge of provincial earth pigment admixtures was successfully applied can be found in [101, 1].

[18]: "As expected, this pigment was found predominantly in the lips and cheek."

The task of pigment set limitation is absolutely necessary. Spectroscopy nicely documents a pigment's fingerprint, but comparison with a spectral database is a problematic and time-consuming task with possibly numerous results. In practice, therefore, this set is limited according to the dating of an artwork (not every pigment was available and commonly used in every era) or the "typical palette" of an author. In [27] the authors apply this principle: *"Knowledge of the expected range of artists' materials to be encountered, their spectral properties, and their particle size can be used to select the spectral and spatial resolutions required for identification and mapping of the pigments."* The relationship between pigment and chemical elements was used in all papers dealing with XRF [71, 48, 49].

[48]: "... Hg for red Co for blue ..."

Application of the spectral fingerprints of paint materials and their principal component analysis (PCA) was used for hypotheses evaluation in several case studies of drawings by Parmigianino in [102]. This paper thoroughly documents the variability of art investigation tasks when an analysis of spectral responses can be useful. In the first case study, stain spectroscopy indicates the different composition and origin of the stains studied, despite a similar stain appearance. The second case

All problems according to Preflight profile
Convert to PDF/A-2u

study evaluates, by means of a similar red pigment spectral response, a hypothesis that two artworks have the same origin and dating. The third case demonstrates an unsuccessful identification of paint materials according to a VIS spectral response and, finally, the fourth hypothesis, concerning authorship and retouching, concludes: *" ... These observations seem to back up the hypothesis regarding a subsequent modification and/or retouching of the original scene, which probably, in its earlier stage, did not include the amphora."*

5.3 ARTWORK CONTEXT

Expert knowledge is crucial when comparing an artwork with contemporary or subsequent art production. This approach was demonstrated in [102], referenced in the previous section.

Our relevant experience is a comparison of similar motifs or whole paintings (original/copy evaluation). Previously, we compared four versions of "*Boy Petting a Bird*" (see Section 10.4 and [103]) and a pair of portraits by Friedrich von Amerling [97]. Rough global registration and suitable visualization are DIP techniques useful for such case studies. A very clear DIP workflow, subjectively adjustable according to expert needs, is important for application.

All problems according to Preflight profile
Convert to PDF/A-2u

Now we will focus on pure mathematical processing of the collected dataset. Our input will be a multispectral or hyperspectral cube, where the dimensions are: painting width x, height y and wavelength λ, which can be the measured reflectance as well as transmittance. Let

$$I\ x, y, \lambda \tag{2}$$

be the intensity of a pixel at position x, y for wavelength λ. It is also necessary to define a pixel neighborhood, i.e. follow spatial information x, y and define neighboring pixels:

$$n\ x, y, r \quad \{\forall\ a, b\ \in \quad ^2 \mid r \geq \sqrt{x - a\ ^2 \quad y - b\ ^2}\} \tag{3}$$

for a certain radius $r \in \quad$. Cardinality of the neighborhood pixel set can vary according to r and in the following text will be denoted as

$$N_r \quad |n\ x, y, r\ | \tag{4}$$

The neighborhood of a pixel is not used in all mathematical constructs, because the spectral reflectance and transmittance of a pixel is often sufficient for the analysis and classification of a pixel. It should be noted that usage of a neighborhood is associated with the curse of dimensionality[1].

Let's denote a pixel's fingerprints as:

$$I_{x,y} \quad I\ x, y, \lambda_1\ , I\ x, y, \lambda_2\ , ..., I\ x, y, \lambda_M\ , \tag{5}$$

where M is the number of modalities at the input. The mapping from fingerprints to descriptors will be:

$$f : \quad ^M \rightarrow \quad ^m, m \in \tag{6}$$

and mapping that takes into account the pixel neighborhood we denote as:

$$g : \quad ^{M\ N_r\ \ 1} \rightarrow \quad ^m, m \in \tag{7}$$

The classification process then attaches one of the C classes $C_{f,i}, i \in \{1..C\}$ according to the f value (g as the case may be):

$$\text{pixel at}\ \ x, y\ \in C_{f,i} \Leftrightarrow \min_{j \in C} \{f\ \ I_{x,y}\ , c_j\} \quad \{f\ \ I_{x,y}\ , c_i\}, \tag{8}$$

1 https://en.wikipedia.org/wiki/Curse_of_dimensionality

All problems according to Preflight profile
Convert to PDF/A-2u

where c_i is a ^{m} vector representing class $C_{f,i}$ and $[v_1, v_2]$ is a distance of vectors v_1 and v_2.

Another perspective involves interpreting hyperspectral data as observed mixtures of partially unknown sources [104]. There we are very close to blind source separation (BSS) theory, in which we work with *source signals* and their mixtures. *"The adjective 'blind' stresses the fact that 1) the source signals are not observed and 2) no information is available about the mixture."*[105]. Therefore, in practice, it has to be carefully defined:

a) what sources are taken into account,

b) whether or not they are observed

and

c) which information is available about the mixture.

Formally written:

$$I\ x, y, \lambda \quad h\ s_1\ x, y\ , s_2\ x, y\ , \cdots , s_{u\ \lambda}\ \ x, y\ \ , \tag{9}$$

where $\{s_1, s_2, \cdots , s_{u\ \lambda}\}$ are source values for $x, y\ ,\ u\ \lambda\ \in$ is the number of sources in mixture/modality λ and h is a mixing function. By intuition, the sources affecting the acquired pixel intensity are paint materials, their level of degradation, illumination, optical system, sensor sensitivity and noise. Other influences also cannot be excluded. Usage of these parameters in a model is always described in a particular paper.

In this chapter, I also append sections focused on visualizations of datasets with reduced dimensionality: f , g ; classification outputs: c_i and sources s, providing deeper insight into an artwork. Visualization techniques correspond to mappings:

$$v : \ ^m \mapsto [0, 1]^3, \tag{10}$$

where the target space is a color space, typically RGB, suitable for visualization.

6.1 PREPROCESSING

By preprocessing, we understand only the mapping $f : \ ^M \rightarrow \ ^M$ and $g : \ ^{M\ N_r\ 1} \rightarrow \ ^M$ i.e. mapping that does not change the dimensionality of pixel vectors. Preprocessing algorithms include gamma correction, contrast enhancement, color balance, focusing, denoising and other basic DIP methods, as well as methods adapted for the needs of art investigation and working with a multimodal dataset. The first

All problems according to Preflight profile
Convert to PDF/A-2u

group of algorithms can be found well described elsewhere [52]. In this section I would like to mention algorithms for the compensation of artifacts related to multimodal acquisition. My experience recognizes two major problems with this group. The first major problem is artifacts in images produced by transmittance acquisition (Section 6.1.1). The second problem is misregistration and mosaicing (Section 6.1.2) of modal images caused by usage of scanners which are not spatially calibrated or spatially limited.

At first glance, this two-item list is not exhaustive; there are many conditions affecting the quality of the acquired images, but in most cases, unwanted artifacts can be eliminated by the appropriate equipment or calibration method, or suitable illumination. Controlling the scanning process leads to better results than usage of DIP methods.

6.1.1 *Transillumination artifacts removal*

Transillumination was introduced to me in 2010 by Igor Fogaš from the Moravian Gallery in Brno.

"X-rays also collect many unwanted image artifacts, including shadows from painting support structures or cradles, canvas stretcher bars, braces, framing, nails, and even holes and trails left behind by wood-eating beetles." [73]

Dataset collection using transillumination[2] makes subsurface layers of the painting stand out in greater contrast than with common reflectograms [106]. Application of this technique is limited by the penetrative ability of the radiation. Therefore it is relevant for X-rays and, in the case of thin support, for THz and IR as well. Apart from painted layers, the intensity of a pixel value is also affected by the canvas, wood structure, nails and other artifacts between the light source and sensor. When solving this problem, we are looking for decomposition (in general, according to equation 9) of the acquired mixture:

$$I \quad I_p \quad I_a \quad \eta, \tag{11}$$

where I is the intensity of the measured pixel (according to equation 2) decomposed into the intensity gain of a painting I_p, intensity gain of unwanted artifacts I_a and noise η. Removal (in other words, decomposition) of the artifacts, i.e.: estimation of $I - I_a$ was solved in [73, 107, 108, 109] as well as in many unpublished case studies using X-ray images.

It is necessary to mention here that "successful removal" is not only the recovered intensity without artifacts, but also an artifact contrast reduction, producing a less disturbing image. Partial reduction positively affects the work of an expert as well as semiautomatic and automatic DIP. I should mention here that multimodal screening often does not provide sufficient information for reasonable application of DIP.

The principle used for the removal of periodic patterns like canvas threads is the usage of a Fourier transform in [107] and [108]. A Fourier frequency spectrum is analyzed, and high peaks near a pattern fre-

2 Transillumination was published in 2012 in [69] but commonly was used in practice before then.

All problems according to Preflight profile
Convert to PDF/A-2u

quency (canvas threads or cradles) are searched and masked. Finally, an inverse Fourier transform produces an image with reduced artifacts.

Alternatively, in [73] Gooch and Tumblin use a gradient map for a rough detection of the cradle borders, which are manually edited by an expert, thus making the sharp edges gradual and less disturbing. The marked artifacts are then removed by Poisson image editing [110].

In [109], automatic removal of cradles from X-ray modality is proposed. A captured X-ray image is decomposed into four images: The cradle itself I_c^0, cradle texture I_c^{text}, cartoon part of a painting I_p^{cart} and texture part of painting I_p^{text}. The mixing function h is a summation of these components:

$$I \quad I_p^{\text{text}} \quad I_p^{\text{cart}} \quad I_c^0 \quad I_c^{\text{text}} \tag{12}$$

The cradle position mask I_c^0 is found according to a maximization of row intensity sum over rotation transformation. For cartoon/texture decomposition, a morphological component analysis (MCA) algorithm is used [111]. Separation of wood texture and painting texture is done by variation of a sparse Bayesian factor model [112] on high-frequency curvelets and shearlets.

Note that in all four case studies referenced here [73, 107, 108, 109], the processing pipeline, composed of existing and more general, but still appropriate DIP algorithms, was made to measure. In general, the usability of the applied techniques is therefore limited.

6.1.2 *Registration*

Registration of two or more images is necessary when a DSLR camera [62, 53] or more than one scanning device [29] has been used for multimodal screening, or when a dataset contains multitemporal images, spatially misregistered. In spite of the existence of scanning devices producing spatially registered images [5], usage of DSLR or multiple scanning devices is a widespread and economical technique. Spatial inaccuracy is caused by lens distortion (optical properties vary for each wavelength), different resolution of the scanning devices used, and also inaccuracy in setting the device in the case of multitemporal acquisition [7]. A special case of registration usage is found in the comparison of multiple artworks with the same motif [113].

The main registration problem is in finding a suitable similarity measure.

Registration improves the ergonomics of manual comparison and also enables application of the following DIP algorithms. In spite of excellent general registration algorithms, the registration of an artwork's multimodal dataset has not yet been fully resolved, due to a lack of useful similarity measures for various modality pairs. The registration task is estimated by the transformation:

All problems according to Preflight profile
Convert to PDF/A-2u

$$t_\lambda : \quad ^2 \rightarrow \quad ^2 \tag{13}$$

$$\text{for which } t_\lambda \; x_\lambda, y_\lambda \qquad \text{pixel at} \quad x, y \tag{14}$$

The complexity of the transformation is given by the number of its parameters. Commonly used global transformations are rigid, affine and perspective. The best performance can be achieved by using a transformation function corresponding to the optical system used for acquisition. It is, as is also the case for DSLR with a standard photographic lens, a radiometric distortion. However, radiometric distortion is hard to estimate from the artwork dataset [114]. For this reason, radiometric distortion has not yet been applied in art investigation. In the case of radial distortion caused by lens distortion, polynomial transformations are useful.

There are two approaches to registration: local and global. The approaches for local and global registration have their own fields of application. Local registration is more useful for multimodal data, where a precise global model depends on lens construction and geometry [115], which we are unable to measure or compute. Global registration, based on projective transformation, is useful for comparing similar motifs [103]; in such cases, local misalignment reduction could be counterproductive because local misalignment is the object of study.

Estimation of transformation parameters is, in most cases, done according to selected tie points [29, 116]. For semiautomatic and automatic registration of tie point positions and pairing, similarity measures such as *cross correlation* [115, 117] and *mutual information* [118, 13] are used. However, application of these similarity measures is problematic. Here, we demonstrate the problem with the cross-correlation that was used in this field. Details on mutual information follow in the Appendix 12.1. Figure 7 visualizes a cross-correlation of multiple bands (from 400 up to 2250nm) on spatially registered images. The more distant wavelengths have a lower cross-correlation, which produces lower gradients near optimal positions of tie points. Registration is slower with decreasing cross-correlation (the gradients are lower) and, in extreme cases, an algorithm can converge to a misregistered local optima.

In case of mutual information, the problematic bands are those with low mutual information (e.g. VIS and X-ray). The problem is similar for the case of low cross-correlation; the gradients decrease, and convergence to a global maximum can be problematic and strongly affected by noise and dissimilar structures. A demonstration in this case, as well as a description of other similarity measures, is beyond our scope here. The selection of a useful similarity measure, e.g. from [119, 120], is still an open problem.

Unacceptable results, especially for multispectral and hyperspectral screening, where the target is pixel spectral response, led in 1989—

All problems according to Preflight profile
Convert to PDF/A-2u

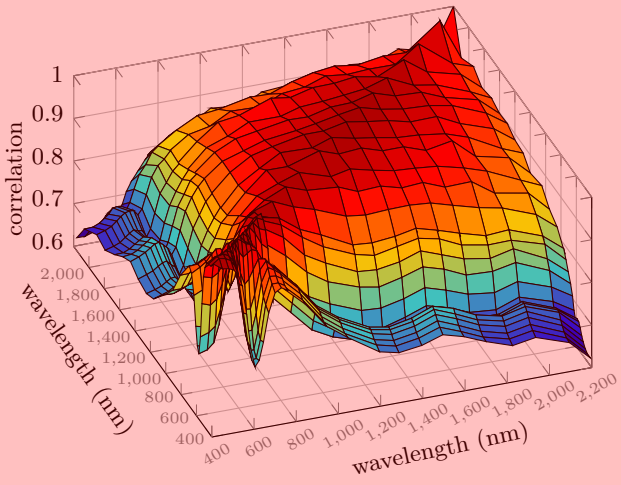


Figure 7: Cross-correlation of 29 spatially registered bands acquired from Leonardo's: *Madonna of the Yarnwinder* (see Figure 9) by VIS-NIR scanner [5]. The correlation of NIR bands is higher than the correlation of VIS bands and, in general, decreases with increasing difference in wavelength.

1992 and 2008 to the development of a scanning device that generates registered multispectral datasets [121, 5] in the UV-VIS-NIR range.

6.2 INFORMATION CONTENT ANALYSIS

In the ideal case, a pixel spectral fingerprint $I_{x,y}$ describes pixel paint material layers well. Formally, there are two representations. The first representation is by f (g as the case may be) mapping from a pixel spectral fingerprint to pixel painted layers, material composition, level of degradation or restoration interventions, and the second representation is by h^{-1} decomposition into the space of searched source signals, which represent layers. In reality, searching such a mapping as well as decomposition are strongly undetermined problems, and the information content of a pixel fingerprint $I_{x,y}$ is limited because not all layers affect the measured value.

In the first representation, where f is the target of estimation, the class behavior is roughly described as f^{-1} by an expert. The class identification is then made according to the mapping f : $^{M} \rightarrow$ and threshold $T_c \in$ for a class C_c such as:

$$\text{pixel at } x, y \in C_c \Leftrightarrow f_c \; I_{x,y} < T. \tag{15}$$

A g-based classification can be made in the same way.

Estimation of h^{-1} (second representation) corresponds to a blind or partially determined decomposition (see equation 9). Classification of a pixel into class C_c is done according to the strongest source signal s_c.

All problems according to Preflight profile
Convert to PDF/A-2u

The recognized sources are then visualized, analyzed and labeled by an expert.

6.2.1 *Dimensionality reduction*

"Dimension reduction algorithms are designed to minimize errors in the procedures performed in the lower dimension."[104]

The motivation for dimensionality reduction is shown in Figure 7, where the correlation is computed for the VIS-NIR bands. The acquired hyperspectral cube contains a lot of redundant information encoded across neighboring modalities. Transformation of the hyperspectral cube into orthogonal dimensions should *"... concentrate significant features into a few representative images, thus facilitating their interpretation"* [122].

We understand f (g as the case may be) mapping (see equations 6, 7), where $m < M$, to be a reduction in the dimensionality of the input. This can be done blindly or with a focus on a specific accentuation of modal content. A blind statistical analysis of pixel spectral fingerprints I does not use a pixel neighborhood $n\ x, y, r$ in most cases, and therefore a f instead of g mapping is constructed (see equation 6), with a focus on reducing the input dimensions while retaining discriminatory power. In addition, there can be requirements for source separation, i.e. noise and painted layers (see Section 6.2.2). The generated outputs, with reduced dimensions, will be easy to visualize for further expert-based evaluation as a few monochromatic images or by false colors (see Section 6.6.1).

The most commonly used compliant algorithm is PCA (used in [122, 123, 124, 5, 125, 9] and many other papers). PCA finds an orthogonal basis, with dimensions ordered by decreasing dimension variance, and in this way concentrates the information content into the first few principal components (i.e. dimensions). It should be noted that the discriminatory power of reduced dimensions is not guaranteed by PCA; classes of low probability will by suppressed by this transformation.

Another popular variant of PCA is maximum noise fraction (MNF) [126], where the signal-to-noise ratio (SNR) is a key parameter for linear decomposition and dimension ordering (instead of variance in PCA). MNF were used, for example, in [127]: *"... to maximize the clarity of the features from the earlier painting"*, in [128] for noise reduction, in [23]: *"..to determine the data dimensionality"* and similarly in [29, 129].

Dimensionality reduction by estimation of the mixing function h (see equation 9) corresponds with an analysis of the spectral signatures of pigments and their mixtures. For a low number of searched signatures (pigments) and an assumption of a linear mixing function h, linear spectral mixture analysis (LSMA) is applicable [130]. Application of LSMA for palimpsests analysis was demonstrated in [131]. An alternative is the visualization of spectral signatures. The typical pigment behavior, high intensity in one band and low in another, is accentuated by using ratios or differences suggested from acquired modal intensities:

All problems according to Preflight profile
Convert to PDF/A-2u

$$\frac{I\ x, y, \lambda_i}{I\ x, y, \lambda_j} \tag{16}$$

$$\text{or } I\ x, y, \lambda_i\ - I\ x, y, \lambda_j\ , \tag{17}$$

for certain modalities λ_i, λ_j. Defining several such ratios and differences can be sufficient for pigment mapping and its visualization. A demonstration of this multimodal analysis is used, e.g. in [132], where several such mappings are used for human-comprehensible visualization by *false colors*.

An h-based dimensionality reduction is also possible by decomposition of n input dimensions, corresponding to spectral sub-bands λ, into components containing noise and other irrelevant information (cracks, artifacts and defects) and components covering information suitable for visualization. Irrelevant components are dropped, and the number of those that are relevant is less than n. These decompositions follow.

6.2.2 *Decomposition techniques*

Decomposition of a hyperspectral data cube into relevant sources/images can use algorithms used for solving similar problems in remote sensing [104, 133]. The most important assumption is whether the observed data is forming a linear or non-linear mixture of searched signals. According to this decision, a suitable method should be constructed. The application of a linear mixing model is simpler, therefore it is necessary to take a critical point of view before its usage.

"If a linear mixing model is used on data where the systematics are nonlinear, the calculated fractions will be significantly in error."[104]

There are ready-to-use algorithms for linear and nonlinear BSS [134], which require fulfillment of some requirements and offer relatively easy application on the acquired dataset. For this reason, a comparison with BSS methods is always present in papers that solve a decomposition problem. In all referenced cases, a comparison with linear independent component analysis (ICA) is provided. A comparison with non-linear ICA is missing[3].

Various algorithms for linear mixture decomposition have been tested, e.g. ICA in [128], where about 20 target components were used *"... to detect components that are only present in a small section of the total analysed image"*; PCA, ICA and orthogonalization in [135]: *"We expect to find in each of these images different independent information and, hopefully, one of them should carry the information about the hidden text that should be retrieved."*; PCA and MNF in cases of the dimensionality reduction mentioned above (see Section 6.2.1); and MCA in [109, 72], sparsely selecting sources from dictionaries of textures and "cartoons".

3 Non-linear ICA is an ill-posed problem with unstable results. The method produces independent components for which dependency on only one source signal is not guaranteed. The creation of extra constraints for the elimination of ill-posedness is often beyond the scope of published case studies.

All problems according to Preflight profile
Convert to PDF/A-2u

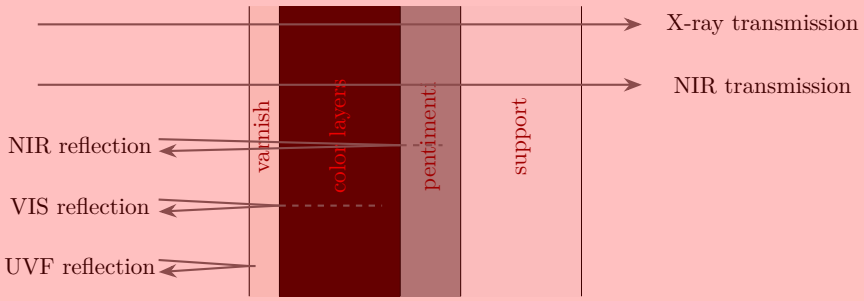


Figure 8: Demonstration of the penetrative ability of particular modalities.

Let's take a look at the decomposition principle. According to the multi-layer model (See Section 3.2.3), pixel intensity $I\ x, y, \lambda$ is affected by those layers which affect the captured rays (see Figure 8). For transmittance, all layers affect the acquired rays, but for reflectance some layers could neither be penetrated nor touched.

For simplicity we denote a vector of source signal values for a pixel x, y :

$$s\ x, y\ _{\lambda} \quad s_1\ x, y\ , \cdots , s_{u\ \lambda}\ x, y\ . \tag{18}$$

The parameter λ indicates that a number of relevant source signals can vary according to modality. The number of these source signals is then denoted as $u\ \lambda$.

Formally, we have, e.g. VIS reflectance and X-ray transmission modalities observed as a mixture of several sources:

$$I\ x, y, \text{VIS} \quad h_{\text{VIS}} \left(s\ x, y\ _{\text{VIS}} \right) \tag{19}$$

$$h_{\text{VIS}} : \quad ^{u\ \text{VIS}} \rightarrow \tag{20}$$

$$I\ x, y, \text{X-ray} \quad h_{\text{X-ray}} \left(s\ x, y\ _{\text{X-ray}} \right) \tag{21}$$

$$h_{\text{X-ray}} : \quad ^{u\ \text{X-ray}} \rightarrow \quad , \tag{22}$$

And it follows from the previous observation:

$$u\ \text{VIS}\ \leq u\ \text{X-ray}\ . \tag{23}$$

From the mentioned observation we can derive that per modality decomposition products are in inclusion according to modality penetration depth:

$$D_{\lambda} \quad \{ s_1, s_2, \cdots , s_{u\ \lambda}\ \} \tag{24}$$

$$D^R_{\text{UVF}} \subseteq D^R_{\text{VIS}} \subseteq D^R_{\text{NIR}} \subseteq D^R_{\text{THz}} \subseteq D^T_{\text{NIR}} \tag{25}$$

$$D^T_{\text{NIR}} \equiv D^T_{\text{THz}} \equiv D^T_{\text{X-ray}}, \tag{26}$$

All problems according to Preflight profile
Convert to PDF/A-2u

where R denotes reflection and T transmission. These relations express modal inclusion according to the commonly respected [1] and empirically verified penetrative ability of the mentioned modalities [10, 26, 37]. Note that exceptions to this inclusion for certain paint material layers may exist.

These inclusions can be effectively used for separation of hidden and visible layers of the painting if we approximate the mixing model h by two mixtures $\underleftarrow{h}$ and $\underrightarrow{h}$ mixed together by $\hat{h}$ such as:

For the existence of $\hat{h}$ the implicit function: $\frac{d\hat{h}}{d\underrightarrow{h}} \frac{d\underrightarrow{h}}{ds} \neq 0$ must be true.

$$h_{\lambda_2}\ \ s_{\lambda_2}\ \approx \hat{h}\left(\underleftarrow{h}_{\lambda_2}\ \ s_{\lambda_1}\ , \underrightarrow{h}_{\lambda_2}\ s_{u\ \lambda_1\ \ 1}, \cdots, s_{u\ \lambda_2}\right) \tag{27}$$

If there exist $h_{\lambda_1}^{-1}$ and $\underleftarrow{h}_{\lambda_2}^{-1}$ inverse mixing functions then $\underleftarrow{h}_{\lambda_2}$ contains the same information as the image from modality λ_1, i.e.: visible layers and symmetrically $\underrightarrow{h}_{\lambda_2}\ s_{u\ \lambda_1\ \ 1}, \cdots, s_{u\ \lambda_2}$ produces an image of hidden layers. When $h_{\lambda_1}^{-1}$ or $\underleftarrow{h}_{\lambda_2}^{-1}$ does not exist, approximate results are obtained by such decomposition.

There are two possibilities: to directly estimate $\underrightarrow{h}_{\lambda_2}$, or estimate $\underleftarrow{h}_{\lambda_2} \circ h_{\lambda}^{-1}$ and according to the implicit function of $\hat{h}$ express $\underrightarrow{h}_{\lambda_2}$. In practical use $\hat{h}$ is not more complicated than a sum [73, 72]:

$$\hat{h}\ A, B \qquad A \quad B \tag{28}$$

In such a case:

$$\underrightarrow{h}_{\lambda_2}\ x, y \qquad I\ x, y, \lambda_2\ - \underleftarrow{h}_{\lambda_2}\left(h_{\lambda}^{-1}\ I\ x, y, \lambda_1\right) \tag{29}$$

Estimation of $\underrightarrow{h}_{\text{X-ray}}$ can be found in [73, 48, 72], where X-ray transmission is decomposed according to other modalities, i.e. VIS - NIR. Deligiannis et al. in [72] decompose an X-ray transmission according to the left- and right-side reflected images of an altar panel. For this purpose, coupled dictionaries were constructed from an RTG image and the *"side information"* obtained from VIS. These dictionaries were then used for separation of RTG images by using modified MCA. Finally, visualization of the RTG, representing the front and back sides of the panel, was created. This approach uses a linear mixing model hidden in an MCA algorithm.

Gooch and Tumblin use a probabilistic approach in [73]. An image from VIS is segmented (i.e. creation of $h_{\lambda_1}^{-}1$) by a mean shift algorithm, and in this way quantized intensity values are translated into X-ray modality by normalization (i.e. normalization corresponds with $\underleftarrow{h}_{\lambda_2}$). The produced image is compared in terms of variance (i.e. subtraction according to equation 29) with X-ray normalized intensities. A hidden layer is created from regions with high influence by tresholding.

Anitha et al. discuss normalized mutual information in [48]. An optimized constraint includes minimization of mutual information between

All problems according to Preflight profile
Convert to PDF/A-2u

h_{λ_1} and $\underrightarrow{h}_{\lambda_2}$ and maximization of mutual information between h_{λ_1} and $\underleftarrow{h}_{\lambda_2}$, which is done separately over wavelet coefficients *"... to maintain coherent image features and avoid pixelwise overfitting"*. The source mixture is simulated here according to equation 29.

In our paper [74], we use an artificial neural network (ANN) for a more penetrative modality approximation. Modality or modalities with lower penetration are used as an input, and those with higher penetration (in our case NIR) as an output. The approximation computed by ANN is then subtracted from the second modal image, which produces *information gain* of the second modality. Rescaling of the *information gain* creates a plausible source signal representation. This method is described in Section 10.12 and uses mixing models h, $\underleftarrow{h}$, and $\underrightarrow{h}$, which are represented by trained ANN, and therefore non-linear and not necessarily invertible. The fusion model for $\hat{h}$ uses addition and scaling:

$$\hat{h}\ A, B \qquad A \quad \frac{1}{B_{max} - B_{min}}\ B - B_{min}\ , \tag{30}$$

where B_{min} and B_{max} are minimal and maximal intensities, respectively, of a pixel in image B. Section 12.1 of the Appendix compares these algorithms in a more detailed manner.

A comparison of mixing functions on the same dataset should justify or reject the application of linear mixing models, as well as the convergence capabilities of constructed constraints, i.e. local vs. global, fast vs. slow.



Figure 9: Attributed to Leonardo da Vinci and another artist: *Madonna with Yarnwinder*, oil on panel. $50.2cm \times 34.6cm$. Private collection, United States.

6.3 PIXEL DESCRIPTORS

In spectral response analysis, DIP is able to produce pixel descriptors. These descriptors are inspired by painted layers (see Section 6.2.2, properties of paint materials (Section 6.3.2), artifacts (Section 6.3.1) and painting tools [98]. This approach is close to dimensionality reduction (Section 6.2.1), with a focus here on certain pixel properties.

In [136], the authors analyzed "Madonna with Yarnwinder" (see Figure 9), attributed to Leonardo da Vinci. The paper *"... supplied interesting information about the pigments used, the restored areas, the preparatory layer, and the binding medium."* All the analytical methods presented there were directed by an expert. According to peaks in the VIS spectral range, two types of blue were identified: ultramarine, available in the Middle Ages, and Thénard's blue, available from the 19th century. According to the NIR response, the content of clay minerals and gypsum in the preparatory layer was identified. Finally, MWIR peak analysis showed the presence of an oil binding medium. It needs to be mentioned at this point that the presented work analyzed peaks in the spectral response of a pixel, according to which the responsible material was determined. This principle underlies a widespread technique whose references I put in Section 6.3.2 Pigment descriptors.

All problems according to Preflight profile
Convert to PDF/A-2u

I denote the localization of underdrawings, varnishes or retouches as a search of ROI. This is a different kind of labeling that broadly uses empirical expert knowledge. In Section 6.3.3 Descriptors for ROI, I will describe an analytical approach that also uses the step from spectral fingerprint to paint material identification but for which the main goal is image segmentation.

6.3.1 *Artifact descriptors*

In Section 6.1.1, I mentioned approaches to transillumination artifact removal. Here, I would like to describe artifacts in the sense of descriptors used for their automatic recognition. All artifacts mentioned here (cradles, nails, lacunas, threads and canvas defects) are present in transmissiongrams and are localized, which makes the pixel neighborhood useful for analysis. Small artifacts like lacunae or nails are clearly visible on modal images and always, as far as I know, marked manually. The same is not valid for periodic and extensive artifacts like canvas threads or cradles presented in a transmissiongram.

Removal of a cradle is first discussed in [14]. This paper is from 2002 and provides an overview of applied techniques, which include the filling of cradle interstices with sugar before a transmissiongram is taken, in order to compensate for cradle defects. The authors suggest a histogram matching algorithm. Identification of pixels with a cradle is done manually. An expert creates a mask with several groups, according to thickness of the wood. The possibility of using edge detectors for determining the cradle borders automatically is discussed here.

Recent automatic and semi-automatic approaches [73, 108, 109] using cradle and canvas pattern descriptors have already been mentioned in Section 6.1.1, where removal of these defects is discussed. Our approach is summarized in Section 10.2.

Description of a canvas by thread distribution was developed by Johnson et al. [137] and followed by Cornelis et al. [138]. The latter authors suggest the usage of Fourier analysis extended by several descriptors, i.e. Fourier features, Haralick features and local binary patterns (LBP) texture descriptors. Fourier and Haralick features represent global descriptors and LBP local ones. These descriptors are then used for recognition, whether the canvas comes from the same or different bolts.

6.3.2 *Pigment descriptors*

The idea of pigment identification non-invasively compels enlargement of the scanned part of the electromagnetic spectrum. Pigment identification according to the measured pigment spectral reflectance was historically done by an expert, but recently in art investigation it is being replaced by semiautomatic and automatic comparison with an existent reference database of pigment mixtures. Pigment identification has al-

All problems according to Preflight profile
Convert to PDF/A-2u

ready been discussed from various perspectives: the model of pigment mixing in Section 3.2.5, the databases of descriptors in Chapter 4 and the expert knowledge and chemical content in Section 5.2. Here we will focus on spectral unmixing techniques, while a comparison of pigment descriptors and application of pigment knowledge in the task of color "reconstruction" will be discussed in sections 6.4 and 7.1.

Manual pigment identification exploits knowledge of peak positions in the material spectral response, e.g. [89, 90, 102, 88, 132]. The same principle is used in XRF-based identification of chemical elements. However, in contrast to XRF, modalities with a longer wavelength produce smoother spectral curves with less significant peaks. Such an interpretation is thus much more complicated. Nowadays, the algorithms used in art investigation emanate from solutions of similar problems in remote sensing. Unmixing of a spectral response to its endmembers is a must for real paintings, where pure pigments are rarely present. This problem is discussed from the perspective of remote sensing in an overview paper [139].

An endmember refers to a pure paint material used for mixtures. In this context, pure pixel means the pure paint material content of a pixel.

Despite general knowledge of advanced algorithms for spectral unmixing, we still do not see their widespread application in art investigation. There are two reasons for this: Firstly, there is no motivation to find the best estimate. The goal of a case study is to discover the story of an artwork, not just precisely identify its pigments, and therefore sub-optimal results are often sufficient. Secondly, demonstrating the performance of these unmixed descriptors, which requires a non-trivial set of analyzed datasets and a comprehensive database of the pigments' spectral fingerprints, is hardly comparable.

Unmixing models was already mentioned above (see Section 6.2.2) in my discussion of linear and non-linear approaches. Due to the ill-posedness of the task of non-linear decomposition, a linear approach is preferred. In [140], the authors introduce the pixel purity index. The pixel purity index uses MNF as preprocessing for a dimensionality reduction. The measured pixel responses are projected into a space with reduced dimensionality, and a convex hull in the form of a convex polyhedron with $n \quad 1$ vertices (were n is the number of reduced dimensions) is searched. These vertices then represent endmembers for the linear mixing of pixel spectral responses. This technique was used in [29, 129, 9]. We understand the descriptors to be the mixing ratio of identified endmembers (the referring spectral response can be obtained by, for example, a single-point KM model).

An alternative approach to endmember identification was published in [141]. Valdiviezo et al. suggest the usage of a lattice of auto-associative memories combined with a k-means algorithm for the identification of pure pixels. Auto-associative memory is trained on per-pixel spectral responses. This step produces two matrices: min-memory W and max-memory M:

All problems according to Preflight profile
Convert to PDF/A-2u

$$W_{ij} \quad \min_{\forall x,y} I\ x,y,\lambda_i\ - I\ x,y,\lambda_j \tag{31}$$

$$M_{ij} \quad \max_{\forall x,y} I\ x,y,\lambda_i\ - I\ x,y,\lambda_j \tag{32}$$

Subset S of the column vectors of M and W is used as a selection of pure pixels present in the dataset. *"This selection is mandatory for the two following reasons. First, contiguous columns including the main diagonal of W (similarly for M) are highly correlated, forming $\sqrt{n}\ \ 1$ groups. Second, the number of columns in S must be much less than n"* [141], where n is the number of dimensions (as in equation 5). This subset is then approximated as the centroids obtained by a k-means algorithm applied on the column vectors. The linear mixing ratio of each endmember is then estimated by non-negative least square minimization.

6.3.3 *Descriptors for ROI*

To conclude this section about descriptors, I would like to summarize the application of all other descriptors used in DIP. Generally speaking, art investigation tasks where the application of descriptors is relevant can be interpreted as a search for the *unknown*, and for the identification of regions of expert interest for further, more detailed analysis. The definition or specification of *unknown* exceeds the scope of this thesis and could be the subject of a case study. It mostly depends on painting stratigraphy, modality capabilities and expert focus, e.g. non-matching underdrawings and overpaintings.

Unknown denotes any important information that can be overlooked by a human.

In the case of underdrawings, we are looking for regions that deviate significantly from the expected mutual information. "Significantly" and "expected" are objects of expert-based estimation here, and the inputs for such computation must be identified. In [73], an overpainted image is studied and a XRF transmissiongram is analyzed for the presence of unexpected pixel intensities. At first, a VIS modal image is segmented by a mean shift algorithm. For each segment, the mean intensity of XRF is computed and compared with XRF values in the segment. The difference in these values describes the unexpectedness of pixel intensity. The suggested algorithm was made to measure for the presented case study; in general, there will be problems with meaningful segmentation, enhancement of noise and regions with high variance.

More general algorithms for ROI identification use statistical moments and probability, and will be presented in Section 12.1.

6.4 CLASSIFICATION

I mentioned in the introduction that each task can be converted into a classification task. Here we will talk about an analytical approach to

All problems according to Preflight profile
Convert to PDF/A-2u

classification, i.e. a comparison of input values and their assignment to known and unknown classes. Art investigation is focused on the description of a painting stratigraphy, which is the more detailed level of a painting's description. We are able to build higher levels, such as the recognition of painting styles, objects or layers, on the known stratigraphy. In most cases, the classification is made manually by an expert, especially when the single value per pixel is a descriptor easily convertible to a grayscale image (Here I was able to find only one exception [73], where an automatic evaluation/visualization was presented). False color of up to three dimensions can be used (see Section 6.6.1), but descriptors with higher dimensionality are not easily interpretable, and a vector difference measurement must be introduced.

At this point I also need to mention the recognition and enhancement of characters in old manuscripts, which can be taken into account and referenced as a classification of art investigation. However, there are several issues: 1) this field of research is far from my knowledge; 2) it is so broad, that providing an overview of the topic would be sufficient material for another PhD thesis; and 3) segmentation of characters and segmentation of unclear objects in a painting are two different types of tasks.

For these reasons, I will present here the classification used for the study of painting stratigraphy. Following is an overview of algorithms for the comparison of pixel descriptors, mentioned in Section 5.2 Pigment descriptors, and spectral fingerprints.

6.4.1 *Pigment identification*

As indicated in previous paragraphs, the main purpose of classification in art investigation is the labeling of pixels with the pigments and chemical elements used. The preferred workflow for the classification and comparison of underdrawings, overpaintings and artifacts is visualization and further expert-based class assignment (see equation 15). The target classes and their borders are often fuzzy, and their identification requires a local, global, and often a structural context as well, which is hard to obtain analytically. In Section 5.2 Pigment descriptors, I introduced analytical descriptors suitable for classification: peak position in the captured spectral response, mixing ratios and unmixing coefficients. In addition to these, the analysis of raw spectral responses is also possible and is often used. The applicability of spectral responses for pigment identification has been demonstrated in many papers [89, 90, 88], but the problem has still not yet been fully resolved [12, 81, 142, 143, 144].

The spectral fingerprint of a pixel is affected by paint materials, as well as their mixtures and layers. Creation of a realistic interaction model composed of these ingredients is too complex and must be sim-

"The main shortcoming regards the fact that reflection-mode spectra can present odd distortions of band shape, position and intensity, which depend on several factors, such as absorption and refraction index and surface

All problems according to Preflight profile
Convert to PDF/A-2u

plified for further classification. There are three main problems with classifier construction:

1. **Huge set of possible paint materials**, which means a lot of classes requiring a scarcely available training set of greater cardinality.
2. **Spectral fingerprint similarity of the paint materials**, which requires a modality (in most cases unavailable) with discriminatory power.
3. Application of a **suitable unmixing approximation**. Approximation by a linear model can lead to unambiguous endmembers (see Section 6.2).

A widespread solution is to reduce the huge set of paint materials that could possibly be used for painting; this must be based on expert knowledge of an artwork's historical context or on invasive analytical methods. Such a reduction partially solves problems 1 and 2.

Classification based on a reduced set of possible paint materials can be seen as identification of the pigment that has the highest influence, or is merely the best match with the database. For both classifications, a similar database search is used.

As mentioned in Section 5.2, hyperspectral data processing in art investigation is inspired by remote sensing research, because similar datasets are available and hyperspectral analysis in art investigation is a relatively smaller field of research. An overview of library search classifiers can be found in [145] (2013), and it fully covers algorithms in the referenced papers. The authors distinguish here between deterministic and stochastic classifiers according to their geometrical/physical or statistical principle: *"The deterministic search algorithms have gained popularity because of their mathematical simplicity and ease of implementation. The stochastic search algorithms offer relatively better accuracy, are mathematically complex and require huge computing resources ..."*[145].

In art investigation, apart from manual classification [89, 90, 132, 146] and least square spectral response fit [147], a widespread library search deterministic classification algorithm is the spectral angle mapper (SAM). This algorithm computes the angle between compared spectral responses:

$$\cos^{-1}\left(\frac{{}_{\lambda}I_1\ \lambda\ I_2\ \lambda}{\sqrt{{}_{\lambda}I_1\ \lambda\ ^2\quad {}_{\lambda}I_2\ \lambda\ ^2}}\right), \tag{33}$$

where I_1 and I_2 correspond to the compared entities and $I\ \lambda$ to its spectral value for wavelength λ. This method is robust to noise and to the multiplication of spectral response (i.e. absolute intensity). The

All problems according to Preflight profile
Convert to PDF/A-2u

SAM was published in 1992 [148] and was applied to pigment identification in [12, 81, 66, 29, 129, 9, 8], etc. Note that the number of pigments taken into account must be limited, and the reference spectral response must have a pigment content as pure as possible. Other methods used for hyperspectral remote sensing datasets, such as spectral correlation mapper (SCM), Euclidean distance, spectral feature fitting and binary encoding, or stochastic methods like spectral information divergence (SID) or constrained energy minimization (CEM) (details in [145]), have not yet been applied or compared in art investigation. An exception in this context is [149], where supervised linear discriminant analysis (for details see [150]) and unsupervised fuzzy C-means [151] algorithms are tested and compared. The fact that there is no need for comparison of effective algorithms for spectral classification highlights the second major problem, namely that the measured spectral response can vary for a single pigment [152], and a context for the measured values in the form of expert knowledge is necessary for reliable classification (or endmember identification). Our testing [34] of paint materials shows that a linear mixing model is insufficient, and a spectral response cannot be taken as a "fingerprint" of pigment content; however, this has not yet been demonstrated on actual paintings. The automatic classification of spectral responses has serious limitations here.

In [153], pigment mixtures are also taken into account. The authors chose the brute force method with a limited number of pigments of known spectral response. For each trio of pigments from a nine-color palette and a 5% step in the mixture ratio, a spectral response is computed. The spectral response of mixed pigments is computed according to the single constant KM theory. According to the best-fitting curve, ratios and pigments are taken into account.

In the case of XRF modality, ratios and pigments are considered according to peaks in the collected spectral response. The "reconstruction" of colors is common in case studies where overpainting has been virtually removed. XRF screening is able to recognize chemical elements but not pigments. Here experts are faced with another classification task, in which the weight ratios of elements are used for pigment identification, and the spectral database refers to the "reconstructed" color. All authors [71, 48, 49] agree that finding a precise mapping from elements to colors is an ill-posed problem with many solutions, and therefore mapping uses expert-based heuristics to search for "the most credible" solution, and the selected output colors are interpreted as *"plausible"* [49].

6.5 SCENE MODELING

For studying the history of painting techniques and the composition of a certain artwork, virtual scene modeling can be useful. For the purpose



Figure 12: Johan
Vermeer: *Girl with a Pearl Earring*, 1665, oi
on canvas.
44.5cm × 39cm

All problems according to Preflight profile
Convert to PDF/A-2u

of a scene model, we assume that a planar painting is a representation of a 3D scene. The projection of a real scene should follow the rules of perspective and the optical properties of real materials. With the assumption that a real scene is presented as a painting, the reverse reconstruction of objects and light source positions supports or rejects this hypothesis. In this regard, published case studies have analyzed composition in the sense of consistency across a whole painting. The position of light sources is estimated in [154] for the *Girl with a Pearl Earring* (see Figure 12) by an exhaustive number of methods. Each method uses a different patch of the painting. Cast-shadow analysis was first used by authors in [155]. Cast-shadow analysis uses painted shadows and their point sources for estimation of the direction of light.

The second method, without 3D reconstruction, is occluding-contour analysis. The main idea is that the occluding contour of a painted surface has well-defined normals perpendicular to the line of sight. According to Lambert's cosine law, the lightness of the contour and contour normal, an estimation of surface albedo and direction of light is possible. Because we have just one equation here with two unknown parameters, more than one point must be used for estimation from the same surface contour. For the best results, least square error is optimized for all considered contour points.

Model-based methods are used for estimation of the light direction according to the painted earring, eyeballs and face. The earring's pearl has been virtually modeled in 3D, and its position and light position is simulated so that the rendered appearance best matches the painting. In the case of eyes, a spherical shape is expected, and the Johnson/-Farid algorithm [156] is used for estimation of the light source direction. The last model-based method creates a 3D model of the face using an expectation-maximization (EM) algorithm. A generic face shape is taken as an input, and its position is set according to the position of the face in the painting. In the steps of EM the albedo of the model is refined, according to which the normals of the modeled face are adjusted. When the convergence point is reached, the light source position is estimated from the refined model.

This approach is similar to our spectral extrapolation in Section 10.12.

Algorithms for studying scene geometry can be demonstrated on one of the most-studied paintings, the *Arnolfini Portrait* by Jan van Eyck (see Figure 13). A room with two figures and a concave mirror with mismatching perspectives absorbs the attention of computer graphics researchers [157, 158, 159]. In [157], the convex mirror with a backward perspective image is analyzed, and its radius is estimated in such a way that most of the "straight" lines are straight. Criminisi et al. assume that the mirror is spherical and, according to this assumption, a "corrected" projection is created. A similar approach to concave mirror image rectification can also be found in [160] and [161], which test the hypothesis that a concave projector was used. The incorrect perspective of the chandelier was demonstrated in [162, 158] using a virtual 3D



Figure 13: Jan van Eyck: *Arnolfini Portrait*, 1434, oil on wood. $82.2cm \times 60cm$. National Gallery, London.

All problems according to Preflight profile
Convert to PDF/A-2u

symmetrical model of the chandelier and its projection, which mismatch the painting. Finally, Jansen and Ruttkay [159] create a complete 3D model of the room with textures, to study vanishing points and perspective. This demonstration shows that the model is highly faithful to the painting, with large local mismatches.

To conclude, scene modeling is a suitable method for evaluating hypotheses relating to motif composition, i.e. whether projectors were used or scenes were composed from several images, whether or not joined in the painted motif.

6.6 VISUALIZATION

A description of the applied visualization techniques used for a final decision is often beyond the scope of published papers. In practice, however, various visualizations are used in dataset presentations, and case studies, for the demonstration of outputs and the results of art investigation. My opinion is that these methods deserve more attention, primarily because visualizations, as well as their analysis and interpretation, represent a major part of art investigation. Visualization techniques are used for searching ROI and comparing various modalities. A lack of advanced visualization methods is mitigated by available simple algorithms such as alpha blending; these are not perfect but fulfill the basic requirement: to visualize the context of two images at once. An expert with knowledge of modality behavior is often able to analyze such a visualization without improvements, but in a time-consuming manner.

Improvement of alpha blending is required when the complexity of a visualization grows, and a context of more than one image and one modality is necessary. Orientation between several blended images is much more complicated. As far as I know, this requirement has not yet been resolved except in our approach, summarized in 10.6.

It is also necessary to visualize high-dimensional data. The standard workflow (since 1988) has been a reduction in input dimensions (see Section 6.2.1 Dimensionality reduction) and the usage of *false colors*. This approach is described in the following section. However, more sophisticated methods, able to compare more than three dimensions, would be useful. Up to now, the application of dimension reduction techniques has been routine and therefore very popular. In general, algorithms for dimension reduction precede visualization. Raw multimodal and hyperspectral dataset comprehensibility is limited, and a reasonable first step is the extraction of features (like pigment classification, layer presence, etc.). An inspiration for multidimensional data visualization can be found in, for example, [163].

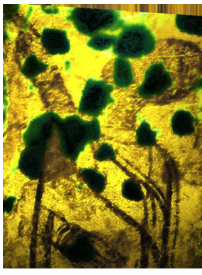


Figure 16: Fusion of UVF and VIS modality in false colors. A fresco from a church in Kostoľány pod Tríbečom

All problems according to Preflight profile
Convert to PDF/A-2u

6.6.1 *False colors*

A visualization technique called *false colors* uses three spectral sub-bands mapped to red, green and blue channels (example given in Figure 16). This principle is derived from analog scanning in 1988 ([164]) to Kodak Ektochrome IR color 135 daylight film. This film consisted of three sensitive layers: the first was sensitive to green, the second to red and the third to NIR, with an upper limit of $900nm$. Because all these sensitive layers were also sensitive to blue light, the blue channel had to be filtered by a Kodak Wratten no. 12 filter. This technique was transferred without change into DIP in [165, 35] or generalized to a three-band mapping to RGB [166]. Visualization by false colors is so popular that there is often neither a reference in articles, nor a description of the mapped sub-bands [124, 73, 3, 32, 167, 21, 49], although exceptions with a detailed sub-band mapping do exist [165, 28, 132]. In [165], Chad Weiner copies the behavior of the original analog method. *"A false color image constructed from the* 700*,* 750*, and* 800nm *images shows that the green, yellow, and lighter orange paints are luminescent in the NIR, whereas the dark orange is less so, and the red paint of the sleeves does not emit at all"*[28]. Usage in [132] is demonstrated and described for the Madonna with Yarnwinder (see Figure 9). Ibidem, multiple combinations are used for material spectral behavior visualization.

All problems according to Preflight profile
Convert to PDF/A-2u

In the current chapter I describe virtual restoration and lacuna filling that does not affect real artwork. There are two main purposes for purely computational modification of an artwork. The first one is to present a certain appearance of an artwork that is not the target of a conservation/restoration process. Such a modification is relevant to the creation of an artwork's story or public presentation. The second purpose is to simulate the restoration/conservation procedure. In this way, a technique (e.g. cleaning) applied on a small part of an artwork can be "extrapolated" to the whole painting without risk of damage [168].

I have split the algorithms for virtual restoration into the following three sections, according to the problem solved. Firstly, there is the cleaning process, where colors are rejuvenated, in Section 7.1. This is followed in Section 7.2 by the elimination through interpolation of small defects like cracks. Inpainting techniques for fixing large-sized lacunae are summarized in Section 7.3.

7.1 COLOR RESTORATION

The motivation is a chemical transformation from substance A to substance B, which changes the ratio of these substances in the measured paint material.

Rejuvenation of an artwork's original appearance always solves the problem of a physical model of aging. In [169] and [153], the authors assume that aging can be modeled as a component for a mixture according to a KM single-constant simplification. In this case, the aging is uniform across the whole painting and presented as an "aging layer". The spectral response of this "aging layer" is then computed from spectroscopic measurements of lead white taken from the painting and "fresh" lead white paint-out.[1] The aging function has also been tested on other pigments used in painting (zinc yellow, vermilion and emerald green).

Shi et al. [170] make the aging function specific for each segment specified by an expert. Here, aging represents a linear interpolation between the starting appearance and ending appearance. The authors indicate that each segment can go through several stages, with different degradation (e.g. red lead → lead white → black lead dioxide).

In a tutorial article from Ribés [63], linear rejuvenation was demonstrated. According to the original blue color, covered and protected by the Mona Lisa frame, the ratio of faded to original appearance per wavelength was calculated, and pixels with the same color (i.e. similar

1 Note that lead-white was often used as a support for a painting and is therefore uniformly distributed over the whole painting.

All problems according to Preflight profile
Convert to PDF/A-2u

spectral response: ±10% in root mean square) were virtually rejuvenated.

Ström et al. [171] rejuvenate colors on tapestries. The authors consider *"the case where there is a referent image, such as a corresponding colored cartoon, which bears unfaded colors."* The image of the cartoon, as well as the faded tapestry, is segmented by a modified k-means algorithm. Not only a pixel's color, but also its position is taken into account for the segmentation. The correspondence of segmented regions is set according to a pairwise cost matrix, for which the weight of the k-means centroid position and color can differ (these parameters are set by an expert). If the correspondence is wrong or missing, the region is not adjusted and rejuvenation is omitted here. *"Finally the tapestry is reconstructed by mapping the colors from the corresponding region in the painting."*

The mapping of pixels to rejuvenated colors is essential, but not always available. Moreover, our study [83] points out that per-part linear models of aging suffer from very rough and possibly erroneous results due, in principle, to their non-linearity.

7.2 CRACK REMOVAL

Small defects of paintings, such as cracks, are a widely and successfully resolved problem. The results of virtual restoration do not differ from the real restoration of these defects. In all referenced papers, reconstruction is split into three tasks: initial segmentation giving a rough crack map, elimination of wrongly identified brush strokes from this map, and reconstruction of crack pixels.

7.2.1 *Rough crack map*

A favorite tool for segmentation of a crack map is morphological operators. Crack structures arise when the surface of a painting is under environmental stress that overcomes the paint material's elasticity. Elasticity of paint materials decreases with age, and crack thickness grows. Morphological operators are able, by setting the size and shape of the structural element, to reflect the varied thickness and orientation of the cracks.

A morphological top-hat function was used in [172, 173, 174, 175]. The authors suggest various sizes of structural elements and a manual setting of the threshold. In [176], opening and erosion with viscous reconstruction is suggested. Cornelis et al. [175] improves this approach in a more automatic manner by using multiple scales of morphological structural elements and automatic Otsu thresholding [52] for classification.

Two other methods for a rough crack map are suggested in [175]. Both methods enhance the cracks for a further step and use thresholding

All problems according to Preflight profile
Convert to PDF/A-2u

for a binary representation of the crack map. The first method uses an elongated directional filter set [177] constructed according to crack orientation. Convolution with these filters enhances the cracks, and a binary crack map is obtained by thresholding. In this case, the threshold is set by an expert.

The second method enhances cracks through a K-SVD algorithm [178]. The K-SVD dictionary is trained by an expert on selected parts of the images, where a minimum of structures other than cracks are present. Image patches are then approximated by a linear combination of words from the dictionary, and in this way an enhanced crack image is obtained. A binary map of the cracks is obtained through the use of thresholding.

All these methods can be combined but always with a focus on an artwork's properties. This rough filtering generates a binary map of thin lines matching the properties of cracks and similar structures. For the elimination of brushstrokes from this set, the following steps are necessary.

7.2.2 *Elimination of brush strokes from crack maps*

The blind application of local filters (morphological structure elements, elongated directional filters or K-SVD words) generates a map with many false positives, because the filters interact with thin brush strokes as well. These false positives are eliminated in the following step.

For this purpose, Giakoumis et al. [172] and Spagnolo and Somma [174] used a typical distribution of the hue and saturation of the crack pixels (hue $\in \langle 0°, 60° \rangle$, saturation $\in \langle 0.3, 0.7 \rangle$) and dark brush strokes (hue $\in \langle 0°, 360° \rangle$, saturation $\in \langle 0, 0.4 \rangle$). Recognition of these two groups is done by ANN based on radial basis functions.

Solanki et al. [173] suggest a semi-automatic region growing algorithm, where seeds are set by an expert and 8-connected cracks/structures are segmented. Uncertain pixels can be identified by using other methods for crack segmentation.

Cornelis et al. [175] improve this step through semi-automatic recognition of structures and cracks by K-means classification and by adding other methods for rough crack pixel set segmentation. Semi-automatic recognition of structures and cracks has two steps. In the first step, K-means classification (into 3 classes) of crack branches (one-pixel-thick lines without branching, obtained from skeletonized segmented pixels by cutting the skeleton in its nodes) is done according to feature vector. In this feature, the vector consists of the mean color of the crack branch, branch length, orientation, eccentricity, surrounding mean color and very important spatial density. The second step involves the application of expert knowledge for recognition and markup of these classes. A final crack map is created from segmented crack branches according to the voting of three methods: top-hat, K-SVD and elongated direc-

All problems according to Preflight profile
Convert to PDF/A-2u

tional filters. A branch is taken into the final crack map if the ratio of pixels, detected by at least two methods, to total pixels in the branch is greater than 0.3.

Using these methods along with the influence of an expert, the rough crack map is refined to contain only the pixels necessary for reconstruction.

7.2.3 *Reconstruction*

When a crack map is obtained, the affected pixels are reconstructed. The quality of the produced reconstruction depends greatly on the formation and properties of the crack. The application of various methods is therefore made-to-measure for the dataset; for example, in [175] the problem of a crack surrounding bright pixels is identified. The author suggests adding these pixels into a set of pixels for reconstruction.

The applied methods, which are computationally effective and easy to implement, contain statistical order methods such as:

a) **Median filters** - median filter, recursive median filter, weighted median filter [173, 172] and modified trimmed means [172].

b) **Iterative methods** such as controlled anisotropic diffusion, which are computationally demanding [172, 173]

and

c) Computationally exhaustive **patch matching algorithms** [174, 175], requiring heuristics for an effective run.

In [174], the authors use c) but reduce the area for patch searching. Reconstruction takes into account the neighborhood of the defective pixel of size $R > D$ and compares each $D \times D$ square in this area with the $D \times D$ area around the pixel (the square around the fixed pixel is excluded from the comparison). The best match of non-defective pixels by means of euclidean distance is used as a source template for fixing the value in a pixel. If this best match value is above some threshold, the pixel value is interpolated from neighboring non-defective pixels.

Cornelis et al. [175] compare current (2013) algorithms used for crack inpainting. In the compared algorithms are anisotropic diffusion, b) and a greedy approach for patch matching used in c) [174], as well as the current state of the art in image inpainting [179]. Fastened patch matching is too slow in comparison with the greedy method and therefore marked as unpractical. The authors suggest a label-constrained patch matching algorithm with patch size adaptation. Constrained matching uses only non-crack pixels and k-means-based labeling to improve the inpainting results. Patch size is adapted according to k-means labeling of the target patch.

The last study [175] highlights the necessity of algorithm adaptation according to crack structure and painted motif. A different algorithm

All problems according to Preflight profile
Convert to PDF/A-2u

is able to create plausible inpainting for a painted book page and is useful for non-characters: faces, objects, etc.

7.3 LACUNA FILLING

Methods denoted as *lacuna filling*, in contrast to crack inpainting, reconstruct fine-grained structures. Two recent papers nicely document two possible approaches. The first one uses statistical self-similarity of image patches, and the second uses a model created according to expert knowledge of an artwork's Byzantine context. See Figure 2, where these two approaches correspond to different directions of research; statistical self-similarity goes from analytical methods (blue left part); by contrast, the 3D model uses expert knowledge (gray right part), and the research uses analytical methods resulting from the gray right part.

In [180], Pei et al. suggest a lacuna synthesis algorithm that works in four steps. First, the affected pixels must be identified, then a possible neighborhood is collected, then auxiliary lines are drawn, and finally a synthesis of missing pixels is made. The synthesis is based on patch matching. For each pixel, a surrounding patch is matched with possible candidates. As a measure of the patch matching, the mean square error is taken. According to the best-fitting patch, the affected middle pixel is reconstructed.

A more complex method, which also takes into account a 3D representation of the damaged object, is described in [181]. Lanitis et al. present a face reconstruction method. This method works with a Byzantine-style specific model constructed from a 3D deformable face model and is customized according to scans of human faces. This model is used for mapping of non-damaged parts of faces and, in this way, ensures that the Byzantine style is preserved.

All problems according to Preflight profile
Convert to PDF/A-2u

OPEN PROBLEMS

Let's follow two outlooks published earlier [168, 57], when the future of DIP for art investigation was being discussed. Barni et al. [168] underscore the problem of unavailable datasets and recommend close cooperation with museums. Fischer and Kakoulli [57] highlight the necessity of extending available modalities.

As I wrote in chapter 2, we are not able to analyze an artwork with the single click of a button, given the current state of the art. The main obstacle is interpretation of multimodal datasets and their transformation into a comprehensible structure. In spite of the growing number of databases of paint materials, the complexity of color mixing makes automatic material recognition almost impossible to achieve, and context-based reduction is still necessary. For this purpose, a physical model of a painting that defines the relation between measured values and optical properties of layers, pigments and binders, will be extremely useful. This brings us to a problem that has not yet been mentioned – paint material aging. Aging is studied much more slowly than paint material itself. The degradation process must be simulated on prepared samples and documented [83, 182]. A necessary step for automatic processing is expression of the degradation through mathematical formulas, or in changes in spectral response through time. However, despite the negative views of fully automatic processing, semiautomatic processing is able to significantly improve the methodology of art investigation.

"... most color-changing mechanisms of pigments are still under intense research, and a neat, clean theory has not yet been established" [170]

REGISTRATION Even though registered hyperspectral data is available in specialized laboratories, in the field of real artwork conservation and restoration much cheaper devices are used, providing only misaligned images. In this regard, precise subpixel registration is a must for the further application of advanced DIP techniques. For this purpose, the development of suitable similarity measures will push the solution to this problem forward. Software that can make a precise registration will also keep the need for expensive special devices to a minimum. A well-suited similarity measure must recognize precise registration from misalignment, be continuous in the sense of transformation parametrization, and provide a minimum of local extremes. These conditions reflect the current state of the art in registration, where gradient descent methods for searching local extremes are often used.

Experiments in various modalities provide good results using current methods in cases where a similar information content in both modalities is present, i.e. UV, VIS, and NIR. When spectral bands are more distant (XRF, X-ray vs. VIS), precise registration is more challenging.

All problems according to Preflight profile
Convert to PDF/A-2u

ALGORITHMIZATION OF EXPERT STEPS Each paper referenced in this thesis documents one or more expert steps that have been automated in the investigation, restoration or conservation of an artwork. Automated processes increase expert independence, reduce the time necessary for creating a visualization, and identify problems in generalizations of these steps. Automation highlights problems with scanning devices and processing algorithms, and indicates insufficiencies in public databases of materials.

In this context, meaningful tasks include the development of a formal description of expert steps and the generalization of these steps. The lack of this is described in Figure 2. In previous chapters I try to summarize the current state of the art, but finer analysis could give a more detailed direction for further research and automation. A comparison of proposed algorithms on a corpus dataset will improve generalization and usability [168, 57].

IMPROVEMENT OF SPECTRAL RESPONSE DISCRIMINABILITY In spite of many successful attempts at non-invasive pigment identification, a successful solution requires strong assumptions. Spectral response discriminability can be improved. A suitable physical model increases the precision of model-based estimations and real values. The curse of dimensionality can be reduced by having a suitable mixing model for pigments, binders and their aging. Other improvements can be made in the field of acquisition techniques, where the goal is faster scanners and new modalities.

We are able to partially solve all these problems with existing DIP algorithms, databases and knowledge of optical rules. All that is needed is a wider context for current methods and the availability of a corpus dataset for evaluation.

All problems according to Preflight profile
Convert to PDF/A-2u

RESEARCH WITHOUT AN IMPACT ON ARTWORK ITSELF

My research would not be complete without mentioning algorithms that were not used for art investigation and restoration, but are nonetheless closely connected with artwork and often use hyperspectral image datasets. Despite the different purpose of DIP development, the main contribution of such research is the development of useful descriptors, which improves the discriminability of artworks and their parts. Therefore, the following sections contain papers focused on the classification of artworks, along with a description of their style and other features.

The data source for this research is discussed in [183]. The authors suggest the usage of WikiArt[1], which to date offers more than 15000 digital images of artworks in VIS.

9.1 PAINTING STYLE

One way of evaluating artworks is based on painting style. Modern art, in particular, is split into many artistic movements, which motivates the development of descriptors for its effective classification. The result of developed descriptors could be better texture synthesis algorithms or similarity measures for image comparison.

In [184], Icoglu et al. define six features for content representation: percentage of dark colors, gradient coefficient, number of local and global maxima in the luminance histogram, color range around peak points, deviation of average gray level of painting parts from the whole, and skew of gray level distribution. All of these methods focus on "light" features introduced in [185].

In his PhD. thesis, Thomas Lombardi [185] created a feature set for the classification of an artwork's painting style. Feature selection according to Lombardi corresponds to human-based classification and is focused on: light, lines, texture and color. The light features are mean, variance, skewness, kurtosis of the image intensity and the distribution of intensity values. For lines, various edge detectors are used including Sobel's and Canny's, total edges, pure intensity edges, a gradient map and block difference of inverse probabilities; in addition, the number of edge pixels is taken as the feature. Lombardi's texture analysis focuses on brushstrokes, but many problems that influence texture descriptors are also mentioned. The descriptors used are based on various transformations including wavelet, Gabor, discrete cosine and fast Fourier, as well as on fractals, gray level co-occurrence matrices and block variation

1 Paintings collected at http://www.wikiart.org

All problems according to Preflight profile
Convert to PDF/A-2u

of local correlation coefficients. Based on the results of this processing, statistical features are selected and the best results are attached to the wavelet transformation level. Finally, palette scope, histogram, color coherence vectors, RGBXY, spatial chromatic histograms, color correlograms and the palette description feature are selected as the color descriptors.

Zujovic et al. recognized abstract impressionism, cubism, impressionism, pop art and realism. In [186], texture, color and edge descriptors are selected for painting representation. As a texture descriptor, steerable filter decomposition [187] on grayscale images is used. A number of edge pixels identified by a Canny edge detector are used as edge descriptors. Various thresholds for Canny's detector were used for identification of strong edges as well as edges with a low-intensity gradient. Finally, for color representation, 3 histograms for hue, saturation and value with 8 bins were used.

Khan et al. [188] distinguish between global and local descriptors. The global descriptors included rotation-invariant, uniform pattern-based local binary patterns [189] for intensity and each color channel, GIST [190], color GIST and PHOG [191] and color PHOG. In the selection of local features, the focus is put on visually salient regions, which are extracted by color names [192], complete LBP [193], SIFT [194], color SIFT [195] and SSIM [196]. The approach of Khan et al. tries to preserve the discriminability of the whole painting through conversion into descriptors, the most relevant of which are shape, texture and color.

All four papers represent a general direction for a painting to feature vector conversion. The inspiration of visually salient regions is the cornerstone for selecting local descriptors of textures, while light, shapes/edges and color are described globally over the whole painting.

9.2 AUTHORSHIP

The motivation for automatic author assignment comes from the economical and historical background. Authorship directly impacts the price of an artwork, and the assignment of an author to a painting is crucial in art history. The approaches to developing a classification machine imitate expert methods. In [197], the authors suggest a classification based on brushstrokes that describes *"... the "handwriting" of an artist, which follows a certain pattern of stroke length and angle"*. For this purpose, an algorithm for brushstroke segmentation was developed in [198]. Brushstroke identification is done according to expert-based characteristics, which assume *[198]: "*

- *Brushstrokes are painted using a fine brush;*
- *Some strokes painted in a wet, and others in a dry manner;*
- *Brushstrokes show some colors;*

All problems according to Preflight profile
Convert to PDF/A-2u

- *Brushstrokes are elongated objects;*
- *Depending on the brush, brushstrokes have a certain length and a width;*
- *Strokes show a direction, which means that there is a point of origin and an end point;*
- *There are combinations of strokes such as: parallel strokes, cross hatched strokes, etc."*

According to these characteristics of brushstroke representation, a processing filter is suggested. A brushstroke is defined by its start and end points, axis of stroke, width at certain position on the axis, and length. Finally, the curvature at the axis position is also taken into account. Detection is made by local filters on gradient images. The filters have eight possible orientations (for details see [198]).

Brushstroke analysis used for classification is also the object of research in [199], where three groups of scientists use wavelet transforms for texture and stroke representation. The wavelets used vary: critical sampling, complex wavelength, Gabor and modulate Gaussian; results are discussed.

The problem of correct feature set selection is demonstrated by [200], where the authors use all available descriptors. Their research points out that more features always means better accuracy in classification, but selection of a more relevant feature subset is still an open challenge. In Lombardi's PhD. thesis [185], experiments show that the color palette is more significant for author identification than distribution of colors over the artwork, but for characterizing style the development of different features is necessary.

9.3 METADATA-BASED IMAGE RETRIEVAL

Another point of view, which does not use the computed descriptors mentioned in previous sections, works with the metadata. Image retrieval can be done not only according to image descriptors, but also according to meta information. Metadata attached to a painting, included thanks to various reasons, represents authors, style, and objects as well as structures in the painting. However, metadata also contains names of features and shortcuts of expert knowledge, which are worthy of deeper analysis and formal description. It should be mentioned that using metadata descriptors for art investigation is far from easy, but nevertheless, metadata can serve as a pool for innovative ideas in computational approaches to art investigation.

In [201], the authors suggest several types of artwork labeling for image retrieval, and a proof of concept was created. Similar approaches can also be found in [202, 203].

All problems according to Preflight profile
Convert to PDF/A-2u

All problems according to Preflight profile
Convert to PDF/A-2u

Part III

OUTLINE: MY CONTRIBUTION TO THE STATE OF THE ART

Shortened presentation of my papers attached in appendix and overview of my contribution to the current state of the art in image processing in art investigation.

All problems according to Preflight profile
Convert to PDF/A-2u

All problems according to Preflight profile
Convert to PDF/A-2u

In general, research in art investigation starts with case studies and goes, via methodology elaboration, to scanning device development.

All sections in Chapter 10 are sorted chronologically. Figure 17 shows that case studies preceded our analytical approach.

In previous parts, I tried to describe the state of the art in DIP used for processing of a multispectral and hyperspectral dataset in the field of art investigation. Here, I want to present the papers we published in this interdisciplinary field. All our papers are ordered chronologically, which also reflects the common workflow of a research group in this interdisciplinary field.

The first step is a searching in the current state of the art methods and their application to a particular case study. In my case, it was my diploma thesis. The application of selected methodology resolves partial and non-scientific problems, and their solution produces the first scientific reports.

In the second step, the researcher analyzes the limitations and assumptions of his methodology and tries to minimize them. In our case, we needed more datasets for comparison, but also needed to improve their quality. Our goal was to acquire knowledge of paint material behavior in non-VIS radiation. To this end, the idea of the m3art database was established, and devices necessary for screening were developed.

After three years of data collecting, we built a knowledge base sufficient for the statistical analysis of datasets and development of material descriptors. This knowledge base includes the m3art database of paint materials (comparable to [91] created in Instituto Nationale di Ottica (INO)) and a dataset composed of case study materials useful for testing new DIP methods. We still have potential for improvement, especially in the field of scanning devices, where the highest-quality dataset is collected in a few laboratories around the world, such as in INO, the National Gallery of Art in Washington, DC and the University of Antwerp. These devices include VIS-NIR scanners producing registered modalities, macro-XRF and other types of scanners (THz T-Ray™4000 by Picometrix; medical X-Ray devices). The development of scanning devices is focused on eliminating shortages in screening processes (and produces the most-cited papers).

Our study of materials was followed by further development of general analytical methods, which is presented as the m3art database [34] and by statistical analysis of VIS-NIR datasets [74]. The link between the presented papers and their usage of analytical and expert-based knowledge is demonstrated in Figure 17. The figure also present the connection with various datasets (and scanning devices) that were used for the research and in the context of the color samples created in Alma laboratory, Prague: FORS and fibre optics transmittance spectroscopy (FOTS) in the Institute of Information Theory and Automation (IITA), and the multimodal VIS-NIR scanner [47] in INO in Florence (Italy).

All problems according to Preflight profile
Convert to PDF/A-2u

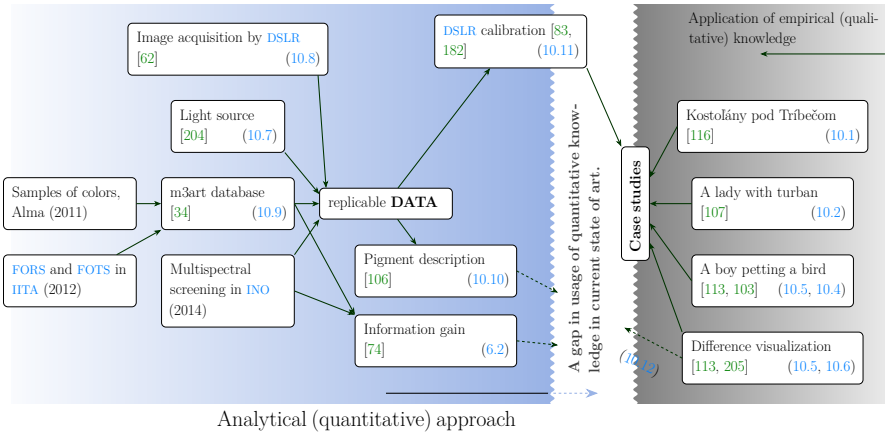


Figure 17: A linkage of the presented articles with regard to an empirical and analytical approach to art multimodal investigation. The box **Case studies** represents all papers focusing on particular artworks and describing the processing of their multimodal dataset. In the blue part the most important is the **DATA** box, which represents databases of descriptors reusable for subsequent case studies. These databases are discussed further in Chapter 4.

All problems according to Preflight profile
Convert to PDF/A-2u

OUTLINE

The following sections summarize our contribution to the attached papers (see Appendix VI). The papers are presented in order of publication, which suitably demonstrates the shift from case studies (right gray part of Figure 17) to the elaboration of methodology for multimodal dataset processing.

10.1 FRESCO RESTORATION: DIGITAL IMAGE PROCESSING APPROACH

The first proceeding was published in 2009, mainly covering my diploma thesis. In this article, we try to apply standard DIP algorithms in one case study (Gothic frescoes in a church in Kostolány pod Tríbečom). Here, we began cooperating with restorers by collectcting their DIP requirements. None of the proposed algorithms uses a deeper knowledge of pigments, colors or other limiting factors. We identified three types of tasks useful for art analysis:

i) registration of multimodal dataset;

ii) fusion of information from various modalities;

and

iii) segmentation tools for improving the readability of degraded frescoes.

We suggest application of image registration by perspective transformation based on control points and mutual information. For this case, such a registration is sufficient because only the visible part of the spectra was collected. In general, the problem is with the physical properties of the optics used for screening. Light rays of various wavelengths are focused differently, and perspective transformation cannot fully compensate for this effect. Note that images must be collected without adjusting DSLR optics and from the same place. A more complex transformation, compensating for lens distortions, should be used here to achieve subpixel precision. Any work that resolves the registration of a multimodal dataset by means of lens distortion has not yet been published due to the ill-posedness of this problem, even though precise registration is essential for further automatic processing (comparison, fusion, visualization).

The second described algorithm was focused on fusion of information by means of PCA (see Section 6.2.1) and visualization in false colors (see Section 6.6.1). We can now say that usage of this method leads to a

All problems according to Preflight profile
Convert to PDF/A-2u

loss of context of the painting modalities, and restorers have a problem with interpretation of results. This context loss is partially resolved in our papers mentioned in Sections 10.6 and 10.12.

We also suggested algorithm for higher-level image analysis: segmentation of lacunae in frescoes and pigments from sampling spots. Usage is possible in the form of a tool for augmenting the collected data.

10.2 REMOVING THE ARTIFACTS FROM ARTWORK CROSS-SECTION IMAGES

In several case studies we were able to use the trans-illumination approach. For studying subsurface layers of a painting, trans-illumination outperforms reflectance images [32]. Trans-illumination can be applied to paintings on thin support (canvas, paper), where all layers can be trans-illuminated, or in cases where high-penetrating modalities are used (e.g. X-ray). The support structure then affects the transmissiongram and decreases the readability of edges. Readability can be improved by removing a pattern of the canvas threads, paper structure or wood structure.

In the second article we successfully adapt and apply an algorithm for the removal of grinding scratches. The algorithm is based on a Fourier transform. In the Fourier spectrum we are looking for lines representing a repeating pattern, which we identify as canvas threads. The two most significant lines (with 90 deg in between) are then masked and an inverse Fourier transform is applied. In this way we obtain an image with a diminished vertical and horizontal thread pattern.

The same problem was resolved by Cornelis et al. [108] (details are summarized in Section 6.1.1).

10.3 IMAGE FUSION FOR ART ANALYSIS

In this article we publish a more general view of image comparison and the fusion of artwork images. We present algorithms for the fusion and comparison of different modalities of the same artwork, as well as an algorithm for comparison of different paintings in VIS. The main contribution is the aggregation of experience from three different case studies for the DIP community.

10.4 DETECTION OF COPIES USING MATHEMATICAL PROCESSING OF IMAGES II: STORY OF A PAINTING ON CANVAS OF A BOY PETTING A BIRD

This article is fully focused on an artwork's story, and presents a case study in which four copies of the same motif were compared. The dataset for processing was really unique, containing a motif of a boy petting a bird with small proportion changes. Three of the compared art-

All problems according to Preflight profile
Convert to PDF/A-2u

works were full-color paintings, while the fourth was a black-and-white reproduction printed on paper. We used the algorithms presented in the following Section 10.5 (registration, comparison and visualization) for the validation of art historians' hypotheses.

10.5 DETECTION OF COPIES USING MATHEMATICAL PROCESSING OF IMAGES I: THEORETICAL BASIS AND METHODOLOGY

This article was published at a conference for restorers and conservators. In short, it presents the applicability of DIP algorithms for digital art dataset processing. Algorithms are mentioned for the following subsections:

REGISTRATION For a registration by means of perspective projection, we suggest manual selection of 4 pairs of corresponding points necessary for the computation of transformation. The position of these points is made more accurate according to the cross-correlation of neighboring pixels.

COMPARISON OF THE SAME MOTIF Comparison of a similar motif is an ill-posed problem. Great compositions of objects in paintings have been reproduced throughout history, and many instances with greater or lesser differences can be found. In such cases, where differences can be suppressed by perspective transformation and brightness can be normalized, we suggested a workflow for comparison of such motifs. Our approach was based on a simple mean square error of intensities (images must be converted to gray-scale) of the normalized input images and offers an intuitive comprehensibility of the output. The application of this approach is very limited and requires expert guidance. However, the results can be really useful, as was demonstrated in the article presented in Section 10.4.

COMPARISON ACROSS MODALITIES Comparison of various modalities requires a more sophisticated approach than just intensity comparison. Image data must be converted to its information values. Therefore we suggest a probability-based measure for color similarity measurement, similar to mutual information. The amount of similarity ζ of a color U from modality λ and a color V from modality κ for corresponding pixels is computed as:

$$\zeta\ U_\lambda, V_\kappa \qquad \frac{p\ U_\lambda, V_\kappa}{p\ U_\lambda\ p\ V_\kappa}, \tag{34}$$

where p denotes the probability and joint probability corresponding to the pixels' colors. Here, we are working with matrix of corresponding intensities (ICM), described in Section 12.1. The best performance can

All problems according to Preflight profile
Convert to PDF/A-2u

be achieved by a suitable number of bins for colors in modalities λ and κ. This approach is very sensitive to registration error and noise and was outperformed by the VIS extrapolation technique published later (see Section 10.12).

DIFFERENCE VISUALIZATION Searching of ROI was motivated by the practical task of comparing four versions of the same motif. It was crucial to be able to distinguish individual paintings in their fused visualization. We have developed a method where the user selects a color per image. Pixels are dyed according to absolute value and the sign of difference of the source images. The provided algorithm uses the hue from HSV color space for setting a color; saturation is set according to the absolute amount of difference; and value is computed as an average of intensities of the compared images, in order to maintain the context.

Development of a similarity measure and difference visualization algorithm was improved even more in the next paper (see Section 10.6, where La*b* color space was used instead of HSV).

10.6 IMAGE FUSION FOR DIFFERENCE VISUALIZATION IN ART ANALYSIS

In 2013 we presented an improved algorithm for color-based comparison of multiple images. We used La*b* color space to achieve maximum comprehension of the comparison by humans.

Three dimensions of La*b* are transposed to hue, saturation and value. Hue is reduced to two values selected by the user and corresponding to the difference sign. Saturation of a pixel corresponds to the absolute value of the difference and, finally, value preserves the context of the original images by averaging the original pixel intensities. In contrast to the algorithm presented in Section 10.5, we work in La*b* instead of HSV.

The visualization technique is independent of the difference measure. Only the difference range is requested, and it must be in $\langle -1; 1 \rangle$. The difference sign reflects which image differs more (e.g. which image has a higher variance for a given pixel), but this parameter is irrelevant for symmetric measures. A graphical representation of this algorithm is shown in Figure 18. In this way, the user is able to preserve the context of compared images by assigning a color to each of the compared images, corresponding to their negative difference.

The method can be useful in other fields of research, where comprehensible visualization is necessary. An improved principle, published in [206], resolves dim colors near zero difference by *"choosing a hue spin"*. Allowing brighter colors near zero saturation breaks the uniformity of a linear transition in La*b*. Hue spin recovers this uniformity.

All problems according to Preflight profile
Convert to PDF/A-2u

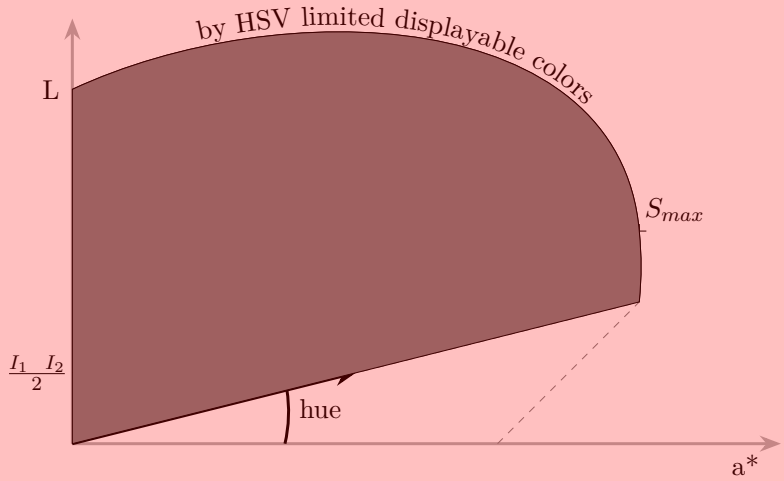


Figure 18: Graphical visualization of difference mapping into La*b* color space. The hue is defined for difference sign by the user, and reduces pixel output color to a set defined by circular sector. Lightness (L) is computed as the average intensity of the compared pixels and reduces the set of possible pixel output colors to a red line of "displayable saturation". S_{max} is computed as the maximal saturation displayable and corresponds to the absolute value of difference equal to 1. Zero difference means zero saturation and corresponds to intersection of the red line with the L axis.

10.7 LEDS IN AN 8-BY-8 MATRIX - TECHNICAL REPORT



Figure 20: LEDs in an 8-by-8 matrix covered with optical filters used for "low-cost acquisition".

Acquisition of a multimodal dataset is a crucial part of art analysis, and it can be very expensive. Spectral sensitivity is given by the sensor, which operates in some range (e.g. VIS, VIS-NIR, X-ray, etc.), while division of this range into sub-bands is done by restricting the wavelength emitted by the light source (or by filtering the reflected/transmitted spectrum). Filtration is possible by using optical filters, while emission is controlled by using a narrow-band light source like light-emitting diodes (LED). In 2012, we developed a fourteen-band light source based on LED, covering a spectral range from $\langle 390, 950 \rangle nm$ (see Figure 21).

The referenced technical report describes the construction parameters of this device. In an article referenced in the following section, we demonstrate the application of a developed light source.

10.8 LOW-COST MOBILE SYSTEM FOR MULTISPECTRAL CULTURAL HERITAGE DATA ACQUISITION

The above-mentioned expensiveness of acquisition devices was the motivation for development of a low-cost VIS-NIR acquisition system. We constructed this system from off-the-shelf products: LED diodes (see Section 10.7), optical filters and a DSLR camera. Usage of these devices for scientific application is conditioned by a well-suited calibration pro-

All problems according to Preflight profile
Convert to PDF/A-2u

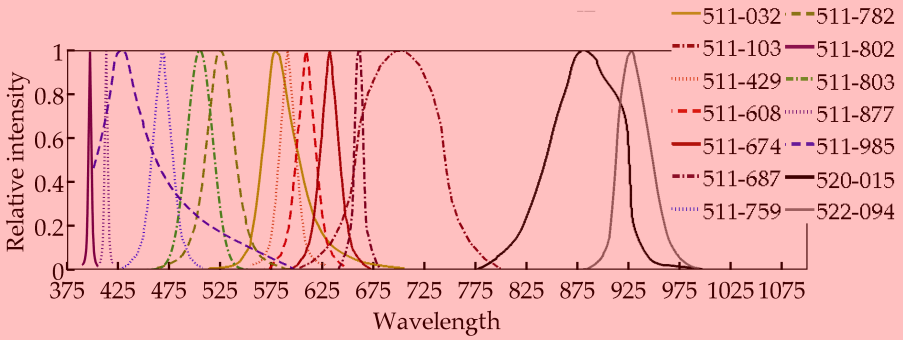


Figure 21: Relative illumination distribution of used LEDs over the VIS-NIR spectrum, described in detail in Section 10.7. Numbers in the legend denote type of LED according to the GME catalogue.

cess that ensures measurement repeatability and reproducibility. In the referenced article we propose two methods for camera sensitivity measurement.

The first method uses a calibrated light source and optical filters (color and NIR filters) with known piecewise constant transmittance. Using the measured intensities per used filter, we obtain a set of linear equations:

$$I \quad A \times S, \tag{35}$$

$$I \quad \begin{pmatrix} I_{R,1} & I_{G,1} & I_{g,1} & I_{B,1} \\ I_{R,2} & I_{G,2} & I_{g,2} & I_{B,2} \\ \vdots & \vdots & \vdots & \vdots \\ I_{R,m} & I_{G,m} & I_{g,m} & I_{B,m} \end{pmatrix}, \tag{36}$$

$$A \quad \begin{pmatrix} l\ \lambda_1\ t_1\ \lambda_1 & l\ \lambda_2\ t_1\ \lambda_2 & \cdots & l\ \lambda_n\ t_1\ \lambda_n \\ l\ \lambda_1\ t_2\ \lambda_1 & l\ \lambda_2\ t_2\ \lambda_2 & \cdots & l\ \lambda_n\ t_2\ \lambda_n \\ \vdots & \vdots & \ddots & \vdots \\ l\ \lambda_1\ t_m\ \lambda_1 & l\ \lambda_2\ t_m\ \lambda_2 & \cdots & l\ \lambda_n\ t_m\ \lambda_n \end{pmatrix}, \tag{37}$$

$$S \quad \begin{pmatrix} s_{R,1} & s_{G,1} & s_{g,1} & s_{B,1} \\ s_{R,2} & s_{G,2} & s_{g,2} & s_{B,2} \\ \vdots & \vdots & \vdots & \vdots \\ s_{R,n} & s_{G,n} & s_{g,n} & s_{B,n} \end{pmatrix}, \tag{38}$$

where I is a matrix of measured intensities (four values for each filter corresponding to the color array in DSLR: Red-Green-green-Blue), $l\ \lambda_j$ represents emitted intensity in wavelength λ_j, $t_i\ \lambda_j$ denotes the transmittance factor of filter i for wavelength λ_j, n is the number of measured spectral sub-bands and m is the number of available filters. Finally, matrix S contains estimated sensitivity factors of the sensor for color element and wavelength. These equations follow from equation 1.

All problems according to Preflight profile
Convert to PDF/A-2u

The second method uses a monochromator instead of optical filters. A single spectral sub-band is directly measured using a monochromator. This corresponds to a diagonal matrix A. Here, the monochromator transmittance factor $d\ \lambda_j$ is presented instead of the filter transmittance factor $t_i\ \lambda_j$, as in the previous approach. This factor must also be measured, and therefore this calibration method is carried out by using a calibrated photodiode for measurement of $d\ \lambda_j$.

A proposed low-cost multimodal screening system was tested on a real painting in Figure 23. Instead of a calibrated light source, an LED panel (see Section 10.7) was used, and therefore only relative values were acquired. From raw VIS data, a true color image was reconstructed.

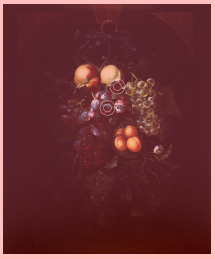


Figure 23: Tomáš Tichý 2008, copy of Fruit Festoon by Nicolaes van Gelder, oil on canvas. $65 \times 50cm$.

10.9 M3ART: A DATABASE OF MODELS OF CANVAS PAINTINGS

With the described equipment, we were able to create a publicly available database of paint materials. Our system for multimodal screening (see Section 3.2.1) was complemented by a spectrometer USB2000+ (OceanOptics^{TM}) and an m3art database was created. This database contains raw measured values on prepared full-scale model samples (see Figure 25). These samples were created in the Alma laboratory and combine materials (pigments and binders) available in the Gothic and Renaissance periods. The main purpose of creating this database was the identification of underdrawings. Therefore half of each sample contains underdrawings. The reflectance of all these samples was measured in the range $[430, 1050]nm$. The measurement of transmittance was possible only on canvases with thin support, and therefore this dataset is only half the size of the whole collection. The database is publicly available in several formats, directly downloadable, for scientific usage.

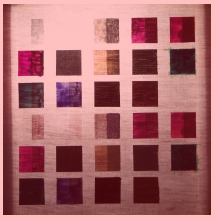


Figure 25: Example of prepared samples: Gothic pigments on white canvas; VIS transmission

10.10 OPTICAL PROPERTIES OF HISTORICAL PAINT PIGMENTS UNDER NEAR-INFRARED RADIATION

Analysis of paint materials from the m3art database demonstrates that even rough pigment classification can be useful for practical usage in a case study. As mentioned in Section 10.9, construction of the m3art database focused on underdrawing visibility in the NIR spectral sub-band. We compared the visibility of underdrawings on reflectograms and transmissiongrams. In the studied dataset, we identified three classes of pigment behavior, according to its reflectance, transmittance, absorbance and ratio. The underdrawing is [106]:

1. *"... invisible due to the negligible transmittance of NIR radiation."*
2. *"... recognisable in reflected light due to the material low reflectivity and high transmittance."*

All problems according to Preflight profile
Convert to PDF/A-2u

3. *"... not recognisable in reflected light ... but it is recognisable in transmitted light"* (The ratio of the reflected to transmitted light is too high, and the contrast of the underdrawing is on the level of noise, or lower).

All 14 pigments were classified into these classes according to their reflection and transmission values. Moreover, the contrast of the unknown underdrawing was computed for a reflectogram and transmissiongram, and both were discussed in the context of the defined class thresholds.

10.11 STATISTICAL EVALUATION OF COLOR CHANGE

In 2014, I was part of a research team that studied the degradation processes of natural fluorite CaF_2 and vivianite. Two articles were produced: "Naturally irradiated fluorite as a historic violet pigment: Raman spectroscopic and X-ray diffraction study" and "Temperature-related degradation and colour changes of historic paintings containing vivianite". In both, a color comparison of samples was necessary with respect to their degradation process. Here, we propose a histogram-based comparison of the acquired samples, which nicely describes their level of degradation and the possible correlation with color change.

In both articles, instead of a histogram-based method, a single-point KM mixing model can also be used.

The sample histograms were produced from VIS images captured under controlled conditions (light source D65, same spatial and DSLR configuration). Statistical relevance was satisfied by the size of the scanned area and the number of acquired pixels. Comparison and evaluation of the created histograms was done by an expert.

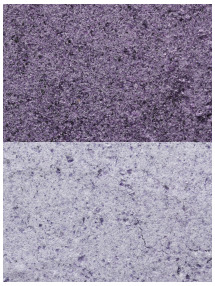


Figure 26: Normalized photograph of two samples of fluorite.

An example of the captured normalized images is presented in Figure 26.

10.12 IMPROVEMENT OF THE VISIBILITY OF CONCEALED FEATURES IN ARTWORK NIR REFLECTOGRAMS BY INFORMATION SEPARATION

The last of the referenced papers turns its focus back to image processing algorithms and statistical analysis of the dataset. After several years of experience in art investigation and measurements of real paint materials, I have to change the understanding of modalities content (see Section 3.2.3).

The most common understanding of artwork is as a multi-layered system. This idea corresponds to real artwork construction but does not reflect modality content. The problem lies in estimation of the penetrative ability of a spectral sub-band. Although this property is (nowadays) not measurable across a whole image, it is of course material-dependent. From the captured dataset, we are not able to identify which layers affected the reflectogram. Furthermore, we are not able to identify layer thickness, refraction index, absorption and other phys-

All problems according to Preflight profile
Convert to PDF/A-2u

ical properties due to the ill-posedness of this problem, insufficient contents of databases and non-existent algorithms for estimation of these properties (these estimations are possible only on simplified single-layer samples).

The relevant perspective is a comparison of information content, which today is commonly done by an expert. As I wrote in the introduction (Section 3.2.3), there are also approaches in DIP [73, 48, 72, 49] that profit from structural or informational analysis of modalities and their separation (see Section 6.2 Information content analysis).

In our paper we try to avoid the problem of model assumption by using ICM (see below). ICM allows for any mapping between modalities' spectral responses. We try to find the limits of blind information separation, i.e. estimation of conditions when information separation based on ICM is possible.

The main idea is estimation of the target modality (in our case NIR) from a less penetrating one (in this case VIS). This is possible because NIR light rays are affected by the visible layer when/if passing through. If we have no restrictions for estimated mapping, the multi-layer ANN is a good choice, as it combines easy application (many existing libraries), advanced gradient descent methods and possible performance tuning.

For our purposes we created fully controlled phantoms based on real paint materials, their spectral response, and the variance of this response. In previous case studies we identified issues related to source separation. Separation is in some cases possible and in others not. We try to evaluate four hypotheses that explain this possibility, or impossibility, of separation and also correspond with our experience in case studies. Our phantoms were constructed with a different underdrawing coverage ratio, size and number of used paint materials. Then we try to train ANN a mapping from VIS to NIR modality. We assume that the information gain of NIR sub-bands cannot be estimated from VIS. The difference between the estimated value and the real value represents the information gain of NIR (and noise). By using ANN with various tuning (depth and width), we create the mapping (for a randomly selected phantom) several times.

Coverage ratio is the ratio between pixels with and without underdrawing, used for ANN training.

Our results are not surprising, but they highlight the situations when information separation is possible, when it is not, and when the results will be poor. A side effect of applied signal separation by ANN is improvement in the visibility of concealed features in an NIR reflectogram, which confirms the legitimacy of the separation and the correspondence with painted layers.

All problems according to Preflight profile
Convert to PDF/A-2u

All problems according to Preflight profile
Convert to PDF/A-2u

Part IV

SUMMARY AND OUTLOOK

Summary of presented work, identification of opened problems and outlook for my future work.

All problems according to Preflight profile
Convert to PDF/A-2u

All problems according to Preflight profile
Convert to PDF/A-2u

CONCLUSION

This thesis summarizes eight years of my cooperation with art restorers and IT specialists on art investigation tasks. We have analyzed image datasets from various modalities and searched for a general model to describe the spectral responses of pigments. In 2008, we began with common DIP algorithms presented in our early papers, followed by measurements of the physical properties of paint materials. For these measurements, we developed a low-cost acquisition system from off-the-shelf products and suggested a calibration methodology for this system. After that, we were able to create a database of paint material spectral responses, their reflectance and transmittance, and also the influence of various underdrawings.

In parallel, but highly influenced by pigment behavior research, we have tried to improve tools for art investigation, such as visualization techniques and image difference measurement (a cross-modal change detection). Experience with real paintings was crucial for gaining deeper insights into the practices of restorers and subsequent development of useful change-detection algorithms.

This thesis, moreover, summarizes the current state of the art of image processing methods in art investigation. I have put our papers into this context and added an outlook in this interdisciplinary field of research from my own perspective.

11.1 CONTRIBUTION

My contribution to the interdisciplinary research field of DIP and art investigation is represented by papers referred to in Part III. First of all, there is a contribution belonging to the field of DIP: signal processing and visualization techniques. We suggest a useful visualization, applicable to an expert-based comparison of multiple paintings/modalities without losing the context of the data source, where experts have the ability to assign each data source a different color. Visualized comparisons then retain this color, which facilitates the comparison task. In the field of signal separation, we have studied separation limits for the multimodal representation of real paintings and the possibility of improving the visibility of concealed features with low contrast in penetrating modalities.

By using our acquisition system for pigment spectral analysis and our methodology for calibration of this system, we have determined basic classes of pigment behavior in the sense of underdrawing visibility. We have created a list of recommendations for the acquisition of under-

All problems according to Preflight profile
Convert to PDF/A-2u

drawings with satisfactory contrast. These recommendations were built on our VIS-NIR m3art database of pigments, built in the years 2012-14, which has open access.

We suggested an inexpensive solution for multimodal (VIS-NIR) artwork screening. We created a system consisting of narrow band LED, photographic filters and an adjusted standard DSLR camera. We also built a LED-based prototype of a light source with an adjustable wavelength.

Finally, there is my own achieved knowledge, represented by my diploma and doctoral thesis followed by several case studies. All of our research stays in the interdisciplinary field due to the immediate application of the knowledge gained to real paintings. We fulfilled expert requirements using a suitable mathematical model, and experts eliminated uncertainties by application of their empirical knowledge.

11.2 OUR OUTLOOK AND FUTURE WORK

Our recent experience highlights how important high-quality inputs are for DIP. Thanks to our acquisition system, we were able to collect a dataset useful for the work of restorers and conservators, but with substantial limitations for the development of widely usable algorithms. At the same time, the processing of a precisely registered multimodal dataset (available through our cooperation with INO) has quickly made a relevant contribution in the field of signal processing. This experience has taught me how important both research directions are for practical applications. While cheap acquisitions and rough recommendations enlarge empirical knowledge and improve the process of art investigation itself, precise measurements allow for the statistical analysis of the spectral behavior of pigments and the derivation of suitable algorithms.

In my future work I would like to extend both these fields. Firstly, there are three publicly available databases of pigments, currently with limited search capabilities. I would like to start with the m3art database and extend it by pigment retrieval according to the spectral response of unknown paint material. For this purpose, the algorithms referred to in Section 6.4.1 will be useful; moreover, a comparison of similarity measures will be produced.

Secondly, a comparison of separation algorithms, presented in Section 12.1, highlights a shortcoming in our last paper, namely the local context of a pixel for signal separation. In addition, we identify a problem in the estimation of the mixing function, which for the sake of applicability is wrongly simplified to addition, and therefore requires a revision. Finally, there is also a problem in identifying the threshold conditions under which the separation results are relevant, partially relevant or irrelevant. All these questions deserve more attention.

Finally, there will be a continuation of multimodal artwork acquisition and an extension of the dataset database, which is crucial for

All problems according to Preflight profile
Convert to PDF/A-2u

understanding problems in the interdisciplinary field of DIP and art investigation.

All problems according to Preflight profile
Convert to PDF/A-2u

All problems according to Preflight profile
Convert to PDF/A-2u

Part V

BIBLIOGRAPHY

All problems according to Preflight profile
Convert to PDF/A-2u

All problems according to Preflight profile
Convert to PDF/A-2u

BIBLIOGRAPHY

1. HRADILOVÁ, Janka; HRADIL, David. *Neinvazivní průzkum malířských výtvarných děl radiografickými a rentgen-fluorescenčními metodami*. Akademie výtvarných umění v Praze, 2015. ISBN 978-80-87108-60-4.
2. ALFELD, Matthias; BROEKAERT, José A. C. Mobile depth profiling and sub-surface imaging techniques for historical paintings - A review. *Spectrochimica Acta - Part B Atomic Spectroscopy*. 2013, vol. 88, pp. 211–230. ISSN 05848547. Available from DOI: 10.1016/j.sab.2013.07.009.
3. CRADDOCK, Paul. *Scientific investigation of copies, fakes and forgeries*. Taylor & Francis, 2009. ISBN 978-0-7506-4205-7. Available from DOI: 10.1051/medsci/2011272214.
4. CREAGH, D.C.; BRADLEY, D.A. *Radiation in Art and Archeometry*. Elsevier Science, 2000. ISBN 978-0-08-054019-1. Available also from: https://books.google.cz/books?id=jhlxNcV6JRQC.
5. BONIFAZZI, Claudio; CARCAGNÌ, Pierluigi; FONTANA, Raffaella; GRECO, Marinella; MASTROIANNI, Maria; MATERAZZI, Marzia; PAMPALONI, Enrico; PEZZATI, Luca; BENCINI, Davide. A scanning device for VIS–NIR multispectral imaging of paintings. *Journal of Optics A: Pure and Applied Optics*. 2008, vol. 10, no. 6, pp. 064011. Available also from: http://stacks.iop.org/1464-4258/10/i=6/a=064011.
6. FONTANA, Raffaella; BARUCCI, Marco; PAMPALONI, Enrico; STRIOVA, Jana; PEZZATI, Luca. From Leonardo to Raffaello: Insights by VIS-IR reflectography. In: *5th ALMA interdisciplinary conference: Interpretation of fine art's analyses in diverse contexts*. 2014, pp. 15–26.
7. BARBARA, Zitová; FILIP, Šroubek. Conservation of" The Last Judgement" mosaic: Image processing. In: DRBOHLAV O., Czech Pattern Recognition Society (ed.). *Proceedings of the 8th Computer Vision Winter Workshop. CVWW'03*. 2003, pp. 169–174.
8. DANIEL, F.; MOUNIER, A.; PÉREZ-ARANTEGUI, J.; PARDOS, C.; PRIETO-TABOADA, N.; VALLEJUELO, S. Fdez-Ortiz de; CASTRO, K. Hyperspectral imaging applied to the analysis of Goya paintings in the Museum of Zaragoza (Spain). *Microchemical Journal*. 2016, vol. 126, pp. 113–120. ISSN 0026-265X. Available from DOI: 10.1016/j.microc.2015.11.044.

All problems according to Preflight profile
Convert to PDF/A-2u

9. CUCCI, Costanza; DELANEY, John K.; PICOLLO, Marcello. Reflectance Hyperspectral Imaging for Investigation of Works of Art: Old Master Paintings and Illuminated Manuscripts. *Accounts of Chemical Research*. 2016, vol. 49, no. 10, pp. 2070–2079. ISSN 0001-4842. Available from DOI: 10.1021/acs.accounts.6b00048.

10. RORIMER, James J. *Ultra-violet Rays and Their Use in the Examination of Works of Art*. Metropolitan Museum of Art in New York, 1931. Available also from: https://books.google.cz/books?id=TVg1AAAAMAAJ.

11. MAIRINGER, Franz. The ultraviolet and fluorescence study of paintings and manuscripts. *Radiation in Art and Archeometry*. 2000, pp. 56–75.

12. PELAGOTTI, Anna; PEZZATI, Luca; BEVILACQUA, Natalia; VASCOTTO, Veronica; REILLON, Vincent; DAFFARA, Claudia. A study of UV fluorescence emission of painting materials. *Art '05–8th International Conference on Non-Destructive Investigations and Microanalysis for the Diagnostics and Conservation of the Cultural and Environmental Heritage*. 2005, pp. A97.

13. PELAGOTTI, A; PEZZATI, L; PIVA, A; DEL MASTIO, A. Multispectral UV fluorescence analysis of painted surfaces. In: *Proceedings of 14th European Signal Processing Conference (EUSIPCO'06)*. 2006.

14. PADFIELD, Joseph; SAUNDERS, David; CUPITT, John; ATKINSON, Robert. Improvements in the Acquisition and Processing of X-Ray Images of Paintings. *National Gallery Technical Bulletin*. 2002, vol. 23, pp. 62–75. ISSN 03612317. Available from DOI: 10.1002/col.5080050319.

15. BRIDGMAN, Charles F. The amazing patent on the radiography of paintings. *Studies of conservation*. 1964, vol. 9, no. 4, pp. 135–139.

16. HELFEN, Lukas; BAUMBACH, Tilo; MIKULÍK, Petr; BARUCHEL, José; PERNOT, Petra; CLOETENS, Peter. High-resolution three-dimensional imaging of flat objects by synchrotron-radiationcomputed laminography. In: *Applied Physics Letters*. 2005, vol. 86, bibrangessep 247–251. No. 7. Available from DOI: 10.1063/1.1854735.

17. KRUG, Kristoph; DIK, Joris; LEEUW, Milko den; WHITSON, Andrea; TORTORA, John; COAN, Paola; NEMOZ, Christian; BRAVIN, Alberto. Visualization of pigment distributions in paintings using synchrotron K-edge imaging. *Applied Physics A*. 2006, vol. 83, no. 2, pp. 247–251. ISSN 1432-0630. Available from DOI: 10.1007/s00339-006-3519-y.

18. DIK, Joris; JANSSENS, Koen; SNICKT, Geert Van der; LOEFF, Luuk van der; RICKERS, Karen; COTTE, Marine. Visualization of a Lost Painting by Vincent van Gogh Using Synchrotron Radiation

All problems according to Preflight profile
Convert to PDF/A-2u

Based X-ray Fluorescence Elemental Mapping. *Analytical Chemistry*. 2008, vol. 80, no. 16, pp. 6436–6442. Available from DOI: 10.1021/ac800965g.

19. ALFELD, Matthias; PEDROSO, Joana Vaz; HOMMES, Margriet van Eikema; SNICKT, Geert Van der; TAUBER, Gwen; BLAAS, Jorik; HASCHKE, Michael; ERLER, Klaus; DIK, Joris; JANSSENS, Koen. A mobile instrument for in situ scanning macro-XRF investigation of historical paintings. *Journal of Analytical Atomic Spectrometry*. 2013, vol. 28, pp. 760–767. Available from DOI: 10.1039/C3JA30341A.

20. RYAN, C. G. et al. The New Maia Detector System: Methods For High Definition Trace Element Imaging Of Natural Material. *AIP Conference Proceedings*. 2010, vol. 1221, no. 1, pp. 9–17. Available from DOI: 10.1063/1.3399266.

21. ROSI, Francesca; HARIG, Roland; MILIANI, Costanza; BRAU, René; SALI, Diego; DAVERI, Alessia; BRUNETTI, Brunetto G.; SGAMELLOTTI, Antonio. Mid-infrared hyperspectral imaging of painting materials. *Optics for Arts, Architecture, and Archaeology IV*. 2013, vol. 8790, pp. 87900Q–1–10. ISSN 0277786X. Available from DOI: 10.1117/12.2020477.

22. ROSI, Francesca; MILIANI, Costanza; BRAUN, René; HARIG, Roland; SALI, Diego; BRUNETTI, Brunetto G.; SGAMELLOTTI, Antonio. Noninvasive Analysis of Paintings by Mid-infrared Hyperspectral Imaging. *Angewandte Chemie International Edition*. 2013, vol. 52, no. 20, pp. 5258–5261. ISSN 1521-3773. Available from DOI: 10.1002/anie.201209929.

23. RICCIARDI, Paola; DELANEY, John K.; FACINI, Michelle; ZEIBEL, Jason G.; PICOLLO, Marcello; LOMAX, Suzanne; LOEW, Murray. Near infrared reflectance imaging spectroscopy to map paint binders in situ on illuminated manuscripts. *Angewandte Chemie - International Edition*. 2012, vol. 51, no. 23, pp. 5607–5610. ISSN 14337851. Available from DOI: 10.1002/anie.201200840.

24. MILIANI, Constanza; ROSI, Francessca; DAVERI, Alessia; BRUNETTI, Brunetto G. Reflection infrared spectroscopy for the non-invasive in situ study of artists' pigments. *Applied Physics A: Materials Science and Processing*. 2012, vol. 106, no. 2, pp. 295–307. Available from DOI: 10.1007/s00339-011-6708-2.

25. AHMAD, M. Z.; KHAN, A. A.; MEZGHANI, S.; PERRIN, E.; MOUHOUBI, K.; BODNAR, J. L.; VRABIE, V. Wavelet subspace decomposition of thermal infrared images for defect detection in artworks. *Infrared Physics and Technology*. 2016, vol. 77, pp. 325–334. ISSN 13504495. Available from DOI: 10.1016/j.infrared.2016.06.018.

All problems according to Preflight profile
Convert to PDF/A-2u

26. BOER, J. R. J. Van Asperen De. Reflectography of Paintings Using an Infrared Vidicon Television System. *Studies in Conservation*. 1969, vol. 14, no. 3, pp. 96–118.

27. DELANEY, John K.; WALMSLEY, Elizabeth; BERRIE, Barbara H.; FLETCHER, Colin F. Multispectral Imaging of Paintings in the Infrared to Detect and Map Blue Pigments. *(Sackler NAS Colloquium) Scientific Examination of Art: Modern Techniques in Conservation and Analysis Front Cover Proceedings of the National Academy of Sciences National Academies Press, Aug 16, 2005*. 2005, pp. 120–136.

28. DELANEY, John K.; ZEIBEL, Jason G.; THOURY, Mathieu; LITTLETON, Roy; MORALES, Kathryn M.; PALMER, Michael; RIE, E. René de la. Visible and infrared reflectance imaging spectroscopy of paintings: pigment mapping and improved infrared reflectography. In: PEZZATI, Luca; SALIMBENI, Renzo (eds.). *Proceedings of SPIE*. Springer International Publishing, 2009, vol. 7391, p. 739103. ISBN 978-0-8194-7674-6. Available from DOI: 10.1117/12.827493.

29. DELANEY, John K.; ZEIBEL, Jason G.; THOURY, Mathieu; LITTLETON, Roy; PALMER, Michael; MORALES, Kathryn M.; RIE, E. René de la; HOENIGSWALD, Ann. Visible and Infrared Imaging Spectroscopy of Picasso's Harlequin Musician: Mapping and Identification of Artist Materials in Situ. *Applied Spectroscopy*. 2010, vol. 64, no. 6, pp. 584–594. ISSN 00037028. Available from DOI: 10.1366/000370210791414443.

30. CSÉFALVAYOVÁ, Linda; STRLIČ, Matija; KARJALAINEN, Harri. Quantitative NIR Chemical Imaging in Heritage Science. *Analytical Chemistry*. 2011, vol. 83, no. 13, pp. 5101–5106. Available from DOI: 10.1021/ac200986p.

31. DAFFARA, Claudia; FONTANA, Raffaella. Multispectral Infrared Reflectography to Differentiate Features in Paintings. *Microscopy and Microanalysis*. 2011, vol. 17, no. 05, pp. 691–695. ISSN 1431-9276. Available from DOI: 10.1017/S1431927611000031.

32. CUCCI, Costanza; CASINI, Andrea; PICOLLO, Marcello; POGGESI, Marco; STEFANI, Lorenzo. A hyper-spectral scanner for high quality image spectroscopy: digital documentation and spectroscopic characterization of polychrome surfaces. *Art '11: 10th international conference on non-destructive investigations and microanalysis for the diagnostics and conservation of cultural and environmental heritage*. 2011, pp. 1–7.

33. PICOLLO, Marcello; BACCI, Mauro; CASINI, A; LOTTI, F; PORCINAI, S; RADICATI, Bruno; STEFANI, L. Fiber Optics Reflectance Spectroscopy: A Non-destructive Technique for the Analysis of Works of Art. In: *Optical Sensors and Microsystems: New Concepts, Materials, Technologies*. Boston, MA: Springer US, 2000, pp. 259–

All problems according to Preflight profile
Convert to PDF/A-2u

265. ISBN 978-0-306-47099-8. Available from DOI: 10.1007/0-306-47099-3{_}23.

34. BLAŽEK, Jan; SOUKUP, Jindřich; ZITOVÁ, Barbara; FLUSSER, Jan; HRADILOVÁ, Janka; HRADIL, David; TICHTABACCK-LUDGE'Y, Tomáš. M3art: A Database of Models of Canvas Paintings. *Digital Heritage. Progress in Cultural Heritage: Documentation, Preservation, and Protection Lecture Notes in Computer Science*. 2014, vol. 8740, no. 1, pp. 176–185.

35. COSENTINO, Antonino. Effects of different binders on technical photography and infrared reflectography of 54 historical pigments. *International Journal of Conservation Science*. 2015, vol. 6, no. 3, pp. 287–298. ISSN 20678223.

36. HU, B. B.; NUSS, M. C. Imaging with terahertz waves. *Optics Letters*. 1995, vol. 20, no. 16, pp. 1716–1718. ISSN 0146-9592. Available from DOI: 10.1364/OL.20.001716.

37. KÖHLER, Wolfram; LABOR, Köhler; PANZER, Michael; KLOTZBACH, Eckhard; WINNERL, Stephan; HELM, Manfred; RUTZ, Frank; JÖRDENS, Christian; KOCH, Martin. Non-destructive investigation of paintings with THz-radiation. *9th ECNDT, Berlin 2006*. 2006, pp. 1–7.

38. FUKUNAGA, Kaori. *THz Technology Applied to Cultural Heritage in Practice*. Springer Japan, 2016. ISBN 978-4-431-55883-5. Available from DOI: 10.1007/978-4-431-55885-9.

39. PICOLLO, Marcello; FUKUNAGA, Kaori. Application of THz-TDS imaging technology to the investigation of panel paintings. *Science, Technology and Cultural Heritage*. 2014, pp. 289–293.

40. ADAM, Aurele J. L.; PLANKEN, Paul C. M.; MELONI, Sabrina; DIK, Joris. Terahertz imaging of hidden paint layers on canvas. In: *2009 34th International Conference on Infrared, Millimeter, and Terahertz Waves*. IEEE, 2009, vol. 17, pp. 1–2. No. 5. ISBN 978-1-4244-5416-7. Available from DOI: 10.1109/ICIMW.2009.5324616.

41. FUKUNAGA, Kaori; PICOLLO, Marcello. Terahertz spectroscopy applied to the analysis of artists' materials. *Applied Physics A*. 2010, vol. 100, no. 3, pp. 591–597. ISSN 1432-0630. Available from DOI: 10.1007/s00339-010-5643-y.

42. ABRAHAM, Emmanuel; YOUNUS, Ayesha; DELAGNES, Jean-Christoph; MOUNAIX, Patrick. Non-invasive investigation of art paintings by terahertz imaging. *Applied Physics A: Materials Science and Processing*. 2010, vol. 100, no. 3, pp. 585–590. Available from DOI: 10.1007/s00339-010-5642-z.

All problems according to Preflight profile
Convert to PDF/A-2u

43. PICOLLO, Marcello; KOHDZUMA, Yohsei; FUKUNAGA, Kaori; HOSAKO, Iwao. Application of terahertz imaging methodologies for the investigation of paintings. *Art '11: 10th international conference on non-destructive investigations and microanalysis for the diagnostics and conservation of cultural and environmental heritage*. 2011.

44. FILIPPIDIS, George; MASSAOUTI, Maria; SELIMIS, Alexandros; GUALDA, Emilio J.; MANCEAU, Jean-Michel; TZORTZAKIS, Stelios. Nonlinear imaging and THz diagnostic tools in the service of Cultural Heritage. *Applied Physics A*. 2012, vol. 106, no. 2, pp. 257–263. ISSN 0947-8396. Available from DOI: 10.1007/s00339-011-6691-7.

45. SECO-MARTORELL, C.; LÓPEZ-DOMI'NGUEZ, V.; ARAUZ-GAROFALO, G.; REDO-SANCHEZ, A.; PALACIOS, J; TEJADA, J. Goya's artwork imaging with Terahertz waves. *Optics Express*. 2013, vol. 21, no. 15, pp. 17800. ISSN 1094-4087. Available from DOI: 10.1364/OE.21.017800.

46. ABRY, P.; KLEIN, A. G.; SETHARES, W. A.; JOHNSON, C. R. Signal Processing for Art Investigation [From the Guest Editors]. *IEEE Signal Processing Magazine*. 2015, vol. 32, no. 4, pp. 14–16. ISSN 1053-5888. Available from DOI: 10.1109/MSP.2015.2419311.

47. BEREZHNOY, Igor; POSTMA, Eric; HERIK, Jaap van den. Digital analysis of Van Gogh's complementary colours. In: *Analysis*. 2004, pp. 163–170. Available also from: http://proceedings.eldoc.ub.rug.nl/FILES/HOME/bnaic/2004/pt1/digital/022digital.pdf.

48. ANITHA, Anila; BRASOVEANU, Andrei; DUARTE, Marco; HUGHES, Shannon; DAUBECHIES, Ingrid; DIK, Joris; JANSSENS, Koen; ALFELD, Matthias. Restoration of X-ray fluorescence images of hidden paintings. *Signal Processing*. 2013, vol. 93, no. 3, pp. 592–604. ISSN 0165-1684. Available from DOI: 10.1016/j.sigpro.2012.09.027. Image Processing for Digital Art Work.

49. THURROWGOOD, David; PATERSON, David; JONGE, Martin D de; KIRKHAM, Robin; THURROWGOOD, Saul; HOWARD, Daryl L. A Hidden Portrait by Edgar Degas. *Scientific Reports*. 2016, vol. 6, pp. 29594. Available from DOI: 10.1038/srep29594.

50. CRIMINISI, Antonio; STORK, David G. Did the great masters use optical projections while painting?: Perspective Comparison of Paintings and Photographs of Renaissance Chandeliers. *Proceedings of the 17th International Conference on Pattern Recognition 2004 ICPR 2004*. 2004, vol. 4, pp. 645–648. ISSN 10514651. Available from DOI: 10.1109/ICPR.2004.1333855.

All problems according to Preflight profile
Convert to PDF/A-2u

51. KALE, David; STORK, David G. Estimating the position of illuminants in paintings under weak model assumptions: an application to the works of two Baroque masters. *Proceedings of SPIE*. 2009, vol. 7240, pp. 72401M–72401M–12. Available from DOI: 10.1117/12.806267.

52. GONZALEZ, Rafael C.; WOODS, Richard E. *Digital Image Processing (3rd Edition)*. Upper Saddle River, NJ, USA: Prentice-Hall, Inc., 2006. ISBN 978-0-13-168728-8.

53. COSENTINO, Antonino. Multispectral imaging system using 12 interference filters for mapping pigments. *Conservar Património*. 2015, vol. 21, pp. 26.

54. LEGRAND, Stijn; VANMEERT, Frederik; VAN DER SNICKT, Geert; ALFELD, Matthias; DE NOLF, Wout; DIK, Joris; JANSSENS, Koen. Examination of historical paintings by state-of-the-art hyperspectral imaging methods: from scanning infra-red spectroscopy to computed X-ray laminography. *Heritage Science*. 2014, vol. 2, no. 1, pp. 1.

55. ŽEMLIČKA, Jan; JAKŮBEK, Jan; DUDÁK, Jan; JANKA, Hradilová. X-ray radiography of paintings with hight resolution (I): testing and measurement with large area pixel detector. In: HRADIL, David; HRADIOVÁ, Janka (eds.). *ACTA ARTIS ACADEMICA 2014*. Praha, CZ, 2014, pp. 51–68.

56. BALAS, C.; EPITROPOU, G.; TSAPRAS, A.; HADJINICOLAOU, N. A novel hyperspectral camera and analysis platform for the non-destructive material identification and mapping: An application in paintings by El Greco. In: *2016 IEEE International Conference on Imaging Systems and Techniques (IST)*. 2016, pp. 211–215. Available from DOI: 10.1109/IST.2016.7738225.

57. FISCHER, Christian; KAKOULLI, Ioanna. Multispectral and hyperspectral imaging technologies in conservation: current research and potential applications. *Reviews in conservation*. 2006, vol. 7, pp. 3–16.

58. DIK, Joris; REISCHIG, Peter; KRUG, Kris; WALLERT, Arie; COERDT, Andrea; HELFEN, Lukas; BAUMBACH, Tilo. Three-dimensional imaging of paint layers and paint substructures with synchrotron radiation computed μ-laminography. *Journal of the American Institute for Conservation*. 2013.

59. BALAS, Costas; PAPADAKIS, Vassilis; PAPADAKIS, Nicolas; PAPADAKIS, Antonis; VAZGIOURAKI, Eleftheria; THEMELIS, George. A novel hyper-spectral imaging apparatus for the non-destructive analysis of objects of artistic and historic value. *Journal of Cultural Heritage*. 2003, vol. 4, pp. 330–337. ISSN 12962074. Available from DOI: 10.1016/S1296-2074(02)01216-5.

All problems according to Preflight profile
Convert to PDF/A-2u

60. RIBÉS, Alejandro; SCHMITT, Francis; BRETTEL, Hans. Calibration and Spectral Reconstruction for an Art Painting Multispectral Acquisition System. *Conference on Colour in Graphics, Imaging, and Vision*. 2004, vol. 2004, no. 1, pp. 403–408. ISSN 2158-6330.

61. BERNS, Roy S; TAPLIN, Lawrence A; URBAN, Philipp; ZHAO, Yonghui. Spectral color reproduction of paintings. In: *Conference on Colour in Graphics, Imaging, and Vision*. 2008, pp. 484–488.

62. BLAŽEK, Jan; SOUKUP, Jindřich; ZITOVÁ, Barbara; FLUSSER, Jan; TICHÝ, Tomáš; HRADILOVÁ, Janka. Low-cost mobile system for multispectral cultural heritage data acquisition. In: *Digital Heritage International Congress (DigitalHeritage), 2013*. 2013, vol. 1, pp. 73–79.

63. RIBÉS, Alejandro; PILLAY, Ruven; SCHMITT, Francis; LAHANIER, Christian. Studying That Smile. *IEEE Signal Processing Magazine*. 2008, vol. 25, no. 4, pp. 14–26. ISSN 1053-5888. Available from DOI: 10.1109/MSP.2008.923091.

64. MAYER, W Stanley Taft; W, James. The Science of Paintings. In: *Measurement Science and Technology*. 2001, vol. 12, pp. 653–653. No. 5. ISBN 978-0-387-98722-4. Available from DOI: 10.1088/0957-0233/12/5/702.

65. EASTAUGH, Nicholas; WALSH, Valentine; CHAPLIN, Tracey; SIDDALL, Ruth. *Pigment Compendium Set: Pigment Compendium: Optical Microscopy of Historical Pigments*. 1st. Elsevier, 2004. ISBN 978-0-7506-4553-9.

66. PELAGOTTI, Anna; MASTIO, Andrea Del; ROSA, Allesia De; PIVA, Alessandro. Multispectral imaging of paintings. *IEEE Signal Processing Magazine*. 2008, vol. 25, no. 4, pp. 27–36.

67. BRILL, T.B. *Light:Its Interaction with Art and Antiquities*. Springer US, 1980. ISBN 978-0-306-40416-0.

68. SIMONOT, Lionel; ELIAS, Mady. Color change due to a varnish layer. *Color Research and Application*. 2004, vol. 29, no. 3, pp. 196–204. ISSN 03612317. Available from DOI: 10.1002/col.20008.

69. CUCCI, Costanza; PICOLLO, Marcello; VERVAT, Muriel. Trans-illumination and trans-irradiation with digital cameras: Potentials and limits of two imaging techniques used for the diagnostic investigation of paintings. *Journal of Cultural Heritage*. 2012, vol. 13, no. 1, pp. 83–88. ISSN 12962074. Available from DOI: 10.1016/j.culher.2011.07.002.

70. GARGANO, M.; LUDWIG, N.; POLDI, G. A new methodology for comparing IR reflectographic systems. *Infrared Physics and Technology*. 2007, vol. 49, no. 3 SPEC. ISS. Pp. 249–253. ISSN 13504495. Available from DOI: 10.1016/j.infrared.2006.06.013.

All problems according to Preflight profile
Convert to PDF/A-2u

71. BULL, Duncan; KREKELER, Anna; ALFELD, Matthias; DIK, Joris; JANSSENS, Koen. An intrusive portrait by Goya. *The Burlington Magazine*. 2011, vol. 153, no. 1303, pp. 668–673. ISSN 0007-6287.

72. DELIGIANNIS, N.; MOTA, J. F. C.; CORNELIS, B.; RODRIGUES, M. R. D.; DAUBECHIES, I. Multi-Modal Dictionary Learning for Image Separation With Application In Art Investigation. *IEEE Transactions on Image Processing*. 2016, vol. PP, no. 99, pp. 1–12. ISSN 1057-7149. Available from DOI: 10.1109/TIP.2016.2623484.

73. GOOCH, AMY AND TUMBLIN, Jack. Visualizing pentimenti: revealing the hidden history of paintings. *Journal of Mathematics and the Arts*. 2007, vol. 00, no. 00, pp. 1–11. ISSN 17513472. Available from DOI: 10.1080/1751347YYxxxxxxxx.

74. BLAŽEK, Jan; STRIOVÁ, Jana; FONTANA, Raffaella; ZITOVÁ, Barbara. Improvement of the visibility of concealed features in artwork NIR reflectograms by information separation. *Digital Signal Processing*. 2017, vol. 60, pp. 140–151.

75. KUBELKA, Paul; MUNK, Franz. Ein Beitrag zur Optik der Farbanstriche. *Zeitschrift für technische Physik*. 1931, vol. 12, pp. 593–601.

76. KUBELKA, Paul. New contributions to the optics of intensely light-scattering materials. Part II: Nonhomogeneous layers. *JOSA*. 1954, vol. 44, no. 4, pp. 330–335.

77. NOBBS, James H. Kubelka—Munk Theory and the Prediction of Reflectance. *Review of Progress in Coloration and Related Topics*. 1985, vol. 15, no. 1, pp. 66–75. ISSN 1478-4408. Available from DOI: 10.1111/j.1478-4408.1985.tb03737.x.

78. ZHAO, Yonghui. *Image Segmentation and Pigment Mapping of Cultural Heritage Based on Spectral Imaging*. 2008. Available also from: http://scholarworks.rit.edu/theses/3029. PhD thesis. Rochester Institute of Technology.

79. DUPUIS, G.; MENU, M. Quantitative characterisation of pigment mixtures used in art by fibre-optics diffuse-reflectance spectroscopy. *Applied Physics A: Materials Science and Processing*. 2006, vol. 83, no. 4, pp. 469–474. Available from DOI: 10.1007/s00339-006-3522-3.

80. LIANG, H; KEITA, K; PERIC, B; VAJZOVIC, T. Pigment identification with optical coherence tomography and multispectral imaging. In: *Proc. OSAV'2008, The 2nd I'ntl Topical Meeting on Optical Sensing and Artificial Vision*. 2008, pp. 33–42. No. May.

81. MASTIO, A Del; PELAGOTTI, A; CAPPELLINI, V. Multispectral and multi-modal imaging data processing for the identification of painting materials. In: PRESS, CRC (ed.). *Lasers in the Conservation of Artworks*. 2008, pp. 453–458. ISBN 978-0-415-47596-9. Available from DOI: doi:10.1201/9780203882085.ch72.

All problems according to Preflight profile
Convert to PDF/A-2u

82. DAVID HRADIL Janka Hradilová, Petr Bezdička. New Criteria for Classification of and Differentiation between Clay and Iron Oxide Pigments of Various Origins. *Acta Artis Academica 2010*. 2010, pp. 107–136.

83. ČERMÁKOVÁ, Zdeňka; ŠVARCOVÁ, Silvie; HRADILOVÁ, Janka; BEZDIČKA, Petr; LANČOK, Adriana; VAŠUTOVÁ, Vlasta; BLAŽEK, Jan; HRADIL, David. Temperature-related degradation and colour changes of historic paintings containing vivianite. *Spectrochimica Acta Part A: Molecular and Biomolecular Spectroscopy*. 2015, vol. 140, pp. 101–110.

84. ALDROVANDI, A.; ALTAMURA, M. L.; CIANFANELLI, M. T.; RITANO, P. I Materiali Pittorici: tavolette campione per la caratterizzazione mediante analisi multispettrale. *OPD Restauro*. 1996, vol. 8, pp. 191–103. ISSN 11202513. Available also from: http://www.jstor.org/stable/24395397.

85. MONTAGNER, Cristina; BACCI, Mauro; BRACCI, Susanna; FREEMAN, Rachel; PICOLLO, Marcello. Library of UV–Vis–NIR reflectance spectra of modern organic dyes from historic pattern–card coloured papers. *Spectrochimica Acta Part A: Molecular and Biomolecular Spectroscopy*. 2011, vol. 79, no. 5, pp. 1669–1680. ISSN 1386–1425. Available from DOI: 10.1016/j.saa.2011.05.033.

86. CAVALERI, Tiziana; GIOVAGNOLI, Annamaria; NERVO, Marco. Pigments and Mixtures Identification by Visible Reflectance Spectroscopy. *Procedia Chemistry*. 2013, vol. 8, pp. 45–54. ISSN 1876-6196. Available from DOI: 10.1016/j.proche.2013.03.007.

87. COTTE, Pascal; DUPRAZ, Damien. Spectral imaging of Leonardo Da Vinci's Mona Lisa: A true color smile without the influence of aged varnish. In: *Conference on Colour in Graphics, Imaging, and Vision*. 2006, vol. 2006, pp. 311–317. No. 1.

88. BACCI, Mauro; PICOLLO, Marcello; TRUMPY, Giorgio; TSUKADA, Masahiko; KUNZELMAN, Diane. Non-Invasive Identification of White Pigments on 20th-Century Oil Paintings by Using Fiber Optic Reflectance Spectroscopy. *Journal of the American Institute for Conservation*. 2007, vol. 46, no. 1, pp. 27–37. ISSN 01971360. Available also from: http://www.jstor.org/stable/40026533.

89. BACCI, Mauro; BARONTI, S; CASINI, A; LOTTI, F; PICOLLO, Marcello; CASAZZA, O. Non-destructive spectroscopic investigations on paintings using optical fibers. In: *Materials issues in art and archaeology III: symposium held April 27-May 1, 1992, San Francisco, California, USA*. 1992, vol. 267, pp. 265–283. No. c. ISBN 978-1-55899-162-0.

All problems according to Preflight profile
Convert to PDF/A-2u

90. BACCI, Mauro. Fibre optics applications to works of art. *Sensors and Actuators: B. Chemical*. 1995, vol. 29, no. 1-3, pp. 190–196. ISSN 09254005. Available from DOI: 10.1016/0925-4005(95)01682-1.

91. RESTORATION LABORATORY OF THE OPIFICIO DELLE PIETRE DURE AND THE APPLIED SPECTROSCOPY LABORATORY OF THE INSTITUTE OF APPLIED PHYSICS "NELLO CARRARA" OF THE ITALIAN NATIONAL RESEARCH COUNCIL. *Fiber Optics Reflectance Spectra (FORS) of Pictorial Materials in the 270-1700 nm range* [http://fors.ifac.cnr.it]. 2016.

92. FLUSSER, Jan; ZITOVÁ, Barbara; BLAŽEK, Jan; BENEŠ, Miroslav; SOUKUP, Jindřich; KOTERA, Jan; HRADILOVÁ, Janka; HRADIL, David; TICHÝ, Tomáš; VAŠUTOVÁ, Vlasta. *m3art database* [http://m3art.utia.cas.cz/db/overview]. 2016.

93. COSENTINO, Antonino. *FORS spectral database* [http://e-conservation.org/images/Issue2/Cosentino/FORS-Spectra-Pigments-CSV.zip]. 2016.

94. HUNTER, Richard S.; HAROLD, Richard W. *The Measurement of Appearance*. Wiley Subscription Services, Inc., A Wiley Company, 1987. ISBN 978-0-471-83006-1.

95. NASSAU, Kurt. The fifteen causes of color: The physics and chemistry of color. *Color Research & Application*. 1987, vol. 12, no. 1, pp. 4–26. ISSN 03612317. Available from DOI: 10.1002/col.5080120105.

96. BEARDEN, J. A. X-ray wavelengths. *Reviews of Modern Physics*. 1967, vol. 39, no. 1, pp. 78–124. ISSN 00346861. Available from DOI: 10.1103/RevModPhys.39.78.

97. HRADILOVÁ, J.; MISLEROVÁ, H. Painting Technique of Portraits Painted in the 19th Century by Friedrich von Amerling. *Acta Artis Academica 2010*. 2010, pp. 137–164.

98. KAMMERER, P.; LETTNER, M.; ZOLDA, E.; SABLATNIG, R. Identification of drawing tools by classification of textural and boundary features of strokes. *Pattern Recognition Letters*. 2007, vol. 28, no. 6, pp. 710–718. ISSN 01678655. Available from DOI: 10.1016/j.patrec.2006.08.003.

99. HRADIL, David; GRYGAR, Tomáš; HRADILOVÁ, Janka; BEZDIČKA, Petr. Clay and iron oxide pigments in the history of painting. *Applied Clay Science*. 2003, vol. 22, no. 5, pp. 223–236. ISSN 01691317. Available from DOI: 10.1016/S0169-1317(03)00076-0.

100. HRADIL, David; BEZDIČKA, Petr; HRADILOVÁ, Janka; VAŠUTOVÁ, Vlasta. Microanalysis of clay-based pigments in paintings by XRD techniques. *Microchemical Journal*. 2016, vol. 125, pp. 10–20. ISSN 0026265X. Available from DOI: 10.1016/j.microc.2015.10.032.

All problems according to Preflight profile
Convert to PDF/A-2u

101. ŠVARCOVÁ, S.; BEZDIČKA, P.; HRADIL, D.; HRADILOVÁ, J.; ŽIŽAK, I. Clay pigment structure characterisation as a guide for provenance determination - a comparison between laboratory powder micro-XRD and synchrotron radiation XRD. *Analytical and Bioanalytical Chemistry*. 2011, vol. 399, pp. 331–336.

102. BACCI, M; CASINI, A; CUCCI, C; MUZZI, A; PORCINAI, S. A study on a set of drawings by Parmigianino: integration of art-historical analysis with imaging spectroscopy. *Journal of Cultural Heritage*. 2005, vol. 6, no. 4, pp. 329–336. ISSN 12962074. Available from DOI: 10.1016/j.culher.2005.07.002.

103. HRADILOVÁ, Janka; VALCHÁŘOVÁ, Blanka; VELÍŠEK, Michal; BLAŽEK, Jan. Detection of Copies Using Mathematicla Processing of Images II: Story of a Painting on Canvas of a Boy Petting a Bird. In: *ACTA ARTIS ACADEMICA 2012: Knowledge and experience in the fine art*. Praha, CZ, 2012, pp. 148–156.

104. KESHAVA, N.; MUSTARD, J.F. Spectral unmixing. *IEEE Signal Processing Magazine*. 2002, vol. 19, no. 1, pp. 44–57. ISSN 10535888. Available from DOI: 10.1109/79.974727.

105. CARDOSO, J-F. Blind signal separation: statistical principles. *Proceedings of the IEEE*. 1998, vol. 86, no. 10, pp. 2009–2025.

106. BLAŽEK, Jan; ZITOVÁ, Barbara; TICHÝ, Tomáš; VAŠUTOVÁ, Vlasta. Optical properties of historical paint pigments under near infrared (NIR) radiation. In: HRADIL DAVID, Hradilová Janka (ed.). *ACTA ARTIS ACADEMICA 2014*. Praha, CZ, 2014, pp. 35–41.

107. BENEŠ, Miroslav; ZITOVÁ, Barbara; BLAŽEK, Jan; HRADILOVÁ, Janka; HRADIL, David. Removing the artifacts from artwork cross-section images. In: *Image Processing (ICIP), 2011 18th IEEE International Conference on*. 2011, pp. 3537–3540.

108. CORNELIS, Bruno; DOOMS, Ann; CORNELIS, Jan; SCHELKENS, Peter. Digital canvas removal in paintings. *Signal Processing*. 2012, vol. 92, no. 4, pp. 1166–1171. ISSN 01651684. Available from DOI: 10.1016/j.sigpro.2011.11.012.

109. YIN, R.; DUNSON, D.; CORNELIS, B.; BROWN, B.; OCON, N.; DAUBECHIES, I. Digital cradle removal in X-ray images of art paintings. In: *2014 IEEE International Conference on Image Processing (ICIP)*. 2014, pp. 4299–4303. Available from DOI: 10.1109/ICIP.2014.7025873.

110. PÉREZ, Patrick; GANGNET, Michel; BLAKE, Andrew. Poisson Image Editing. *ACM Trans. Graph.* 2003, vol. 22, no. 3, pp. 313–318. ISSN 0730-0301. Available from DOI: 10.1145/882262.882269.

All problems according to Preflight profile
Convert to PDF/A-2u

111. ELAD, Michael; STARCK, J.L.; QUERRE, Philippe; DONOHO, David L. Simultaneous cartoon and texture image inpainting using morphological component analysis (mca). *Applied and Computational Harmonic Analysis*. 2005, vol. 19, no. 3, pp. 340–358.

112. BHATTACHARYA, Anirban; DUNSON, David B. Sparse bayesian infinite factor models. *Biometrika*. 2011, vol. 98, no. 2, pp. 291–306.

113. BLAŽEK, Jan; HRADILOVÁ, Janka; ZITOVÁ, Barbara; KAMENICKÝ, Jan. Odhalování kopií pomocí matematického zpracování obrazu, část I: teoretická východiska a princip metody. In: *ACTA ARTIS ACADEMICA 2012: Knowledge and experience in the fine art*. Praha, CZ, 2012, pp. 141–147.

114. MA, Lili; CHEN, YQ; MOORE, KL. Rational radial distortion models of camera lenses with analytical solution for distortion correction. *International Journal of Information Acquisition*. 2004, no. 435, pp. 1–12. Available also from: http://www.worldscientific.com/doi/abs/10.1142/S0219878904000173.

115. LETTNER, M; KLEBER, F; SABLATNIG, R; MIKLAS, H. Contrast Enhancement in Multispectral Images by Emphasizing Text Regions. In: *The 8th IAPR International Workshop on Document Analysis Systems DAS*. 2008, pp. 225–232. Available from DOI: 10.1109/DAS.2008.68.

116. BLAŽEK, Jan; ZITOVÁ, Barbara; BENEŠ, Miroslav; HRADILOVÁ, Janka. Fresco restoration: digital image processing approach. In: *Signal Processing Conference, 2009 17th European*. 2009, pp. 1210–1214.

117. CONOVER, Damon M.; DELANEY, John K.; LOEW, Murray H. Automatic registration and mosaicking of technical images of Old Master paintings. *Applied Physics A: Materials Science and Processing*. 2015, vol. 8790, pp. 1–8. ISSN 14320630. Available from DOI: 10.1007/s00339-015-9140-1.

118. CAPPELLINI, V.; DEL MASTIO, A.; DE ROSA, A.; PIVA, A.; PELAGOTTI, A.; EL YAMANI, H. An automatic registration algorithm for cultural heritage images. In: *IEEE International Conference on Image Processing 2005*. IEEE, 2005, pp. II–566. ISBN 978-0-7803-9134-5. Available from DOI: 10.1109/ICIP.2005.1530118.

119. ROGELJ, Peter; KOVAČIČ, Stanislav; GEE, James C. Point similarity measures for non-rigid registration of multi-modal data. *Computer Vision and Image Understanding*. 2003, vol. 92, no. 1, pp. 112–140. ISSN 1077-3142. Available from DOI: 10.1016/S1077-3142(03)00116-4.

120. RUSSAKOFF, Daniel B.; TOMASI, Carlo; ROHLFING, Torsten; MAURER, Calvin R. Image Similarity Using Mutual Information of Regions. *Lecture Notes in Computer Science - European Con-*

All problems according to Preflight profile
Convert to PDF/A-2u

ference on Computer Vision. 2004, vol. 3023, pp. 596–607. ISSN 03029743. Available from DOI: 10.1007/978-3-540-24672-5_47.

121. SAUNDERS, D.; CUPITT, J. Image Processing at the National Gallery: The VASARI Project. In: *National Gallery Technical Bulletin*. 1993, vol. 14, pp. 72–85.

122. BARONTI, S.; CASINI, A.; LOTTI, F.; PORCINAI, S. Multispectral imaging system for the mapping of pigments in works of art by use of principal-component analysis. *Appl. Opt.* 1998, vol. 37, no. 8, pp. 1299–1309. Available from DOI: 10.1364/AO.37.001299.

123. ATTAS, Michael; CLOUTIS, Edward; COLLINS, Catherine; GOLTZ, Douglas; MAJZELS, Claudine; MANSFIELD, James R; MANTSCH, Henry H. Near-infrared spectroscopic imaging in art conservation: investigation of drawing constituents. *Journal of Cultural Heritage*. 2003, vol. 4, no. 2, pp. 127–136.

124. DIEM, M; LETTNER, M; SABLATNIG, R. Multi-Spectral Image Acquisition and Registration of Ancient Manuscripts. In: *Proc of 31st AAPROAGM Workshop*. 2007, pp. 129–136. Available also from: http://www.caa.tuwien.ac.at/cvl/people/diem/paper/diem-oagm07.pdf.

125. PICOLLO, Marcello; BACCI, Mauro; CASINI, Andrea; LOTTI, Franco; POGGESI, Marco; STEFANI, Lorenzo. Hyperspectral image spectroscopy: a 2D approach to the investigation of polychrome surfaces. *Conservation Science 2007: papers from the conference held in Milan, Italy, 10-11 May 2007*. 2008, pp. 162–168.

126. GREEN, A A; BERMAN, M; SWITZER, P; GRAIG, M D. A transformation for ordering multispectral data in term of image quality with implications for noise removal. *IEEE Transactions on Geoscience and Remote Sensing*. 1988, vol. 26, no. 1, pp. 65–74. ISSN 01962892. Available from DOI: 10.1109/36.3001.

127. VAN DER SNICKT, Geert; MARTINS, Ana; DELANEY, John; JANSSENS, Koen; ZEIBEL, Jason; DUFFY, Michael; MCGLINCHEY, Chris; VAN DRIEL, Birgit; DIK, Joris. Exploring a hidden painting below the surface of René Magritte's Le portrait. *Applied Spectroscopy*. 2016, vol. 70, no. 1, pp. 57–67. ISSN 19433530. Available from DOI: 10.1177/0003702815617123.

128. SNIJDERS, Ludo; ZAMAN, Tim; HOWELL, David. Using hyperspectral imaging to reveal a hidden precolonial Mesoamerican codex. *Journal of Archaeological Science: Reports*. 2016, vol. 9, pp. 143–149. ISSN 2352409X. Available from DOI: 10.1016/j.jasrep.2016.07.019.

129. DELANEY, John K.; RICCIARDI, Paola; GLINSMAN, Lisha Deming; FACINI, Michelle; THOURY, Mathieu; PALMER, Michael; RIE, E. René De La. Use of imaging spectroscopy, fiber optic reflectance spectroscopy, and X-ray fluorescence to map and identify pigments

All problems according to Preflight profile
Convert to PDF/A-2u

in illuminated manuscripts. *Studies in Conservation*. 2014, vol. 59, no. 2, pp. 91–101. ISSN 0039-3630. Available from DOI: 10.1179/2047058412Y.0000000078.

130. HEINZ, Daniel C.; CHANG, Chein I. Fully constrained least squares linear spectral mixture analysis method for material quantification in hyperspectral imagery. *IEEE Transactions on Geoscience and Remote Sensing*. 2001, vol. 39, no. 3, pp. 529–545. ISSN 01962892. Available from DOI: 10.1109/36.911111.

131. RAPANTZIKOS, Konstantinos; BALAS, Costas. Hyperspectral Imaging : Potential in Non-Destructive Analysis of Palimpsets. *IEEE International Conference on Image Processing, 2005 (ICIP 2005)*. 2005, pp. II – 618–21. Available from DOI: 10.1109/ICIP.2005.1530131.

132. FONTANA, R.; BARUCCI, M.; CARCAGNÌ, P.; DAFFARA, C.; PAMPALONI, E.; PEZZATI, L. Autofocus laser system for multi-NIR scanning imaging of painting surfaces. In: PEZZATI, Luca; SALIMBENI, Renzo (eds.). *Archaeology*. 2011, vol. 8084, pp. 808405–9. ISBN 978-0-8194-8680-6. Available from DOI: 10.1117/12.889487.

133. KESHAVA, N. Distance metrics and band selection in hyperspectral processing with applications to material identification and spectral libraries. *IEEE Transactions on Geoscience and Remote Sensing*. 2004, vol. 42, no. 7, pp. 1552–1565. ISSN 0196-2892. Available from DOI: 10.1109/TGRS.2004.830549.

134. ALMEIDA, Luis B. Nonlinear Source Separation. *Synthesis Lectures on Signal Processing*. 2006, vol. 1, no. 1, pp. 1–114. ISSN 1932-1236. Available from DOI: 10.2200/S00016ED1V01Y200\-602SPR002.

135. LEGNAIOLI, Stefano; GRIFONI, Emanuela; LORENZETTI, Giulia; MARRAS, Luciano; PARDINI, Lorenzo; PALLESCHI, Vincenzo; SALERNO, Emanuele; TONAZZINI, Anna. Enhancement of hidden patterns in paintings using statistical analysis. *Journal of Cultural Heritage*. 2013, vol. 14, no. 3, Supplement, pp. S66–S70. ISSN 1296-2074. Available from DOI: 10.1016/j.culher.2012.11.013. Science and Technology for the Safeguard of Cultural Heritage in the Mediterranean Basin.

136. BACCI, Mauro; BELLUCCI, R; CUCCI, C; FROSININI, C; PICOLLO, Marcello; PORCINAI, S; RADICATI, Bruno. Fiber Optics Reflectance Spectroscopy in the Entire VIS-IR Range: a Powerful Tool for the Non-invasive Characterization of Paintings. *MRS Proceedings*. 2004, vol. 852, no. February, pp. OO2.4. ISSN 1946-4274. Available from DOI: 10.1557/PROC-852-OO2.4.

137. JOHNSON, D.H.; JOHNSON, C.R.; KLEIN, A.G.; SETHARES, W.A.; LEE, H; HENDRIKS, E. A thread counting algorithm for art forensics. In: *2009 IEEE 13th Digital Signal Processing Workshop*

All problems according to Preflight profile
Convert to PDF/A-2u

and 5th IEEE Signal Processing Education Workshop. IEEE, 2009, pp. 679–684. ISBN 978-1-4244-3677-4. Available from DOI: 10.1109/DSP.2009.4786009.

138. CORNELIS, Bruno; DOOMS, Ann; MUNTEANU, Adrian; CORNELIS, Jan; SCHELKENS, Peter. Experimental study of canvas characterization for paintings. *Analysis*. 2010, vol. 7531, pp. 753103–753103–12. ISSN 0277786X. Available from DOI: 10.1117/12.838345.

139. BIOUCAS-DIAS, José M.; PLAZA, Antonio; DOBIGEON, Nicolas; PARENTE, Mario; DU, Qian; GADER, Paul; CHANUSSOT, Jocelyn. Hyperspectral unmixing overview: Geometrical, statistical, and sparse regression-based approaches. In: *IEEE Journal of Selected Topics in Applied Earth Observations and Remote Sensing*. 2012, vol. 5, pp. 354–379. No. 2. ISBN 978-0-8194-8347-8. Available from DOI: 10.1109/JSTARS.2012.2194696.

140. BOARDMAN, Joseph. Automating Spectral Unmixing of AVIRIS data using Convex Geometry Concepts. In: *Fourth JPL Airborne Geoscience Workshop*. 1993, vol. 1, pp. 11–14. No. 93-26. Available also from: http://ntrs.nasa.gov/search.jsp?R=19950017428.

141. VALDIVIEZO, Juan C.; URCID, Gonzalo; LECHUGA, Edwin. Digital restoration of damaged color documents based on hyperspectral imaging and lattice associative memories. *Signal, Image and Video Processing*. 2016. ISSN 1863-1703. Available from DOI: 10.1007/s11760-016-1042-y.

142. ROSI, F.; DAVERI, A.; MILIANI, C.; VERRI, G.; BENEDETTI, P.; PIQUÉ, F.; BRUNETTI, B. G.; SGAMELLOTTI, A. Non-invasive identification of organic materials in wall paintings by fiber optic reflectance infrared spectroscopy: a statistical multivariate approach. *Analytical and Bioanalytical Chemistry*. 2009, vol. 395, no. 7, pp. 2097–2106. ISSN 1618-2650. Available from DOI: 10.1007/s00216-009-3108-y.

143. PLOEGER, Rebecca; CHIANTORE, Oscar; SCALARONE, Dominique; POLI, Tommaso. Mid-Infrared Fiber-Optic Reflection Spectroscopy (FORS) Analysis of Artists' Alkyd Paints on Different Supports. *Applied Spectroscopy*. 2011, vol. 65, no. 4, pp. 429–435. Available from DOI: 10.1366/10-06059.

144. PRONTI, Lucilla; FERRARA, Pasquale; UCCHEDDU, Francesca; PELAGOTTI, Anna; PIVA, Alessandro. Identification of pictorial materials by means of optimized multispectral reflectance image processing. *2015 IEEE International Workshop on Information Forensics and Security, WIFS 2015 - Proceedings*. 2015. Available from DOI: 10.1109/WIFS.2015.7368561.

All problems according to Preflight profile
Convert to PDF/A-2u

145. VISHNU, S; NIDAMANURI, R R; BREMANANTH, R. Spectral material mapping using hyperspectral imagery: a review of spectral matching and library search methods. *Geocarto International*. 2013, vol. 28, no. 2, pp. 171–190. ISSN 1010-6049. Available from DOI: Doi10.1080/10106049.2012.665498.

146. COSENTINO, Antonino. Identification of pigments by multispectral imaging; a flowchart method. *Heritage Science*. 2014, vol. 2, no. 1, pp. 8. ISSN 2050-7445. Available from DOI: 10.1186/2050-7445-2-8.

147. DUPUIS, Guillaume; ELIAS, Mady; SIMONOT, Lionel. Pigment Identification by Fiber-Optics Diffuse Reflectance Spectroscopy. *Appl. Spectrosc.* 2002, vol. 56, no. 10, pp. 1329–1336. Available also from: http://as.osa.org/abstract.cfm?URI=as-56-10-1329.

148. YUHAS, RH; GOETZ, Alexander F H; BOARDMAN, Joe W. Descrimination among semi-arid landscape endmembers using the Spectral Angle Mapper (SAM) algorithm. *Summaries of the Third Annual JPL Airborne Geoscience Workshop*. 1992, vol. 1, pp. 147–149.

149. MANSFIELD, James R; SOWA, Michael G; MAJZELS, Claudine; COLLINS, Cathy; CLOUTIS, Edward; MANTSCH, Henry H. Near infrared spectroscopic reflectance imaging: supervised vs. unsupervised analysis using an art conservation application. *Vibrational Spectroscopy*. 1999, vol. 19, no. 1, pp. 33–45. ISSN 09242031. Available from DOI: 10.1016/S0924-2031(99)00004-1.

150. RAO, C. Radhakrishna. The Utilization of Multiple Measurements in Problems of Biological Classification. *Journal of the Royal Statistical Society. Series B (Methodological)*. 1948, vol. 10, no. 2, pp. 159–203. ISSN 00359246. Available also from: http://www.jstor.org/stable/2983775.

151. DUNN, J. C. A Fuzzy Relative of the ISODATA Process and Its Use in Detecting Compact Well-Separated Clusters. *Journal of Cybernetics*. 1974, vol. 3, no. 3, pp. 32–57. ISSN 0022-0280. Available from DOI: 10.1080/01969727308546046.

152. BRUNI, S.; CARIATI, F.; CASADIO, F.; TONIOLO, L. Spectrochemical characterization by micro-FTIR spectroscopy of blue pigments in different polychrome works of art. *Vibrational Spectroscopy*. 1999, vol. 20, no. 1, pp. 15–25. ISSN 09242031. Available from DOI: 10.1016/S0924-2031(98)00096-4.

153. ZHAO, Yonghui; BERNS, Roy S; TAPLIN, Lawrence a; CODDINGTON, James. An investigation of multispectral imaging for the mapping of pigments in paintings. *Proceedings of SPIE (International Society for Optical Engineering)*. 2008. ISSN 0277786X. Available from DOI: 10.1117/12.765711.

All problems according to Preflight profile
Convert to PDF/A-2u

154. JOHNSON, Micah K.; STORK, David G.; BISWAS, Soma; FURUICHI, Yasuo. Inferring illumination direction estimated from disparate sources in paintings: an investigation into Jan Vermeer's Girl with a pearl earring. *Proc. SPIE*. 2008, vol. 6810, pp. 68100I–12. Available from DOI: 10.1117/12.759726.

155. STORK, David G. Did Georges de la Tour use optical projections while painting Christ in the Carpenter"s Studio? In: SAID, Amir; APOSTOLOPOULOS, John G. (eds.). *Proceedings of SPIE*. 2005, vol. 5685, p. 214. Available from DOI: 10.1117/12.582984.

156. JOHNSON, Micah K.; FARID, Hany. Exposing digital forgeries by detecting inconsistencies in lighting. *Proceedings of the 7th workshop on Multimedia and security - MM&Sec '05*. 2005, pp. 1–10. ISSN 1053-587X. Available from DOI: 10.1145/1073170.1073171.

157. CRIMINISI, Antonio; KEMP, Martin; SING BING KANG. Reflections of Reality in Jan van Eyck and Robert Campin. *Historical Methods*. 2004, vol. 37, no. 3, pp. 109–121. ISSN 0161-5440. Available from DOI: 10.3200/HMTS.37.3.109-122.

158. STORK, David G. Optics and Realism in Renaissance Art. *Scientific American*. 2004, vol. 291, no. 6, pp. 76–83. ISSN 0036-8733. Available from DOI: 10.1038/scientificamerican1204-76.

159. JANSEN, P.H.; RUTTKAY, Z.M. The Arnolfini Portrait in 3d: Creating Virtual World of a Painting with Inconsistent Perspective. In: ARNOLD, D. B.; FERKO, A. (eds.). *Annual Conference of the European Association for Computer Graphics, Eurographics 2007 Cultural Heitage Papers*. The Eurographics Association, 2007, pp. 25–32. Available also from: http://doc.utwente.nl/61965/.

160. SAVARESE, Silvio; SPRONK, Ron; STORK, David G.; DELPOZO, Andrey. Reflections on praxis and facture in a devotional portrait diptych: a computer analysis of the mirror in Hans Memling's Virgin and Child and Maarten van Nieuwenhove. *Proc. SPIE*. 2008, vol. 6810, pp. 68100G–10. Available from DOI: 10.1117/12.761226.

161. ROBINSON, Dirk; STORK, David G. Aberration analysis of the putative projector for Lorenzo Lotto's Husband and wife: image analysis through computer ray-tracing. In: *Computer Image Analysis in the Study of Art*. SPIE, 2008, vol. 6810, 68100H–11. Available from DOI: 10.1117/12.768315.

162. STORK, David G. Were optical projections used in early Renaissance painting? A geometric vision analysis of Jan van Eyck's Arnolfini portrait and Robert Campin's Merode Altarpiece. In: LATECKI, Longin J.; MOUNT, David M.; WU, Angela Y. (eds.). *SPIE Electronic Imaging: Vision Geometry XII*. Bellingham, WA: SPIE, 2004, vol. 5300, pp. 23–30.

All problems according to Preflight profile
Convert to PDF/A-2u

163. DZEMYDA, Gintautas; KURASOVA, Olga; ZILINSKAS, Julius. *Multidimensional Data Visualization: Methods and Applications*. Springer Publishing Company, Incorporated, 2012.

164. ALDROVANDI, A.; BERTANI, D.; CETICA, M.; MATTEINI, M.; MOLES, A.; POGGI, P.; TIANO, P. Multispectral image processing of paintings. *Studies in Conservation*. 1988, vol. 33, no. 3, pp. 154–159. Available from DOI: 10.1179/sic.1988.33.3.154.

165. WEINER, Chad. *Improved Acquisition of Underdrawings in Oil-Paintings Using IR-Reflectography*. 1998. Technical report. Rochester Institute of Technology.

166. VILASECA, Meritxell; PUJOL, Jaume; ARJONA, Montserrat; MARTÍNEZ-VERDÚS, Francisco Miguel. Color visualization system for near-infrared multispectral images. *Journal of Imaging Science and Technology*. 2005, vol. 49, no. 3, pp. 246–255.

167. CORNELIS, Bruno; DOOMS, Ann; CORNELIS, Jan; LEEN, Frederik; SCHELKENS, Peter. Digital Painting Analysis, at the Cross Section Of Engeneering, Mathematics and Culture. In: *19th European Signal Processing Conference*. Barcelona, 2011, pp. 1254–1258. No. Eusipco.

168. BARNI, Mauro; PELAGOTTI, Anna; PIVA, Alessandro. Image Processing for the Analysis and Conservation of Paintings: Opportunities and Challenges. *IEEE Signal Processing Magazine*. 2005, no. September, pp. 141–144.

169. BERNS, Roy S.; BYRNS, Siobhan; CASADIO, Francesca; FIEDLER, Inge; GALLAGHER, Christopher; IMAI, Francisco H.; NEWMAN, Alan; TAPLIN, Lawrence A. Rejuvenating the color palette of Georges Seurat's A sunday on La Grande Jatte - 1884: A simulation. *Color Research and Application*. 2006, vol. 31, no. 4, pp. 278–293. ISSN 03612317. Available from DOI: 10.1002/col.20223.

170. SHI, Xifan; LU, Dongming; LIU, Jianming. Color Changing and Fading Simulation for Frescoes Based on Empirical Knowledge from Artists. In: *Advances in Multimedia Information Processing - PCM 2006: 7th Pacific Rim Conference on Multimedia, Hangzhou, China, November 2-4, 2006. Proceedings*. Ed. by ZHUANG, Yueting; YANG, Shi-Qiang; RUI, Yong; HE, Qinming. Berlin, Heidelberg: Springer Berlin Heidelberg, 2006, pp. 861–869. ISBN 978-3-540-48769-2. Available from DOI: 10.1007/11922162_98.

171. STRÖM, M.; JOHANSSON, E.; STORK, D. G. Mapping colors from paintings to tapestries: rejuvenating the faded colors in tapestries based on colors in reference paintings. In: *Human Vision and Electronic Imaging XVII*. 2012, vol. 8291, 82911F. Available from DOI: 10.1117/12.905275.

All problems according to Preflight profile
Convert to PDF/A-2u

172. GIAKOUMIS, Ioannis; NIKOLAIDIS, Nikos; PITAS, Ioannis. Digital image processing techniques for the detection and removal of cracks in digitized paintings. *IEEE Transactions on Image Processing*. 2006, vol. 15, no. 1, pp. 178–188.

173. SOLANKI, Mr Sachin V; MAHAJAN, Mrs AR. Cracks inspection and interpolation in digitized artistic picture using image processing approach. *Int. J. of Recent Trends in Engineering and Technology*. 2009, vol. 1, no. 2.

174. SPAGNOLO, G Schirripa; SOMMA, F. Virtual restoration of cracks in digitized image of paintings. *Journal of Physics: Conference Series*. 2010, vol. 249, no. 1, pp. 012059. Available also from: http://stacks.iop.org/1742-6596/249/i=1/a=012059.

175. CORNELIS, B.; RUŽIĆ, T.; GEZELS, E.; DOOMS, A.; PIŽURICA, A.; PLATIŠA, L.; CORNELIS, J.; MARTENS, M.; MEY, M. De; DAUBECHIES, I. Crack detection and inpainting for virtual restoration of paintings: The case of the Ghent Altarpiece. *Signal Processing*. 2013, vol. 93, no. 3, pp. 605–619. ISSN 0165-1684. Available from DOI: 10.1016/j.sigpro.2012.07.022. Image Processing for Digital Art Work.

176. KAMMERER, Paul; ZOLDA, Ernestine; SABLATNIG, Robert. Computer Aided Analysis of Underdrawings in Infrared Reflectograms. In: ARNOLD; CHALMERS; NICCOLUCCI (eds.). *4th International Symposium on Virtual Reality, Archaeology and Intelligent Cultural Heritage*. 2003, vol. 1, pp. 1–9.

177. POLI, Riccardo; VALLI, Guido. An algorithm for real-time vessel enhancement and detection. *Computer Methods and Programs in Biomedicine*. 1997, vol. 52, no. 1, pp. 1–22. ISSN 01692607. Available from DOI: 10.1016/S0169-2607(96)01773-7.

178. AHARON, Michal; ELAD, Michael; BRUCKSTEIN, Alfred. K-SVD: An algorithm for designing overcomplete dictionaries for sparse representation. *IEEE Transactions on Signal Processing*. 2006, vol. 54, no. 11, pp. 4311–4322. ISSN 1053587X. Available from DOI: 10.1109/TSP.2006.881199.

179. KOMODAKIS, N.; TZIRITAS, G. Image Completion Using Efficient Belief Propagation Via Priority Scheduling and Dynamic Pruning. *IEEE Transactions on Image Processing*. 2007, vol. 16, no. 11, pp. 2649–2661. ISSN 1057-7149. Available from DOI: 10.1109/TIP.2007.906269.

180. PEI, Soo-Chang; ZENG, Yi-Chong; CHANG, Ching-Hua. Virtual restoration of ancient Chinese paintings using color contrast enhancement and lacuna texture synthesis. *IEEE Transactions on Image Processing*. 2004, vol. 13, no. 3, pp. 416–429.

All problems according to Preflight profile
Convert to PDF/A-2u

181. LANITIS, Andreas; STYLIANOU, Georgios; VOUTOUNOS, Chrysanthos. Virtual restoration of faces appearing in byzantine icons. *Journal of Cultural Heritage*. 2012, vol. 13, no. 4, pp. 404–412. ISSN 1296-2074. Available from DOI: 10.1016/j.culher.2012.01.001.

182. ČERMÁKOVÁ, Zdeňka; BEZDIČKA, Petr; NĚMEC, Ivan; HRADILOVÁ, Janka; ŠREIN, Vladimír; BLAŽEK, Jan; HRADIL, David. Naturally irradiated fluorite as a historic violet pigment: Raman spectroscopic and X-ray diffraction study. *Journal of Raman Spectroscopy*. 2015, vol. 46, no. 2, pp. 236–243.

183. TAN, Wei Ren; CHAN, Chee Seng; AGUIRRE, Hernan E.; TANAKA, Kiyoshi. Ceci n'est pas une pipe: A deep convolutional network for fine-art paintings classification. *2016 IEEE International Conference on Image Processing (ICIP)*. 2016, pp. 3703–3707. Available from DOI: 10.1109/ICIP.2016.7533051.

184. ICOGLU, Oguz; GUNSEL, Bilge; SARIEL, Sanem. Classification and Indexing of Paintings Based on Art Movements. In: *European Signal Processing Conference*. 2004, pp. 749–752.

185. LOMBARDI, Thomas Edward. *The classification of style in fine-art painting*. 2005. PhD thesis. Pace University.

186. ZUJOVIC, Jana; GANDY, Lisa; FRIEDMAN, Scott; PARDO, Bryan; PAPPAS, Thrasyvoulos N. Classifying paintings by artistic genre: An analysis of features & classifiers. In: *2009 IEEE International Workshop on Multimedia Signal Processing, MMSP '09*. IEEE, 2009, pp. 1–5. ISBN 978-1-4244-4464-9. Available from DOI: 10.1109/MMSP.2009.5293271.

187. PORTILLA, Javier; SIMONCELLI, Eero P. A Parametric Texture Model Based on Joint Statistics of Complex Wavelet Coefficients. *International Journal of Computer Vision*. 2000, vol. 40, no. 1, pp. 49–70. ISSN 1573-1405. Available from DOI: 10.1023/A:1026553619983.

188. KHAN, Fahad Shahbaz; BEIGPOUR, Shida; VAN DE WEIJER, Joost; FELSBERG, Michael. Painting-91: a large scale database for computational painting categorization. *Machine vision and applications*. 2014, vol. 25, no. 6, pp. 1385–1397.

189. OJALA, Timo; PIETIKAINEN, Matti; MAENPAA, Topi. Multiresolution gray-scale and rotation invariant texture classification with local binary patterns. *IEEE Transactions on pattern analysis and machine intelligence*. 2002, vol. 24, no. 7, pp. 971–987.

190. OLIVA, Aude; TORRALBA, Antonio. Modeling the Shape of the Scene: A Holistic Representation of the Spatial Envelope. *International Journal of Computer Vision*. 2001, vol. 42, no. 3, pp. 145–175. ISSN 1573-1405. Available from DOI: 10.1023/A:1011139631724.

All problems according to Preflight profile
Convert to PDF/A-2u

191. BOSCH, Anna; ZISSERMAN, Andrew; MUNOZ, Xavier. Representing shape with a spatial pyramid kernel. In: *Proceedings of the 6th ACM international conference on Image and video retrieval*. 2007, pp. 401–408.

192. WEIJER, Joost van de; SCHMID, Cordelia; VERBEEK, Jakob; LARLUS, Diane. Learning Color Names for Real-world Applications. *Trans. Img. Proc.* 2009, vol. 18, no. 7, pp. 1512–1523. ISSN 1057-7149. Available from DOI: 10.1109/TIP.2009.2019809.

193. GUO, Zhenhua; ZHANG, Lei; ZHANG, David. A completed modeling of local binary pattern operator for texture classification. *IEEE Transactions on Image Processing*. 2010, vol. 19, no. 6, pp. 1657–1663.

194. LOWE, David G. Distinctive Image Features from Scale-Invariant Keypoints. *Int. J. Comput. Vision*. 2004, vol. 60, no. 2, pp. 91–110. ISSN 0920-5691. Available from DOI: 10.1023/B:VISI.0000029664.99615.94.

195. VAN DE SANDE, Koen; GEVERS, Theo; SNOEK, Cees. Evaluating color descriptors for object and scene recognition. *IEEE transactions on pattern analysis and machine intelligence*. 2010, vol. 32, no. 9, pp. 1582–1596.

196. SHECHTMAN, Eli; IRANI, Michal. Matching local self-similarities across images and videos. In: *2007 IEEE Conference on Computer Vision and Pattern Recognition*. 2007, pp. 1–8.

197. SABLATNIG, Robert; KAMMERER, Paul; ZOLDA, Ernestine. Hierarchical classification of paintings using face and brush stroke models. In: *Pattern Recognition, 1998. Proceedings. Fourteenth International Conference on*. 1998, vol. 1, pp. 172–174.

198. SABLATNIG, Robert; KAMMERER, Paul; ZOLDA, Ernestine. Structural analysis of paintings based on brush strokes. In: *Photonics West'98 Electronic Imaging*. 1998, pp. 87–98.

199. JOHNSON JR., C. Richard; HENDRIKS, Ella; BEREZHNOY, Igor J.; BREVDO, Eugene; HUGHES, Shannon M.; DAUBECHIES, Ingrid; LI, Jia; POSTMA, Eric; WANG, James Z. Image processing for artist identification. *Signal Processing Magazine, IEEE*. 2008, vol. 25, no. 4, pp. 37–48.

200. SHAMIR, Lior; MACURA, Tomasz; ORLOV, Nikita; ECKLEY, D Mark; GOLDBERG, Ilya G. Impressionism, expressionism, surrealism: Automated recognition of painters and schools of art. *ACM Transactions on Applied Perception (TAP)*. 2010, vol. 7, no. 2, pp. 8.

All problems according to Preflight profile
Convert to PDF/A-2u

201. HOLLINK, Laura; SCHREIBER, Guus; WIELEMAKER, Jan; WIELINGA, Bob. Semantic Annotation of Image Collections. In: *In Workshop on Knowledge Markup and Semantic Annotation, KCAP'03*. 2003, pp. 1–3. Available also from: http://www.cs.vu.nl/%5C%CB%9Cguus.

202. JIANG, Shuqiang; HUANG, Tiejun; GAO, Wen. An Ontology-based Approach to Retrieve Digitized Art Images. In: *IEEE/WIC/ACM International Conference on Web Intelligence (WI'04*. 2006, pp. 131–137.

203. LI, Q.; LUO, S.; SHI, Z. Semantics-Based Art Image Retrieval Using Linguistic Variable. In: *Fourth International Conference on Fuzzy Systems and Knowledge Discovery (FSKD 2007)*. 2007, vol. 2, pp. 406–410. Available from DOI: 10.1109/FSKD.2007.511.

204. KUNEŠ, Michal; BLAŽEK, Jan. *Pole LED v matici 8x8*. Pod Vodárenskou věží 8, 182 08 Praha 8, CZ, 2013. Technical report. Ústav teorie informace a automatizace, AV ČR.

205. BLAŽEK, Jan; ZITOVÁ, Barbara; FLUSSER, Jan. Image fusion for difference visualization in art analysis. In: *Digital Heritage International Congress (DigitalHeritage), 2013*. 2013, vol. 1, pp. 653–656.

206. MORELAND, Kenneth; MORELAND, Kenneth. Diverging Color Maps for Scienti c Visualization. *5th International Symposium, ISVC 2009*. 2009, pp. 92–103. Available from DOI: 10.1007/978-3-642-10520-3_9.

207. COMANICIU, D.; MEER, P. Mean shift: a robust approach toward feature space analysis. *IEEE Transactions on Pattern Analysis and Machine Intelligence*. 2002, vol. 24, no. 5, pp. 603–619. ISSN 0162-8828. Available from DOI: 10.1109/34.1000236.

208. CHOW, C; LIU, Cong. Approximating discrete probability distributions with dependence trees. *IEEE transactions on Information Theory*. 1968, vol. 14, no. 3, pp. 462–467.

All problems according to Preflight profile
Convert to PDF/A-2u

All problems according to Preflight profile
Convert to PDF/A-2u

Part VI

APPENDIX

All articles summarized in this thesis and their supplementary materials.

All problems according to Preflight profile
Convert to PDF/A-2u

All problems according to Preflight profile
Convert to PDF/A-2u

APPENDIX

The following pages contain all original articles referenced in Chapter 10 and published during my PhD. studies. The last published paper [74] is fulfilled here by supplementary material in Section 12.1.

All problems according to Preflight profile
Convert to PDF/A-2u

FRESCO RESTORATION: DIGITAL IMAGE PROCESSING APPROACH

Jan Blažek [1], *Barbara Zitová* [2], *Miroslav Beneš*[1,2], *and Janka Hradilová*[3]

[1]Faculty of Mathematics and Physics, Charles University
Malostranské nám. 25
Prague, Czech Republic
E-mail: gimli@centrum.cz

[2]Institute of Information Theory and Automation
Academy of Sciences of the Czech Republic
Pod Vodárenskou věží 4
Prague, Czech Republic
E-mail: {zitova,benem9am}@utia.cas.cz

[3]Academic Laboratory of Materials Research of Paintings
Academy of Fine Arts
U Akademie, Prague, Czech Republic
E-mail: janka@avu.cz

ABSTRACT

In this paper, we present an application of digital image processing algorithms for the process of fresco restoration. Modern methods for image preprocessing and evaluation such as image registration, image fusion, and image segmentation are applied on images of the fresco, obtained in different modalities (visual and ultraviolet spectra) and at different times. Moreover, local chemical analyzes are taken into account during the image analysis. The robustness of proposed algorithms should be high due to the bad state of the fresco. Achieved results can give to art restorers better insight into the evolution of the fresco aging and in this way a proper conservation method can be chosen. Developed methods are illustrated by generated output images.

1. INTRODUCTION

Nowadays, methods belonging to digital image processing can help even in the restoration of historical art pieces. During the conservation process various sensors working in different modalities (UV - ultraviolet, IR - infrared, or complete evaluation by means of spectroscopy, when up to 32 various filters are employed) are often used and efficient preprocessing of these data is crucial for their further evaluation [1]. These algorithms take as an input all the acquired images available and their aim is to fuse the contained information and in this way achieve a content-rich detailed image, which parts are distributed among the input images but they are difficult to perceive all in once. Sometimes even such details can be generated which are not recognizable in any of the individual input images.

From digital image processing point of view we are working with a data set taken in different modalities, possibly from different viewpoints and at different times. That is why we face the problem of multi-modal and multi-temporal **image registration**, when data taken within different geometrical coordinates and differing in modality (captured wavelength spectrum) and possibly originating in different times have to be geometrically aligned. The image registration is very well studied, there are several survey papers on this topic [2]. After the data alignment, the very image processing analysis can start. At this moment, the corresponding parts of the images depict the same parts of the scene and thus they can be automatically compared or fused.

In the **image fusion** result various information sources are combined in order to see all important features and relations, which can be derived, in one multi-informational image. In this way we can see for example under-drawings (apparent in infrared images) and patterns created by applied biological materials (captured by ultraviolet spectra) at the same time in the resulting fused image. Such data visualization can be very useful and without computer-based assistance can be done just by very experienced restoration experts. The image fusion can work on the pixel-wise level, when the output values are function of the intensity values of the corresponding pixels from all data sources or their close neighborhoods. Otherwise, the output can be constructed from the input data using some more higher level image analyzes such as object segmentation, data denoising, edge detection, etc. to stress out the scene content. The pixel-wise fusion is for example very well studied for the processing of the Earth remote sensing imaging [3] and the higher level fusion can make a use of the various existing methods for object segmentation and other mentioned image processing tasks.

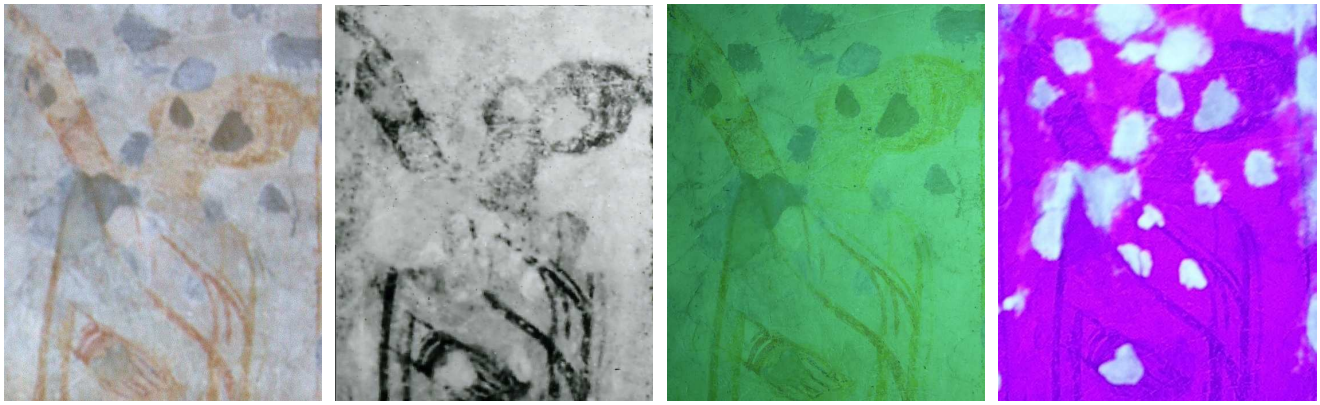


Figure 1: One of the part of the Kostolany pod Tribečom fresco. There is apparent current bad state of the fresco. The white areas are windows.

There are several possibilities how the acquired data sets and the fused results can be used. One of them is virtual restoration of the analyzed art piece [4], [5], when the aim is the visualization of the original state of the artwork. It is sometimes a little bit controversial issue, when aging and possible destruction is removed. Even the real art restorers' intentions to "improve" the state of the art piece can be questioned to which extent it is really valuable and responsible.

On the other hand, such virtual restoration can be used as a preliminarily test, which restoration method would be the most appropriate. In this manner, no harm is done and better knowledge necessary for final decision was collected. An interesting possibility is to use virtual restoration for tourist purposes, because the visualization of the original beauty of the historical pieces can attract more visitors, both virtual and

All problems according to Preflight profile
Convert to PDF/A-2u



(a) (b) (c) (d)

Figure 2: An example of the data set for the fresco: (a) - a visible spectrum image of the recent state (VS); (b) - a visible spectrum image from the 60's (BWS); (c) - a broad-band ultraviolet spectrum image (UVB); (d) - a narrow-band (with the spectrum maxima at 368 nm) ultraviolet spectrum images (UVN)

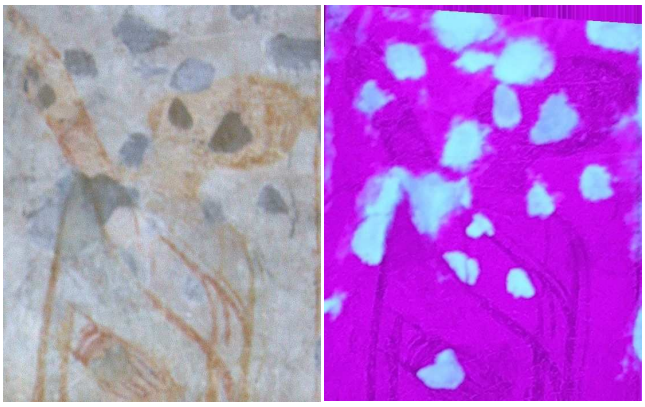
real ones.

Our application belongs to the category of the virtual restoration for the decision about the best restoration method. We were asked to joint the team of the restorers and try to figure out as much as possible from the data they have. The more effective analysis and visualization of measured data will help to achieve deeper understanding of the art piece evolution and structure, which materials were used and what is the material distribution across the fresco. The goal of proposed method was to combine all available images of the fresco (from different time and taken using different modalities) in order to emphasize the structure details of the fresco. Secondly, using the generated structural information, we were asked to expand the point-wise results of chemical analysis across the detected segments of the fresco. We use for the method development the data set of multi-modal and multi-temporal images together with results of locally taken chemical analyzes. It is necessary to mention that the robustness of proposed algorithms should be high due to the bad state of the fresco. Moreover, the reliability of the method was difficult to validate because of the not sufficient set of testing data due to the delayed site analysis. The proposed approach was designed for the described case, however the general ideas can be utilized in similar situations, when the virtual restauration of such extent is needed.

The rest of the paper is organized as follows. In Section 2, the studied object will be introduced together with the data set used for experiments. Section 3 covers individual steps of the data processing - image registration, image fusion, and image higher level analyzes - together with illustrative results. Finally, last Section 4 concludes our achievements and lists our plan for the future.

2. FRESCO

The data set we worked on comes from the fresco (Fig.1) situated in the 11th century church in Kostolany pod Tribečom, a small village in the Slovak Republic. The whole fresco covers quite large area of the inner church walls and as it is apparent from the picture (Fig.1) that it is in quite bad state. Restoration works have been started recently. Small subsections of the fresco were used for the method development in our laboratory, an example of which you can see in Fig.2.



(a) (b)

Figure 3: An example of the reference and corresponding registered images: (a) - visual spectra (VS); (b) - near band ultraviolet spectrum (UVN). See top right part of the (b) image for the geometry difference.

We obtained the fresco photographs in the visible spectrum (VS) and ultraviolet broad-band spectrum (UVB), and ultraviolet narrow band spectrum (UVN) with the spectrum maxima at 368 nm, see Fig.2 (a), (c), and (d), respectively. Next to this, we have black and white photographs (BWS) of the fresco from the 60's (see Fig.2 (b)), which captured the fresco before aging changes during last forty years. All the recent image data were taken by the Czech-Geo company.

Microscopic minute samples were manually taken out at several locations on the fresco, which are of the high interest for art restorers. Then they were tested using spectrometry. In this way, full chemical description of these samples was found out and these results were included to the data processing stream. The grid of the sampling spots is up to now not regular and quite sparse but this situation will be changed in the future.

3. IMAGE ANALYSIS

As it was stated before we are facing problem of the multi-modal and the multi-temporal registration, followed by the

All problems according to Preflight profile
Convert to PDF/A-2u

image fusion. Scene details should be stressed out. Moreover, the extra results from the sampling spots, which are representing chemical content of individual points, should be included into the result, too. They should be spread within the neighborhoods, defined by the structural information contained in data (edges, object shapes).

The used methods can be divided into three categories:

- image registration
- image fusion
- image higher level analysis

3.1 Image registration

Image registration is the process of transforming one image into the coordinate system of another image. Here, the process is complicated by the fact that the images can differ by the modality [6] used for scanning and possibly by the acquisition time [2]. In our case the most complex task is the registration of the BWS old photographs to the reference coordinate system (the one of the VS images). As it is apparent from the Fig.2 (b), there has been a big change in the fresco state.

The multi-modal and multi-temporal parts of registration were solved separately. In the later case feature points for the estimation of necessary geometric transform were chosen manually in both images (VS and BWS) and then the transformation parameters were computed, using known correspondences (significant differences due to multimodal nature of the data violated any automatic feature detection method). The first, multi-modal case was solved by means of the *mutual information* [7], which represents usual method for such cases. An example of the registered data can be seen in Fig.3 (see the top right corner for geometric difference). In the end, we have set of four images, which coordinate system corresponds to each other and we can directly compare and combine pixel values, because they depict the same object from the scene.

3.2 Image fusion

The goal of the image fusion is to find data combination and hidden dependencies which are difficult to find by looking at images separately. There exists many methods, often we can meet them in remote sensing applications (combining high spatial - panchromatic and frequency - multispectral resolution images) or in medical imaging (fusing functional - fMRI, PET information with the structural one - CT, MRI). The algorithms working on pixel-wise basis are using various image transforms such as principle component analysis (PCA) [8], independent component analysis (ICA) [8], or wavelet transform [9]. The very combination is then done in the chosen transform domain.

Here, we have tried wavelet transform and PCA transform. In the wavelet case, higher coefficients in the wavelet decomposition of images are combined, while PCA looks for the reduction of the dimensionality of the fresco representation and it sorts individual dimensions according to their importance. The latter solution gave us better results with respect to the detail visibility and distinctive features combination. One example is shown in Fig. 4. Details, which were hardly recognizable or distributed among several modalities,

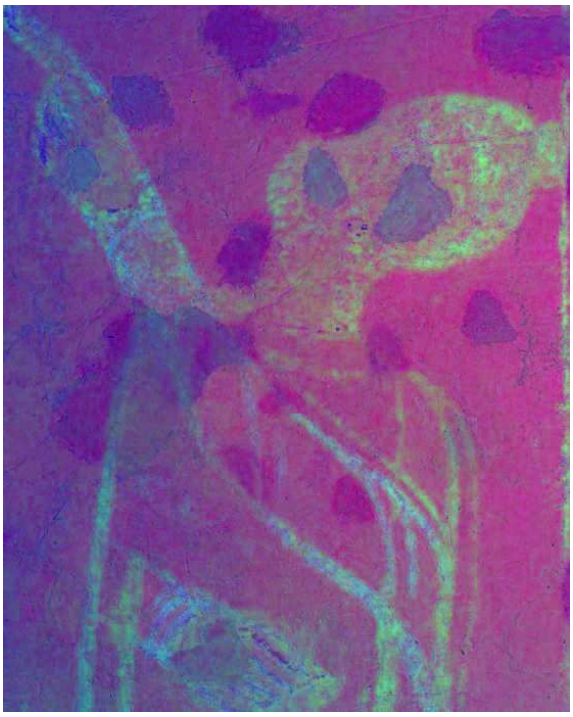
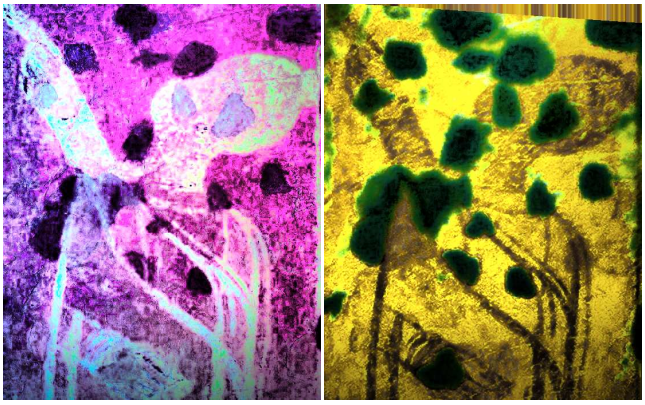


Figure 4: An example of the fused data using PCA transform. There are visible details, which were hardly recognizable before, such as the collar part or the stripes around the wrist.



(a) (b)

Figure 5: An example of the PCA fused data, when their contrast has been locally improved. The images differ in the chosen combination of input sources - (a): VS + UVN; (b) UVN + BWS.

appeared in the resulting image (the collar details, the stripes around the wrist).

It is difficult to judge automatically which source combination can be more useful for the art restorers thus we provide them with several combinations. Moreover, local contrast enhancement was implemented for better visualization. In Fig.5. achieved improvement can be seen. Fig.5 (a) is an enhanced image from Fig. 4, (b) part depicts the enhanced version of the fused UV narrow-band image (UVN) and the old fresco photograph (BWS). It is noticeable, that on these two images different features are captured depending on used

All problems according to Preflight profile
Convert to PDF/A-2u

modalities ((a) represents better the depicted person while the (b) image reflects more the destruction of the fresco).

3.3 Image higher level analysis

While in the previous section we did not care too much about objects depicted on the images, this last part of our approach is interested mainly in these structures. If any further virtual restoration should be considered than it is necessary to have an idea where are object boundaries and which parts of the image belongs to each other. Using the fused as well as the registered original data, we have applied edge detection and segmentation algorithms to achieve the notion of the scene content. This part of the project is still under progress so we would present our preliminary results.

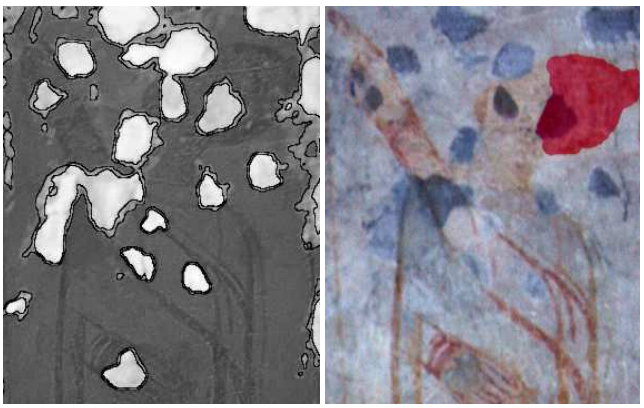
As it is apparent from the Fig.2 (b) image, the fresco was heavily destroyed and repaired afterwards, sometimes very insensitively. One of the interests of the art restorers is the detection of these lacunas. The Canny edge detector [10] run on the quantized UV data source followed by morphological post-processing gave us borders of these areas, as you can see in the Fig. 6 (a). These can be leaved out from further material analyzes as they are not native to the fresco. Original visual content of these areas is lost forever, however their filling up [11], [12] will be discussed in the Conclusion Section.

The second part of the image higher level analysis considered the sampling spots and usage of their information. There is the sparse grid of the sampling spots where we know exact chemical analysis (spectrometry) of the fresco content (the density of grid should be increased in the future in-site measures). Knowing the spot coordinates and the structure of the scene - the distribution of edges, borders, and flat areas - we can spread the content knowledge thorough the uniform neighborhoods till any border is reached. The idea behind is that if the intensity color is the same in the acquired images the chemical content is probably the same as well.

The robustness of such approach can be increased using the higher level content when we put individual borders and flat areas into the mutual relations. An outcome of the proposed solution is better visualization of the fresco colors and efficient representation of the chemical analyzes results - their extrapolation to the plane, because even that they are taken point-wise, they should represent an area and not just single points (see Fig. 6(b) for the person's hat representation).

4. CONCLUSIONS

In our paper we present the application of the digital image processing methods used during the fresco restoration. The art restorers have images of the fresco in three modalities - perceived in the visual, the narrow-band ultraviolet, and the broad-band ultraviolet wavelength spectra and, moreover, the old black and white photograph of the fresco from the 60's. Our aim was to combine all available information in a way to see all details in one fused image which enables better evaluate the state of the artwork. The second reason for the fresco processing is better visualization of the chemical analyzes, done on the sparse grid of the sampling spots. To achieve given goals, we have applied multi-modal (mutual information) and multi-temporal (it was done semi-automatically) registration. The registered data were fused by means of the PCA transform. Wavelet fusion did not return any good results. For the sampling spots value spread image higher level analysis was realized, including the edge detection (Canny edge detection followed by morphological post-processing) and segmentation. Achieved results are illustrated by several Figures.



(a) (b)

Figure 6: Image analysis results. (a) - lacunas: segmented areas, where the fresco was destroyed and then artificially repaired. (b) - spread information from the sampling spot about the chemical content (spectrometry), limited by structure-based neighborhood.

The project of an application of image processing methods for such fresco restoration is still running. All the work is done in tight cooperation with the restoration experts, because the applicability of the results has to be re-evaluated for every change of experiment settings. Moreover, the state of the fresco is very bad, thus it is often difficult to find robust enough algorithms.

In the near future we would like to point our attention to the inpainting for more tempting visualization of the fresco. As we mentioned in the Section 3., this is quite controversial issue, however we believe we could find reasonable consensus with the art restorers. The extrapolation of structures and textures across missing corrupted areas could improve the perception of such valuable art pieces. Once again, due to the bad state of the fresco we expect semiautomatic solution, allowing the experts interactively influence the output.

5. ACKNOWLEDGEMENT

All the work was done in the cooperation with the ALMA, a joint workplace of the Academy of Fine Arts in Prague and the Institute of Inorganic Chemistry of the Academy of Sciences of the Czech Republic. The project has been financed by the Projects of Ministry of Education of the Czech Republic no. MSM6046144603 and no. 1M0572, and by the Project of Grant Agency of the Czech Republic no. 203/07/1324.

REFERENCES

[1] M. Barni, A. Pelagotti, and A. Piva, "Image Processing for the Analysis and Conservation of Paintings: Opportunities and Challenges," IEEE Signal processing magazine, vol. 141, pp. 141-144, September 2005.

[2] B. Zitova and J. Flusser, "Image Registration Methods:

All problems according to Preflight profile
Convert to PDF/A-2u

A Survey" Image and Vision Computing," vol. 21, pp. 977-1000, 2003.

[3] G. Simone, A. Farina, F. C. Morabito, S. B. Serpico, and L. Bruzzone, "Image fusion techniques for remote sensing applications," Information Fusion, vol. 3, pp. 3-15, 2002.

[4] A. D. Mastio, V. Cappellini, R. Caldelli, A. D. Rosa, and A. Piva, "Virtual restoration and protection of cultural heritage images," in 15th International Conference on Digital Signal Processing, pp. 471-474, 2007.

[5] M. Pappas and I. Pitas, "Digital color restoration of old paintings," IEEE Transactions on Image Processing, vol. 9, pp. 291-294, 2000.

[6] F. Kleber, M. Lettner, M. Diem, M.C. Vill, R. Sablatnig, H. Miklas, and M. Gau, "Multispectral Acquisition and Analysis of Ancient Documents", in: Conference on Virtual Systems and MultiMedia (VSMM'08), pp. 184-191, Cyprus, 2008.

[7] P. Viola and W. M.Wells III, "Alignment by Maximization of Mutual Information," International Journal of Computer Vision, 24(2), pp. 137154, 1997.

[8] C. H. Chen, and Z. Xiaohui, "On the roles of PCA and ICA in data fusion," Proceedings on Geoscience and Remote Sensing Symposium, vol. 6, pp. 2620-2622, 2000.

[9] H. Li , B. S. Manjunath , S. K. Mitra, "Multisensor image fusion using the wavelet transform," Graphical Models and Image Processing, v.57 n.3, p.235-245, May 1995.

[10] J. Canny, " A Computational Approach To Edge Detection," IEEE Trans. Pattern Analysis and Machine Intelligence, 8:679-714, 1986.

[11] S.-C. Pei, Y.-C. Zeng, and C.-H. Chang, "Virtual restoration of ancient chinese paintings using color contrast enhancement and lacuna texture synthesis," IEEE Trans. Image Processing (Special Issue on Image Processing for Cultural Heritage), vol. 13, no. 3, pp. 416429, Mar. 2004.

[12] A. De Rosa, A. M. Bonacehi, V. Cappellini, and M. Barni, "Image segmentation and region filling for virtual restoration of artworks," Proceedings of International Conference on Image Processing, Issue 1, pp. 562-565, 2001.

All problems according to Preflight profile
Convert to PDF/A-2u

REMOVING THE ARTIFACTS FROM ARTWORK CROSS-SECTION IMAGES

Miroslav Beneš [b] *Barbara Zitová* [a] *Jan Blažek* [a] *Janka Hradilová* [c] *David Hradil* [d]

[b] Department of Software Engineering, Faculty of Mathematics and Physics,
Charles University, Prague, Czech Republic – benem9am@utia.cas.cz
[a] Institute of Information Theory and Automation, Academy of Sciences of the Czech Republic,
Prague, Czech Republic – zitova@utia.cas.cz
[c] Academic Laboratory of Materials Research of Paintings, Academy of Fine Arts,
Prague, Czech Republic – janka@avu.cz
[d] Institute of Inorganic Chemistry, Academy of Sciences of the Czech Republic,
Řež, Czech Republic – hradil@iic.cas.cz

ABSTRACT

In this paper we propose a method for automatic removal of artifacts from artwork cross-section images. Cross-section images of minute samples are acquired during the painting material research of an artwork before actual conservation is performed. Such images are unfortunately damaged by the artifacts from grinding of the resin in which the sample is embedded. Removing those artifacts can improve the outcome of image segmentation and other image processing methods. The proposed algorithm can also simplify an analysis of underdrawings by reducing the canvas structure after infrared acquisition. Despite the idea is not entirely original, the application to cultural heritage data is novel and the implementation does not require user interaction.

Index Terms— Image processing, image enhancement, cultural heritage

1. INTRODUCTION

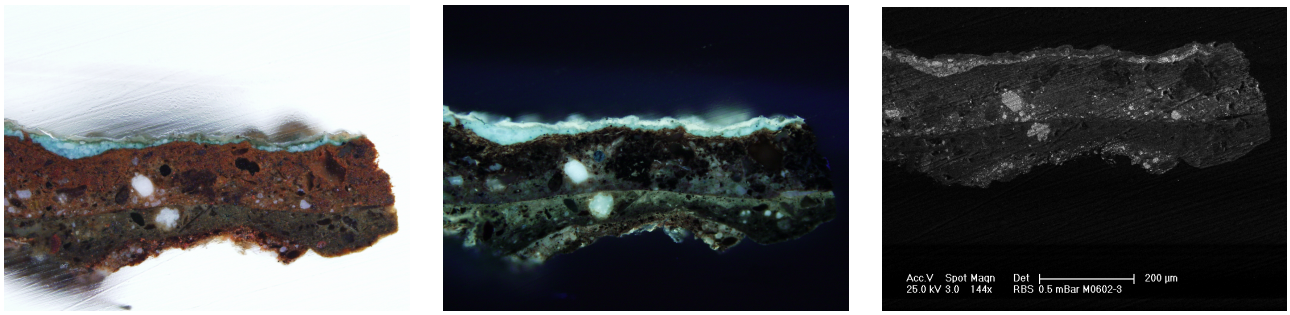
Today, the exploitation of digital image processing (DIP) approaches can be seen even in very distant areas such as art restoration applications. The ability to provide flexible analyzing tools and to improve quality and interpretability of input data obtained from processed artworks can make the DIP algorithms very useful and valuable for art conservators. Initially, DIP methods originally developed for other application areas such as medical research, industrial quality control, or remote sensing were applied. However, new approaches have been developed recently particularly for cultural heritage purposes, reflecting their special needs and aspects of processed artworks. One of the straightforward application of DIP methods is so called virtual restoration, aiming at the visualization of the original state of the artwork [1]. In addition, we can use achieved results for preliminary tests and suggestions, which restoration method would be the most appropriate [2]. The DIP methods can classify authors of the artwork [3] or even judge the genuineness of the studied painting [4]. There are many scientific papers dealing with individual tasks of artwork restoration, as well as complex systems, trying to offer unified solution (for example ArtShop [5]).

The main focus of our work lies in the application of DIP methods in materials research for art restoration/conservation and in the following report management and archiving [6]. Achieved results come from the fruitful cooperation between the Institute of Information Theory and Automation, Czech Academy of Sciences, ALMA, a joint workplace of the Academy of Fine Arts in Prague, the Institute of Inorganic Chemistry of the Academy of Sciences of the Czech Republic, and the Hamilton Kerr Institute, University of Cambridge, UK. Art conservators, materials scientists, and digital image processing researchers proposed and have been creating the system, which should reflect the demands of all participating sides.

Our paper presents recent achievement in the image data preprocessing in the developed system. In order to improve the quality of the data segmentation (dividing the image into meaningful segments) we have to deal with often low quality input images due to the data acquisition process and the sample preparation, respectively. We propose a method for automatic removal of the artifacts from artwork cross-section images of samples, acquired during the painting material research before actual conservation is performed. Section 2 introduces the overall system developed for the artwork restoration support, section 3 deals with the artifacts removal itself, section 4 describes experimental results, and, finally, section 5 concludes our paper.

The work was supported by the Academy of Sciences of the Czech Republic under the project no. M100750901 (financial support for international cooperation) and by the Ministry of Education of the Czech Republic under the project no. 1M0572 (research center) and no. MSM6046144603.

All problems according to Preflight profile
Convert to PDF/A-2u



(a) VIS image (b) UV image (c) SEM image

Fig. 1. The images are acquired in three modalities - visible spectrum (VIS), ultraviolet spectrum (UV) and electron microscope (SEM)

2. SYSTEM NEPHELE AND IMAGE PROCESSING

Nephele is an extended database system developed to facilitate the work of art conservator. When some artwork is considered to be conserved, the painting material research report is assorted. The report describes the process of material research of given artwork. It contains all the acquired information about the object, e.g. general information about author and artwork, information about samples taken off of the artwork by an invasive method, results of chemical analyses etc. The database reflects the structure of report and can afterwards serve as a knowledge base for further research.

The report access is supported by means of a search engine. User can take advantage of two different approaches: traditional text-based retrieval and content-based image retrieval. The latter is enabled thanks to the image processing modules incorporated to the Nephele system, which handle the input image data acquired during the material research - microscopic images of minute surface samples. The samples are taken off of the selected areas of the artwork, embedded in a polyester resin, and grounded at a right angle to the surface plane to expose the painting layers. Due to grinding of the resin noisy artifacts form in the background. The images are acquired in several modalities. Stratigraphy (learning about painting layers) is usually studied in visible spectrum (VIS) and ultraviolet spectrum (UV) images, where the UV analysis makes use of the luminescence. Images from electron microscope (SEM) further extend the data set (see figure 1).

The multimodal input data have to be preprocessed before they can be used for image retrieval or material classification purposes. VIS, UV and SEM image triplets of the sample are often geometrically misaligned due to manipulation errors. SEM image has also different resolution. Therefore spatial alignment issue of the images has to be solved by image registration. Likewise, image segmentation is involved in preprocessing of the input data set. The noisy background encloses the cross-section and has to be removed. Also preliminary layer segmentation is performed. Unfortunately, present artifacts complicate these tasks and decrease the performance of the modules (see figure 4. The proposed method removes the artifacts and improves the outcome of image processing stage.

3. ARTIFACTS REMOVING

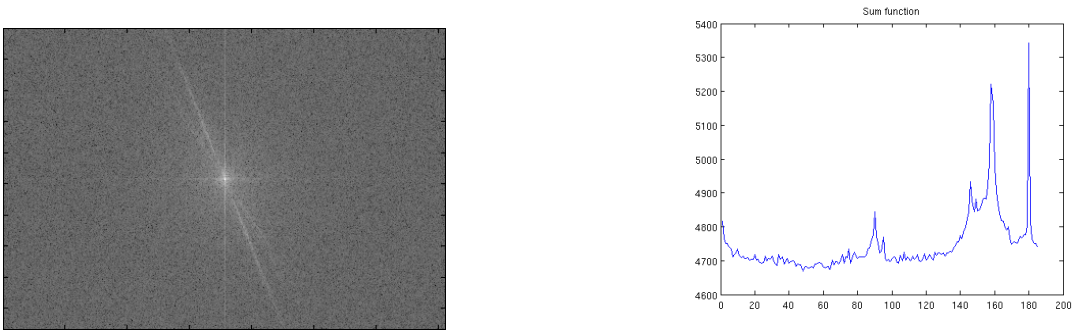
As stated before, the artifacts in the images originate from the grinding of the polyester resin, which is necessary to reveal the painting layers of the given sample. The proposed method can remove the artifacts completely or at least significantly diminished them.

Figure 1 shows the properties of the artifacts. They are omnipresent and in form of parallel lines. If we apply common Fourier transform to the grayscale input image, we can observe considerable amplitude response in a direction perpendicular to the original artifacts lines (see figure 2 (a)). In case of SEM images it is important to equalize the histogram first, which makes the lines more distinctive. Otherwise, the response would be weak. It is also better to remove the label from the image. Given the response, masking the Fourier spectrum and applying inverse Fourier transform provides demanded action to remove the artifacts in the image domain.

To achieve this, the function of column sums needs to be constructed. Fourier spectrum is rotated by one degree for all angles between zero and 180. In each step the values in columns are summed up and the maximum of the column sums is taken (with regard to the character of Fourier transform it is always in the middle). Thus, for each angle we have maximum response (see figure 2 (b)). Due to the properties of cross-section sample there is often strong response for angles 90 and 180. Other distinct peak determines the response of the artifacts, therefore its orientation. Sum function is smoothed to inhibit impact of distortions and peaks are found automatically (only the 3 highest peaks are considered).

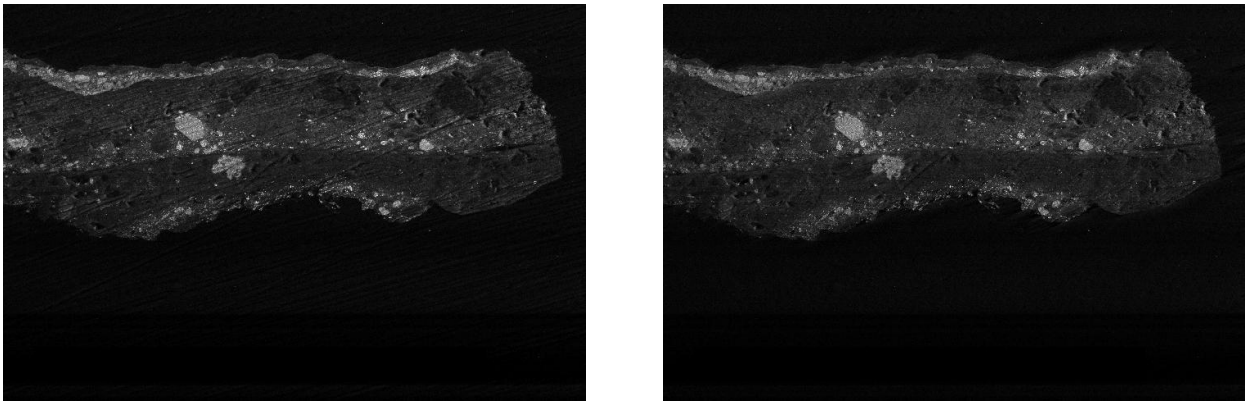
Now we have enough information to make up binary mask, which will be used for removing the response from the Fourier spectrum. Afterwards, inverse Fourier transform is

All problems according to Preflight profile
Convert to PDF/A-2u



(a) Fourier spectrum (b) Sum function

Fig. 2. Fourier spectrum of SEM image and sum function with several distinctive peaks



(a) SEM image before enhancement (b) SEM image after enhancement

Fig. 3. Example of an enhanced SEM image. Besides the improvement in the background, a texture of cross-section is adjusted.

applied to modified spectrum and enhanced result is acquired (see figure 3). Mask must be smoothed, otherwise the ringing effect is involved [7]. The parameters of the algorithm were tuned to have a minimal impact on the cross-section in terms of sharpness and level of detail.

4. EXPERIMENTS AND RESULTS

The images in the data set come from Academic Materials Research Laboratory of Painted Artworks (ALMA). It mainly consists of VIS and UV pairs, or VIS, UV and SEM triplets. Therefore, we have 76 VIS images, 62 UV images and 46 SEM images for testing purposes. The proposed algorithm was executed on each modality separately.

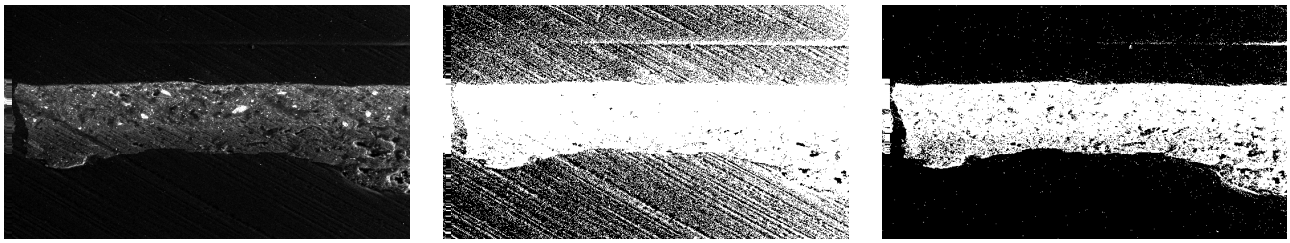
In case of VIS image data set, 71 images out of 76 were successfully enhanced (which means the artifacts were removed or significantly diminished). Concerning 5 dissatisfactory results, the response in Fourier spectrum was indistinctive or an appropriate peak was not correctly marked. Only 1 out of 46 SEM images was not processed in a satisfactory manner.

The algorithm performed poorly on UV data set. The responses in spectra were almost negligible. The background of the images is dark and the artifacts are nearly invisible, and thus they do not affect image segmentation and other image processing methods too much.

Figure 4 illustrates the influence of the grinding artifacts on outcome of specific image segmentation algorithm (Triangle, see [8]). The left image is the original SEM image with apparent artifacts in the background. Second image is binarized using the Triangle algorithms. Finally the right image shows the result of binarization applied to enhanced SEM image. The improvement of the algorithm performance is clear.

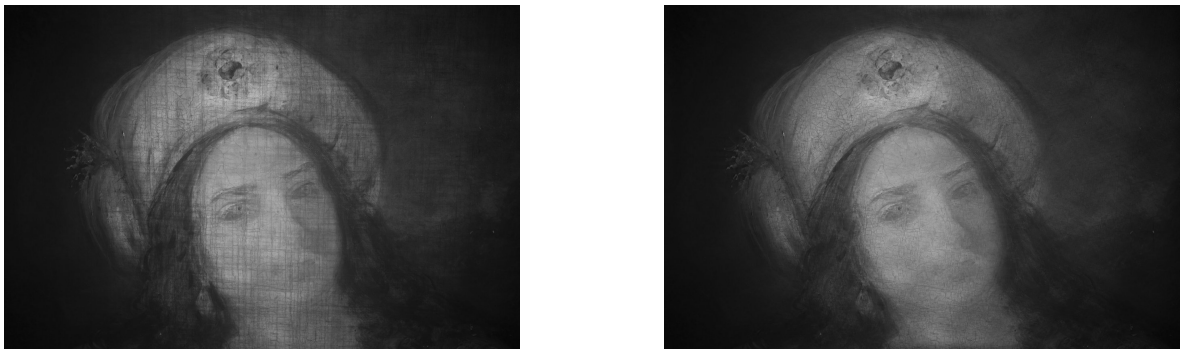
Also a different area of cultural heritage can exploit the performance of the proposed method, processing of infrared (IR) images of old paintings. The IR light enables to see hidden underdrawing, which capture the painter's original intentions. Unfortunately, IR backlighting captures also the canvas structure and its inhomogeneity. The algorithm helps to remove them and simplifies further analysis (see figure 5).

All problems according to Preflight profile
Convert to PDF/A-2u



SEM image | Binarized SEM image | Binarized enhanced SEM image

Fig. 4. The background artifacts might influence the outcome of the segmentation algorithm.



(a) Original image (b) Image after enhancement using the proposed algorithm

Fig. 5. Beside the underdrawings the IR backlighting shows also the canvas structure, which can be removed by the proposed method. The original underdrawing texture is well preserved. Thanks to Igor Fogaš, Moravian Gallery in Brno.

5. CONCLUSION

We proposed a method for automatic removal of the artifacts in cross-section images of given artwork. This improves the performance of following image processing modules such as image segmentation and image restoration. The algorithm was incorporated to Nephele system, which facilitates the work of material scientists and artwork conservators. It is fully automatic and stable.

6. REFERENCES

[1] M. Pappas and I. Pitas, "Digital color restoration of old paintings," *IEEE Transactions on Image Processing*, vol. 9, pp. 291–294, 2000.

[2] A.D. Mastio, V. Cappellini, R. Caldelli, A.D. Rosa, and A. Piva, "Virtual restoration and protection of cultural heritage images," in *15th International Conference on Digital Signal Processing*, 2007, pp. 471–474.

[3] R. Sablatnig, P. Kammerer, and E. Zolda, "Hierarchical classification of paintings using face and brush stroke models," in *Proceedings of 14th International Conference on Pattern Recognition*, 1998, pp. 172–174.

[4] C.R. Johnson Jr., E. Hendriks, I. Berezhnoy, E. Brevdo, S.M. Hughes, I. Daubechies, J. Li, E. Postma, and J. Wang, "Image processing for artist identification: Brushwok in the paintings of vincent van gogh," *IEEE Signal Processing Magazine, Special Issue on Visual Cultural Heritage*, 2008.

[5] V. Cappellini, M. Barni, M. Corsini, A. De Rosa, and A. Piva, "Artshop: an art-oriented image processing tool for cultural heritage applications," *Journal of Visualization and Computer Animation*, vol. 14, no. 3, pp. 149–158, 2003.

[6] M. Beneš, B. Zitová, J. Flusser, J. Hradilová, and D. Hradil, "The image processing system for art specimens: Nephele," in *Proceedings of 14th European Signal Processing Conference EUSIPCO 2006*, 2006, pp. 1–5.

[7] R.L. Easton Jr. and R.L. Easton, *Fourier Methods in Imaging*, John Wiley & Sons, 2010.

[8] G.W. Zack and W.E. Rogers, "Automatic measurement of sister chromatid exchange frequency," *Journal of Histochemistry and Cytochemistry*, vol. 25, no. 7, pp. 741–753, 1977.

All problems according to Preflight profile
Convert to PDF/A-2u

Image fusion for art analysis

Barbara Zitová[a] and Miroslav Beneš[a,b] and Jan Blažek[a,b]

[a]Institute of Information Theory and Automation, Academy of Sciences of the Czech Republic, Pod Vodárenskou věží 4, Prague, Czech Republic

[b]Faculty of Mathematics and Physics, Charles University, Malostranské nám. 25, Prague, Czech Republic

ABSTRACT

Our paper addresses problem of multi-modal data acquisition and the following data visualization for art analysis and interpretation. Various types of modalities for acquisition of digital images are used for art analysis. The data we can obtain using various modalities differ in two ways. The acquired images can differ by their mutual geometry and possibly by their radiometric quality. These are the differences we would like to remove. The group of differences we are interested in are details or characteristics of an artwork, which are apparent just in the certain modality and which bring us new information. The two listed groups represent two categories of image processing methods we have to deal with. The first one is represented by image preprocessing methods such as data enhancement and restoration algorithms, the second class includes effective ways how to combine the acquired information into one image - image fusion. In our paper we present image quality enhancement for microscopic multi-modal data and their segmentation and recent results in data fusion and visualization for art analysis are demonstrated from the second category of methods.

Keywords: Image fusion; visualization; art analysis.

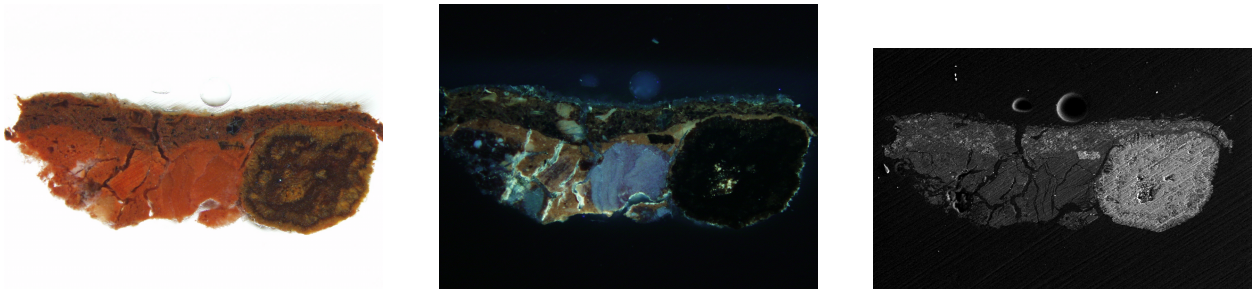
1. INTRODUCTION

Image fusion tries to create an efficient combination of information contained in multiple input images to provide more accurate description of the studied object than any of these individual input images. The one resulting compact image is visualizing all acquired information at once and in this way the end-user has often better possibility to perceive the details not apparent otherwise. The image fusion methods strive to reduce the dimensionality of acquired data while preserving or even stressing details, important for the end-user. Nowadays, the number of possible modalities for image data acquisition is growing (visible spectra, infrared in different wavelength bands, ultraviolet in different wavelength bands, to name the most widely used) and we are able to capture more and more subtle details of objects of interest, of their structure and functionality. The methods for effective combination of revealed information are very important. They enable to perceive paintings which were lost by overpainting (i.e. Patch of Grass by Vincent van Gogh[1]) or see the virtually reconstructed and valuable gems of cultural heritage in their original beauty (Mona Lisa, restored using virtual methods[2]).

Image fusion methods can be found in different application domains such as medical imaging, remote sensing, material science, and surveillance, to name the most important ones. Art analysis can gain a lot from the fusion methodology, combining multispectral data in an effective manner. The multispectral data acquisition itself is widely used for analysis[3] of artworks. Such data sets have to be usually preprocessed to minimize geometrical and radiometrical differences in the acquisition process - different camera setting, different camera viewpoint, different filter sensitivity and noise robustness, etc. We face the problem of multimodal/multitemporal image registration, when data taken within different geometrical coordinates and differing in modality and possibly originating in different times have to be geometrically aligned. The image registration is well studied problem, there are several survey papers[4] on this topic.

Further author information: (Send correspondence to Barbara Zitová)
Barbara Zitová: E-mail: zitova@utia.cas.cz, WWW: zoi.utia.cz
Miroslav Beneš: E-mail: benem9am@utia.cas.cz
Jan Blažek: E-mail: blazek@utia.cas.cz

All problems according to Preflight profile
Convert to PDF/A-2u



(a) VIS image (b) UV image (c) SEM image

Figure 1. The cross-section images for artwork material analysis are acquired in three modalities - (a): visible spectrum (VIS); (b): ultraviolet spectrum (UV); (c): scanning electron microscope (SEM)

Removal of radiometrical differences and related image enhancement is discussed in Section 2. Section 3 presents segmentation methodology for microscopic cross-sections, Section 4 demonstrates results of image fusion in three different projects. Finally, Section 5 concludes our paper.

Image enhancement

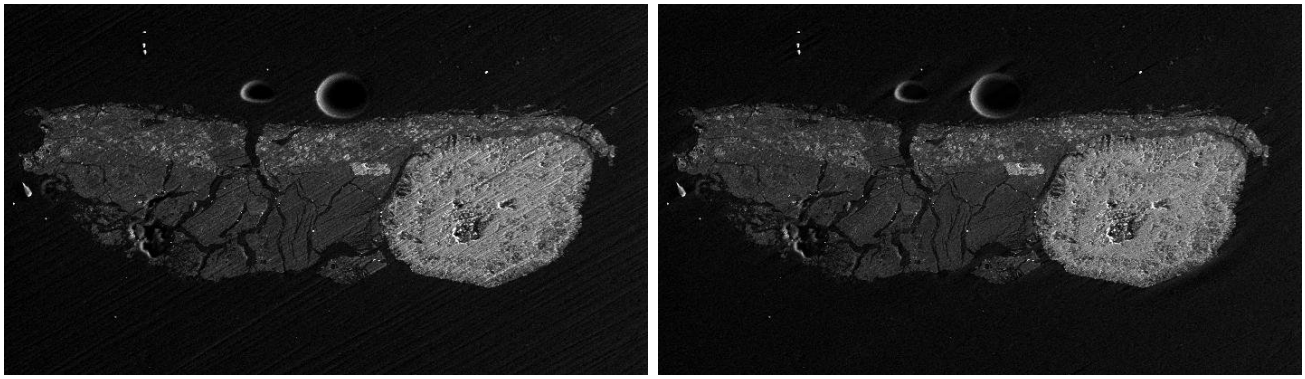
Image enhancement tries to improve the quality of the processed image so further processing can bring better results. Diminishing of radiometrical differences such as noise or blur, removal of various acquisition artifacts - these algorithms are examples of image enhancement methods. First method introduced here is related to material research of image artwork. Art conservators are taking several minute surface samples from the studied artwork. The samples are taken off at the selected areas to be able to capture material composition of the artwork and they are scanned using several modalities – visible spectrum (VIS), ultraviolet spectrum (UV) and images from scanning electron microscope (SEM) (see Fig.1).

During the preparation for scanning, the samples are embedded in a polyester resin and grounded at a right angle to the surface plane to expose individual painting layers. Grinding of the resin produces noisy artifacts in form of parallel lines (see Fig.2) on the cutting surface due to the mechanical properties of the material. They are affecting image quality of both the background and the studied sample (the foreground) and in this way they are negatively influencing further image processing. Moreover, the cutting pattern cannot be easily removed mechanically by material polishing, because this operation could negatively influence the surface quality of the studied sample due to friction and consecutive temperature increase. Thus, the multimodal input data have to be preprocessed before any higher level image processing can be performed (e.g. image retrieval, material classification).

The proposed method removes the artifacts completely or at least significantly diminishes them and thus improves the performance of image processing. As it was stated, the artifacts are omnipresent and in form of parallel lines. If Fourier transform is applied on the input image, considerable amplitude response can be observed in the direction perpendicular to the artifact lines. Thus, masking the Fourier spectrum and applying inverse Fourier transform can provide required result - removal of the artifacts in image domain.

The method is based on the construction of an appropriate directional masking filter corresponding to the direction of these parallel lines. The first step consists of the direction estimation. We exploit the idea that the orientation of the artifact response should corresponds to a distinct peak of the column sum function. This auxiliary function is constructed by consecutive stepwise rotation within the interval $< 0^\circ, 180^\circ >$ of the Fourier spectrum with the step equals to 1°. In each step, the values in columns are summed up and the maximum of the column sums is taken. The sum function is smoothed to inhibit impact of distortions and peaks are found automatically. The directional masking filter is then created in the determined direction and the inverse Fourier transform of the filtered data is computed. The achievable result are shown in Fig.2, where the right image demonstrates the diminishing of the cutting regular pattern. The consequences for further image preprocessing will be shown in the next Section.

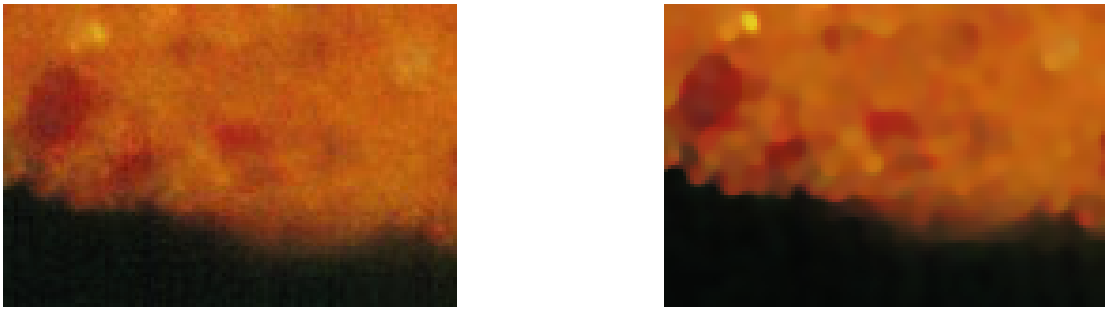
All problems according to Preflight profile
Convert to PDF/A-2u



(a) SEM image before enhancement (b) SEM image after enhancement

Figure 2. Example of an enhanced SEM image. (a) Original SEM image, the cutting pattern - parallel lines at 45 ° angle - is apparent. (b) Enhanced filtered image - besides the improvement in the background, the texture of cross-section is as well enhanced.

Another frequently present imperfection of the image data is out of focus blur due to the wrong setting of the acquisition camera. This type of radiometrical degradation can be removed by an appropriate deconvolution technique. We expect the model of the present blur to be in the form of Gaussian function and by application of the method described in[5] sufficient improvement for further segmentation or other image processing can be achieved (see Fig.3). Transitions between materials are now much sharper and the boundary of the sample is more distinct, too.



(a) VIS image before enhancement (b) VIS image after enhancement

Figure 3. Example of the deconvolved VIS image. (a) Original VIS image with out of focus blur. (b) Enhanced VIS image with sharper material transitions, more suitable for further segmentation. Consulting M. Sorel

Image segmentation

The aim of image segmentation, another image preprocessing method, is to divide the input image to several regions, which share similar characteristic (e.g. color, texture). One of the subtasks may be image binarization, i.e. division of the input image to two different classes. Therefore one of the two labels is assigned to each pixel in the picture. In our case it is either background or foreground label, because the cross-section has to be isolated from the noisy background, which is formed by the polyester resin.

Due to the distinctive characteristics of the microscopic cross-sections and their polyester resin background the segmentation is difficult. Dozen of binarization algorithm was tested, but only few proved to give satisfactory results. The variance of the algorithms performance can be observed in Fig.4, where binary results of three different algorithms on two different SEM images are presented. Huang[6] algorithm uses fuzzy thresholding method. Intermodes[7] computes the threshold from smoothed histogram and IsoData[8] is an iterative selection method based on ISODATA algorithm. In the top row (sample A) the binary masks are almost identical. On the other hand in the bottom row (sample B) the outputs of the algorithms differ quite radically.

All problems according to Preflight profile
Convert to PDF/A-2u

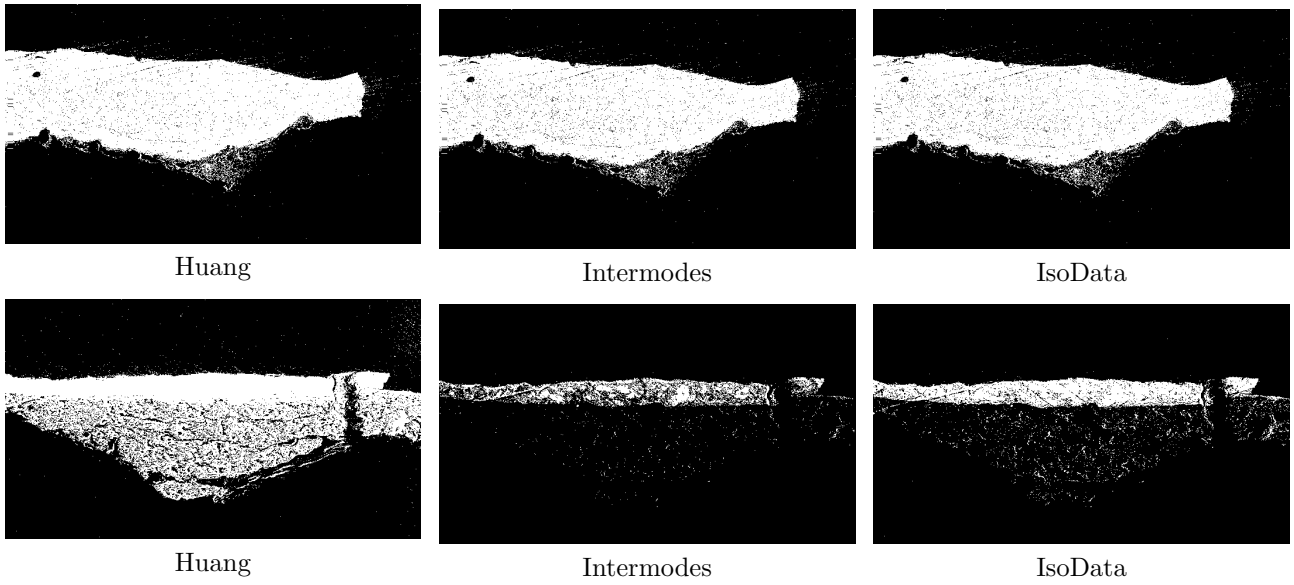


Figure 4. Performance variation of three different binarization algorithms (Huang,[6] Intermodes,[7] and IsoData[8]) on two different SEM images. There are almost identical results in the top row (sample A) and very different results of the algorithms in the bottom row (sample B).

Fig.5 illustrates the impact of the background artifacts on outcome of various algorithms. In this case the method by Triangle[9] was applied. The left image is the original SEM image with the grinding artifacts (parallel lines). In the middle there is a result of binarization algorithm, which was applied to the original SEM image. Finally, the right image shows the result of the binarization algorithm applied to the preprocessed SEM image, after the artifacts were removed using the introduced image enhancement technique. The improvement in the resulting foreground/background segmentation is apparent.



Figure 5. The influence of the background grinding artifacts. The original SEM image (left) is either directly binarized (middle) or the grinding artifacts are firstly diminished using the introduced enhancement method and then binarized (right).

Exhaustive testing of binarization methods was realized in order to determine suitable image segmentation method for each modality (VIS, UV and SEM). In all three cases the Huang algorithm[6] seems to be the most promising. The quality of its output corresponds the most with the needs of the next steps of image processing workflow.

Image fusion

As it was stated the aim of image fusion is to find such combination of input images that all the important and interesting details stay preserved while the dimensionality of the data is reduced. Final output image is much easier to comprehend than the original data stream for human understanding. The fusion algorithms can work

All problems according to Preflight profile
Convert to PDF/A-2u



(a) Visible image



(b) Infrared image



(c) Fused image



(a) Fused image - detail

Figure 6. Mary Magdalene painting. The input images for image fusion: (a) visual spectra image; (b) infrared spectra image. The fused image (c) and the detailed version: the triangle structure above the forehead (d).

pixel-wise, based on the mapping of the input pixel values to the output information and not taking into account the image structure and the content (good example is well-known alpha blending). The second category of fusion methods are based on the multiscale decomposition, often using wavelet decomposition applied on input images and followed by particular decision criterion for the output data formation.[10] The low- and high-frequency data drive the fusion in these cases. The last group is based on higher level information about an object of interest, so-called object based image fusion. Detected objects from one data channel are here substituted into the other data channel to form the multimodal representation. The special category of image fusion methods is formed by biologically motivated approaches based on human vision system.

In the art analysis, there are several possibilities how the input data entering the fusion process should be interpreted and as a result what type of image fusion is the most appropriate. In this paper we will address three examples of them on the projects we were involved in.

In the first one, the data set consists of the multispectral images of the Mary Magdalene painting. The images were acquired in the visible spectra and in the infrared spectra IR (an infrared-enabled camera with Hoya R72 filter, 720-1200 nm). Fig.6 shows the intensity images in the visible (a) and in the infrared (b) wavelengths. The painting itself was heavily damaged so both the visual and the computer based evaluation was extremely difficult. Visual inspection uncovered differences in the underdrawing sketches and the surface painting. An

All problems according to Preflight profile
Convert to PDF/A-2u



(a) Slovak version (b) Croatien version (c) Fused image

Figure 7. The oil paintings of Marianne Norman Earl Ehrenfels by F. Amerling. Two versions from the Slovak Republic (a) and from the Croatia (b), respectively. The resulting fused image - the more bright intensity represents the more prominent difference.

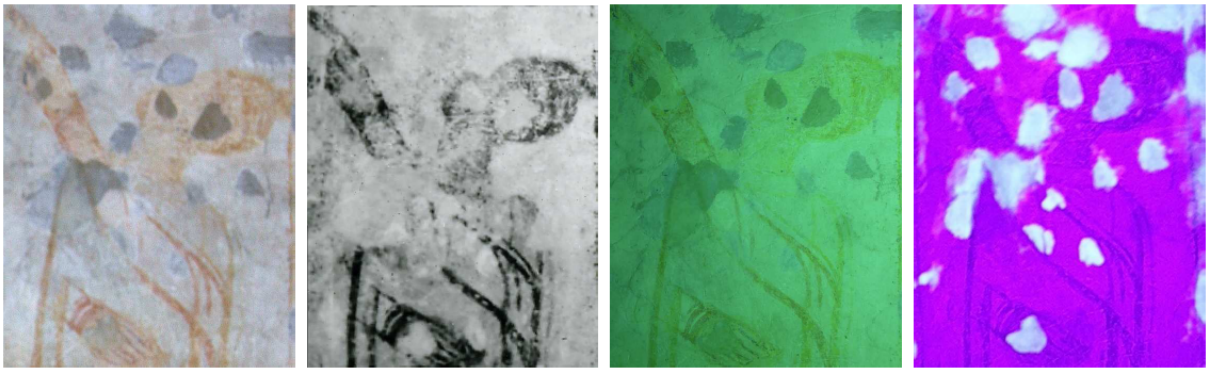
underdrawing is a preparatory drawing for a painting sketched directly on the ground. It can be found in many artworks, typically outlined with charcoal, but artists have also been known to use chalk, pencil or paint. The underdrawings are later covered with the artists medium. The drafts vary in detail from artist to artist, from simple perspective outlines to detailed sketches. Therefore, the underdrawing can provide much insight into the creative process of an individual artist. Often image acquisition in the infrared modality is used for underdrawing visualization, because the infrared waves are often capable of passing through the paint layer where the visible radiation is reflected by it.

For the image fusion, we applied contrast preserving color fusion,[11] which is a representative of the pixel-based color fusion and tries to preserve intensity changes in the input images equally, independently of the other modality. Here, the 2D rectangular color mapping scheme used for image fusion is created in such a way, that color differences as perceived by the human eye in all points are nearly the same. Fig. 6(c) shows the fused image, created from the visible and IR input images, using the blue-red color space. These part, which are depicted in almost white color, are common in both modalities, while the red and blue parts correspond to the visual and IR modality, respectively.

On the Mary Magdalene painting the IR image shows the difference in the mouth area, detected during visual inspection. While the original IR sketch (Fig. 6(b)) shows the smile on the woman face, the final painting (Fig. 6(a)) much more resembles sad, serious facial expression. However, this finding, done visually, is an example of situation, when the computer assisted approach failed. While people are trained in recognition of human expressions and moods, for automatic image processing the ratio of the difference we are interested in with respect to the painting scratches, lacunas, ageing, noise, etc. speaks for the negative influence of the painting damage, disabling any automatic analysis. We failed to detect automatically this facial difference. On the other hand, there was hidden other detail, where on the contrary the human perception failed.

Fig. 6(d) shows the close-up of the face of the lady. As it was stated, white lines correspond to sketches which are common for both modalities and red and blue color represent differences. The interesting part is the one just above the forehead. There are three line-like structures, formed into the triangle, representing the scarf folding. Such similar structures are apparent in the white color, located just below. The visual inspection is able to perceive these structures in the individual input images (see Fig. 6 (a) and (b)), however it is difficult to judge if they are located at the same place or not. The fused image clearly indicates the difference in geometry of this triangle structure in visible and IR domain.

All problems according to Preflight profile
Convert to PDF/A-2u



(a) Input images [VIS, BWS, UVB, UVN]



(b) Fresco



(b) Fused image

Figure 8. The fresco, located in Kostolany pod Tribečom, the Slovak Republic. (a) - the visible spectrum (VS) image; the old black and white photograph (BWS) from the 60s; the ultraviolet broad-band spectrum (UVB) image; the ultraviolet narrow band spectrum (UVN) image. (b) - the fresco in the church. (d) - the fused image with more profound details. Consulting R. Furbach.

The second example how the goal of the image fusion can be seen is based on the comparison of two different paintings.[12] In Fig. 7 you can see two oil paintings created by F. Amerling in 1851. The painting (a) is from the collection of Spis Muzeum in Levoča, Slovak Republic, while the (b) painting belongs to the Osijek Art Gallery in Osijek, Croatia. Both paintings represent Marianne Norman Earl Ehrenfels. The Slovak painting was not signed, the authorship was decided later. In the list of F. Amerling's painting by G. Probszt is mentioned the Croatien version. In both portraits there are the rose in the hair and small gold earring. The identity of the depicted women is very probable, however not proven. They are very similar, but the dresses and background are not identical.

There are theories the paintings were created in different times. One theory by B. Balen claims that the Slovak version is the copy of the Croatien one. However, this would imply that the copy outperforms the original. The Slovak version is more relaxed, its details are more elaborated (the rose, the collar). The second theory by J. Hradilova et al. claims that the Slovak version is the earlier version, even that the time difference was small. After the image registration of the two images we fused them to obtain the difference between the images. The squared difference of the normalized images gives us the resulting image (see Fig. 7(c)), with impressive level

All problems according to Preflight profile
Convert to PDF/A-2u

of the congruency. The fused image, where the more bright intensity represents the more prominent difference, prove the theory of the single depicted persons and, moreover, the differences encourage the idea of the Slovak original - the differences, visualized in more exact form than by their description, are exactly as expected, referring to the more smooth and not so elaborated and detailed version from the Croatia (the rose, the neck, the nose proportion).

Finally, the last application of image fusion will be presented on the wall fresco data.[13] The aim here is similar as in the first example, however the number of used modalities is higher so the source combination is even more complicated for the human observer. We would like to fuse all data into one detailed image, capturing all important aspects from all information sources.

The fresco (Fig. 8(b)) is situated in the 11th century church in Kostolany pod Tribečom, a small village in the Slovak Republic. The fresco covers large area of the inner church walls and it is heavily damaged. Restoration works have been started recently. The fresco images were acquired in the visible spectrum (VS), in the ultraviolet broad-band spectrum (UVB), and in the ultraviolet narrow band spectrum (UVN) with the spectrum maxima at 368 nm, see Fig.8 (a). Next to this, we have black and white photographs (BWS) of the fresco from the 60s (see Fig.8 (a)), which captures the fresco before aging changes during last fifty years (this channel was not used for the image fusion). All the recent image data were taken by the Czech-Geo company.

The main idea of our approach is to use principle component analysis (PCA) for the normalization of each modality channel. The resulting vectors are then averaged across the adaptively normalized channels. The resulting output image is generated from the averaged vectors by means of the neural network without hidden layers with three input and three output neurons. The neural network is trained on the combination of the input VIS image and resulting output data. In Fig. 8(c) the resulting fused image is presented. The line-like artifacts at the top right corner comes from the image registration (all the input channels had to be geometrically aligned before the fusion itself and not all modality images covers this part of the scene). The quality of the fresco is not improved, we did not used any higher level processing here, however the details from all channels are visible now at once, the details are more apparent and profound (see the cap of the person).

CONCLUSIONS

Our paper addresses problem of multi-modal data acquisition and following data visualization for art analysis and interpretation. The methodology for preprocessing the microscopic cross-section images, taken in visible and ultraviolet spectra and by means of the scanning electron microscope was presented, consisting of the image enhancement using the frequency representation of images, of the image deconvolution, and finally of image segmentation. In the second part of the paper three different image fusion techniques were demonstrated on the multispectral images and on the images acquired from different paintings, respectively. The proposed algorithms were applied on data sets from ALMA, a joint workplace of the Academy of Fine Arts in Prague and the Institute of Inorganic Chemistry of the Academy of Sciences of the Czech Republic, and from the Hamilton Kerr Institute (Dr. Spike Bucklow), University of Cambridge, United Kingdom.

ACKNOWLEDGEMENTS

The work was supported by the Grant Agency of the Czech Republic under the project No. 102/08/1593, by the Academy of Sciences of the Czech Republic under the project M100750901(financial support for international cooperation), and by the the Ministry of Education of the Czech Republic under the project No. 1M0572 (research center).

REFERENCES

[1] Hughes, S., Daubechies, I., Brasoveanu, A., Duarte, M., and Dik, J., "Underpainting Recovery with Xray Synchrotron Imaging and Image Processing," *Proceedings of The Third International Workshop on Image Processing for Art Investigation IP4AI3, USA* , 15–16 (2010).

[2] Elias, M. and Cotte, P., "Multispectral camera and radiative transfer equation used to depict Leonardo's sfumato in Mona Lisa," *Appl. Opt.* **47**, 2146–2154 (2008).

All problems according to Preflight profile
Convert to PDF/A-2u

[3] Pelagotti, A., Mastio, A. D., Rosa, A. D., and Piva, A., "Multispectral imaging of paintings," *Signal Processing Magazine IEEE* **25**, 27 – 36 (2008).

[4] Zitova, B. and Flusser, J., "Image registration methods: a survey," *Image and Vision Computing* **21**(11), 977–1000 (2003).

[5] Chambolle, A. and Lions, P., "Image recovery via total variation minimization and related problems," *Numer. Math.* **76**(2), 167188 (1997).

[6] Huang, L.-K. and Wang, M.-J., "Image thresholding by minimizing the measures of fuzziness," *Pattern Recognition* **28**(1), 41–51 (1995).

[7] Prewitt, J. and Mendelsohn, M., "The analysis of cel images," *Annals of the New York Academy of Sciences* **128**, 1035–1053 (1966).

[8] Ridler, T. and Calvard, S., "Picture thresholding using an iterative selection method," *IEEE Transactions on Systems, Man and Cybernetics* **8**, 630–632 (1978).

[9] Zack, G. and Rogers, W., "Automatic measurement of sister chromatid exchange frequency," *Journal of Histochemistry and Cytochemistry* **25**(7), 741–753 (1977).

[10] Li, H., Manjunath, B. S., and Mitra, S. K., "Multisensor image fusion using the wavelet transform," *CVGIP: Graphical Model and Image Processing* **57**(3), 235–245 (1995).

[11] Kamenicky, J. and Zitova, B., "Contrast Preserving Color Fusion," *Proceedings of SPIE IS T/SPIE Electronic Imaging 2011* , 1–6 (2011).

[12] Hradilova, J. and Mislerova, H., "Technika malby portretu 19.stoleti od Friedricha Von Amerlinga," *Acta Artis Academica* , 140–154 (2010).

[13] Blazek, J., Zitova, B., Benes, M., and Hradilova, J., "Fresco restoration: digital image processing approach," *Proceedings of the 17th European Signal Processing Conference EUSIPCO 2009* , 1–5 (2009).

All problems according to Preflight profile
Convert to PDF/A-2u



ODHALOVÁNÍ KOPIÍ POMOCÍ MATEMATICKÉHO ZPRACOVÁNÍ OBRAZU II.

PŘÍBĚH MALBY NA PLÁTNĚ S NÁMĚTEM CHLAPCE HLADÍCÍHO PTÁČKA

Janka Hradilová
Akademie výtvarných umění v Praze
Laboratoř ALMA
U Akademie 4
170 22 Praha 7
hradilovaj@volny.cz

Blanka Valchářová
soukromý restaurátor
Gagarinova 12
746 01 Opava
prudentia@volny.cz

Michal Velíšek
odborný historik
Gagarinova 12
746 01 Opava
prudentia@volny.cz

Jan Blažek
Ústav teorie informace a automatizace AV ČR, v.v.i.
Odd. zpracování obrazové informace
Pod vodárenskou věží 4
182 08 Praha 8
blazek@utia.cas.cz

ABSTRAKT

Materiálovým výzkumem neznámého obrazu byla zjištěna italská provenience anonymního díla. Vznik díla je přesněji možno zařadit jistě před konec 17. století. Na rubové stránce obrazu byl odhalen nápis *Monsù Bernardo* - možná signatura malíře Franze Wernera von Tamm. Pečlivým pátráním se nám podařilo nalézt předlohu této malby – původní obraz malovaný dánským malířem Bernhardem Keilhauem (1624 Helsingborg – 1687 Řím) a také podobnou kopii nacházející se v Polsku. Díky novému způsobu matematického zpracování obrazových dat jsme byli schopni určit, že jak český tak polský obraz jsou volnými kopiemi výše uvedeného díla, vzájemně však spolu nesouvisejí. Byly vytvořeny jinými malíři a pravděpodobně v odlišném období.

KLÍČOVÁ SLOVA: **Bernhard Keilhau alias Monsù Bernardo, Franz Werner von Tamm, komparace digitálních snímků kopií**

Datace a provenience podle materiálů

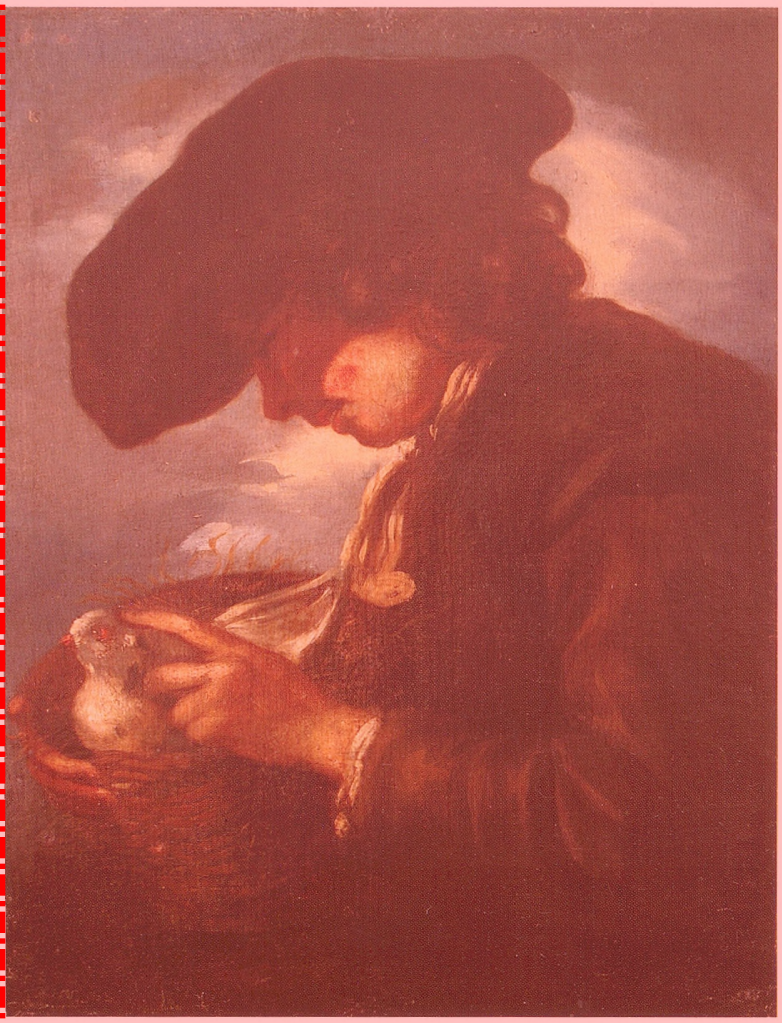
V rámci předběžného restaurátorského průzkumu[1] neznámého uměleckého díla (*obr. 1*) byla provedena i materiálová analýza dvou odebraných fragmentů. Zpočátku se zdálo, že půjde jen o rutinu a nic nenasvědčovalo tomu, že nakonec dojde k nesporné autorizaci díla. Olejomalba na plátně s rozměry 65,5x49,5 cm pochází ze soukromé sbírky a její historie nebyla vůbec známá.

Analýzou fragmentů[2] odebraných z obrazu v místě zápěstí levé ruky a v modrém pozadí bylo zjištěno, že na originální nerovnoměrně tkané lněné plátno s řídkou osnovou (v průměru 10x10 cm² nití) byl nanesen hlinkový podklad, který je směsí jílovitých hlinek a dolomitické křídy a je dále tónovaný uhlíkatou černí a miniem (Pb_3O_4). Jde tedy o podklad, který byl záměrně dobarvován. Byl nanášen ve dvou nátěrech (vrstvy 1a, b na *obr. 2*) a je pojen proteiny, pravděpodobně ve spodní části podkladu. Ve svrchním nátěru pak převládá olejové pojivo.

1 Blanka Valchářová: Restaurátorská zpráva o konzervaci obrazu.

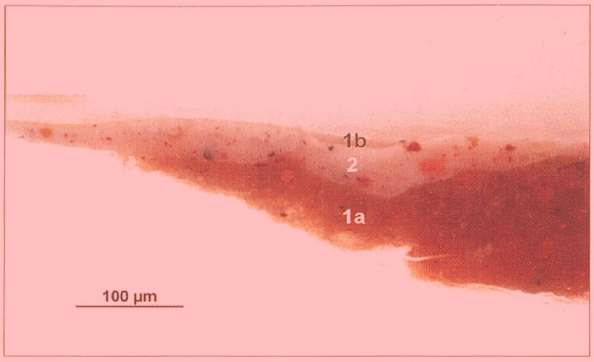
2 Drobné fragmenty byly zality do polyesterové pryskyřice Neukadur PE 45. Následně se připravily nábrusy na brusce Kompakt 1031 (Hrazdil). Studium stratigrafie bylo provedeno na mikroskopu Olympus BX 60 při zvětšení 320x v odraženém bílém světle v kombinaci bočního osvětlení a fluorescence (Hg výbojka, typ záření UVA 330-380nm) byla snímána s univerzálním UV filtrem Olympus digitálním fotoaparátem DP70. Identifikace organických látek byla provedena standardními histochemickými testy na proteiny a olej. Prvková analýza byla provedena rastrovacím elektronovým mikroskopem Philips SEM XL30 CP v Ústavě anorganické chemie AV ČR, v.v.i. v Řeži u Prahy při pracovním napětí 25kV s užitím Robinsonova detektoru odražených elektronů (RBS) a EDAX detektoru RTG záření. RTG mikrodifrakce fragmentu podkladu byla provedena v Ústavě anorganické chemie AV ČR, v.v.i. v Řeži a byla použita k přímé detekci krystalických fází. Fragment podkladové vrstvy byl měřen na difraktometru Philips X'Pert PRO s použitím monokapiláry zužující primární svazek rentgenového záření do stopy o průměru cca 150 μm.

All problems according to Preflight profile
Convert to PDF/A-2u



1 Obraz *„Chlapec hladící ptáka“* česká soukromá sbírka, stav po konzervaci díla (foto B. Valchářová)

Podle klasifikace hlinkových podkladů[3] jde o podklad typu D, obsahující jílové minerály chlorit a illit, který byl používán v italské malbě konce 16. a v průběhu 17. století. Jednovrstvá olejomalba inkarnátu (*obr. 2*) pak obsahovala olovnatou bělobu s příměsí křídy (uhličitanu vápenatého) jemně pigmentovanou miniem, rumělkou (HgS), uhlíkatou černí a smíšenou olovnatou žlutí ($Pb_2Sn_2Sb_{1.5}O_{6.75}$). Tento typ neapolské žluti je dopován cínem, který částečně zastupuje ve své struktuře antimon (Sb). V literatuře[4] je výskyt



2 Stratigrafie inkarnátu: 1. hlinkový podklad, 2. olejomalba inkarnátu (foto J. Hradilová, příčný popis v textu článku)

této směsné žluti spojen výhradně s italskou malbou 16. a 17. století, my jsme pak tento pigment identifikovali jen v malbě 19. století v okruhu vídeňské školy.[5] Tyto malby jsou však podloženy zcela odlišným typem podkladu.

Podklad typu D, který byl identifikován na tomto zkoumaném obraze, používali dle našich dosavadních srovnávacích analýz malíři působící v Itálii, např. Caravaggio (1571-1610), Jakob van de Kerckhoven zvaný také Giacomo da Castello (Antverpy 1637 - Benátky 1712), F. Bassano (1549-1592) nebo S. Magnasco (1635-1670).[6]

Je známo, že v době 17. a 18. století hodně vlámských malířů v Itálii navštěvovalo. Pro dataci spíše do 17. století ale kromě podkladu a směsné olovnaté žluti svědčí i výskyt modrého indiga v pozadí malby. Indigo je totiž starý typ modrého pigmentu, který byl postupně nahrazován umělě vyráběnou Pruskou modří. První zmínky o Pruské modři (nebo také jinak Berlínské modři) pocházejí z Berlína již z raného 17. století a je známo, že byl tento pigment dostupný a používaný na Pruské akademii umění v Berlíně nejpozději nejpozději v r. 1709.[7] Pak si Pruská modř rychle našla cestu do Paříže a dalších evropských měst (Rotterdam aj.) – to vše začátkem 18. století. Závěr materiálového průzkumu dvou vzorků tak byl překvapivě jednoznačný – jedná se o italskou malbu ze

3 Hradil D., Hradilová J., Bezdička P.: Nová kritéria pro klasifikaci a rozlišení jílových a příležitostných pigmentů různého původu - New Criteria for Classification of and Differentiation between Clay and Iron Oxide Pigments of Various Origins. In: Hradil D., Hradilová J. (Eds.), *Acta Artis Academica*, 2010 – Proceedings of the 3rd interdisciplinary conference of ALMA, Prague, November 24-25, AVU Praha, 2010, 107-136.

4 Roy A. and Berie B.H.: A new lead-based yellow in the seventeenth century. Painting Technique History, Materials and Studio Practice. Dublin Congress 7-11 Sept. 1996, 1998, 160-165 a informace z přednášky Claudia Seccaroniho na konferenci Technart 2007, Lisabon, Portugalsko.

5 Hradilová J., Mislerová H.: Technika malby portrétů 19. století od Friedricha von Amerlinga-Painting Technique of Portraits painted in the 19th Century by Friedrich von Amerling. In: Hradil D., Hradilová J. (Eds.), *Acta Artis Academica*, 2010 – Proceedings of the 3rd interdisciplinary conference of ALMA, Prague, November 24-25, AVU Praha, 2010, 137-164.

6 Hradil D., Hradilová J., Bezdička P.: Nová kritéria pro klasifikaci a rozlišení jílových a příležitostných pigmentů různého původu - New Criteria for Classification of and Differentiation between Clay and Iron Oxide Pigments of Various Origins. In: Hradil D., Hradilová J. (Eds.), *Acta Artis Academica*, 2010 – Proceedings of the 3rd interdisciplinary conference of ALMA, Prague, November 24-25, AVU Praha, 2010, 107-136 a Nepublikované zprávy archivu laboratoře Alma AVU Praha.

7 Bartoll J.: The Early Use of Prussian Blue in Painting, Art 2008, 9th International Conference, Jerusalem, Israel May 25-30, 2008, 43.

All problems according to Preflight profile
Convert to PDF/A-2u



3 Kopie obrazu Bernharda Keilhaua detto Monsù Bernardo *"Chlapec hladící ptáka"* ze sbírek Muzea Jagellonské univerzity v Krakově reprodukce z knihy: Anna Jasińska, Kopia wg. Bernharda Keilhau, Helsingborg 1624 – Rzym 1687 (Bernhard Keilhau, Helsingborg 1624 – Rome 1687) *„Chłopiec głaskający ptaka"* (A Boy Petting a Bird), Malarstwo obce w zbiorach Collegium Maius, Muzeum Universytetu Jagiellońskiego, Katalog, tom II, Wydawnictwo Uniwersytetu Jagiellońskiego, Kraków, 2003, p. 122

17. století. Toto zjištění výrazně zvýšilo zájem o dané dílo a otevřelo cestu k následnému komparativnímu výzkumu.

Hledání podobných obrazů

Polský obraz

Námětem i kompozicí velmi podobné dílo se podařilo nalézt v polském katalogu (*obr. 3*)[8], kde je tento téměř shodný obraz veden jako *„Kopie Bernharda Keilhaua - Chlapec hladící ptáka"*. Jedná se o olejomalbu na plátně s rozměry 62x47,5 cm, obraz je bez signatury s evidenčním číslem 5732. Je datován na rozhraní 17. a 18. století a pochází ze sbírky Muzea Jagellonské univerzity v Krakově.

V textu polského katalogu nechybí zmínka o původní předloze, kterou je údajně obraz od dán-

8 Jasińska A.: Kopia wg. Bernharda Keilhau, Helsingborg 1624 – Rzym 1687 (Bernhard Keilhau, after Helsingborg 1624 – Rome 1687) „Chłopiec głaskający ptaka (A Boy Petting a Bird), Malarstwo obce w zbiorach Collegium Maius, Muzeum Universytetu Jagiellońskiego, Katalog, tom II, Wydawnictwo Uniwersytetu Jagiellońskiego, Kraków 2003, 122–123.



4 *„Chlapec hladící ptáka"* neboli *„Alegorie hmatu"*, kolem r. 1652; olej na plátně soukromá sbírka v Paříži; reprodukce z knihy: Minna Heimbürger, Bernard Keilhau detto Monsù Bernardo,Ugo Bozzi Editoriale, Roma, 1988, p.175, katalogové číslo 50

ského malíře Bernharda Keilhaua (1624 Helsingborg – 1687 Řím), nacházející se v soukromé sbírce v Paříži[9] (*obr. 4*). Podle polské historičky umění Anny Jasińské (2003)[10] obraz představuje scénu, která je alegorií hmatu, což je námět typický pro holandskou malbu.

Obraz od Bernharda Keilhaua a jeho inspirace podle mědirytin

Olejomalba na plátně o rozměrech 65x49 cm (*obr. 4*) *„Chlapec hladící ptáka"* (neboli *„Alegorie hmatu"*), je datována přibližně do roku 1652 a popsána je v knize od Minny Heimdürger (1988). Autorka[11] popisuje originální malbu od Bernharda Keilhaua, známého také v italském prostředí pod jménem Monsù Ber-

9 Heimbürger M.: Bernardo Keilhau detto Monsù Bernardo, Ugo Bozzi Editoriale, Roma, 1988, 175. Katalogové číslo obrazu 50.

10 Jasińska A.: Kopia wg. Bernarda Keilhau, Helsingborg 1624 – Rzym 1687 (Bernard Keilhau, after Helsingborg 1624 – Rome 1687) „Chłopiec głaskający ptaka (A Boy Petting a Bird), Malarstwo obce w zbiorach Collegium Maius, Muzeum Universytetu Jagiellońskiego, Katalog, tom II, Wydawnictwo Uniwersytetu Jagiellońskiego, Kraków 2003, 122 -123.

11 Heimbürger M.: Bernardo Keilhau detto Monsù Bernardo, Ugo Bozzi Editoriale, Roma, 1988, 175. Katalogové číslo obrazu 50.

All problems according to Preflight profile
Convert to PDF/A-2u



5 Rytina *„Dítě s ptačím hnízdem v opici“* od Cornelise Bloemaerta, 1625, © The Trustees of the British Museum



6 Rytina *„Chlapec a ptáček v kleci“* od Cornelise Bloemaerta, 1625, © The Trustees of the British Museum

nardo. Podle ní malíř prezentuje nepatrně pozměněnou verzi vlámsko-holandské malby s námětem dívky nebo chlapce (v některých případech obou) s ptáčkem v kleci nebo z klece vyletujícího. V tomto případě je klasický motiv [illegible] pozměněn (klec byla nahrazena hnízdem).[12]

Dále se Minna Heimdürger (1988) ve své knize zmiňuje, že *“významným kompozičním prvkem u malíře je motiv klobouku se širokým lemem monumentálním způsobem ohraničující hlavu, přičemž autor využívá efektu vznikajícího proti prosvětlenému pozadí. Tento prvek vychází z Utrechtské školy – tj. školy Utrechtských carravaggistů – a stal se jedním z oblíbených Keilhauových motivů.*

Obraz od Bernharda Keilhaua alias Monsù Bernardo byl podle Minny Heimbürger inspirován rytinou *„Dítě s ptačím hnízdem v opici“* od Cornelise Bloemaerta[13] (*obr. 5*). Malířská rytina pochází z roku 1625 a je o rozměrech 16,7x11,8 cm.[14] Cornelis tvořil rytiny podle kompozice malby svého bratra Hendricka Bloemaerta.[15] V katalogu prací Cornelise Bloemaerta[16] na podobné téma byla nalezena také rytina s námětem *„Chlapec a ptáček v kleci“* (*obr. 6*) o shodných rozměrech: 16,7x11,8 cm. Ve sbírce britského muzea je datována rokem 1625 a je opět údajně inspirovaná malbou svého bratra Hendricka nebo otce Abrahama. V Muzeu Boymans-van Beuningen v Rotterdamu existuje kresba *„Chlapec s ptáčkem v kleci“* (*obr. 7*) od Abrahama Bloemaerta z roku 1566 o rozměrech 13x12 cm. Proti rytině od Cornelise Bloemarta je ale stranově obrácena.[17]

12 Heimbürger M.: Bernardo Keilhau detto Monsù Bernardo, Ugo Bozzi Editoriale, Roma, 1988, 175. Katalogové číslo obrazu 50.

13 Cornelis Bloemaert II (1603 Utrecht – 1692 Řím) se vyučil jako malíř, ale věnoval se převážně grafické tvorbě. Po roce 1630 pracoval v Paříži, posléze v roce 1633 odešel do Říma. V Itálii vytvářel podle malířských předloh rytiny mnoha italských obrazů (podle knihy od Arthur Mayger Hind, A history of engraving & etching, Menno Hertzberger, Amsterdam, Koch & Knuttel at Gouda, 1963, 122) a http://en.wikipedia.org/wiki/Cornelio_Bloemaert, 19.8. 2012.

14 Holstein H. F. W.: Dutch and Flemish Etchings, Engravings and Woodcuts ca 1450-1700, Berckheyde - Bodding, 2, Berckheyde-Bodding, Amsterdam, Koch & Knuttel at Gouda, 1888-1957, 70-82. Dílo je uvedeno pod katalogovým číslem 293.

15 Hendrick Bloemaert (1601 nebo 1602 Utrecht - 1672 Utrecht) byl malířem a bratr Cornelise Bloemearta a nejstarší syn Abrahama Bloemerta, byl považován za dědečtího člena utrechtských Caravaggistů.

16 Holstein H. F. W.: Dutch and Flemish Etchings, Engravings and Woodcuts ca 1450-1700, Berckheyde - Bodding, 2, Berckheyde-Bodding, Amsterdam, Koch & Knuttel at Gouda, 1888–1957, 70–82. Dílo je uvedeno pod katalogovým číslem 294.

17 Reproduction H. Kleinmann & Co. Haarlem, (13x12 cm). Series IV, plate 46.

All problems according to Preflight profile
Convert to PDF/A-2u



7 Kresba *„Chlapec a ptáče v kleci“* od Abrahama Bloemaerta, 1566, © Niederländische Zeichnungen, Band VI, 46

V knize Minny Heimbürger dále stojí za povšimnutí, že jak u obrazu *„Chlapec krmící ptáče“* (neboli *„Alegorie chuti“*)[18] tak i u námi sledovaného obrazu *„Chlapec hladící ptáče“ („Alegorie hmatu“)* je zmíněna pozdější existence pandantu hlubotisku od britské tiskařky Caroline Watson (1760–1814) (*obr. 8*). Podle William Stirling-Maxwell (1873) grafiky o rozměrech 9,1x7 cm vznikly v roce 1781.[19] Obě olejomalby dnes připisované Monsù Bernardo byly v minulosti připisovány Bartolomé Esteban Murillovi.[20]

Kdo byl Bernhard (Eberhard) Keilhau alias Monsù Bernardo

Bernhard (Eberhard) Keilhau se narodil roku 1624 v Helsingborgu v rodině německého malíře Caspara Kegelhoffa (Keilhau), který se usadil v Dánském království. První umělecké schopnosti získal od svého otce. Pracoval v dílně dánského malíře Mortena van Steenwinckela (1595–1646). V letech 1642–51 působil v Holandsku ve městech Utrecht a Amsterdam, tři roky potom (1642-1644) strávil v atelieru Rembrandta Harmenszoon van Rijn. Krátce pak působil ve Frankfurtu, Mohuči, Ausburgu a v Kolíně nad Rýnem. Od roku 1651 pracoval v Benátkách a Bergamu. Po roce 1656 se odstěhoval do Říma, kde strávil druhou část svého pohnutého života. Vytvořil nový umělecký styl, v Itálii nazývaný stylem „Monsù Bernardo“. Žánrové obrazy mistra byly úspěšné, a proto se v Římě usadil natrvalo. V roce 1687 zemřel.[21] Někteří historici označují tohoto malíře i jako německo-dánského.



8 Hlubotisk od britské tiskařky Caroline Watson (1781); reprodukce z knihy: Minna Heimbürger, Bernardo Keilhau detto Monsù Bernardo, Ugo Bozzi Editoriale, Roma, 1988, p. 175, katalogové číslo 50

Odhalení skrytého autorství

Při prohledávání rubové strany obrazu v rámci předběžného průzkumu[22] byl na dublovacím lněném plátně tkaném nerovnoměrně s hustotou osnovy 10x8 nití na cm² zjištěn nápis *F. H. angekauft 1854*. Jde zřejmě o zmínku o přírůstku do sbírky. Po sejmutí starého dublovacího plátna se ale objevila rubová strana originálu s hrubou osnovou, na jejímž povrchu byl nápis jiný *Monsù Après*. Nápis byl psaný černou barvou v jemných liniích (*obr. 9*).

Termín *Après* (*d'après*) se sice ve francouzštině používá pro určení předlohy (ve smyslu „podle“), správně by však potom mělo být *Après Monsù Bernardo*. Tento nápis ve francouzštině by musel být doplněn někde ve frankofonních zemích, což zatím není nikterak nezávisle zdokumentováno. Podle zjištění archivů[23], by se ale v tomto případě mohlo jednat i o vlastní podpis autora. Jeden malíř totiž podpis

8 Heimbürger M.: Bernardo Keilhau detto Monsù Bernardo, Ugo Bozzi Editoriale, Roma, 1988, 174. Katalogové číslo obrazu 49.

9 Stirling-Maxwell W.: Essay Towards a Catalogue of Prints engraved from the Works of Diego Rodríguez de Silva y Velázquez and Esteban Murillo, London, 1873, 114.

20 Angulo Iñiguez, Diego, Murillo: Su vida, su arte, su obra, Madrid, 1981, vol. 1-3: Catàlogo critico, under no. 2516, 2515, Espada-Calpe a William Stirling-Maxwell, Essay Towards a Catalogue of Prints engraved from the Works of Diego Rodríguez de Silva y Velázquez and Esteban Murillo, London, 1873, 114.

21 Heimbürger M.: Bernardo Keilhau detto Monsù Bernardo, Ugo Bozzi Editoriale, Roma, 1988, 8-106; Filippo Baldinucci, Domenico Maria Manni, Eberhard Keilhau (Kailo) Di Helsingor in Danimarca pittore detto Fra Noi Monsù Bernardo Discepolo di Rembrant Van Rein (1624-1687) Notizie dei professori del disegno da Cimabue in qua, 1812, 413-428 a http://it.wikipedia.org/wiki/Mons%C3%B9_Bernardo, 19. 8. 2012.

22 Ibidem 1

23 James M. Bower, Murtha B. Getty, Union List of Artist Names: Aa-Dzw, Thomson Gale, 1994 a http://www.getty.edu/vow/ULANFullDisplay?find=Tamm%2C+Franz+Werner+von&role=painter&nation=german&page=1&subjectid=-1&checked=500017541, 19. 8. 2011.

All problems according to Preflight profile
Convert to PDF/A-2u



9 Signatura Monsù d'Apré na rubové straně originálního plátna obrazu z české soukromé sbírky „*Chlapec hladící ptáča*" (foto B. Valchářová)



10 IR reflektografie obrazu z české soukromé sbírky „*Chlapec hladící ptáča*" (foto J. Blažek)

Monsù d'Apré skutečně používal - jmenoval se Franz Werner von Tamm (1658-1724).

Franz Werner von Tamm se narodil v Hamburku. Byl to italsko-vlámsky orientovaný malíř kvetinových a loveckých zátiší. Von Tamm používal jeho dalších devatenáct různých podpisů z německého, francouzského a italského jazyka (např. *Monsieur da Pré, Mons.r Duprat, Monsù Daprait*) aj.[24] Podle Rijksbureau voor Kunsthistorische Documentatie (RDK) v Hágu byla jeho přezdívka také *Dapper* nebo *Aprêt*.

Na vývoj Franze Wernera měli v rané fázi vliv Dietrich von Sosten a Johann Joachim Pfeiffer. Později ovlivnil von Tamm z Hamburku odešel do Říma, kde v letech 1685-1695 výtvarně působil. Byl členem spolku Bentvueghels[25] podobně jako Cornelis Bloemaert a David de Konick, kterými byl také ovlivněn.

Po desetiletém italském období odchází Franz Werner von Tamm v roce 1702 do Pasova a dále působí jako dvorní malíř u císaře Leopolda I. na rakouském císařském dvoře ve Vídni, kde také v roce 1724 umírá. Lichtenštejnské muzeum (bývalá Die fürstlich Liechtensteinsche Galerie) a také obrazárna Uměnecko-historického muzea (Kunsthistorisches Museum) ve Vídni jsou vlastníkem několika jeho obrazů.[26]

Bernhard Keilhau detto Monsù Bernardo (autor originálního obrazu) zemřel dva roky po Tammově příchodu do Itálie. Je tak otázkou, zda von Tamm vytvořil kopii jeho za života Keilhaua, nebo byla kopie až posmrtným odkazem k původní malbě. Sociální život von Tamma v Itálii je znám v hrubých obrysech - práce s Peterem van Bloemenem, Karlem van Vogelaerem a jeho tvůrčí vztah s Carlem Marattim. V literatuře[27] existuje i zmínka, že Franz Werner von Tamm měl v Římě svého žáka jménem Pietro Navarra. Ten se údajně zúčastnil workshopu Bernharda Keilhaua jako student v roce 1686. Dokládá snad tato stopa, že se Franz Werner von Tamm a Bernhard Keilhau osobně znali a přímo spolupracovali?

Předesílám, abychom mohli potvrdit, že naše anonymní dílo je skutečně malbou Franze Wernera von Tamm, bylo by užitečné obraz porovnat s malbami podepsanými *Monsù d'Apré* vzniklými v Itálii. Zatím se nám ale tato možnost nenaskytla a navíc figurální

24 James M. Bower, Murtha B. Getty, Union List of Artist Names: Aa-Dzw, Thomson Gale, 1994 a http://www.getty.edu/vow/ULANFullDisplay?find=Tamm%2C+Franz+Werner+von&role=painter&nation=german&page=1&subjectid=-1&checked=500017541, 19. 8. 2011.

25 Spolek nebo společnost sdružující kolem 70-ti holandských nebo vlámských – a obecně „severských" -umělců (malířů, sochařů, grafiků a básníků), působících v Římě od roku asi 1620 do roku 1720. Jejich bujará činnost byla papežem Klimentem XI. v roce 1720 zakázána. Členem této společnosti byl podle RDK i Karel Škréta.

26 Lier, Hermann Arthur, „Tamm, Franz Werner", in: Allgemeine Deutsche Biographie 37 (1894), 363-364 [Onlinefassung]; URL: http://www.deutschebiographie.de/pnd11935540X.html?anchor=adb, 19. 8. 2012.

27 Heimbürger M.:, Bernardo Keilhau detto Monsù Bernardo,Ugo Bozzi Editoriale, Roma, 1988, 244. Jde o popis obrazu se signaturou P.N., přisuzovaného Pietro Navarrovi, žáku Franze Wernera von Tamm. Katalogové číslo obrazu 183.

All problems according to Preflight profile
Convert to PDF/A-2u



A B C

11 Digitální porovnání obrazů s motivem chlapce hladícího ptáčka metodou barevného odlišení - porovnání jasu dvou obrázků (viz 1. část tohoto příspěvku od Blažka a kol. v tomto sborníku); (A) porovnání grafiky od Caroline Watson (1781) oválného tvaru (červená) a originálního obrazu od Monsú Bernardo (zelená); (B) porovnání grafiky od Caroline Watson (1781) oválného tvaru (červená) a polské kopie obrazu z Muzea Jagellonské univerzity v Krakově (modrá); (C) porovnání grafiky od Caroline Watson (1781) oválného tvaru (červená) a kopie obrazu z české soukromé sbírky (žlutá); červená barva převládá v místech, kde je malba rytiny proti obrazům světlejší; zelená, modrá nebo žlutá barva je vždy dominantní tam, kde je světlejší příslušný obraz

malba nebyla pro tohoto autora zrovna typická.[28]

Infračervená fotografie[29] ukazuje na kresbu a místa pořízení malby (*obr. 10*). Čitelnost infračervené fotografie je ovlivněná malým kontrastním podkladem,

28 Podle informací od Dr. Z. Kazlepky Franz Werner von Tamm byl vynikajícím malířem dekorativních zátiší a drobného zvířectva, figurální složku (např. putti) do jeho děl malovali jiní malíři. Obrazy ve Vizovicích a Valticích od Franze Wernera Tama jsou signovány italsky „Frances(co) v. tam f. …“ a „Fran(co) v. tam f. …“ V městském muzeu Hazebrouck ve Francii s limitovanou sbírkou obrazů vlámské a francouzské provenience se však od daného umělce vyskytuje obraz „Le Boucher (Řezník)“, který je figurální malbou a je malován technikou obrysu.

29 Pořízeno upraveným fotoaparátem Canon EOS 50 pro snímání v IR spektru. Pro pořízení byly použity pásmové filtry pro viditelné spektrum (480–680) a blízké IR spektrum (950nm). Po osvětlení bylo využito denní světlo (viditelné spektrum) a tepelné žárovkové spektrum (NIR). Obraz byl nasvícen zezadu (doporučení I. Fogaš).

All problems according to Preflight profile
Convert to PDF/A-2u


A


B


C

12 Vzájemné digitální porovnání obrazů s motivem chlapce hladícího ptáčka metodou barevného odlišení - porovnání jasu dvou obrázků (viz 1. část tohoto příspěvku od Blažka a kol. v tomto sborníku); (A) porovnání originálního obrazu od Monsu Bernardo (zelená) s kopií obrazu z české soukromé sbírky (žlutá) a polské kopie obrazu z Muzea Jagellonské univerzity v Krakově (modrá); (B) porovnání kopie obrazu z české soukromé sbírky (žlutá) s originálním obrazem od Monsu Bernardo (zelená); (C) porovnání polské kopie obrazu z Muzea Jagellonské univerzity v Krakově (modrá) a kopie obrazu z české soukromé sbírky (žlutá); zelená, modrá [illegible] žlutá barva je vždy dominantní tam, kde je příslušný obraz svůj

který není bílý. Podklad obsahuje hlinky. Kresba je průsvitná, dobře patrná. Jde o malbu vysoké kvality. Ve světlých místech jsou vidět drobná vrstevnatá položení tváře chlapce, krku s vlasy a ruky hladící ptáčka. Známé položení je viditelné v hnízdě ptáčka pod jeho tělíčkem a v proutěném košíku. Stejná položení lze sledovat i na všech okrajích obrazu. Kresba proporčně sedí s malbou italského obrazu od Monsu Bernardo.

Matematické zpracování obrazů

Komparace hlubotisku s olejomalbami

Všechny tři srovnávané obrazy (český, polský a původní) jsme nejprve porovnali s hlubotiskem z roku 1781 (*obr. 7*) přisuzovaným britské tiskařce

All problems according to Preflight profile
Convert to PDF/A-2u

Caroline Watson (1760–1814). P[illegible] digitálním porovnání metodou barevného odli[illegible]ní, kdy porovnáváme [illegible]as dvou obrázk[illegible] (viz první [illegible]ást tohoto p[illegible]spěvku – [illegible]lík a kol.), jsme vygenerovali celkem t[illegible] slo[illegible]né digitální obrázky *(obr. 11 a, b, c)*. Porovnáním hlubotisku oválného tvaru ([illegible]ervená) s reprodukcí p[illegible]vodního obrazu od Mons[illegible] Bernardo (zelená) (reprodukce z knihy M. Heimdürger, 1988) *(obr. 11a)* jsme zjistili, [illegible]e u malby jsou viditelné rozdíly ve velikosti t[illegible]a a hlavy chlapce, dále ve velikosti klobouku a v posunu oka, v umíst[illegible]ní a velikosti pt[illegible]ka. [illegible]ervená barva p[illegible]vládá v místech, kde je malba rytiny oproti obrazu sv[illegible]lejší a zelená barva je zase dominantní tam, kde je sv[illegible]lejší obraz. U malby v[illegible]ho rukávu na rytin[illegible] je posunuta záplata na rameni kord[illegible]le. Na obraze chybí malba [illegible]ad patrná v grafice. Posunutá je ruka dr[illegible]cí hnízdo pt[illegible]ka. V malb[illegible] hladící ruky jsou prodlou[illegible]ené prsty a viditelné i jemné posuny prst[illegible] Šátek je v[illegible]razn[illegible]jší než u grafického tisku.

Z komparace hlubotisku ([illegible]ervená) s reprodukcí polského obrazu (modrá) vznikl rovn[illegible]ž slo[illegible]ený obrázek *(obr. 11b)*. Modrá barva p[illegible]vládá v místech, kde v malb[illegible] polského obrazu jsou místa oproti rytin[illegible] sv[illegible]lejší, a [illegible]ervená barva je zase dominantní tam, kde je sv[illegible]lejší rytina.

Podle komparace je vid[illegible], [illegible]e proporce a kompozice malby jsou t[illegible]m[illegible]r shodné. Viditelná shoda je p[illegible]edevším v malb[illegible] rukávu s rukou hladící pt[illegible]ka. Hlava pt[illegible]ka (kromě rozdílu v oku) zcela kopíruje zobrazení na grafice. Velmi zajímavá je i v[illegible]razná shoda prout[illegible]ného kon[illegible]ku, a oka chlapce. Klobouk je ale tvarov[illegible] odli[illegible]ný. Záplata a malba rukávu u vestičky kabátku je jiná. Úpln[illegible] jiný je na grafice fald v podpa[illegible]. Tělo pt[illegible]ka zcela kopíruje grafiku s v[illegible]jimkou kord[illegible]el. Mezi proutím kon[illegible]ku prosvítá bílé pe[illegible] operen[illegible]ce. Malba oka chlapce se p[illegible]bližuje zobrazení na grafice. Vyniká zde v[illegible]k[illegible]dlité ukon[illegible]ení [illegible]atku. V[illegible]znamný rozdíl je i v množství slámy [illegible]ouhající z hnízda – malé množství stébel se více podobá originálnímu obrazu od Mons[illegible] Bernardo než hlubotisku. I p[illegible]es n[illegible]které tyto rozdíly je ale smysluplné se ptát, zda-li malí[illegible] polského [illegible]brazu znal i hlubotisk. Vylou[illegible]eno to není, proto[illegible]e polský obraz byl pouze p[illegible]ibližn[illegible] datován na p[illegible]elom 17. a 18. století, může b[illegible]t ale i pozd[illegible]ji. Tato otázka naopak nemá smysl v p[illegible]ípad[illegible] obrazu z [illegible]ské soukromé sbírky. P[illegible] jeho srovnání ([illegible]lutá) s hlubotiskem ([illegible]ervená) *(obr. 11 c)* byly totiž zji[illegible]t[illegible]ny v[illegible]razné proporční rozdíly. Souvislost s grafikou tu tedy není, což je logické, uvá[illegible]íme-li již dolo[illegible]ený vznik [illegible]brazu v 17. století a grafiky v roce 1781.

U v[illegible]ech obraz[illegible] chybí oproti hlubotisku st[illegible], na kterém je polo[illegible]ené hnízdo. Je tak zřejmé, [illegible]e kompozice grafiky je ovlivn[illegible]na jiným námětem od Mons[illegible] Bernardo (viz. v[illegible]še).[30]

30 Jde o obraz uveden[illegible] v poznámce 18.

Vzájemná komparace [illegible]leje[illegible]male[illegible]

Na obrázku 12a (*obr. 12a*) je porovnána reprodukce obrazu od Mons[illegible] Bernardo (zelená) a polského obrazu [illegible]modrá]. Malba mohutn[illegible]ho rukávu s faldy u polského obrazu kopíruje ruku [illegible]brazu malovaného Mons[illegible] Bernardo. Témě[illegible] shodn[illegible] je fald v podpa[illegible]. Zde namalovan[illegible] fald se nevyskytuje na grafice (viz výše). Obrazy se proporčn[illegible] neshodují v malb[illegible] hlavy pt[illegible]ka a ve velikosti jeho t[illegible]la. Bohatší je malba [illegible]atku kolem krku chlapce u polského obrazu. Malba polského obrazu je celkov[illegible] posunuta sm[illegible]rem dol[illegible] P[illegible] srovnání v bílém sv[illegible]le má chlapec v[illegible]razn[illegible] zakon[illegible]ení tmavé vestičky. Kopista dodr[illegible]el i [illegible]lutou barevnost rukávu kord[illegible]le.

Srovnání kopie z [illegible]ské soukromé sbírky ([illegible]lutá) s reprodukcí obrazu od Mons[illegible] Bernardo (zelená) *(obr. 12b)* poukazuje na ur[illegible]té rozdíly v malb[illegible] klobouk[illegible] U [illegible]ského obrazu je del[illegible] ruka u rukávu kord[illegible]le s tkaninou. Jinak jsou ale proporce obraz[illegible] témě[illegible] srovnatelné. Posuny prst[illegible] v malb[illegible] hladící ruky souvisí s del[illegible]m rukávem. V[illegible]razná shoda je v malb[illegible] hlavy (tváře, ústa) a ruky dr[illegible]cí hnízdo. Zm[illegible]ny jsou patrné v malb[illegible] [illegible]atku kolem krku. Jiné ve snímcích v bílém sv[illegible]le jsou jasné zm[illegible]ny barevnosti v malb[illegible] hn[illegible]dého kabátku chlapce a modrého pozadí (srovnej *obr. 1 a 4*). Obraz z [illegible]ské sbírky zjednodušen[illegible] zobrazuje malbu slámy lemující prout[illegible]ný kon[illegible]k. Žánrová malba volně prochází do malby pozadí. V pozadí prosvítá podklad. Obraz byl již n[illegible]kdy restaurován. V minulosti byl podlepen nov[illegible]m plátnem za pomoci klihu. Okraje lemovala nevhodná papírová lepící páska. Došlo k aplikaci nevyhovujícího laku, a proto se na povrchu vytvo[illegible]ily stékance. Laková vrstva posléze ztmavla a došlo k jejímu zakalení, což v[illegible]razn[illegible] omezilo [illegible]itelnost malby. Z matematického srovnání nicmén[illegible] vyplývá, [illegible]e jde pravd[illegible]podobn[illegible] o volnou kopii obrazu od Mons[illegible] Bernardo.

Na komparaci polského obrazu (modrá) a obrazu z [illegible]ské sbírky ([illegible]lutá) *(obr. 12c)* je vid[illegible] v[illegible]razný vzájemný posun. Znač[illegible]nou robustnost[illegible] je polská kopie. Viditeln[illegible] je rozdíl v malb[illegible] rukávu s bílou tkaninou a v malb[illegible] prst[illegible] dr[illegible]cích prout[illegible]ný kon[illegible]k. Je celkem viditelné, [illegible]e obrazy nejsou rozm[illegible]rov[illegible] shodné, a je tedy více než pravd[illegible]podobné, [illegible]e je nemaloval stejný malí[illegible] Nebyly ani vytvo[illegible]eny jeden podle druhého. V obou p[illegible]ípadech jde sice o volné kopie originální malby od Mons[illegible] Bernardo, spolu v[illegible]ak vzájemn[illegible] nesouvisejí. Toto tvrzení by se m[illegible]lo je[illegible] potvrdit srovnáním materiálového pr[illegible]zkumu obou obraz[illegible] V sou[illegible]asné dob[illegible] ale nebylo možné tento komparativní v[illegible]zkum provést.

Závěr

Matematické zpracování digitálního obrazu nám usnadnilo prokázat, [illegible]e anonymní obraz z [illegible]ské soukromé sbírky s námětem chlapce hladícího pt[illegible]ka

All problems according to Preflight profile
Convert to PDF/A-2u

„*Alegorie hmatu*" je volnou kopií obrazu od Bernharda Keilhaua alias Monsù Bernardo (1624–1687), který byl namalován pravděpodobně v roce 1652. Materiálový výzkum podkladu malby a pigmentů jednoznačně dokládá, že tato kopie je italské provenience a vznikla nejpravděpodobněji také v 17. století. Jejím autorem by mohl být Franz Werner von Tamm (1658–1724), coţ by vedle kvality malby mohla dokládat (možná) originální signatura nebo popis autorství *Monsù d'Apré* na zadní straně původního plátna, kterou tento malíř prokazatelně používal (vedle jiných). Oba malíři se také nejen kolem roku 1686 potkali, ale po krátkou dobu snad i spolupracovali.

Další podobná olejomalba, tentokrát ze sbírky Muzea Jagellonské univerzity v Krakově je rovněţ volnou kopií stejného výchozího díla. Obrazová analýza však vylouţila moţnost, ţe by obě kopie (česká a polská) byly navzájem ovlivněny. Polská kopie byla podobně datována na přelom 17. a 18. století, je ale možné, že vznikla i později. Neznámý kopista totiţ zřejmě znal grafické listy se stejným námětem od Caroline Watson (1781) – určité významné podobnosti srovnávací obrazová analýza ukazuje. Abychom mohli lépe určit původ polské kopie, bylo by třeba provést materiálovou analýzu.

Výsledky, vedoucí k určení datace, provenience a autorství anonymního obrazu z české soukromé sbírky jsou založeny na nedestruktivních metodách, matematickém zpracování obrazových dat, historické rešerši a jsou podepřeny materiálovou analýzou pouze dvou odebraných vzorků. S využitím moderních postupů komparativního přístupu a nálezů znalosti věcí s mezioborovým přesahem tak mohou být velmi cenná a přesná data získána maximálně šetrným způsobem.

PODĚKOVÁNÍ

Autoři článku děkují za provedení a interpretaci instrumentálních analýz kolegům z laboratoře ALMA D. Hradilovi, P. Bezdičkovi a S. Švarcové. Dále děkují V. Kotrbové a P. Bauerové za pomoc při hledání obtíţně dostupné literatury. Výzkum byl proveden za podpory grantu GAČR P103/12/2211.

All problems according to Preflight profile
Convert to PDF/A-2u



DETECTION OF COPIES USING MATHEMATICAL PROCESSING OF IMAGES II.

STORY OF A PAINTING ON CANVAS OF A BOY PETTING A BIRD

Janka Hradilová
Academy of Fine Arts in Prague
Laboratory ALMA
U Akademie 4
170 22 Praha 7
Czech Republic
hradilovaj@volny.cz

Blanka Valchářová
freelance restorer
Gagarinova 12
746 01 Opava
Czech Republic
prudentia@volny.cz

Michal Velíšek
professional historian
Gagarinova 12
746 01 Opava
Czech Republic
prudentia@volny.cz

Jan Blažek
Institute of Information
Theory and Automation
of the AS CR, v.v.i.
Image processing department
Pod vodárenskou věží 4
182 08 Praha 8
Czech Republic
blazek@utia.cas.cz

ABSTRACT

Material investigation of a painting by an unknown author has identified its Italian provenience. The origin of the work of art can be definitely dated back before the end of the 17th century. The inscription Monsù Bernardo Apré was found on the back side of the painting – a possible signature by the painter Franz Werner von Tamm. Our detailed search has lead to identification of a model of this picture – original painting by the Danish painter Bernhard Keilhau (1624 Helsingborg – 1687 Rome) and also to finding of another similar copy in Poland. Thanks to a new method of mathematical image data processing, we have been able to determine that both the Czech and the Polish paintings are loose copies of the artwork identified above, however without any mutual relation between them. They were created by different painters and probably at different times.

KEY WORDS: **Bernhard Keilhau alias Monsù Bernardo, Franz Werner von Tamm, comparison of digital images of copies**

Dating and provenience based on the materials

A preliminary restoration investigation of an anonymous artwork *(Fig. 1)*[1] included a material analysis of two fragment samples. Initially, the analysis was considered a routine activity and nothing suggested that the author of the work of art would be eventually positively identified. The oil painting on canvas 65.5x49.5 cm came from a private collection and its history was completely unknown.

The analysis of the fragments[2] collected from the painting from the left hand wrist and from the blue background has shown that the original uneven woven flax linen with a light warp (on average 10x10 thread per cm^2) was covered with an earthy ground, which was a mixture of iron earths and dolomitic chalk, and subsequently tinted with carbon black and red lead (Pb_3O_4). This means that the ground was intentionally toned. It was applied in two coats and proteins were used as binders, mostly in the bottom coat of the ground. Oil binder prevailed in the upper coat. In reference to classification of earthy

1 Valchářová B.: Restorer´s report about the painting conservation.

2 Small fragments were embedded in polyester resin Neukadur PE 45. Subsequently, specimens were prepared on the Kompakt 1031 grinder (Hrazdil). Stratigraphy was examined with the Olympus BX 60 microscope using 320x magnification in reflected white light in combination with lateral illumination and fluorescence (Hg discharge lamp, UVA 330-380nm) was recorded with the Olympus digital camera DP70 with a universal UV filter. Identification of organic stuff was performed by means of standard histochemical tests for proteins and oil. Elemental analysis was performed by means of the scanning electron microscope Philips SEM XL30 CP in the Institute of Inorganic Chemistry of the Academy of Sciences of the Czech Republic (AV ČR, v.v.i.) in Řež using the working voltage of 25kV and Robinson Backscattered Electron (RBS) detector and EDAX detector of X-rays. X-ray microdiffraction of a ground fragment was performed in the Institute of Inorganic Chemistry of AV ČR, v.v.i. in Řež and it was used for direct detection of crystalline phases. A fragment of the ground was measured on the Philips X'Pert PRO diffractometer using a monocapillary which constricts the primary X-ray beam into a track with the diameter of ca. 150 μm.

All problems according to Preflight profile
Convert to PDF/A-2u

grounds, this is the type D, containing clay minerals, specifically chlorite and illite, used in Italian paintings at the end of the 16th and in the 17th century. A one-layer oil painting of the incarnate (*Fig. 2*) contained lead white with an admixture of chalk (calcium carbonate), slightly pigmented with red lead, cinnabar (HgS), carbon black and mixed lead yellow ($Pb_2Sn_2Sb_{1.5}O_{6.75}$). This type of Naples yellow contains an admixture of tin, which partly replaces antimony (Sb) in its structure. In literature,[4] occurrence of this mixed yellow is connected exclusively with Italian painting in the 17th century (or sometimes also in the late 16th century), while we have identified this pigment also in 19th century paintings belonging to the Vienna Academy circle.[5] The latter paintings, however, had a completely different type of a ground.

The earthy grounds of the D type, as identified on the examined painting, was used, according to our previous comparative analyses, by painters working in Italy, e.g. Caravaggio (1571–1610), Jakob van de Kerckhoven alias Giacomo da Castello (Antwerp 1637 – Venice 1712), F. Bassano (1549–1592) or S. Magnasco (1635–1670).[6]

It is a know fact that in the 17th and 18th century many Flemish painters visited Italy. Moreover, apart from the earthy ground and the mixed lead yellow, the dating in the 17th century is also supported by presence of blue indigo on the background of the painting. Indigo is actually an older type of blue pigment, which was gradually replaced by artificially produced Prussian blue. First references to Prussian blue (or Berlin blue) came from Berlin already in the early 17th century and it is known that the pigment was available and actually used at the Prussian Art Academy in Berlin, not later that in 1709.[7] Then, the royal blue found quickly its way to Paris and other European towns (Rotterdam etc.) at the beginning of the 18th century. Conclusions from the material investigation of two samples were, therefore, surprisingly unambiguous – the painting is Italian and it dates back to the 17th century. This finding significantly increased the interest in the concerned work of art and opened a way to its subsequent comparative examination.

Search for similar paintings

Polish painting

A very similar painting, in terms of the topic and composition, was found in a Polish catalogue (*Fig. 3*),[8] where a nearly identical painting is recorded as a "*Copy of a picture by Bernhard Keilhau – Boy petting a bird*". The latter is an oil painting on canvas, 62x47.5 cm, without a signature and with the registration number 5732. It is dated to the turn of the 17th and 18th century and it comes from a collection of the Museum of the Jagiellonian University in Krakow.

The text in the Polish catalogue mentions the original model, allegedly a painting by the Danish painter Bernhard Keilhau (Helsingborg 1624 – Rome 1687), held in a private collection in Paris[9] (*Fig. 4*). According to the Polish art historian Anna Jasińska (2003)[10], the painting is an allegory of the sense of touch, which is a topic typical for Dutch painting.

Original painting by Bernhard Keilhau and its inspiration by copper engraving

The oil painting, size 65x49 cm (*Fig. 4*), "*Boy petting a bird*" *(or "Allegory of the sense of touch")*, has been dated approximately to 1652 and it has been

3 Hradil D., Hradilová J., Bezdička P.: Nová kritéria pro klasifikaci a rozlišení jílových a železitých pigmentů různého původu - New Criteria for Classification of and Differentiation between Clay and Iron Oxide Pigments of Various Origins. In: Hradil D., Hradilová J. (Eds.), *Acta Artis Academica*, 2010 – Proceedings of the 3rd interdisciplinary conference of ALMA, Prague, November 24-25, Academy of Fine Arts in Prague, 2010, 107-136.

4 Roy A. and Berie B.H.: A new lead-based yellow in the seventeenth century. Painting Techniques History, Materials and Studio Practice. Dublin Congress 7-11 Sept. 1996, 1998, p. 160-165 and information from a lecture read by Claudio Seccaroni at the Technart 2007 conference, Lisboa, Portugal.

5 Hradilová J., Mislerová H.: Technika malby portrétů 19. století od Friedricha von Amerlinga-Painting Technique of Portraits painted in the 19th Century by Friedrich von Amerling. In: Hradil D., Hradilová J. (Eds.), *Acta Artis Academica*, 2010 – Proceedings of the 3rd interdisciplinary conference of ALMA, Prague, November 24-25, Academy of Fine Arts in Prague, 2010, 137-164.

6 Hradil D., Hradilová J., Bezdička P.: Nová kritéria pro klasifikaci a rozlišení jílových a železitých pigmentů různého původu - New Criteria for Classification of and Differentiation between Clay and Iron Oxide Pigments of Various Origins. In: Hradil D., Hradilová J. (Eds.), *Acta Artis Academica*, 2010 – Proceedings of the 3rd interdisciplinary conference of ALMA, Prague, November 24-25, Academy of Fine Arts in Prague, 2010, 107-136 and unpublished reports in the archive of the Alma laboratory at Academy of Fine Arts in Prague.

7 Bartoll J.: The Early Use of Prussian Blue in Painting, Art 2008, 9th International Conference, Jerusalem, Israel May 25-30, 2008, 43.

8 Jasińska A.: Kopia wg. Bernharda Keilhau, Helsingborg 1624 –Rzym 1687 (Bernhard Keilhau, after Helsingborg 1624 – Rome 1687) „Chłopiec głaskający ptaka (A Boy Petting a Bird), Malarstwo obce w zbiorach Collegium Maius, Muzeum Universytetu Jagiellońskiego, Katalog, tom II, Wydawnictwo Uniwersytetu Jagiellońskiego, Krakow 2003, 122 -123.

9 Heimbürger M.: Bernardo Keilhau detto Monsù Bernardo, Ugo Bozzi Editoriale, Roma, 1988, 175. Catalogue number of the painting 50.

10 Jasińska A.: Kopia wg. Bernharda Keilhau, Helsingborg 1624 –Rzym 1687 (Bernhard Keilhau, after Helsingborg 1624 – Rome 1687) „Chłopiec głaskający ptaka (A Boy Petting a Bird), Malarstwo obce w zbiorach Collegium Maius, Muzeum Universytetu Jagiellońskiego, Katalog, tom II, Wydawnictwo Uniwersytetu Jagiellońskiego, Kraków 2003, 122 -123.

All problems according to Preflight profile
Convert to PDF/A-2u

described in a book by Minna Heimdürger (1988). The author[11] describes the original painting by Bernhard Keilhau, who was also known as Monsù Bernardo in Italy. The author believes that the painter presented a slightly modified version of a Flemish –Dutch painting of a girl or boy (in some cases both) with a bird inside a cage or flying out of the cage. In this case the classical motif has been slightly altered (the cage has been replaced with a nest).[12]

Further, Minna Heimdürger (1988) in her book mentions that a *"significant composition element used by the painter was a hat with a broad brim, which monumentally defines the head, while the painter used the effect of a brightened background. This element comes from the Utrecht school – the so-called Ultrecht Carravaggisti - and it became one of Keilhau´s favorite motifs "*.

According to Minna Heimbürger, the painting by Bernhard Keilhau, alias Monsù Bernardo, was inspired by the copper engraving "Boy with a bird nest in a cap" by Cornelis Bloemaert[13] (*Fig.5*). The engraving comes from 1625, size 16.7x11.8 cm.[14] Cornelis made copper engravings based on compositions of paintings made by his brother Hendrick Bloemaert.[15] In a catalogue of works by Cornelis Bloemaert[16] on similar topics a engraving was found called "*Boy with a bird in a cage*" (*Fig.6*), which had the same size: 16.7x11.8 cm. In the collection of the British Museum it is dated back to 1625 and, again, it was allegedly inspired by a painting of his brother Hendrick or his father Abraham. The Museum Boymans-van Beuningen in Rotterdam keeps a drawing called "*Boy with a bird in a cage*" (*Fig.7*) by Abraham Bloemaert of 1566, size 13x12 cm. However, in comparison with Cornelis Bloemaert's engraving it is side-reversed.[17]

11 Heimbürger M.: Bernardo Keilhau detto Monsù Bernardo,Ugo Bozzi Editoriale, Roma, 1988, 175. Catalogue number of the painting 50.

12 Ibidem 11.

13 Cornelis Bloemeart II (1603 Utrecht – 1692 Rome) was trained as a painter but he mostly dealt with graphic art; after 1630 he worked in Paris and in 1633 he left for Rome. In Italy he produced engravings based on numerous Italian paintings (see the book by Arthur Mayger Hind, A history of engraving & etching, Menno Hertzberger, Amsterdam, Koch & Knuttel at Gouda, 1963, 122 and http://en.wikipedia.org/wiki/Cornelio_Bloemaert, 19.8. 2012)

14 Holstein H. F. W.: Dutch and Flemish Etchings, Engravings and Woodcuts ca. 1450-1700, Berckheyde - Bodding, 2, Amsterdam, Koch & Knuttel at Gouda, 1888–1957, 70–82. The artwork is listed under the catalogue number 293.

15 Hendrick Bloemaert (1601 or 1602 Utrecht - 1672 Utrecht), painter and brother of Cornelis Bloemeart, the oldest son of Abraham Bloemert, was considered a prominent member of the Ultrecht Carravaggisti group.

16 Holstein H. F. W.: Dutch and Flemish Etchings, Engravings and Woodcuts ca 1450-1700, Berckheyde - Bodding, 2, Amsterdam, Koch & Knuttel at Gouda, 1888–1957, 70–82. The artwork is listed under the catalogue number 294.

17 Reproduction H. Kleinmann & Co. Haarlem, (13x12 cm). Series IV, plate 46.

It should be noted, that in her book Minna Heimbürger also mentions later existence of an engraving by the British printmaker Caroline Watson (1760–1814) (*Fig.8*), both in connection with the painting "*Boy feeding a little dog*" (or "*Allegory of the sense of taste*")[18] and in connection with our painting of "*Boy petting a bird*" ("*Allegory of the sense of touch*"). According to William Stirling-Maxwell (1873), these small engravings (9.1x7 cm large) have been created in 1781.[19] Both the oil paintings, now ascribed to Monsù Bernardo, had been, in the past, ascribed to Bartolomé Esteban Murillo.[20]

Who was Bernhard (Eberhard) Keilhau alias Monsù Bernardo

Bernhard (Ebenrhart) Keilhau was born in 1624 in Helsingborg in a family of a German painter Caspar Kegelhoff (Keilhau), who settled down in the Danish kingdom. He learned his first artistic skills from his father. He worked in a workshop of the Danish painter Morten van Steenwinckel (1595–1646). In 1642–51 he worked in Holland, in the towns of Utrecht and Amsterdam, and spent three years (1642–1644) in the studio of Rembrandt Harmenszoon van Rijn. Later, he shortly worked in Frankfurt, Mainz, Ausburg and Cologne. From 1651, he worked in Venice and Bergamo. After 1656, he moved to Rome, where he spent the second half of his eventful life. He created a new artistic style, in Italy called "Monsù Bernardo style". His genre paintings were successful and, therefore, he settled down in Rome for good. He died in 1687.[21] Some historians refer to him as a German-Danish painter.

Discovery of the hidden authorship

When examining the back side of the painting as a part of the preliminary investigation,[22] the inscription *F. H. angekauft 1854* was found on the sup-

18 Heimbürger M.: Bernardo Keilhau detto Monsù Bernardo, Ugo Bozzi Editoriale, Rome, 1988, 174. Catalogue number of the painting 49.

19 Stirling-Maxwell W.: Essay Towards a Catalogue of Prints engraved from the Works of Diego Rodríguez de Silva y Velázquez and Esteban Murillo, London, 1873, 114.

20 Angulo Iñiguez, Diego, Murillo: Su vida, su arte, su obra, Madrid, 1981, vol. 1-3: Catàlogo crìtico, under no. 2516, 2515, Espada-Calpe and William Stirling- Maxwell, Essay Towards a Catalogue of Prints engraved from the Works of Diego Rodriguey de Silva Y Velazguez qnd Estéban Murillo, London, 1873, 114.

21 Heimbürger M.: Bernardo Keilhau detto Monsù Bernardo, Ugo Bozzi Editoriale, Roma, 1988, 8-106; Filippo Baldinucci, Domenico Maria Manni, Eberhard Keilhau (Kailo) Di Helsingor in Danimarca pittore detto Fra Noi Monsù Bernardo Discepolo di Rembrant van Rein (1624-1687) Notizie dei professori del disegno da Cimabue in qua, 1812, 413-428 a http://it.wikipedia.org/wiki/Mons%C3%B9_Bernardo, 19. 8. 2012.

22 Ibidem 1

All problems according to Preflight profile
Convert to PDF/A-2u

porting flax canvas with uneven warp density 10x8 thread per cm². It is probably a reference to its acquisition into a collection. However, after removing the old supporting canvas, the back side of the original appeared, with a thinner warp and with a different inscription: *Monsù d'Apré*. The inscription was written with fine black lines (*Fig. 9*).

If the term *d'apré* (or *d'après*) is used in French to identify the model (meaning "according to"), the correct wording would have been *d'après Monsù Bernardo*. This inscription must have been made somewhere in French speaking countries, which has not been independently confirmed yet. However, according to information from archives[23], the inscription could be also the author´s own signature. One painter actually used the signature *Monsù d'Apré* - his name was Franz Werner von Tamm (1658–1724).

Franz Werner von Tamm was born in Hamburg and he was an Italian-Flemish oriented painter of floral and hunting still lifes. Von Tamm used nineteen other signatures in German, French and Italian (e.g. *Monsieur da Pré, Monsu Duprat, Monsù Daprait*) etc.[24] According to Rijksbureau voor Kunsthistorische Documentatie (RDK) in Haague, he also used nicknames *Dapper* or *Aprêt*.

In his early stage of development, Franz Werner was influenced by Dietrich von Sosten and Johann Joachim Pfeiffer. Later, however, von Tamm left Hamburg for Rome, where he worked in 1685–1695. He was a member of the Bentvueghels group[25], similarly as Cornelis Bloemaert and David de Konick, who had also influenced him.

Ten years later, in 1702, Franz Werner von Tamm left for Passau and then he worked as a court painter of the emperor Leopold I at the Austrian imperial court in Vienna, where he died in 1724. The Lichtenstein Museum (the former Die fürstlich Liechtensteinsche Galerie) and also the picture gallery of the Art-history Museum (Kunsthistorisches Museum) in Vienna own several of his paintings.[26]

Bernhard Keilhau alias Monsù Bernardo (the author of the original painting) died two years after the Tamm´s arrival to Italy. Therefore, it is not clear whether von Tamm made the copy while Keilhau was still alive, or as a postmortem reference to the original. The information about the von Tamm´s social life in Italy is only very general - he worked with Peter van Bloemen, Karl van Vogelaer and he had a creative relation with Carl Maratti. Literature[27] suggests that Franz Werner von Tamm had a student in Rome, whose name was Pietro Navarra. The latter allegedly attended a workshop by Bernhard Keilhau, perhaps as a student in 1686. Is this the evidence that the Franz Werner von Tamm and Bernhard Keilhau personally knew each other or even worked together?

In order to confirm that the investigated anonymous work was truly painted by Franz Werner von Tamm, we need to compare the painting with other pictures signed by *Monsù d'Apré* and made in Italy. However, we lacked the opportunity to do so and, moreover, figural painting was not actually typical for this painter.[28]

An infrared photography[29] shows the drawing and places, where the painting is damaged (*Fig. 10*). The legibility of the infrared photography is influenced by its little contrasting ground that is not white. The ground contains earth pigments. The drawing is convincing and well legible. The painting is of high quality. Numerous fine damages are visible in light areas on the boy´s face, neck with hair and on his hand petting the bird. A substantial damage is visible in the bird´s nest under its body and on the wicker basket. The same damages are visible on all edges of the painting. The drawing proportionally fits with the Italian painting by Monsù Bernardo.

Mathematical processing of images

Comparison of the engraving with the old paintings

Initially, we compared all the three concerned paintings (Czech, Polish and the original one) with the engraving (*Fig. 7*) ascribed to the British printer

23 James M. Bower, Murtha B. Getty, Union List of Artist Names: Aa-Dzw, Thomson Gale, 1994 and http://www.getty.edu/vow/ULANFullDisplay?find=Tamm%2C+Franz+Werner+von&role=painter&nation=german&page=1&subjectid=-1&checked=500017541, 19. 8. 2011.

24 Ibidem.

25 A society of ca. 70 Dutch or Flemish – or generally "Nordic" - artists (painters, sculptors, graphic artists and poets), operating in Rome ca. from 1620 to 1720. Their boisterous activities were banned by the pope Kliment XI in 1720. According to RDK, Karel Škréta was also a member of the society.

26 Lier, Hermann Arthur, „Tamm, Franz Werner", in: Allgemeine Deutsche Biographie 37 (1894), 363-364 [Onlinefassung]; URL: http://www.deutschebiographie.de/pnd11935540X.html?anchor=adb, 19. 8. 2012.

27 Heimbürger M.: Bernardo Keilhau detto Monsù Bernardo, Ugo Bozzi Editoriale, Roma, 1988, 244. It is a description of a painting with initials P.N., ascribed to Pietro Navarra, student of Franz Werner von Tamm. Catalogue number of the painting 183.

28 According to the information provided by Dr. Z. Kazlepka, Franz Werner von Tamm was an outstanding painter of decorative still lifes and small animals, while the figural component (e.g. putti) in his works was painted by other painters. Paintings by Franz Werner von Tamm in Vizovice and Valtice are signed in Italian "Frances(co) v. tam f. ..." or „Fran(co) v. tam f. ..." However, the town museum Hazebrouck in France, which has a limited collection of paintings of Flemish and French provenience, has a painting by the same author called "Le Boucher" (The Butcher), a figural painting using the chiaroscuro technique.

29 The image has been taken with the modified camera Canon EOS 50 for IR spectrum. Zone filters were used for the visible spectrum (480-680) and near IR spectrum (950nm). The illumination was provided by daylight (visible spectrum) and thermal lamp spectrum (NIR). The painting was illuminated from the rear (based on a recommendation by I. Fogaš).

All problems according to Preflight profile
Convert to PDF/A-2u

Caroline Watson (1760–1814). Based on a digital comparison using the method of colour distinction, where the brightness of two images is compared (see the first part of this contribution – Blažek et al.), we have generated three composed pictures *(Fig. 11a, b, c)*. By comparing the oval engraving (red) with a reproduction of the original painting by Monsù Bernardo (green) (reproduction from the M. Heimdürgen's book, 1988) (*Fig. 11a*), we found out that there are visible differences in the size of the boy´s body and head, as well as in the size of the hat, shift of the eye and in the location of the bird and its size. The red colour predominates in areas, where the engraving is brighter than a painting, and vice versa, the green colour predominates in areas where the painting is brighter. A patch on a bigger sleeve shoulder is shifted on the painting. The painting lacks the painted back that is visible in the print. The painting of the petting hand has extended fingers and also slight shifts of the fingers are visible. The scarf is more distinct in the engraving.

Based on a comparison of the engraving (red) with a reproduction of the Polish painting (blue) *(Fig. 11b),* a composed picture was also created. The red colour predominates in areas, where the engraving is brighter than a painting, and vice versa, the blue colour predominates in areas, where the painting is brighter.

The comparison indicates that proportions and a composition of the painting are nearly identical. The agreement is visible, particularly in the painting of the sleeve of the hand petting the bird. The bird's head (except the difference in the eye) completely copies the image of the print. Very interesting is the significant agreement on the wicker basket and the boy´s cheek and eye. The shapes of the hat, however, are different. The patch and the sleeve of the coat are different. Completely different is the fold under the arm in the print. The bird's body in the print is much bigger. White feathers are visible through the basket. Locations of the boy´s eye are similar in the painting and in the graphic print. However, the end of the scarf is distinctly visible. Another substantial difference consists in the quantity of straw protruding from the nest – the small number of straws in the painting resembles more the original painting by Monsù Bernardo than the engraving. Despite the differences, a question should be asked whether the author of the Polish painting knew also the graphic print (not only the original painting). This is not excluded, as the Polish painting has been preliminarily dated to the turn of the 17th and 18th century but it may have been painted later as well.

This question, however, does not make sense for the painting from the Czech private collection. It is because its comparison (yellow) with the engraving (red) (*Fig. 11c*) identified significant proportion differences. Obviously, it has no connection with the graphic print, which is logical, as the painting has been documented to come from the 17th century, while the graphic print was made in 1781.

Unlike the engraving, none of the paintings feature a table on which the nest is resting. Therefore it is obvious that the composition of the graphic print must have been influenced also by another theme used by Monsù Bernardo (see above).[30]

Mutual comparison of the oil paintings

The figure 12a (*Fig. 12a*) compares a reproduction of the painting by Monsù Bernardo (green) and the Polish painting (blue). The bigger sleeve with folds on the Polish painting copies the hand on the painting by Monsù Bernardo. The fold under the arm is nearly identical. The fold shown in the painting is not present in the graphic print (see above). The paintings are not proportionally identical in respect to the bird's head and the size of its body. The painting of the scarf around the boy´s neck is richer in the Polish painting. The Polish painting is generally shifted downwards. When compared in white light, the boy has a more distinct edge of the dark vest. The artist, who made the copy, also observed the yellow color on the shirt sleeve.

A comparison of the copy from a Czech private collection (yellow) with a reproduction of the painting by Monsù Bernardo (green) (*Fig. 12b)* shows certain differences between the hats. In the Czech painting,, the arm in the sleeve with a lace is longer. Otherwise, however, the proportions of the two paintings are nearly identical. Shifted fingers of the petting hand are related to the longer sleeve. There is a significant agreement in the head (cheek, mouth) and the hand holding the nest. Differences are visible on the scarf around the neck. Even the snapshots made in white light demonstrate clear changes in the colours of the boy´s brown coat and the blue background (compare *Figs. 1 and 4*). The painting from a Czech collection shows a simplified image of the straw lining the wicker basket. The genre painting loosely penetrates the background. The base coat shows through in the background. The painting had been insensitively restored. In the past, it was glued on a new canvas. The edges were lined with an inappropriate paper adhesive tape. Also an unsuitable varnish was applied and, therefore, creeping appeared on the surface. The varnish layer subsequently turned dark and dimmed, which has significantly reduced legibility of the painting. Nevertheless, the mathematical comparison indicates that the painting is probably a loose copy of the painting by Monsù Bernardo.

30 The painting is identified in the footnote No. 18.

All problems according to Preflight profile
Convert to PDF/A-2u

A comparison of the Polish painting (blue) and the painting from a Czech collection (yellow) (*Fig. 12c*) shows significant differences. The Polish copy is significantly more robust. There are visible differences on the sleeve with a white lace and on fingers holding the wicker basket. It is quite well visible that the sizes of the paintings are not identical and, therefore, it is more than probable that they were not made by the same painter. None of them was made as a copy of the other one either. In both cases the paintings are loose copies of the original painting by Monsù Bernardo, however, there is no mutual relation between the two. This statement remains to be confirmed by a comparative materials research of the two paintings. However, it was impossible to perform this research in time for this paper.

Conclusion

Mathematical processing of the digital images made it possible for us to prove that the anonymous painting from a Czech private collection with a motif of a boy petting a bird – "*Allegory of the sense of touch*" is a loose copy of the painting by Bernhard Keilhau alias Monsù Bernardo (1624–1687), painted ca. in 1652. The material investigation of the ground of the painting and the pigments has positively documented that the copy is of Italian provenience and that it was most probably made also in the 17th century. Its author may have been Franz Werner von Tamm (1658-1724), as documented by the quality of the painting and also the (potentially) original signature or ascription of authorship to *Monsù Après* on the rear side of the original canvas, which is a signature demonstrably used (apart from other signatures) by the painter. The two painters not only met each other around 1686, but they may have worked together for a short period of time.

Another similar oil painting, this time from the collection of the Museum of the Jagiellonian University in Krakow, is also a loose copy of the same original work of art. The image analysis, however, excluded the option that both the copies (the Czech and the Polish ones) mutually influenced each other. The Polish copy has been preliminarily dated to the turn of the 17th and 18th century but it may have also originated later. The unknown copyist may have been familiar with graphic prints using the same topic made by Caroline Watson (1781) – the comparative analysis has indeed shown certain significant similarities. Its material investigation is needed in order to better determine the origin of the Polish copy.

Results leading to specification of the time of origin, provenience and author of the anonymous painting from a Czech private collection are based on non-destructive methods, mathematical processing of image data and historical search and they are supported by material analysis of only two samples. This indicates that modern techniques, comparative approach and appropriate interdisciplinary expertise make it possible to obtain very valuable and accurate data with a minimum disruption of the work of art.

Acknowledgment

We would like to express our thanks for execution and interpretation of instrumental analyses to our colleagues D. Hradil, P. Bezdička and S. Švarcová from the ALMA laboratory. We also thank V. Kovářová and P. Bauerová for their assistance in searching for not readily available literature. The research was carried out with support of Czech Science Foundation – project No. GAČR P103/12/2211.

All problems according to Preflight profile
Convert to PDF/A-2u

LIST OF FIGURES

1 Painting *"Boy petting a bird"* from a Czech private collection, condition after the artwork conservation (Photo by B. Valchářová)

2 Stratigraphy of the incarnate: 1. earthy ground, 2. oil painting of the incarnate (Photo by J. Hradilová; for more detailed description see the article)

3 Copy of the painting *"Boy petting a bird"* by Bernhard Keilhau alias Monsù Bernardo, from the collections of the Museum of the Jagiellonian University in Krakow; reproduction from a book: Anna Jasińska, Kopia wg. Bernharda Keilhau, Helsingborg 1624 – Rzym 1687 (Bernhard Keilhau, Helsingborg 1624 – Rome 1687) *„Chłopiec głaskający ptaka"* (A Boy Petting a Bird), Malarstwo obce w zbiorach Collegium Maius, Muzeum Universytetu Jagiellońskiego, Katalog, tom II, Wydawnictwo Uniwersytetu Jagiellońskiego, Kraków, 2003, p. 122

4 *"Boy petting a bird"* or *"Allegory of the sense of touch"*, around 1652; oil on canvas, private collection in Paris; reproduction from a book: Minna Heimbürger, Bernard Keilhau detto Monsù Bernardo, Ugo Bozzi Editoriale, Roma, 1988, p. 175, catalogue number 50

5 Engraving *"Boy with a bird's nest in a cap"* by Cornelis Bloemaert, 1625, © The Trustees of the British Museum

6 Engraving *"Boy with a bird in a cage"* by Cornelis Bloemaert, 1625, © The Trustees of the British Museum

7 Drawing *"Boy with a bird in a cage"* by Abraham Bloemaert, 1566, © Niederländische Zeichnungen, Band VI, 46

8 Engraving by the British printer Caroline Watson (1760–1814); reproduction from a book: Minna Heimbürger, Bernardo Keilhau detto Monsù Bernardo, Ugo Bozzi Editoriale, Roma, 1988, p.175, catalogue number 50

9 Signature Monsù d´Apré on the back side of the original canvas of the painting from a Czech private collection *"Boy petting a bird"* (Photo by B. Valchářová)

10 IR reflectography of the painting from a Czech private collection *"Boy petting a bird"* (Photo by J. Blažek)

11 Digital comparison of paintings with a motif of a boy petting a bird using the colour distinction technique based on brightness comparison of two images (see the 1st part of the contribution by Blažek in these proceedings); (a) comparison of the oval engraving by Caroline Watson (1760–1814) (yellow) and the original painting by Monsù Bernardo (blue); (b) comparison of the oval engraving by Caroline Watson (1760–1814) (yellow) and a copy of the Polish painting from the Museum of the Jagiellonian University in Krakow (blue); (c) comparison of the oval engraving by Caroline Watson (1760–1814) (yellow) and a copy of the painting from a Czech private collection (blue); the red colour predominates in areas, where the engraving is brighter than the painting, and vice versa, the green, blue or yellow colour predominates in areas, where the painting is brighter

12 Mutual digital comparison of paintings with a motif of a boy petting a bird using the colour distinction technique based on brightness comparison of two images (see the 1st part of the contribution by Blažek in these proceedings); (a) comparison of the original painting by Monsù Bernardo (blue) and the Polish copy of the painting from the Museum of the Jagiellonian University in Krakow (yellow); (b) comparison of a copy of the painting from a Czech private collection (blue) with the original by Monsù Bernardo (yellow); (c) comparison of the Polish copy of the painting from the Museum of the Jagiellonian University in Krakow (blue) and a copy of the painting from a Czech private collection (yellow); the green, blue or yellow colour predominates in areas, where the respective painting is brighter

All problems according to Preflight profile
Convert to PDF/A-2u



ODHALOVÁNÍ KOPIÍ POMOCÍ MATEMATICKÉHO ZPRACOVÁNÍ OBRAZU I.

TEORETICKÁ VÝCHODISKA A PRINCIP METODY

Jan Blažek
Ústav teorie informace a automatizace AV ČR, v.v.i.
Odd. zpracování obrazové informace
Pod vodárenskou věží 4
182 08 Praha 8
blazek@utia.cas.cz

Janka Hradilová
Akademie výtvarných umění v Praze
Laboratoř ALMA
U Akademie 4
170 22 Praha 7
hradilovaj@volny.cz

Jan Kamenický
Ústav teorie informace a automatizace AV ČR, v.v.i.
Odd. zpracování obrazové informace
Pod vodárenskou věží 4
182 08 Praha 8
kamenik@utia.cas.cz

Barbara Zitová
Ústav teorie informace a automatizace AV ČR, v.v.i.
Odd. zpracování obrazové informace
Pod vodárenskou věží 4
182 08 Praha 8
zitova@utia.cas.cz

ABSTRAKT

Navrhujeme poloautomatické metody pro geometrické sesazení (dále jen registraci) a pro komparaci digitálních snímků uměleckých děl. Algoritmus registrace je založen na odhadu perspektivní transformace pomocí kontrolních bodů. Porovnání snímků je založeno na statistické analýze snímků normalizaci jasu a absolutní odchylce. Vhodnost různých metod porovnání je demonstrována na příkladech. Výstupem algoritmů jsou srozumitelné rozdílové mapy. Navrhované metody jsou implementovány ve veřejně dostupné aplikaci *Fresco*.

KLÍČOVÁ SLOVA: **perspektivní transformace, perspektiva, rozdíl snímků, grafický software**

Úvod

Při analýze uměleckého díla restaurátor často pořizuje digitální snímky. Ty dokumentují stav díla. Využívá se zde různých vlnových spekter (NIR, UV), je-li dostupná potřebná technika.[2] Zpracování snímků probíhá nejčastěji s časovým odstupem, neboť analýza "in-situ" často není možná (nedostatečné vybavení, nedostatek času).

Cílem digitální dokumentace je porovnání snímků.[3] Porovnání jsou nejrůznějšího typu. Porovnávají se snímky mezi sebou[4]: UV a bílé světlo, NIR a bílé světlo, snímky dokumentující restaurátorský zásah, snímky z jiného časového období (například předchozí restaurátorský zásah).[5] Výjimkou nejsou ani porovnání snímků různých kopií téhož obrazu. Pořízené snímky je nutné často předzpracovat tak, abychom potlačili odchylky snímků, které nechceme měřit. Jedná se o různou intenzitu osvětlení, odlesky, geometrickou deformaci (pořízení snímku z úhlu) a posunutí UV, NIR snímků vůči sobě. Různou intenzitu osvětlení lze odstranit v mnoha dostupných softwarech téměř automaticky (často se však liší kvalita této normalizace). Odstranění odlesků jiných v digitalizované podobě je problematické a je jednodušší jim zamezit použitím polarizačního filtru a difuzéru při snímání. Problém nejčastěji nastává u snímků geometricky deformovaných a posunutých.

Zamezení geometrickým vadám je značně problematické a často ani není možné. Proces pořizování vyžaduje konstrukci lešení a stativ s tlumením otřesů. Snímání v UV a NIR navíc vyžaduje různě

1 Falco C. M.: High resolution digital camera for infrared reflectography (invited Article), *Review of Scientific Instruments* 80/7, 2009.

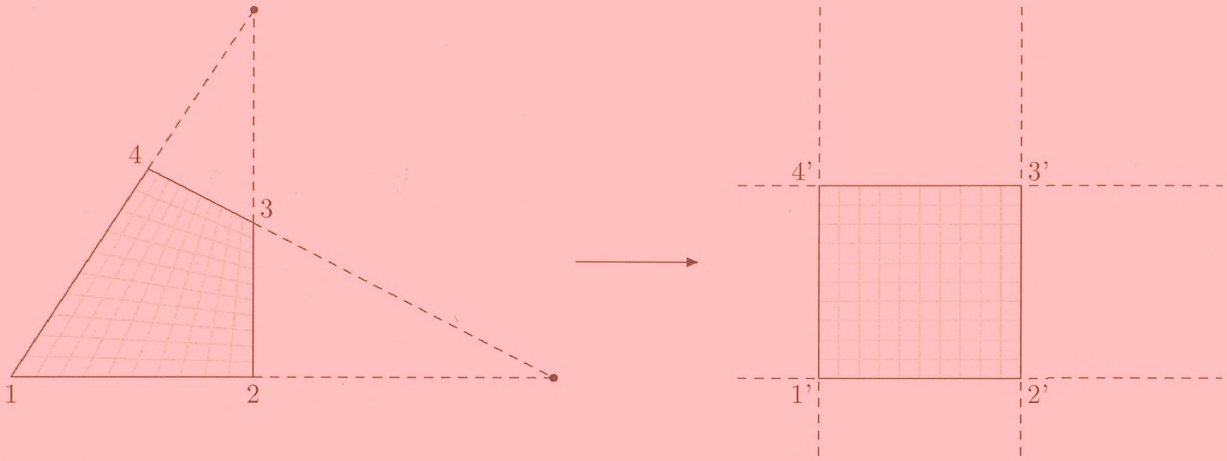
2 Boer J. R. J. V. A. D.: Reflectography of paintings using an infrared vidicon television system, *Studies in Conservation* 14/ 3 (1969), 96–118.

3 Berezhnoy I. E., Postma E. O., van den Herik J.: Computer analysis of van Gogh's complementary colours, *Pattern Recognition Letters* 28/ 6 (2006), 703–709; Berezhnoy I., Postma E., Herik D.: Digital analysis of Van Gogh's complementary colours, *Analysis* (2004), 163–170.

4 Delaney J. K., Metzger C., Walmsley E., Fletcher C.: Examination of the visibility of underdrawing lines as a function of wavelength In: *Proceedings of the 10th Triennal ICOM–CC Meeting*, vol. I, pp. 15–19, 1993.

5 Zitová B., Flusser J., Šroubek F.: Conservation of „The Last Judgement" mosaic: Image processing. In: *Proceedings of the 8th Computer Vision Winter Workshop*. CVWW'03, p. 169-174.

All problems according to Preflight profile
Convert to PDF/A-2u



1 Perspektivní transformace – úbo[illegible]níky se posunou do nekone[illegible]na, tvar [illegible]la se vyrovná do obdélníku; čísla znázor[illegible]ují dvojice referen[illegible]ních bod[illegible] řádé [illegible]ry ozna[illegible]ují zkreslení



2 *„Dáma s turbanem"* (Moravská galerie Brno) – snímek po[illegible]zen[illegible]pro ú[illegible]ely studie; pozice úb[illegible]níků dokazuje lev[illegible]pod-hled pozorovatele (foto Jan Bla[illegible]ek)



3 *„Dáma s turbanem"* (Moravská galerie Brno) – vyrovnan[illegible] snímek do optimální roviny pohledu; perspektivní úb[illegible]níky jsou v nekone[illegible]nu (aplikace Fresco, autor Jan Bla[illegible]ek)

zaost[illegible]ný fotoaparát, [illegible]li drobn[illegible]m posunem se p[illegible] snímání dostupnou fotografickou technikou nem[illegible]žeme vyhnout. Zejména [illegible]asová náro[illegible]nost takového p[illegible]stupu se pak stává neúnosnou.

Je b[illegible]žným zvykem registraci snímk[illegible] provád[illegible] pomocí softwaru. I zde se ale velmi li[illegible] kvalita r[illegible]zných programů. Součástí naší práce je i hledání software, kter[illegible] je možné pro odstran[illegible]ní výše zmín[illegible]ných vad použít. Nalezli jsme [illegible]ešitelné [illegible]ení v podob[illegible] Adobe Photoshop s instalovaným plug-inem Perspective Transformation, který jako jediný umož[illegible]uje napravit fotografické defekty (pořízení snímku z úhlu, hloubka ostrosti) ve smyslu perspektivy. Ostatní b[illegible]žně dostupné softwary nabízí p[illegible]evážně lokální transformace, s nep[illegible]íjemně intuitivní zadávání transforma[illegible]ních parametr[illegible] (úhel a zkosení, které se navzájem ovliv[illegible]ují). Lokální transformace následné komparaci mohou spíše uškodit (u t[illegible]chto algoritm[illegible] se nepředpokládá plochost snímaného díla). Ručně upravené dílo pomocí lokálních transformací také místo neodpovídá originálu (jeho promítnutí do roviny pozorovatele).

Při použití více programátorského p[illegible]stupu lze registraci provést například v programu Matlab se souborem nástroj[illegible] pro zpracování obrazu (toolbox Image Processing). Mezi nekomer[illegible]ními softwary jsme požadovanou funk[illegible]nost nenašli.

Zam[illegible]ili jsme se tedy na vývoj vhodného software, ve kterém je možné jak registraci, tak i komparaci snadno provád[illegible]t. Komparaci se snažíme usnadnit ozna[illegible]ením oblastí zájmu pomocí diferen[illegible]ních snímků. Samotné porovnání t[illegible]chto oblastí je usnadn[illegible]no nastavitelnou pr[illegible]hledností snímků i jejich obarvením. Oblasti zájmu jsou vybírány na

All problems according to Preflight profile
Convert to PDF/A-2u

základě matematických modelů pro určení rozdílnosti a budou popsány níže. V následujících řádcích popíšeme funkci našich algoritmů. Matematickou dokumentaci přitom zredukujeme na nutné minimum a doplníme sadou ukázek na zpracovávaných snímcích.

Registrace

Při konstrukci registračního algoritmu předpokládáme, že na snímku je zachyceno ploché dílo (obraz / nástěnná malba / mozaika atd.) a proto využíváme vlastností perspektivní transformace.[6] Zřídkakdy je tento předpoklad splněn (prověs plátna, nerovnost stěny). Malé odchylky však způsobí pouze malou chybu ve výsledném snímku. Defekty po transformaci mají podobu rozmazání v oblastech nerovností. Transformace je tedy stabilní. U 3D objektů jako jsou sochy a podobně je nutné zvolit jinou techniku skládání z více snímků která je nad rámec tohoto příspěvku.

První fází při zpracování snímků je transformace do pohledové roviny (*obr. 1*), a to zejména v případech, kdy bylo dílo snímáno z velkého úhlu. Chceme tak dosáhnout pohledu, kdy se na dílo díváme přímo. Přejdeme na fotografii potřebné perspektivní úbytkové zachycující obraz v prostoru (*obr. 2*) a získáme představu o pozici pozorovatele. Pozice úběžníků při přímém pohledu na střed obrazu (to je náš idealizovaný pohled) je v nekonečnu (*obr. 3*) na horizontální a vertikální ose. Tyto známe v podstatě dobře popsaný počítání i cílový stav.

Korespondující čtveřice bodů

Technika registrace pomocí referenčních bodů byla v našem případě zvolena díky své srozumitelnosti a snadné konfiguraci. Uživatel zadá čtyři dvojice bodů na obrazech, podle nichž se potřebné parametry transformace automaticky dopočítají.

Na cílovém snímku (*obr. 1*) má dílo tvar obdélníku, na počítaném snímku tvar obecného (konvexního) čtyřúhelníku. Vrcholy obou těchto čtyřúhelníků se navzájem odpovídají a navíc dobře definují transformaci potřebnou k provedení snímku. Výběr referenčních bodů ponecháváme na uživateli, neboť automatické heuristiky nemusí body zvolit správně. Ze čtyř dvojic bodů se spočtou parametry perspektivní transformace:

$$u_i = \frac{ax_i + by_i + c}{gx_i + hy_i + 1} \qquad v_i = \frac{dx_i + ey_i + f}{gx_i + hy_i + 1}$$

kde $[x_i, y_i], [u_i, v_i]$ jsou souřadnice vybraných bodů, a, b, c, d, e, f, g, h parametry transformace. Získáváme tak soustavu osmi lineárních rovnic. Pokud souřadnice transformovaných bodů mají neceločíselné hodnoty, barva v těchto bodech se dopočítá pomocí bilineární interpolace.[7]

Dle získaných parametrů je vstupní snímek (*obr. 2*) transformován na referenční snímek (v našem případě obdélník požadovaných rozměrů) a to tak, aby byl orientován dle zadaných bodů a měl stejné rozlišení (*obr. 3*).

Korekce zadání na vzájemné korelace

Protože zadávání bodů se provádí ručně, může být nepřesné. Pro tento účel používáme zpřesnění pomocí maximalizace vzájemné korelace[8], spočtené jako:

$$\frac{\Sigma_{i \in S}(m_i - \mu_{M_S})(n_i - \mu_{N_S})}{|S|}$$

kde S je okolí porovnávaného bodu (kruhové nebo čtvercové), i index do tohoto okolí, m respektive n hodnota pixelu v obrazech M respektive N a μ_{MS}, μ_{NS} střední hodnoty pixelů v okolí S na obrazech M respektive N.

Okolí zadaných bodů (± 20 bodů) se prochází bod po bodu a porovnává se vzájemná korelace okolí (velikost byla na základě experimentů stanovena jako kruh o velikosti 7 % rozlišení snímků) obou bodů. Maximální hodnota náleží správnému referenčnímu bodu. Nové body jsou tedy přidány jako parametry perspektivní transformace.

Komparace

Cílem počítačové komparace digitálních snímků je nalezení oblastí zájmu, které se na vstupních datech liší. Tento postup je motivován náročností komparace bez pomoci počítače a charakterem hledaných rozdílů. Níže uvedené metody používáme zejména pro odhalení proporčních rozdílů (kopie obrazů) a rozdílů v různých vlnových spektrech.

Předzpracování

Počítačové vidění je na rozdíl od vidění lidského absolutní. Barevné tóny nezávisí na barvách použitých v okolí, ale jsou definovány pomocí hodnot RGB.[9] Rovněž stín zakrývající část obrazu může mít katastrofální dopad na komparaci snímků neboť způsobí posun "skutečných" barev směrem k barvě černé. Například jedna barva použitá v nasvícené i temné části obrazu bude z pohledu počítače charakterizována různě (*obr. 4*). Velkou roli hraje i teplota zdroje

6 Perspektivní transformace - http://en.wikipedia.org/wiki/Perspective_transform

7 Bilineární interpolace - http://en.wikipedia.org/wiki/Bilinear_interpolation

8 Korelace - http://simple.wikipedia.org/wiki/Correlation

9 Barevný prostor RGB - http://en.wikipedia.org/wiki/RGB_color_space

All problems according to Preflight profile
Convert to PDF/A-2u



4 „*Zavraždění sv. Václava*" (Loket, kostel sv. Václava) – snímání prosvitu plátna; nepovedený snímek vykazuje velké rozdíly v jasu v různých místech obrazu (foto Jan Blaček)



5 „*Zavraždění sv. Václava*" (Loket, kostel sv. Václava) – úprava kontrastu lokálním vyrovnáním histogramu; střed obrazu není prosvětlen jako na obr. 7, naopak jsou vidět i detaily klepadla dveří ovládaného Václavem (aplikace Fresco, autor Jan Blaček)

světla použitá k nasvícení díla. Pro eliminaci rozdílu kontrastu (*obr. 5*) používáme metodu lokální normalizace kontrastu[10] (varianta CLAHE, velikost regionu a práh jsou nastaveny uživatelem). Normalizace barev vstupních snímků je prováděna posunem a měřítkováním hodnot jednotlivých barevných kanálech:

$$v_{target} = \left(v_{current} - \mu_{current}\right)\frac{\sigma_{target}}{\sigma_{current}} + \mu_{target}$$

kde v je hodnota pixelu, μ a σ průměr a rozptyl hodnot z celého snímku; *target* a *current* značí počáteční (před normalizací) a cílovou (po normalizaci) hodnotu. Normalizuje se každý z RGB kanálů zvlášť (*obr. 6*).

Alternativou pro lokální normalizaci kontrastu je globální normalizace. Lze ji použít v případech, kdy je nasvícení uměleckého díla homogenní, ale nedostatečné, a byl použit polarizační filtr a barvy jsou "vybledlé". Globální zvýšení kontrastu snímků je vhodné zejména pro oživení barev a je dostupné v mnoha komerčních softwarech (*obr. 7*). Globální zvýšení kontrastu je ekvivalentní metodě lokální s nastavením velikosti regionu na velikost celého snímku.

Komparace pomocí odečtení

Základní námi používanou metodou komparace obrazů je porovnání absolutních odchylek.[11] Pokud vstupní snímky *A* a *B* normalizujeme pomocí metod zmíněných výše, je možné hodnoty RGB v korespondujících pixelech od sebe odečíst (rozdílový snímek bude mít nenulovou vypovídající schopnost). Protože však rozdíl barev není intuitivně srozumitelný používáme rozdíl v šedé stále (*obr. 8a*). Hodnotu odchylky bereme v úvahu v absolutní hodnotě (nezajímá nás, zda je rozdíl v prvním nebo druhém snímku, ale to, že v daném místě rozdíl je). Předpokladem pro použití metody je normalizovaný kontrast i vyvážení bílé (vyvážení bílé lze ekvivalentně nahradit centrováním rozdílových hodnot). V naší aplikaci uvažujeme pouze černobílé snímky (komponenta Y z barevného prostoru Yuv)[12]. Při zachování značení dostáváme pro každý pixel:

$$Y = 0{,}3v_{target}[R] + 0{,}59v_{target}[B] + 0{,}11v_{target}[B]$$

kde *R*, *G* a *B* jsou jednotlivé barevné kanály z barevného prostoru RGB. Hodnota pixelu ve výsledném snímku je určena jako:

$$|Y_A - Y_B|$$

Důvodem je lepší srozumitelnost výsledku pro restaurátora. Pro porovnání barevnosti navrhujeme složitější metody.

10 Lokální normalizace kontrastu - http://en.wikipedia.org/wiki/Adaptive_histogram_equalization

11 Odchylka rozdílu čtverců - http://en.wikipedia.org/wiki/Mean_squared_error

12 Barevný prostor Yuv - http://en.wikipedia.org/wiki/YUV

All problems according to Preflight profile
Convert to PDF/A-2u



6 „*Ukřižování*" (Stěbořice u Opavy) – ukázka posunu barev; původní obraz (vlevo) byl snímán fotoaparátem upraveným pro snímání v NIR - převládá červená složka způsobená NIR zářením; upravený obraz (vpravo) má potlačenou červenou složku a zvýšený rozptyl modrých a zelených odstínů (foto Jan Blaček)



7 „*Zavraždění sv. Václava*" (Loket, kostel sv. Václava) – úprava kontrastu globálním vyrovnáním histogramu; příklad nevhodné aplikace na díle s nehomogenním osvětlením (aplikace GIMP, autor Jan Blaček)

Pravděpodobnostní přístup

Pravděpodobnostní porovnání je založeno na předpokladu, že barva *U* v prvním obrazu odpovídá barvě *V* v obrazu druhém. Rozdíl detekujeme v místech, kde barvě *U* odpovídá jiná barva, než barva *V*. Zobecnění této metody nám umožní kvantifikovat rozdílnost. Řekneme, že nejméně rozdílná barva od barvy *U* je taková, která barvě *U* odpovídá nejvíce. Nejrozdílnější je naopak ta, která barvě *V* odpovídá nejméně často. Zapsáno formálně

$$podobnost\,(U,V) = \frac{p(U,V)}{p(U)p(V)}$$

kde p značí pravděpodobnost na množině pixelů celého snímku. V případě kopie obrazu je idea taková, že se kopista snažil zachovat barevnost (co bylo modré, je modré i na kopii). V případech, kde kopista dodržel proporce originálu, bude rozdíl malý, protože shodných oblastí bude nejvíce (vychází se z předpokladu, že se jedná o kopii). Pokud se však koncept dodržet nepodařilo (ruka je deformovaná, obličej je malíčko pootočený) dochází k velkým změnám (kde byl obličej, je kontura a pozadí).

Z širokého spektra statistických metod tuto základní ideu kopíruje korelace[13], vzájemná informace[14] a variace informace[15]. Tyto míry jsou globální a charakterizují, jak moc jsou si obrázky "podobné".

13 Korelace - http://simple.wikipedia.org/wiki/Correlation

14 Wells W.M., Viola P., Atsumi H., Nakajima S., Kikinis R.: Multi-modal volume registration by maximization of mutual information, *Medical Image Analysis* 1 (1) (1996), 35–51.

15 Variance informace - http://en.wikipedia.org/wiki/Variation_of_information

All problems according to Preflight profile
Convert to PDF/A-2u



a



b



c

8 „*Dáma s turbanem*" (Moravská galerie Brno) **a** – odečtení normalizovaných intenzit snímků v bílém a NIR světle - tmavá barva znamená velký rozdílnost; metoda je stabilní vůči malým změnám intenzity, citlivě reaguje na textury ve svrchní malbě (neobsažené v podkresbě (aplikace Fresco, autor Jan Blažek); **b** – pravděpodobnostní rozdíl intenzit snímků v bílém a NIR světle; tmavá barva znamená velký rozdílnost; stabilita vůči malým změnám intenzity (v případě vhodného nastavení metody) i vůči texturám ve svrchní malbě oblasti zájmu jsou patrné v okolí očí (duhovky), obrysu turbanu a obličeje (podkresba); chyba metody je vidět v pravém horním rohu, kde byl ve viditelném světle odlesk (Matlab, autor Jan Blažek); **c** – barevné odlišení NIR a viditelného spektra; zelená barva znamená velký jas v NIR spektru, červená v bílém světle; odstíny žluti znamenají shodná místa (aplikace Fresco, autor Jan Blažek)

Pro použití při vizualizaci rozdílů jsme museli tyto metody rozšířit o lokální význam (původní vzorec). Výsledky porovnání pomocí pravděpodobnostního přístupu ukazuje obrázek 8b (*obr. 8b*).

Barevné odlišení

Barevné odlišení je metoda vycházející z nejběžněji používané komparační techniky, kdy si restaurátor promítá oba snímky přes sebe. Používají se nejčastěji plnobarevné snímky, protože detekce rozdílů je v takovém případě složitější. Náš postup kombinuje tuto metodu s barevným odlišením obou snímků. Poté se oba snímky normalizují (pomocí metod popsaných výše) tak, aby měly stejný kontrast, a převedou se do šedé stupně. Snímky převedené do odstínů šedi následně obarvíme (nastavíme odstín a saturaci v barevném prostoru HSV[16]) a složíme výslednou rozdílovou mapu. Samotné skládání je provedeno podle algoritmu pro skládání průhledných vrstev.[17] Pro obarvení může být použito jednoduché schéma, kdy se dva barevné kanály z RGB nahradí intenzitami šedých snímků. Výborného odlišení lze dosáhnout nahrazením šedých stupňů dvojicemi modrá - žlutá nebo červená - zelená (*obr. 8c*).

Na rozdíl od předchozích metod barevné odlišení neidentifikuje rozdílná místa. Všechny metody zde zmíněné je možné kombinovat. Pro dosažení lepších komparačních map lze zkombinovat oba způsoby měření rozdílů a diferenční mapy obarvit. Pro přehlednější zvýraznění rozdílů lze obarvit pouze oblasti s rozdíly a zbytek ponechat v šedé stupně.

Závěry

Naše práce se snaží upozornit na široké možnosti digitálního zpracování obrazu, které je vhodné zapojit při analýze uměleckých děl. Snažíme se, aby naše metody byly dostupné a aby srozumitelnost výsledků

16 Barevný prostor HSV - http://en.wikipedia.org/wiki/HSL_and_HSV

17 Alfa skládání barev - http://en.wikipedia.org/wiki/Alpha_compositing

All problems according to Preflight profile
Convert to PDF/A-2u

byla maximální. Použití co nejjednodušších algoritmů v tomto případě napomáhá srozumitelnosti a zároveň vychází z doposud používaných technik.

Veškerý software vyvíjíme v jazyce Java pod GPL licencí a přímo jej nabízíme na našich webových stránkách. Není nutná žádná instalace pro jeho použití, na klientském počítači pouze musí být nainstalována Java. Algoritmy, které byly úspěšně otestovány, jsou kontinuálně do softwaru přidávány. Na vývoji softwaru má možnost podílet se každý. Podpora uživatelům je realizována zatím pouze v podobě možnosti hlášení nalezených chyb v software a v emailové diskusi.

Využití našeho softwaru je zatím sporadické zejména kvůli úzkému povědomí o podobné aplikaci. Do budoucna se hodláme zabývat vývojem chybějících manuálů a vývojem plně automatických algoritmů bez nutnosti ladění parametrů. Nadále pokračujeme ve vývoji vhodných registračních a komparačních algoritmů.

Je na odborném posouzení zda předložené výsledky jsou užitečné a má smysl je dále rozvíjet. V současné době se můžeme opřít o pozitivní ohlasy a spolupráci s laboratoří ALMA, ve které i nadále pokračujeme. Využití popsaných algoritmů pak demonstruje následující druhá část tohoto příspěvku – Hradilová *a kol.*

Poděkování

Výzkum byl proveden za podpory grantu GAČR P103/12/2211.

All problems according to Preflight profile
Convert to PDF/A-2u

DETECTION OF COPIES USING MATHEMATICAL PROCESSING OF IMAGES I.

THEORETICAL BASIS AND METHODOLOGY

Jan Blažek
Institute of Information Theory and Automation of the AS CR, v.v.i.
Image processing department
Pod vodárenskou věží 4
182 08 Praha 8
Czech Republic
blazek@utia.cas.cz

Janka Hradilová
Academy of Fine Arts in Prague
Laboratory ALMA
U Akademie 4
170 22 Praha 7
Czech Republic
hradilovaj@volny.cz

Jan Kamenický
Institute of Information Theory and Automation of the AS CR, v.v.i.
Image processing department
Pod vodárenskou věží 4
182 08 Praha 8
Czech Republic
kamenik@utia.cas.cz

Barbara Zitová
Institute of Information Theory and Automation of the AS CR, v.v.i.
Image processing department
Pod vodárenskou věží 4
182 08 Praha 8
Czech Republic
zitova@utia.cas.cz

ABSTRACT

We propose semi-automatic methods for registration and comparison of digital images of fine art. The registration algorithm is based on the estimation of perspective transformation parameters by the means of control points. The image comparison is based on the statistical analysis of images, the normalization of brightness and the absolute deviation. The suitability of the different algorithms of comparison is demonstrated on examples. An output of algorithms' comparison is intelligible differential maps.

KEY WORDS: **Perspective transformation, perspective, images' difference, graphical software**

INTRODUCTION

Very often, restorers use digital images during the analysis of fine art. These images are documenting the state of the artwork. Different light spectra are used (NIR[1], UV), if the necessary technology is available.[2] Commonly, the image processing is performed after a time gap, because analysis "in situ" is often impossible (insufficient equipment, lack of time).

The goal of the digital documentation is the image comparison.[3] There are several types of comparison[4] – the comparison of different images[5] (of the ones taken in UV and white light, NIR and white light, documentary images of restorer's intervention, images taken in different time (a preceding restorer's intervention)[6] and, finally, comparison of different copies of the same original.

1 Falco C. M.: High resolution digital camera for infrared reflectography (invited Article), *Review of Scientific Instruments* 80/7, 2009.

2 Boer J. G. J. V. A. D.: Reflectography of paintings using an infrared vidicon television system, *Studies in Conservation* 14/3 (1969), 96–118.

3 Berezhnoy I. E., Postma E. O., van den Herik J.: Computer analysis of van Gogh's complementary colours, *Pattern Recognition Letters* 28/ 6 (2006), 703–709; Berezhnoy I., Postma E., Herik D.: Digital analysis of Van Gogh's complementary colours, Analysis (2004), 163–170.

4 Bridgman C. F., Gibson H. L.: Infrared luminescence in the photographic examination of paintings and other art objects, *Studies in Conservation* 8/3 (1963), 77–83; Buzzegoli E., Keller A.: Ultraviolet/Infrared false colour imaging. In: *Scientific Examination for the Investigation of Painting. A Handbook for Conservator-restorers*, 2009; Carcagni P., Della Patria A., Fontana R., Greco M., Mastroianni M., Materazzi M., Pampaloni E., Pezzati L., Piccolo R.: Spectral and colorimetric characterisation of painted surfaces: a scanning device for the imaging analysis of paintings. In: *Proc. SPIE*, 2005, vol. 5857, pp. 235–244.

5 Delaney J. K., Metzger C., Walmsley E., Fletcher C.: Examination of the visibility of underdrawing lines as a function of wavelength In: *Proceedings of the 10th Triennal ICOM–CC Meeting*, vol. I, pp. 15–19, 1993.

6 Zitová B., Flusser J., Šroubek F.: Conservation of "The Last Judgement" mosaic: Image processing. In: *Proceedings of the 8th Computer Vision Winter Workshop*. CVWW'03, p. 169–174.

All problems according to Preflight profile
Convert to PDF/A-2u

It is necessary to pre-process the taken images in order to eliminate the differences that we don't want to measure, i.e. a different light intensity reflections, geometrical deformations (taking an image in an angle) or shift of UV, NIR images in relation to each other. It is possible to remove different light intensity in many available types of software in an almost automatic way (but there are significant differences between these normalizations). Removing the reflections in digitalized images is problematic and it is better to prevent them by using polarized filters or diffusing media during the image acquisition. The most common problems are the geometric deformations and the image shift.

The prevention of geometrical deformation is highly problematic and often impossible. The process of image acquisition requires setting up scaffold or vibration-absorption tripod. In addition, taking images in UV or NIR requires different focus of the camera; therefore, it is impossible to prevent all the deformation during image acquisition process. Such approach is very time consuming and, thus, unacceptable.

It is common to register images by the means of specialized software. However, also in this case, the quality of the results differs. As a part of our work, we look for useful software, which is capable of removing the above mentioned deformations. We found a partial solution in Adobe Photoshop with a plug-in for Perspective Transformation, which is able to correct photographic defects (taking image in an angle, depth of field) of the perspective. Other commonly used software offers mostly only local transformations or a non-intuitive entering of transformation parameters (the angle and the bevel, which affect each other). A local transformation can be detrimental for the subsequent comparison (these algorithms don't take into account the flatness of the object). An image manually corrected by local transformations also often does not match the original (its projection into the plane of the observer).

It is possible to perform the registration in Matlab with a toolbox for Image Processing. This approach requires more programming experience. This functionality was not found among the non-commercial software.

We focus on the development of useful software, in which it is possible to perform registration as well as the comparison. The comparison is simplified by the highlighting of the area of interest. These areas are shown on differential images. The comparison of the areas of interest is facilitated by an adjustable transparency of the images or by their discolouring. The selection of the areas of interest is based on mathematical models, which determine the differences. These models will be described below. In the following part, we will describe our algorithms. We reduce the mathematical parts to a minimum extent and we complement them with a set of results obtained on the processed images.

Registration

For the purpose of the construction of the registration algorithm, we assume that the taken image contains flat artwork (painting/wall painting/mosaic etc.) and, therefore, we use the properties of perspective transformation.[7] Such assumption is fulfilled only rarely (canvas slacking, wall unevenness). In spite of that, small deviations cause only small error in the result. After transformation, the defects look like blurred area in the place of unevenness. Thus, the transformation is stable. For three-dimensional objects, i.e. sculptures, it is necessary to choose another technique for image joining, which is beyond the scope of this article.

The first phase of the image processing is the transformation into the plane of the observer (*Fig. 1*). This is necessary especially in cases, when the image of the artwork was taken in a large angle. A straight view is our goal. We add the necessary perspective vanishing points that set the image in space (*Fig. 2*). We get an idea of the observer's position. In the straight view on the middle of the image (which is our ideal view), the position of the vanishing points is in the infinity (*Fig. 3*). That describes the initial and the final state of the transformation.

Four corresponding pairs of points

The registration technique was chosen based on intelligibility and easy configuration. The user select four points in each image and the transformation parameters are computed according to these pairs of points.

The final state of the image has the shape of a rectangle (*Fig. 1*), the initial state has the shape of a general (convex) quadrangle. The corners of these quadrangles correspond to each other and they define well the transformation needed for the image transformation. The selection of the reference points is made by the user, because the automatic heuristics may not select the points correctly. From the four pairs of points, we compute the parameters of the transformation as follows:

$$u_i = \frac{ax_i + by_i + c}{gx_i + hy_i + 1} \qquad v_i = \frac{dx_i + ey_i + f}{gx_i + hy_i + 1}$$

where $[x_i, y_i], [u_i, v_i]$ are coordinates of the selected points, and a, b, c, d, e, f, g, h are the parameters of the transformation. We obtain the system of eight linear equations. If coordinates of the transformed points are not integer, the colour, in these points, is computed by the means of bilinear interpolation.[8]

7 http://en.wikipedia.org/wiki/Perspective_transform
8 http://en.wikipedia.org/wiki/Bilinear_interpolation

All problems according to Preflight profile
Convert to PDF/A-2u

The initial image (*Fig. 2*) is transformed according to the computed parameters into the reference image (in our case into a correctly oriented rectangle shape with a defined resolution) (*Fig. 3*).

Correction of point setting by cross-correlation

Because the setting of the corresponding points is done manually, it can be inaccurate. Therefore, we use final specification of the point location according to the maximization of the cross-correlation.[9] The cross-correlation is computed as follows:

$$\frac{\Sigma_{i\,S}\left(m_i-\mu_{M_S}\right)\left(n_i-\mu_{N_S}\right)}{\|S\|}$$

where S is a surrounding area of a specified point (radial or rectangular), i pixel index in this area, m and n values of pixel in images M and N, respectively, and μ_{MS}, μ_{NS} the average values of pixels in the area S in the image M and N, respectively.

The area around a set pixel (± 20 pixels) is searched pixel by pixel and the mutual correlation of the areas is compared (the size and shape of this area was set experimentally: a circle with a size of 1/1600 of image resolution). The maximal value of the cross-correlation indicates the correct reference point. These points are used for the computation of the perspective transformation parameters.

Comparison

The goal of a digital image comparison is to find areas of interest, which differ in input data. This goal is inspired by the complexity of this process, when no automation is at hand, and by the characteristics of the differences, which are being searched for. We use the following methods especially for the detection of the disproportions (artwork's copies) and the differences between different wavelength spectra (underdrawing).

Pre-processing

The computer vision is, compared to that of human, absolute. The colour tones are independent of the colours used in the nearest area and they are defined by the values of RGB.[10] The shadow covering a part of a taken image could have a catastrophic impact on the comparison of images. Such shadow causes shift of the colours in colour space and, therefore, the same colour can have a different representation in a digital colour space (*Fig. 4*). The temperature of the light source is also important. To eliminate the differences in contrast (*Fig. 5*), we use the method of local normalization of contrast[11] (variation CLAHE, the size of the area and the threshold are set by the user). The normalization of the colours is made by shifting and scaling the values in individual colour channels:

$$v_{target} = \left(v_{current} - \mu_{current}\right)\frac{\sigma_{target}}{\sigma_{current}} + \mu_{target}$$

where v is the value of a pixel, μ and σ the average and the variance of values of the whole image; *target* and *current* means initial (before normalization) and final (after normalization) value. We normalize each RGB channel separately (*Fig. 6*).

An alternative of local normalization of contrast is a global normalization. It is possible to use global normalization in cases, when lighting of the artwork is homogeneous, but insufficient, or a polarizing filter was used and the colours are faded. A global contrast enhancement of the images is useful to saturate the colours, and it is available in most of the commercial software (*Fig. 7*). A global contrast enhancement is equivalent to a local method having the size of the area equal to the size of the image.

Comparison based on subtraction

The basic method we use for the image comparison is based on the comparison of absolute deviations.[12] If input images A and B are normalized according to the above-mentioned methods, it is possible to subtract values of RGB space of the corresponding pixels (the differential image has nonzero informative ability). The problem of such an image are colours. A coloured image is not intuitively intelligible, therefore, we use grey-scale images (*Fig. 8a*). The value of the subtraction is used in its absolute value (we are not interested in whether the difference is in the first image or in the second one, but in the difference itself). The prerequisites for the use of the method are a normalized contrast and a white equalization (which can be substituted by centring of subtracted values). In our application, we take into account only grey-scale images (the component Y from the colour space Yuv[13]). With the previously used nomenclature, we get the following equation for each pixel:

$$Y = 0{,}3v_{target}[R] + 0{,}59v_{target}[B] + 0{,}11v_{target}[B]$$

where R,G and B are the colour channels from RGB space. The value of the pixel in a final image is computed as:

$$|Y_A - Y_B|$$

9 http://simple.wikipedia.org/wiki/Correlation
10 http://en.wikipedia.org/wiki/RGB_color_space
11 http://en.wikipedia.org/wiki/Adaptive_histogram_equalization
12 http://en.wikipedia.org/wiki/Mean_squared_error
13 http://en.wikipedia.org/wiki/YUV

All problems according to Preflight profile
Convert to PDF/A-2u

so the restorer will better understand the result. For the comparison of colours, we propose more complex methods.

Approach based on probability

Probability-based comparison is based on assumption that the colour U in the first image corresponds to the colour V in the second one. The difference is detected in areas, where colour U corresponds to a different colour than the colour V. The generalization of this method allows us to scale the difference. We suggest that the colour, which is the most similar to colour U, is the colour that corresponds to colour U the most often. The most dissimilar is the colour, which corresponds to colour U the most rarely. Formally expressed as:

$$similarity(U, V) \approx \frac{p(U, V)}{p(U)\,p(V)}$$

where p is the probability applied on a set of pixels of the whole image. The idea is that the copyist of an artwork tries to produce similar colours (blue is blue also in a copy). If the copyist maintains the proportions of the original, the difference will be small, because the number of similar areas will be very high, assuming it is a copy of an artwork. If the concept of the original was not preserved (a deformed hand, face slightly rotated), high values of difference are reached (in the area of the face is now a contour or a background).

From the wide spectra of statistical methods, this basic idea corresponds to correlation[14], mutual information[15], and variation of information.[16] These measures are global and characterize how much the images are similar. For use in difference visualization, we have to extend this method to local relevance (the formula above). The result of the comparison according to the probability method is depicted in Figure 9 (*Fig. 8b*).

Colour differentiation

The method of colour differentiation is based on a basic restorer's comparison technique, when the images are projected over each other. In most cases, full colour images are used, even though the detection of differences is in that case harder. Our approach combines this method with the colour differentiation of the images. Both images are contrast-normalized (by the methods described above) and transformed to greyscale. Subsequently, the grey images are coloured (we set the hue and the saturation in a colour space HSV)[17] and the final differential map is composed. The composition itself is made by the algorithm for alpha blending.[18] A simple schema is used for the colouring – two channels from RGB are substituted by intensity of the greyscale images. An excellent differentiation is reachable by substitution of greyscale intensities by blue-yellow or red-green colour tones (*Fig. 8c*).

Unlike the above-mentioned methods, the colour differentiation does not identify areas of interest. It is possible to combine all the methods discussed above. For obtaining better comparison maps, it is possible to combine both methods of difference measurement and colour the areas of interest in the subtraction maps and keep the rest of the image in greyscale.

Conclusions

Our approach shows a wide applicability of the digital image processing in relation to the analysis of artworks. Our goals are to maximize the intelligibility of the results and to make these methods widely available. The use of simple methods and algorithms, which are based on existing algorithms for image processing, is helpful for the intelligibility of the results.

The whole software is developed in Java under GPL license and we offer it directly on our website. No installation is necessary, only Java Runtime Environment has to be installed on the client's computer. The algorithms, which have been successfully tested, are continuously added into the software. It is also possible to join the development team as a developer or a restorer-analyst. The user-support is under construction; issues can be reported and discussed in an email conference.

The use of our Fresco software is, so far, rare. It is caused by low awareness of our software. In the future, we want to develop the missing manuals and to improve our algorithms to a level of full automatic use without the necessity of alignment of the parameters. We also continue in development of new algorithms for registration and comparison.

It is on restorer's community to judge the usefulness of our work and whether it is important or not to continue in the development. Nowadays, we successfully cooperate with the ALMA laboratory and the demonstration of our results can be found in the second part of this article – Hradilová et al.

Acknowledgement

The reserach was carried out with support of Czech Science Foundation – project No. GAČR P103/12/2211.

14 http://simple.wikipedia.org/wiki/Correlation

15 Wells W.M., Viola P., Atsumi H., Nakajima S., Kikinis R.: Multi-modal volume registration by maximization of mutual information, *Medical Image Analysis* 1 (1) (1996), 35–51.

16 http://en.wikipedia.org/wiki/Variation_of_information

17 http://en.wikipedia.org/wiki/HSL_and_HSV

18 http://en.wikipedia.org/wiki/Alpha_compositing

All problems according to Preflight profile
Convert to PDF/A-2u

List of Figures

1 Perspective transformation – vanishing points are shifted to infinity; the shape of the artwork is corrected to rectangular shape; the numbers represent the corresponding pairs of reference points; grey lines show the distortion

2 „*Lady with a turban*" (Moravian gallery in Brno) – the image taken for the purposes of this article; the position of the vanishing points indicates observer's left view from below (Photo Jan Blaček)

3 „*Lady with a turban*" (Moravian gallery in Brno) – an image transformed into the optimal plane of the viewer; vanishing points are in the infinity (Application Fresco, author Jan Blaček)

4 „*Murder of St. Wenceslas*" (Loket, St. Wenceslas' church) – the recording of the canvas' transparency; a failed image shows high differences in brightness in different parts of the artwork (Photo Jan Blaček)

5 „*Murder of St. Wenceslas*" (Loket, St. Wenceslas' church) – adjustment of the contrast by local equalization of the histogram; the centre of the image is not overexposed as in Fig. 7; on the contrary, the details of the doorknocker hold by St. Wenceslas are visible (Application Fresco, author Jan Blaček)

6 „*Crucifixion*" (Stěkořice u Opavy) – an example of the colour shifting method; the original image (a) was taken by camera adjusted for taking images in NIR spectrum; the red tint of the whole image is caused by the NIR radiation; the corrected image (b) has a suppressed red component and extended range of blue and green components (Photo Jan Blaček)

7 „*Murder of St. Wenceslas*" (Loket, St. Wenceslas' church) – an image adjusted by global contrast enhancement; an example of unsuitable application on the image that is non-homogeneously illuminated (Application GIMP, author Jan Blaček)

8 „*Lady with a turban*" (Moravian gallery in Brno) **a** – the subtraction of normalized intensities in visible and NIR spectra; darker colour represents parts with higher differences; method is stable in relation to small changes of intensities and responds badly to texture in the upper layer of the painting (which is not present in the under-drawing); **b** – a probability difference of intensities in visible and NIR spectra; darker colour represents parts with higher differences; method is stable in relation to small changes in intensity (in case the parameters are correctly set) as well as to textures in the upper layer of the painting; the areas of interest are visible in the eyes (irises), in the outline of the turban and in the face (under-drawing); the error of this method is visible in the right top corner, where there was reflection in the visible light spectrum (Matlab, author Jan Blaček); **c** – „Lady with a turban" (Moravian gallery in Brno) – colour differentiation of NIR and visible light spectra; the green colour represents higher brightness in the NIR spectrum, red colour represents high brightness in the visible spectrum; grey areas indicate similar areas in both images (Application Fresco, author Jan Blaček)

All problems according to Preflight profile
Convert to PDF/A-2u

Image Fusion for Difference Visualization in Art Analysis

Jan Blažek, Barbara Zitová, Jan Flusser
Institute of Information Theory and Automation
Academy of Sciences of Czech Republic, Prague, Czech Republic
Email: [blazek — zitova — flusser]@utia.cas.cz

***Abstract*—A new method for difference visualization is presented, oriented on the art analysis application. Compared images are combined into one fused image without losing important image context. Dissimilar regions are highlighted by color, which encodes localized differences. The method was developed for comparison of artwork copies, but it can be applied for general image comparison, too. The method is based on diverging color maps. The color representation of the difference is comprehensible, naturally ordered, and has maximal displayable resolution. The applicability of the method is demonstrated on hierarchy ordering of the copies of the "A boy with a bird" painting by Mons Bernardo (1624-1687).**

I. Introduction

A new method for base level image difference visualization is presented. The method was developed for a comparative analysis used in artwork investigation, when it is important to be able to display changes in composition (in case of underdrawings and underpaintings) and proportion deviations (multiple copies of the same artwork). Recent development creates high demand for such effective visualization algorithms, where all the important details are preserved and/or accentuated while the data dimensionality is reduced so we are able better understand captured scenes. Our method is meant for comparison of artwork copies, but it can be applied for image comparison in general, without exact specification of the "difference". The method is based on diverging color maps.

The comparison is based on the low level information, gained from pixel intensity values in HSV (Hue, Saturation, Value) color space and on any suitable local difference measure. The measure has to fulfill two conditions - it can have both positive and negative values and its zero value should represent a situation with no difference. These three dimensions - pixel intensities in both the original and the compared images, respectively, and the difference values - are combined into the HSV color representation.

New Value (V) is computed as an average intensity of both images. Spatially coherent fusion of the input images is necessary for good localization of the image difference. Hue (H) and Saturation (S) are reserved for the difference representation. New Hue reflects a sign of the estimated difference. New Saturation represents the absolute value of the estimated difference. Proposed color representation of the difference is comprehensible, aesthetic (according to the user selection), naturally ordered, and has maximal displayable resolution.

The difference measure, which has to be chosen in advance, has to reflect the data type of the compared structures. For multimodal images or images with different coloring any information-based measure can be applied, such as mutual information [4], Rényi distance, etc. We were comparing different copies of the same artwork and we decided to use the intensity difference of normalized and perspectively registered images. This approach gives us exact knowledge about the proportion deviation of the copyist.

The main goal of the proposed method was to highlight regions of expert interest (ROIs) and to visualize *difference values* specified by any appropriate difference measure for the further decision of an expert. Requirements for good visualization are:

(i) Visualization should be comprehensible.
(ii) Visualization should be aesthetic.
(iii) ROIs should be visualized in the context of compared images.
(iv) The whole scale of the similarity measure values should be recognizable.
(v) More than two images are compared without context loss.

Comprehensible visualization (i) is highly dependent on the selection of a *similarity measure*. Therefore we suggest similarity measure, which is comprehensible by an expert, who will use the visualization. We propose to use measures based on the low level information and which are defined for each pixel separately. Finally, the measure values should be real numbers in the interval containing the zero value, which represents "no difference". Positive values represent the difference in the first image and negative values the difference in the second image, respectively.

For the visualization, global measures must be adjusted for the local meaning and semi-local (region based) measures must be interpolated. We successfully tested localized measures of the information [3] and the normalized intensity difference of both images.

The method will be presented in the Section 2. Section 3 is demonstrating achieved results together with the illustrative visualizations. Finally, Section 3 concludes the paper and presents plans for the future work.

All problems according to Preflight profile
Convert to PDF/A-2u

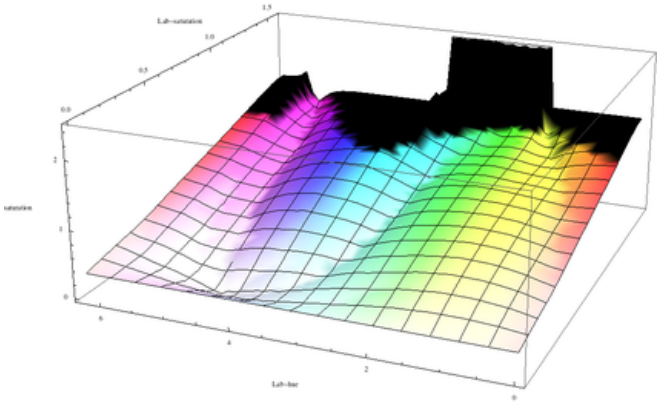


Fig. 1. The restriction of the saturation in CIELAB to the saturation in HSV color space. According to the hue and the saturation in CIELAB, the HSV saturation is perceived as continuous and linear. Black area contains colors out of the displayable range of the HSV color space. The lowest value of the *saturation* is in the white point - in this case D65 was used



Fig. 2. The comparison of two portraits of general Windischgrätz. The difference of the normalized intensity values of each corresponding pixel pair was employed as the difference measure.

II. Visualization method

The method is based on the fusion of the image intensities of both the original and the compared images, respectively and of their *difference value*. These values are evaluated for each pixel separately.

We work in CIELAB color space [2] where we define Hue and Saturation. However, the final result is visualized in HSV color space. The reason for the computation in CIELAB color space is the linearity of this space for human visual system and therefore better discriminability of ROIs in the resulting image. The HSV color space is used for visualization because we have to take into account limitations of an output device (typically a LED monitor).

The method workflow is as follows:

(1) Hues for each of the compared images are selected, based on the user preferences.

Hue selection is realized by the user input, electronically, and therefore due to the hardware limitations this selection is made in the HSV color space. In the output visualized image the negative and the positive difference values will be manifested by the first and by the second of the selected *hues*, respectively.

(2) Mapping of HSV *saturation* to the *difference values* is realized.

The saturation (S) in CIELAB we define as an angle between our color vector and L axis. The range of CIE–saturation values is then restricted according to the selected *hue* transformed to CIE–hue, which is an angle between a axis and projection of color vector into $a * b$ plane, and HSV limitations (see figure 1). For a 'positive' *hue* we obtain angles in the range $[0°, \alpha]$ and for a 'negative' *hue* another range $[0°, \beta]$. According to these ranges the difference values are mapped into the range $[-\beta, \alpha]$ and then transformed to HSV–*saturation*.

(3) The HSV coordinates computation for each pixel.

The new *Hue* (H) reflects the sign of the computed difference measure (1). The new *saturation* (S) represents the absolute value of the chosen difference measure (2). Finally, the new *value* (V) is the average value of intensities of compared images, pixelwise.

(4) The resulting fused image is displayed.

III. Results

The proposed method was successfully applied for several art investigation cases. The methodology proved to be useful for art experts and helped them to get better insight into the studied art pieces. Two of them are shown here. Firstly, the comparison of two portraits of general Windischgrätz was realized. Here, the difference of the normalized intensity values of each corresponding pixel pair was employed as the difference measure (see fig. 2). Slight scale differences and changes in the head position are apparent.

In the second case, the method was employed in the investigation of the painting analysis. The art experts have four images depicting almost the same scene - the 'Boy with the bird' (see fig. 3). One of them was the original painting by Monsú Bernardo (1624-1687). Then, they have one original engraving and two copies, one found in Poland and one in Czech Republic. The image registration was done by the perspective transformation according to the manually selected point pairs. The applied difference measure is the difference in the normalized pixel intensities. The visualization of the proportion deviation was successfully applied to estimate the

All problems according to Preflight profile
Convert to PDF/A-2u



Fig. 3. The 'Boy with the bird' painting - different versions. From the left - the original image by Monsú Bernardo, the engraving according to the original, the copy found in Poland, the copy found in Czech Republic.

hierarchy ordering.

The comparison was realized pairwise, the original painting (green) with the Polish copy (blue), with the engraving (red) and with the Czech (yellow) version, respectively. The best proportion matching is visible on the comparison with the Czech version (see fig. 4). The comparison of the copies themselves (fig. 5) shown that the Polish version is probably the copy of the engraving or vice-versa, see the significant matching of these two pairs (fig. 5, left image).

IV. Conclusions and future work

The new method for base level image difference visualization was presented. The method was developed for a comparative analysis used in artwork investigation. The method can be applied for image comparison in general, too, without exact specification of the "difference". The method is based on diverging color maps.

The comparison is based on the pixel intensity values in HSV color space and on any suitable local difference measure, such as the difference in the normalized pixel intensities. Proposed color representation of the difference is comprehensible, based on the consultations with the art experts. As far as we know such comparison task in the field of cultural heritage has been commonly solved by the image registration followed by the comparison made manually in Photoshop by warping and alpha blending.

The proposed method fulfills our requirements:

(i) Our method has an improving effect on the comprehension of the difference visualization, based on the reactions of the restores and art conservators. The identification of ROIs is faster and more precise.

(ii) The image context is kept with the image fusion approach of both input images in the HSV *value* (V) and with the coloring of the fused resulting image. In general, the difference sign identifies the image where the difference is present. The absolute value of the *similarity* measure is mapped to the final *saturation* (S).

(iii) The difference mapping is linear for human visual system by using CIELAB color space for the computation, which is important for further difference importance understanding.

(iv) For the comparison of more than two images (see figure 3) we propose to use the same hue (H) per image for all the fused image pairs (see figures 4 and IV).

(v) Finally, the coloring of the fused image is made by two hues harmonized by the user. The aesthetic requirement mostly depends on the user preferences.

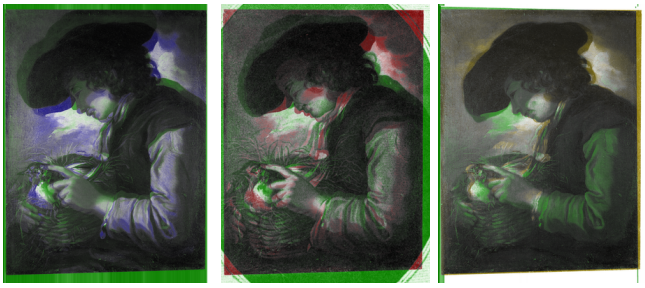


Fig. 4. The comparison of the original (green) with (from the left) the Polish (blue), with the engraving (red) and with the Czech (yellow) version, respectively. The best proportion matching is visible on the comparison with the Czech version. The registration was made by the perspective transformation according to the manually selected point pairs. The difference measure is the difference in the normalized pixel intensities.

For the future we plan to study the influence of the similarity measure choice. The selection of the difference measure is the most problematic part in our practice. Such measure has to match the type of the data to be compared. We often work with multitemporal or multimodal images. Very often we have to deal with different versions/copies of the same painting. For the difference measure we successfully used the difference in the normalized intensity values, the difference of the most significant principal component [1] and other information measures [3]. We would like to offer methodology for the universal difference measure.

All problems according to Preflight profile
Convert to PDF/A-2u



Fig. 5. The comparison of the three non-original pairs. The same colors and the difference measure as in figure 4 were applied. We can see significant matching of the engraving with the Polish version. Probably one was used as the model for creation of the second.

The presented method was developed in the cooperation with the Academic Materials Research Laboratory of Painted Artworks where it has been successfully used in the art investigation process. Matlab implementation can be found at Matlab Central - File Exchange. Java implementation is included in our project software Fresco (http://m3art.utia.cas.cz/fresco.php). This software can be used for free.

Our experience proved usefulness of the method for the image comparison. Moreover, it could be applied for the visual valuation of the image registration or of the segmentation precision.

ACKNOWLEDGMENT

This work has been supported by Czech Science Fundation, (project no. P103/12/2211).

REFERENCES

[1] I.T. Jolliffe. *Principal Component Analysis*. Springer Series in Statistics. Springer, 2002.

[2] Kenneth Moreland. Diverging color maps for scientific visualization. In *Proceedings of the 5th International Symposium on Advances in Visual Computing: Part II*, ISVC '09, pages 92–103, Berlin, Heidelberg, 2009. Springer-Verlag.

[3] J.P.W. Pluim, J.B.A. Maintz, and M.A. Viergever. f-information measures in medical image registration. *Medical Imaging, IEEE Transactions on*, 23(12):1508 –1516, dec. 2004.

[4] W. M. Wells III, P. Viola, H. Atsumi, S. Nakajima, and R. Kikinis. Multi-modal volume registration by maximization of mutual information. *Medical Image Analysis 1*, 1:35 – 51, 1996.

All problems according to Preflight profile
Convert to PDF/A-2u

Pole LED v matici 8x8

Prototyp

Ing. Michal Kuneš,
Mgr. Jan Blaček

Department of Image Processing
Institute of Information Theory and Automation of the ASCR
Pod Vodárenskou věží 4, CZ-182 08, Praha 8, Czech Republic
+420 26605 2470, http://zoi.utia.cas.cz
{xkunes, blazek}@utia.cas.cz

Obsah

1. Úvod 2
2. Vybrané LED diody 2
3. Napájecí obvody 4
4. Vstupní napětí: 5
5. Další součástky 5
6. Schéma DPS 6
7. Výroba DPS 9
8. Použití prototypu 11
9. Závěr 12
10. Literatura 13

Revize

Revize	Datum	Autor	Popis změn v dokumentu
0	21.1.2013	M.K.	Vytvoření dokumentu
1			
2			

Tento prototyp byl podpořen projektem: P103/12/2211: Methods for multimodal image processing based on mathematical models of optical properties of paint materials for artwork analys

All problems according to Preflight profile
Convert to PDF/A-2u

1. Úvod

Cílem tohoto dokumentu je popsat návrh a zhotovení pole LED (svítivých diod), které bylo vytvořeno v rámci projektu P103/12/2211: Methods for multimodal image processing based on mathematical models of optical properties of paint materials for artwork analys.

Úkolem bylo vytvořit trojúhelníkovou matici LED se stranou o délce 5 cm tak, aby jednotlivé LED s co nejní šší šířkou pásma a s co nevyšší homogenitou vyzařovaného světla pokrývaly co nejvyšší pásmo vlnových délek (viditelného) světla od 350 do 1000nm, v celkové velikosti 8 x 8 LED.Tedy je třeba zvolit vhodný počet LED na pokrytí pásma od 350 do 1000nm, tak aby bylo celé pásmo dostatečně pokryto a naopak, aby každá jednotlivá LED svítila v co nejužší pásmu s co nejvyšší homogenitou světelného kužele.

2. Vybrané LED diody

Pro prozkoumání dostupných druhů LED, byly vybrány LED s vlnovými délkami 398nm a 405nm pro ultrafialové, 466nm a 700nm pro viditelné a 880nm a 950nm pro infračervené spektrum (viz. tabulka 1). Každá LED svítí v rozsahu přibližně ± 50nm, kromě UV LED, které mají šířku pásma mnohem užší (asi ± 5nm) viz. GME [1].

	vlnová délka			vyzařovací úhel	vyzařovací výkon		katalog. číslo gme.cz	U	I	název LED / součástky
	20% od	80% do								
	[nm]	[nm]	[nm]	[°]	[mc]	[mW]		[V]	[mA]	
1	395	401	398	30	--	2	511-802	3.5	20	330MUV9C - UV 2000uW/30°
2	402	408	405	30	--	4	511-877	3.5	20	530MUV9C - UV 4000uW/30°
3	400	470	466	60	90	--	511-985	4	20	L-53MBDL - BLUE 90/60°
4	450	480	470	25	2500	--	511-759	3,3	20	530PB6C - BLUE 3000/40° CREE
5	470	530	506	30	6500	--	511-803	3,5	30	530PG0C - BUEGREEN 8000/30°
6	500	550	525	30	7000	--	511-782	3,3	20	530PG2C - PURE GREEN 8000/30°
7	550	580	565	24	250	--	511-032	2,1	30	L-HLMP-3950 - GREEN 200/24°
8	560	610	590	40	3500	--	511-429	2,1	30	540MY8C - YELLOW 3500/40°
9	580	625	605	20	4000	--	511-608	2,1	20	530MO0C - ORANGE 4000/20°
10	600	650	620	20	5000	--	511-674	2,1	20	520MR2C - RED 5000/20°
11	650	670	660	30	2000	--	511-687	2,5	20	L-53SRC-DW - RED 2000/30°
12	670	730	700	50	8	--	511-103	2,2	20	BL-BHG274 - REG/(GREAN) 8/(50)/50°
13	825	925	880	20	--	25	520-015	1,5	100	SFH485-2 - IR >25mW@100mA 20°
14	930	1000	950	50	--	10	511-094	1,3	100	LD271 IR - >=10mW/sr@100mA
15	--	--	--	--	--	--	832-040	--	20	Dutinková lišta BL804G (2 piny)
16	--	--	--	--	--	--	832-040	--	30	Dutinková lišta BL804G (2 piny)
17	--	--	--	--	--	--	832-040	--	100	Dutinková lišta BL804G (2 piny)

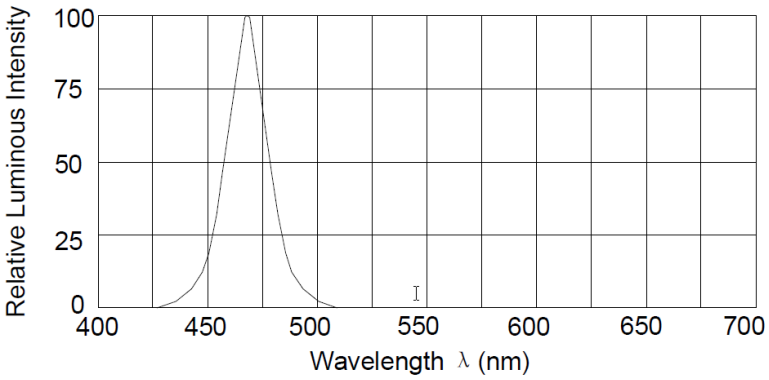
Tabulka 1 Seznam použitých LED

Pro vyšší flexibilitu návrhu byly použity i dutinkové lišty (č. 15, 16, 17 tab. 1) s 2 piny pro možnost připojení dalších LED zasunutím do dutinek, pokud to bude při využití desky potřeba.

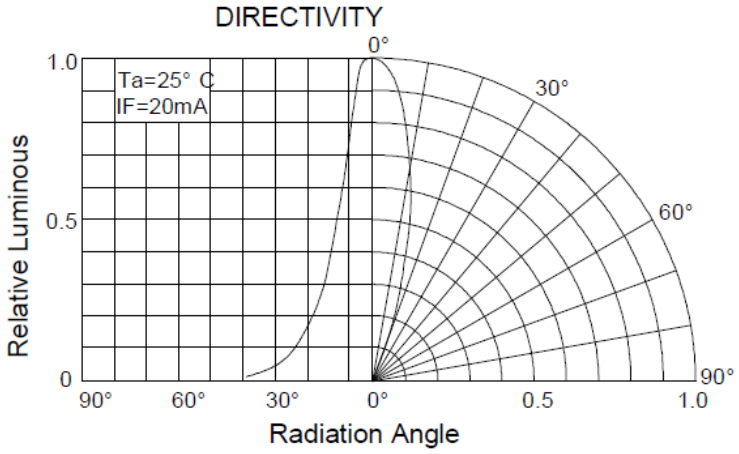
Poznámka 1: LED 700nm č.12 BL-BHG274 je dvoubarevná (červená 700nm a zelená 568nm) a je zapojena pouze jako červená pro vlnovou délku 700nm.

Poznámka 2: LED byly vybrány v internetovém obchodě GME [1], kde je ke většině součástek možné dohledat potřebnou dokumentaci podle katalogového čísla z tabulky 1.

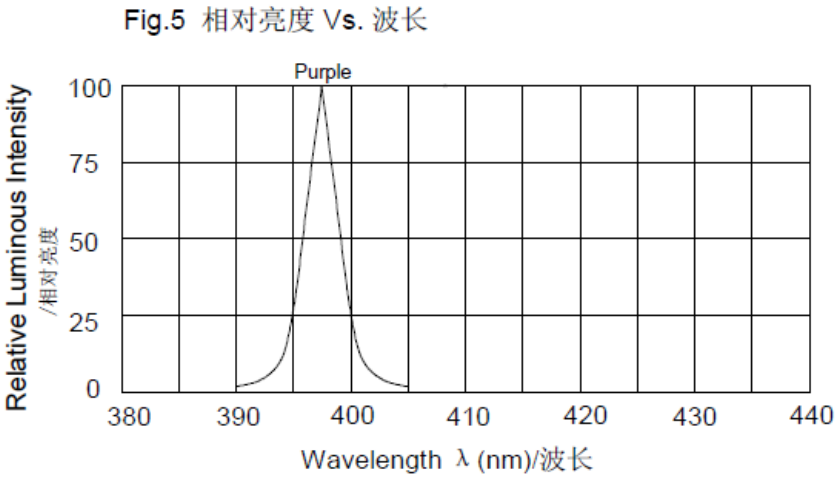
Příklad grafu intenzity vyzařování světla u LED 530PB6C - BLUE 3000/40° CREE ([1] GME 123-005 511-759)
- v závislosti na vlnové délce:



- v závislosti na úhlu vyzařování:



Příklad svítivosti UV LED 330MUV9C - UV 2000uW/30° 511-802 v závislosti na vlnové délce:

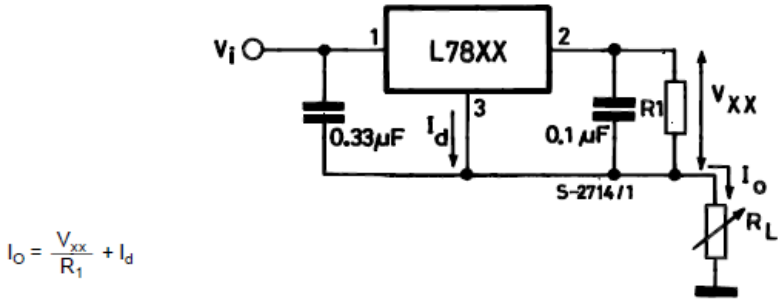


3. Napájecí obvody

Led jsou rozmístěny do matice 8x8, napájení je rozděleno do osmi vláken po 8 LED podle specifikace výrobce jednotlivých LED:

8x 20mA = 160mA
8x 30mA = 240mA
8x 100mA = 800mA

Pro první dvě varianty byl vytvořen napájecí zdroj proudu pomocí stabilizátoru napětí 5V - L7805 ([1] GME kód produktu: 330-149) s kondenzátory 0,33uF/63V ([1] GME 123-005) na vstupu a 100nF/50V ([1] GME 120-060) na výstupu podle standardního zapojení (viz. dokumentace k obvodu L7805 [1] GME 330-149):



Obrázek 1 Zapojení L7805 jako zdroje proudu

Kde pro naše obvody L7805 je:
V_{xx} = 5V (pro L7805)
I_d = 6mA
I_o = požadovaný proud pro LED (zátěž R_L – 160 / 240mA)

Pro 160mA dostaneme:

R_1 = 4 x 130Ω (paralelně) = 32,5Ω
I_o = 5 / (130 / 4) + 6 = 5 / 32,5 + 6 = 153,8 + 6 = 159,8mA

Ztrátový výkon rezistoru: $P_R = R \times I^2 = 130 \times (0{,}1538/4)^2 = 0{,}2W$
(Byly použity rezistory z řady RR 130R 0,6W.)

Pro 240mA dostaneme:

R_1 = 21,2Ω ((2 x 68Ω) || 56Ω (paralelně))
Io = V_{xx} / R_1 + I_d = 5 / 21,2 + 6 = 153,8 + 6 = 242,3mA

Ztrátový výkon rezistoru:
$P_{R68} = U^2 / R = 5^2 / 68 = 0{,}37$ W
$P_{R56} = U^2 / R = 5^2 / 56 = 0{,}45$ W
(Byly použity rezistory z řady RR 68R W1 a RR 56R W1 - 1W.)

Pro 800mA je využit obvod LDD-700H ([1] GME 332-390), který je určen pro napájení LED s proudem 700mA a napětím 2 až 52V, Vstup 9 až 56V tím sice dostaneme proud 700mA místo 800mA, ale to je pro naše účely dostačující. Obvod značně zjednoduší návrh a ušetří potíže s chlazením obvodů L7805, které lze sice využít do proudu 1A (eventuálně 2A pro 78S05), ale při proudu 1A a předpokládaném napětí až 32V je třeba obvod výrazně chladit.

Výstupy všech tří napájecích obvodů jsou pro případné měření fyzicky odděleny od LED pomocí oboustranného kolíku ([1] GME 832-168) (2 paralelně pro nižší ztrátový odpor) a jsou v případě běžného provozu propojeny zkratovací propojkou (jumper ([1] GME 832-140). Kolíky je dále možné použít pro měřící a testovací účely.

4. Vstupní napětí

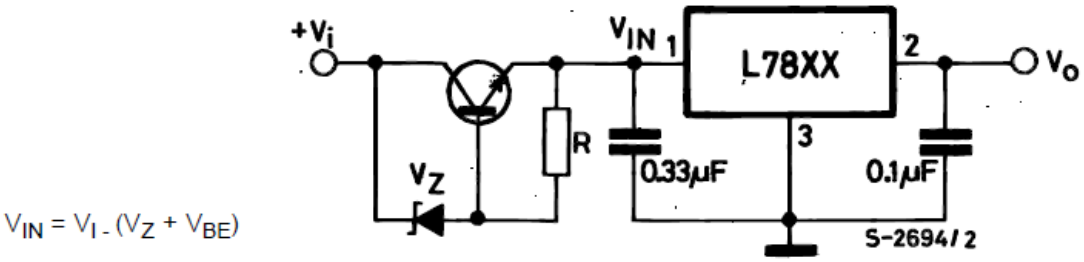
Jednotlivé druhy LED vykazují značný rozdíl v napětí U_f pro požadovaný proud. Využijeme-li nejnižší napětí pro prodávané LED a to 1,2V a nejvyšší 4V máme výsledné rozpětí napětí 8x1,2V a 8x4V, tedy 9,6 a 32V pro sériové řazení 8 LED.

Minimální pracovní napětí pro obvod L7805 je 7V (2V pro vlastní L7805 + 5V pro výstup L7805) a maximální pak 35V. Tím dostaneme požadovaný rozsah napětí pro obvody s LED 1,2V a L7805 jako: U_{MAX12} = 35 + 9,6 = 44,6V a U_{MIN12}= 7 + 9,6 = 16,6V. Pro 4V LED je to pak U_{MAX4} = 35 + 32 = 67V a U_{MIN4}= 7 + 32 = 39V.
Je dobré, že maximální napětí pro 1,2V je vyšší než minimální pro 4V a obvod lze tedy použít.

Pro 10x LED dostaneme U_{MAX12} = U_{MIN4} = 47V, což znamená, že můžeme obvod L7805 použít maximálně pro napájení 10x LED, pro 11x LED a minimálním napětí 1,2V by došlo k nárůstu napětí na obvodu L7805 nad povolenou hranici 35V. (Požadované napětí pro 11x LED 4V je 51V a napětí na obvodu L7805 pro LED 1,2 je pak 11 x 4 + 7 – 11 x 1,2 = 37,5V.)

Potřebujeme tedy napájení minimálně 39V a maximálně 44,6V pro obvod L7805.
Předpokládáme-li na vstupní blokovací usměrňovací diodu (úbytek 0,8V) a diodu (úbytek 1,35V) před obvody L7805 dostáváme se na 47V. Použijeme-li dostupný zdroj 48V / 1,35A, znamená to, že potřebujeme napětí snížit minimálně o 1V a maximálně o 6V, tak aby jsme dosáhli požadovaného rozsahu 39V a 44,6V.

Snížíme jej tedy o 5V pomocí tranzistoru. Použijeme ST13005 ([1] GME 211-225), Zenerovu diodu BZX83V004.7 ([1] GME 222-017) a RR 100R 0,6W ([1] GME 110-049) podle zapojení obvodu L7805 pro vysoké vstupní napětí:



Obrázek 2 Zapojení L7805 pro vysoké vstupní napětí

Tím dostaneme úbytek 5,6V (namířeno).

Před každou větev s L7805 je ještě vložena ochranná usměrňovací dioda BY500-1000 ([1] GME 110-049) s úbytkem 1,35V.

5. Další součástky

Napájení
DPS je napájena napájecím adaptérem síťovým 48V/1350mA s konektorem 2,1mm ([1] GME 751-151). Na vstupu desky je pak za vstupním spínačem ([1] GME 631-236) pojistka 1,6A 60V ([1] GME 633-347), ochranná dioda proti přepólování 5A s úbytkem 0,85V ([1] GME 223-171), následuje blokovací kondenzátor 100nF/63V ([1] GME 120-060) a elektrolytický kondenzátor 330u/100V ([1] GME 123-785) pro odstranění případných výkyvů vstupního napětí.

Otočné spínače
Pro řazení vývodů, kterých máme 10x 160mA, 4x 240mA a 3x700mA použijeme pro jednoduchost otočné spínače do DPS 1x12, 3x4 a 4x3. 3x4 a 4x3 využijeme na paralelní spojení kontaktů tak, aby se spínač nepřetěžoval vysokým proudem. Spínače je navržen pro proudové zatížení do 150mA (katalogová hodnota). 1x12 bude tedy malinko přetížen. Přepínač 3x4 máme 3x150mA = 450mA, což využijeme pro přenesení 240mA a pro přepínač 4x3 máme 3x150mA = 600mA a ten by 700mA také měl zvládnout.

Protože je těžké sehnat otočné spínače pro vyšší proudové zatížení, bylo by vhodné pro případné vyšší zatížení a dlouhodobé využití spínače nahradit pomocí spínacích relé či spínacích tranzistorů.

Páčkové spínače do DPS
Před každou větví je pak páčkový spínač přepínač ([1] GME 631-236) pro vypnutí/zapnutí napájení dané proudové větve (160/240/700mA).

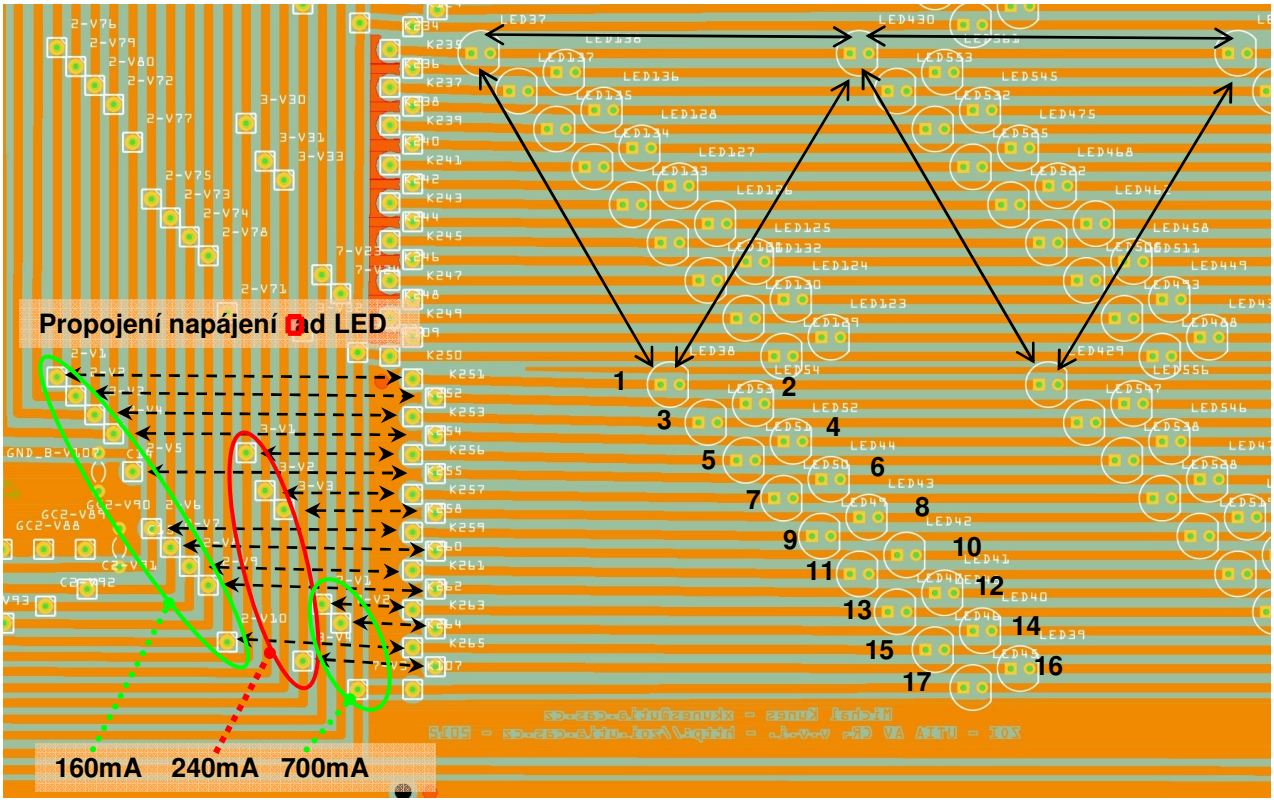
V napájecích v[illegible]vích (160/240/700mA) je elektrolytický kondenzátor 470u/63V ([1] GME 123-777) pro stabilizaci vykyv[illegible] vstupního nap[illegible]tí.

V ka dé v[illegible]vi LED je dále za oto[illegible]ním spína[illegible]em umíst[illegible]n blokovací kondenzátor 100nF/63V (3x) ([1] GME 120-060) pro LDD-700H, respektive 100nF/50V ([1] GME 120-060) pro v[illegible]tve s obvody L7805 (14x).

Propojovací matice

Jeliko pou íváme jednovrstvou desku pro plošné spoje, je ob[illegible]as nutné e it k[illegible]ení spoj. Jediný problém u našeho návrhu nastal pu propojování v[illegible]vi LED. Pro jednoduchost zde byly pro propojení pou ity propojky (rezistory s nulovým odporem RR 0R ([1] GME119-145)) a pro pu bojení k plus (Obr. 3) a k mínus pólu u 100mA v[illegible]tve, která vy aduje vlastní mínus pól (vzhledem k pou iti obvodu LDD-700H [1] GME 332-390).

Rozmíst[illegible]ní LED v matici



Obrázek 3 Matice LED a projení npájení jednotlivých [illegible]d LED

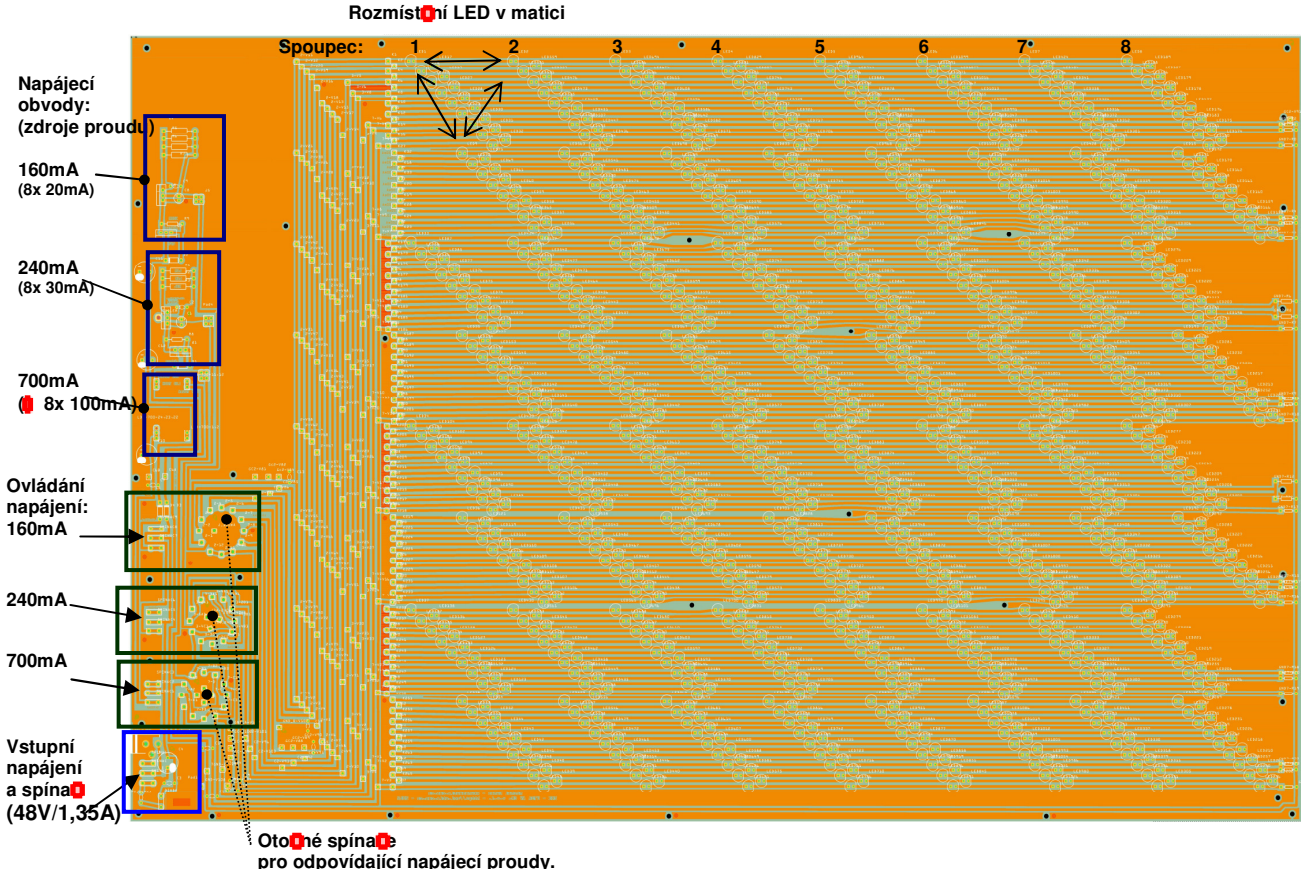
6. Schéma DPS

Pro návrh DPS byl vyu it open-source program Fritzing V0.7.10 b6551 [2], který je jednoduchý na ovládání a ikdy nedosahuje kvality komer[illegible]ních softwar[illegible] zejména v sou[illegible]ástkové základn[illegible] je pro naše ú[illegible]ely dosta[illegible]ující.

Program je distribuován pod GNU Gpl V3 [3].

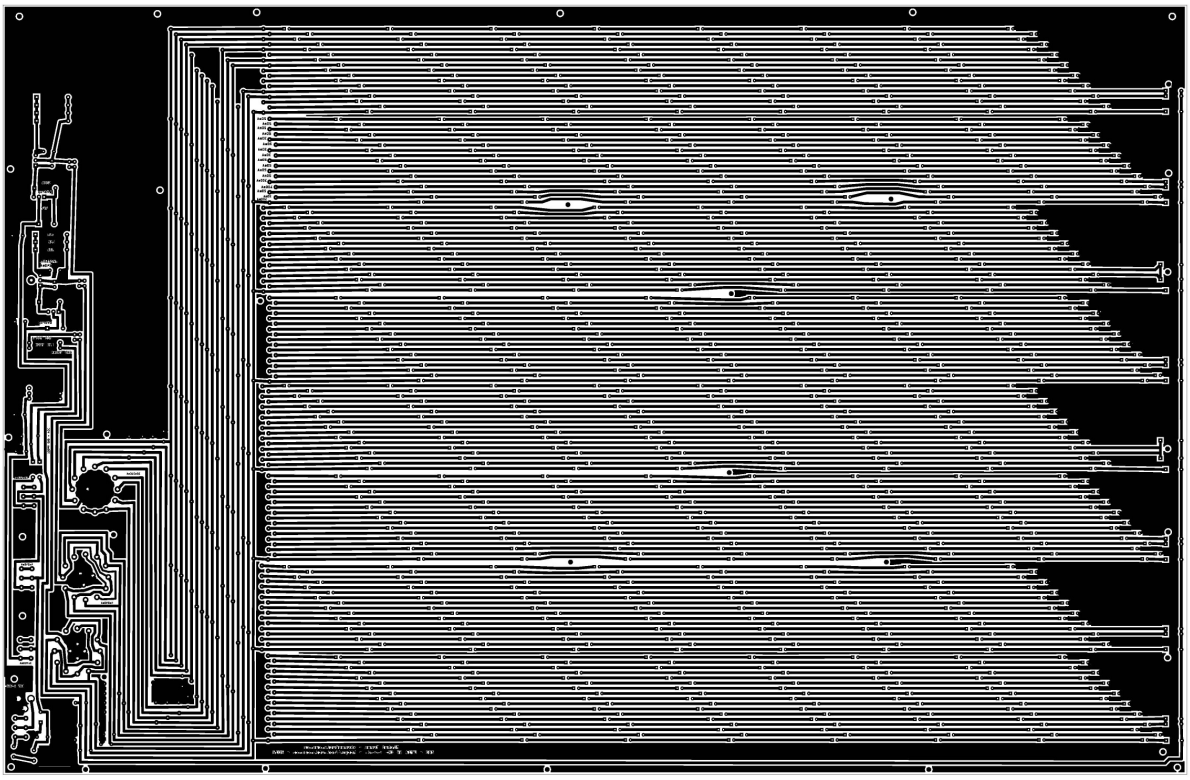
Schéma DPS v programu Fritzing:

Na následujícím schématu jsou zvýrazněny ovládací části napájení: hlavní spínač a vstup pro napájení, ovládání a přepínání jednotlivých LED větví 160 / 240 / 700mA a vlastní zdroje proudu pro jednotlivé větve.
Ve schématu je také zobrazeno rozmístění odpovídajících si LED do trojúhelníkové matice se stranou 5cm.



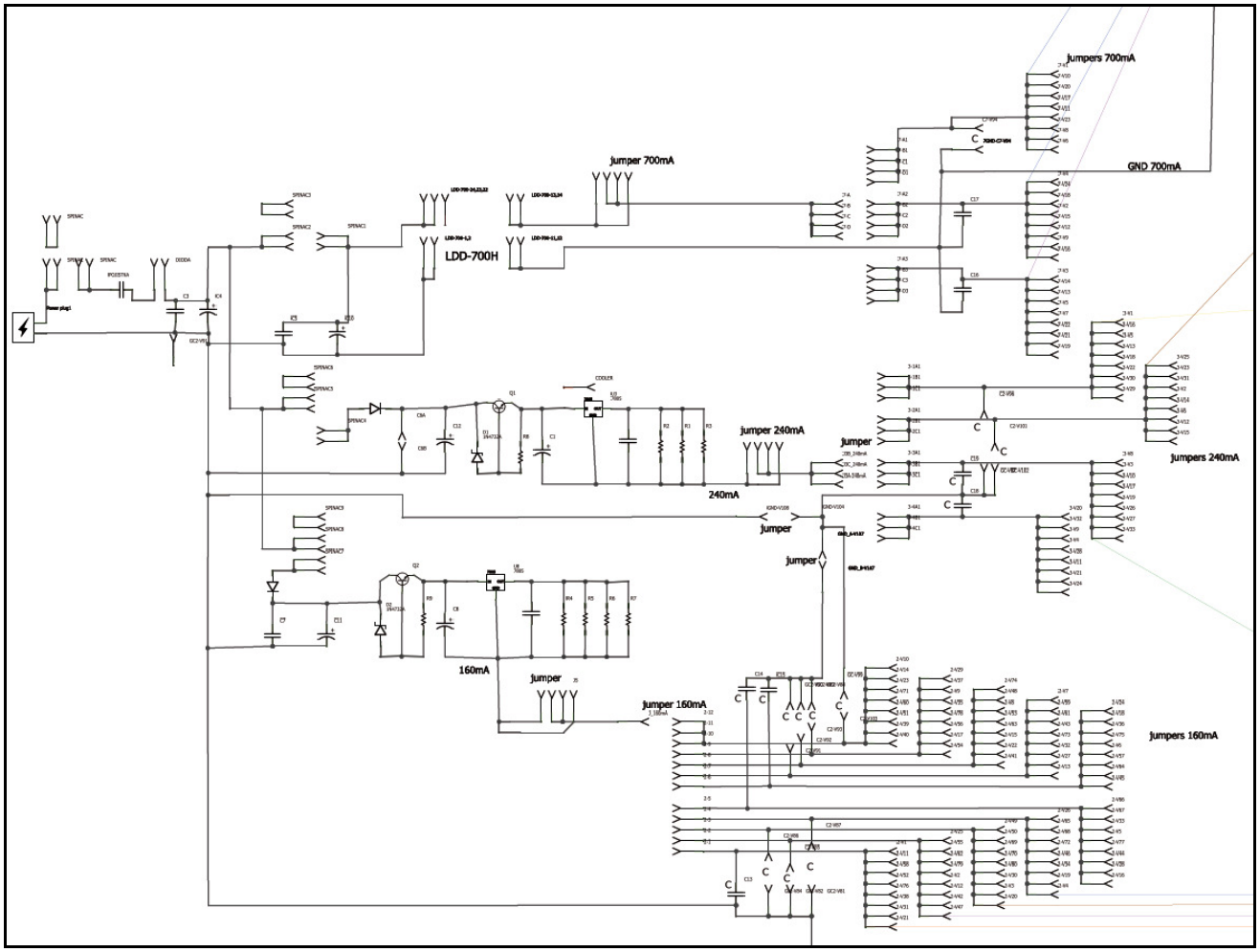
Obrázek 4 Schéma DPS

Schéma DPS pro výrobu z programu Fritzing:



Obrázek 5 Podklady pro výrobu DPS

Ukázka části schématu zobrazující napájecí části obvodu s přepínači:



Obrázek 6 Schéma napájecí části obvodu

Schéma (Obr. 6) zobrazuje napájecí obvody (zdroje proudu) s obvodem LDD-700H a s obvody L7805 se spínači, kondenzátory, diodami a tranzistory. Obvody L7805 jsou v zapojení pro vysoké vstupní napětí podle schématu na obr. 2. Pak jsou na schématu naznačeny kontakty pro kruhové přepínače a propojky pro jednotlivé větve LED a dutinkové lišty.

(Celé schéma viz přiložené soubory.)

Seznam použitých součástek:

Název	KS	kód GME [1]
Fotocuprextit 600x400x1,5 jednovrstvý	1	661-121
Fix pro kreslení DPS S-FIX PLS0.3	1	746-001
Fix pro kreslení DPS S-FIX PLS1.0	1	746-002
Ochranný lak na DPS ELCHEMCO S-LAK PAJITE 50ml	1	741-007
Leptací roztok na DPS ELCHEMCO S-LEPT.ROZ.2	3	740-004
Ochranný lak na DPS ELCHEMCO S-LAK NA DPS	1	741-008
sprej Transparent 21	1	749-003
Vývojka pro pozitivní fotoemulzi ELCHEMCO S-VYVOJKA-500	3	740-002
Cínová pájka SOLDER S-Sn60Pb40E-100g - 1mm F1	1	745-069
Napájecí adaptér síťový 48V/1350mA, T3, výstup 2,1mm	1	751-151
Napájecí souosý konektor PC-GK2.1	1	806-312
Spínač-P-B068EP do DPS	4	631-236
pojistka vstupní 1,6A 60V	1	633-347
dioda 5A, (0,85V)	1	223-171
BY500-1000, 1,35V	6	223-099
Přepínač 3x4 (210mA - 4x)	1	631-039
Přepínač 12 (140mA - 7x)	1	631-089
Přepínač 4x3 (4x150 .. 700mA 3x)	1	631-099
RR 130R (0,6W)	4	110-052
RR W1 68R	2	114-121
RR W1 56R	1	114-452
RR 0R	152	119-145
CE 330u/100VT JAM-TK 12,5x25 RM5 BULK	1	123-785
CE 470u/63V JAM-SK 12,5x20 RM5 BULK	3	123-777
CK 100N/63V	20	120-060
100nF/50V	20	120-106
CE 0,33u/63V JAM-SS 4x7 RM1,5 BULK	3	123-005
7805 TTO 220	2	330-149
chladič V7100	4	620-022
chladič V7142B BLACK	1	620-058
LDD-700H (56V)	1	332-390
ST13005	2	211-225
Zenerova dioda BZX83V004.7	2	222-017
RR 100R , 0,6W	2	110-049
U-KM-NOZICKA	10	622-171
Plastová matice KSS SKP-M03P	10	622-027
Distanční sloupek plastový M3 M/F KSS KDA6M3X15 W	10	623-106
Dutinková lišta BL804G (5pin mechanicky rozdělena na 2x2p)	96	832-040
Zkratovací propojka JUMP-SW OPEN BLACK (30mOhm) 2,54	6	832-140
Oboustranný kolík S2G10 2mm	2	832-168

© 25.1.2013 UTIA AV CR, v.v.i. ZOI

7. Výroba DPS

Deska byla vytvořena fotocestou na fotocuprextit 600x400x1,5 jednovrstvý ([1] GME 661-121).

Po vytištění předlohy na papír A2, přiložení předlohy na fotocuprextit byla předloha nastříkána sprejem Transparent 21([1] GME 749-003). Tím dojde k zprůhlednění papíru s předlohou k UV záření. Deska byla osvícena 64 UV LED po dobu asi 13min. Vzhledem k velikosti desky, bylo nutné UV LED pohybovat nad deskou a svítit na desku klasickým osvětlením v místnosti – zatmívkami a i tak nebylo osvícení zcela dokonalé.

Po osvícení byla deska omyta od spreje Transparent 21. Po vložení do vývojky (vývojka pro pozitivní fotoemulzi ELCHEMCO S-VYVOJKA-500 [1] GME 740-002) byly některé části, které měly být odleptány, pro jistotu proškrábnuty špičkou nože. I to se nakonec ukázalo jako nedostatečné, protože některé části spojů nebyly dostatečně odleptány a to zejména v části kolem napájecích obvodů. Schéma bylo nakonec na několika místech opraveno lihovým fixem.

Posledním krokem je leptání v leptacím roztoku pro výrobu plošných spojů - FeCl3 ([1] GME 740-004). Po omytí, ručním opravení několika spojů, zejména v oblasti napájecích obvodů, byla deska natřena ochranným pájitelným lakem ([1] GME 740-007).

Výsledná deska po navrtání otvorů a osazení:



Obrázek 7 Prototyp - osazená DPS

Po odleptání a mechanické opravení spojů byla deska v příslušných místech navrtána a osazena součástkami. Výsledná osazená deska (prototyp) je zobrazena na obrázku 7.

Deska s plošným spojem a součástkami je navíc ze spodní části vyztužena dřevěným rámem z bukového dřevěného hranolu o straně 20x14x900mm, který byl podle velikosti desky sešroubován do obdélníku a deska byla na rám připevněna šrouby. Deska je ze spodní strany navíc podepřena na několika místech plastovými sloupky s gumovými nožičkami, tak aby se neprohýbala při manipulaci s přepínači.

p i ou it prototypu

1. Po p ipojení napájecího zdroje 48V / 1,35A se deska zapne/vypne hlavním spína em.
2. Podle po adované LED (po adované vlnové délky viz. tabulka 1 a jejího napájecího proudu) zvolíme napájecí v tev a otoným spína em vybereme správnou v tev LED (20-1 a 20-10 / 30-1 a 30-4 / 100-1 a 100-3).
3. Poté je mo né zapnout napájení jednotlivých v tví pro 160 / 240 / 700mA. Je mo né zapnout i všechny v tve najednou, ale to není pro naše ú ely nutné (svítí pak a 3 řady LED).

	vlnová délka			Vtev spína e	I	název LED / sou ástky
	20% od [nm]	80% do [nm]	[nm]		[mA]	
1	395	401	398	20-1	20	330MUV9C - UV 2000uW/30°
2	402	408	405	20-2	20	530MUV9C - UV 4000uW/30°
3	400	470	466	20-3	20	L-53MBDL - BLUE 90/60°
4	450	480	470	20-4	20	530PB6C - BLUE 3000/40° CREE
5	470	530	506	30-1	30	530PG0C - BUEGREEN 8000/30°
6	500	550	525	20-5	20	530PG2C - PURE GREEN 8000/30°
7	550	580	565	30-2	30	L-HLMP-3950 - GREEN 200/24°
8	560	610	590	30-3	30	540MY8C - YELLOW 3500/40°
9	580	625	605	20-6	20	530MO0C - ORANGE 4000/20°
10	600	650	620	20-7	20	520MR2C - RED 5000/20°
11	650	670	660	20-8	20	L-53SRC-DW - RED 2000/30°
12	670	730	700	20-9	20	BL-BHG274 - REG/(GREAN) 8/(50)/50°
13	825	925	880	100-1	100	SFH485-2 - IR >25mW@100mA 20°
14	930	1000	950	100-1	100	LD271 IR - >=10mW/sr@100mA
15				20-10	20	Dutinková lišta BL804G
16				30-4	30	Dutinková lišta BL804G
17				100-1	100	Dutinková lišta BL804G

Tabulka 2 Seznam pou itých LED

Doporu ení:

- Vzhledem k relativn jednoduchému chlazení obvod je vhodné **nenechávat desku zapnutou p li dlouhou dobu** (do cca 30min).
- P i **vypnutí LED jedné z v tví 20 (160) nebo 30 (240) mA je vhodné p ed dalším m ením po kat asi 5 min** ne dojde ke kompletnímu vybití kondenzátor v napájecím obvodu, proto e LED dané v tve ješt chvíli viditeln svítí (pokud to p i pou ití desky vadí). Tento krok se dá obejít kompletním **odpojením napájecího obvodu dané v tve odstran ním zkratovacích propojek**, viz. propojky na obrázku 7.

P íklad pou ití:

Tedy pro LED 605nm (9 tab. 2) pot ebujeme otoný spína otoit do polohy 20-6 (viz. obrázek 7), aktivovat spína pro 20mA (160mA) v tev a zapnout napájení celé desky hlavním spína em.

Pokud v následujícím kroku chceme pou ít LED 590nm (8 tab. 2) je vhodné vypnout celou desku hlavním spína em, po té vypnout spína pro 20mA (160mA) v tev, otoit otoný spína pro danou v tev do polohy 30-3 a zapnout spína pro 30mA (240mA) v tev,.

P ed zapnutím desky je vhodné po kat a p estane zcela svítit p vodní LED 605nm v d sledku vybíjení kondenzátor v napájecím obvodu. Tento krok lze urychlit odpojením LED od napájení odstran ním zkratovací propojky v 20mA (160mA) v tví (viz. obrázek 7.). Pak je mo né zapnout hlavní spína e pro rozsvícení po adované LED 590nm.
(Po dokon ení práce a vypnutí desky hlavním spína em je vhodné vrátit p padné odstran né zkratovací propojky na p vodní místo pro p ípad dalšího pou ívání a zejména pro dodate né vybití napájecích kondenzátor)

Nam[illegible] hodnoty ubytk[illegible] nap[illegible] na všech LED a obvodu L7805:

	vlnová délka				U	naměřeno		I	název
	20%	80%	jm.			U_f	U		
	od	do				8xLED	7805		
	[nm]	[nm]	[nm]	gme.cz	[V]	[V]	[V]	[mA]	
1	395	401	**398**	511-802	3,5	**25,4**	**11,5**	20	330MUV9C - UV 2000uW/30°
2	402	408	**405**	511-877	3,5	**25,6**	**11,3**	20	530MUV9C - UV 4000uW/30°
3	400	470	**466**	511-985	4	**32,3**	**4,5**	20	L-53MBDL - BLUE 90/60°
4	450	480	**470**	511-759	3,3	**24,7**	**11,9**	20	530PB6C - BLUE 3000/40° CREE
5	470	530	**506**	511-803	3,5	**26,8**	**9,2**	30	530PG0C - BUEGREEN 8000/30°
6	500	550	**525**	511-782	3,3	**26,2**	**10,5**	20	530PG2C - PURE GREEN 8000/30°
7	550	580	**565**	511-032	2,2	**18,1**	**17,8**	30	L-HLMP-3950 - GREEN 200/24°
8	560	610	**590**	511-429	2,1	**16,6**	**19,3**	30	540MY8C - YELLOW 3500/40°
9	580	625	**605**	511-608	2,1	**15,1**	**21,7**	20	530MO0C - ORANGE 4000/20°
10	600	650	**620**	511-674	2,1	**16,2**	**20,6**	20	520MR2C - RED 5000/20°
11	650	670	**660**	511-687	2,5	**14,7**	**22,0**	20	L-53SRC-DW - RED 2000/30°
12	670	730	**700**	511-103	2,2	**17,6**	**19,2**	20	BL-BHG274 - REG/(GREAN) 8/(50)/50°
13	825	925	**880**	520-015	1,5	**12,2**	**N/A**	100	SFH485-2 - IR >25mW@100mA 20°
14	930	1000	**950**	511-094	1,3	**11,8**	**N/A**	100	LD271 IR - >=10mW/sr@100mA

Nam[illegible]ené hodnoty ukazují, [illegible]e nap[illegible]tí na obvodu L7805 a jednotlivých LED se dr[illegible]í v p[illegible]edpokládaných hranicích 2,a 30V na obvodu I 7805. Nam[illegible]ené hodnoty nap[illegible]tí na jednotlivých LED pak odpovídají katalogovým hodnotám.

P[illegible]lo[illegible]ené soubory

readme.txt – tento odstavec
Seznam.xls – seznam pou[illegible]itých LED a ostatních sou[illegible]ástek
Schema_V37_large.fzz – schéma desky s plošným spojem vytvo[illegible]ené v programu Fritzing V0.7.10 b6551 [2]

Výstupy z programu Fritzing (DPS - deska s plošnými spoji):

Schema_V37_large_etch_copper_bottom.pdf - spodní [illegible]ást DPS – m[illegible]
Schema_V37_large_etch_copper_bottom_mirror.pdf - spodní [illegible]ást DPS – m[illegible], zrcadlov[illegible] oto[illegible]ená
Schema_V37_large_etch_mask_bottom.pdf - maska DPS
Schema_V37_large_etch_mask_bottom_mirror.pdf - maska DPS, zrcadlov[illegible] oto[illegible]ená
Schema_V37_large_etch_silk_top.pdf - popisky DPS
Schema_V37_large_etch_silk_top_mirror.pdf - popisky DPS, zrcadlov[illegible] oto[illegible]ená

© 25.1.2013 UTIA AV CR, v.v.i. ZOI

All problems according to Preflight profile
Convert to PDF/A-2u

9. Závěr

Zde popisované pole LED o velikosti 8x8 LED, rozmístěných do rovnostranného trojúhelníku o straně 5cm se podařilo úspěšně vytvořit a odzkoušet. Pole je navrženo tak, aby se relativně jednoduše ovládalo a bylo možné jej případně přenášet.

Další využití pole LED v projektu teprve ukáže kvalitu realizace a zejména vhodnost zvolených LED pro pokrytí zadání (zejména šířku pásma vyzařovaného světla a homogenitu vyzařovaného světelného kužele). Pro tento účel pole také obsahuje 3 volné patice, kam je možné umístit případné nové LED s jinou vlnovou délkou či jinými parametry vyzařování a tím ověřit jejich využití přímo v požadovaném rozmístění.

Využití v projektu také ukáže, zda zvolené rozmístění do trojúhelníkové matice o vzdálenosti 5 cm a celkové velikosti 8x8 je dostačující pro potřeby projektu. V tomto směru by však bylo nutné vytvořit LED pole nové.

10. Literatura

[1] *GME,* [online], URL : < http://www.gme.cz/ > [citováno 21. ledna 2013]

[2] *Fritzing,* [online], URL: < http://http://fritzing.org/ > [citováno 21. ledna 2013]

[3] *GNU GPL V3,* [online], URL: < http://www.gnu.org/copyleft/gpl.html > [citováno 21. ledna 2013]

All problems according to Preflight profile
Convert to PDF/A-2u

Low-cost mobile system for multispectral cultural heritage data acquisition

Jan Blažek, Jindřich Soukup, Barbara Zitová, Jan Flusser
Institute of Information Theory and Automation, ASCR
Academy of Sciences of Czech Republic, Prague, Czech Republic
Email:[blazek—soukupj—zitova—flusser]@utia.cas.cz

Tomáš Tichý and Janka Hradilová
ALMA Laboratory, Academy of Fine Arts
Prague, Czech Republic
Email: tomas.tichy.cz@gmail.com, hradilovaj@volny.cz

***Abstract*—In the paper we propose an alternative approach to the multispectral data acquisition of the cultural heritage artifacts. The demonstrated solution is mobile, affordable, and consists only of commercial off-the-shelf products. It could be used for the data acquisition in-situ without limitations. It was designed for multispectral scanning of cultural heritage artifacts for their first analysis, for multimedia presentations dedicated to public, and, of course, for art conservation studies. The presented solution contains next to the hardware part as well the description of pre-analysis step - two alternative ways of the photometric calibration - to ensure the anticipated precision. The applicability of the framework was demonstrated on the case study, the preliminary spectral analysis. The proposed methodology is successfully used in the art restoration practice.**

***Index Terms*—Multispectral data acquisition, cultural heritage, photometric calibration.**

I. Introduction

Multispectral imaging is nowadays an established technology for an acquisition of cultural heritage data, including paintings [15], large-sized pictorial surfaces such as frescoed halls [2], or even 3D structures like walls or monuments [8]. It is a non-destructive technique for analysis of paintings and other art objects. It provides spectral and colorimetric characterization of the artifact, which helps to document the current state of an artwork, its creation progress, and the restoration interventions, too.

The scanning systems produce datasets representing the studied artifacts in various wavebands (infrared, ultraviolet). The multispectral scans provide information about the art composition, it helps to achieve faithful color reproduction, it can effectively reveal the artwork creation. Such information can create valuable insight into the painting. It could bring near the history of the painting, demonstrate the painter's original intentions and show the tracks of the restoration interventions.

There are many solutions for multispectral cultural heritage data acquisition. They differ in their mobility (in-situ or laboratory-only data acquisition), in their spectral resolution, in their allowed spatial as well as spectral measured extent. The price can differ significantly, too. Today, the topic of the multispectral imaging attracts big attention. The survey of the 3D and multispectral data acquisition for cultural heritage applications was recently published [4]. They present the state of the art and existing registration techniques for creation of 3D models with multispectral texture. There were several large project studying this topic like MARC - Methodology for Art Reproduction in Colour [12], VASARI - Visual Arts System for Archiving and Retrieval of Images [13], or CRISATEL - [6]). In the CRISATEL project the high resolution multispectral image acquisition system was built for digitizing art paintings. The system consists of a multispectral digital camera and of light projectors. They have utilized the developed system to scan famous Mona Lisa painting [9]. The acquired data were used for better understanding of this masterpiece as well as for the attempts to apply virtual restoration. The tutorial on the multispectral imaging where Mona Lisa is used as a case study was published in [16].

Novati et al. [14] proposed the exploitation of the multispectral imaging for the image acquisition in a digital museum. They addressed two approaches to multispectral acquisition using narrow-band and wide-band sensors. They proposed new framework for wideband acquisition, which could be affordable for cultural institutions archives. Paviotti et al. [2] concentrated on multispectral acquisition of large-sized pictorial surfaces. They paid special attention to the practical issues related to the size of the scanned objects as well as to their illumination. Carcagni et al. [5] proposed their multispectral scanning system ($380\,\mathrm{nm}$ up to $800\,\mathrm{nm}$), developed to overcome problems related to the systems based on CCD or Vidicon cameras. They work with the spectrometer for contact-less single-point spectral measurements, moved by two orthogonally mounted translation stages. Bianco et al. [3] studied the multispectral data acquisition, producing already geometrically registered data using the specialized focus control system. They demonstrated the applicability on the document analysis.

Despite listed references the multispectral technology is often still understood as something available only to special cultural laboratories. In our paper we propose multispectral acquisition framework which is mobile and adjustable. We believe that such solution could spread even among the individual specialists and thus the multispectral acquisition could became available for general interested public.

It is composed of commercial off-the-shelf products and it has low purchase price. It is mobile so it could be used for the data acquisition "in situ" without any limitations. We foresee its applicability in the data acquisition for cultural heritage artifacts for first analysis, for multimedia presentations,

978-1-4799-3169-9/13/$31.00 ©2013 IEEE

All problems according to Preflight profile
Convert to PDF/A-2u

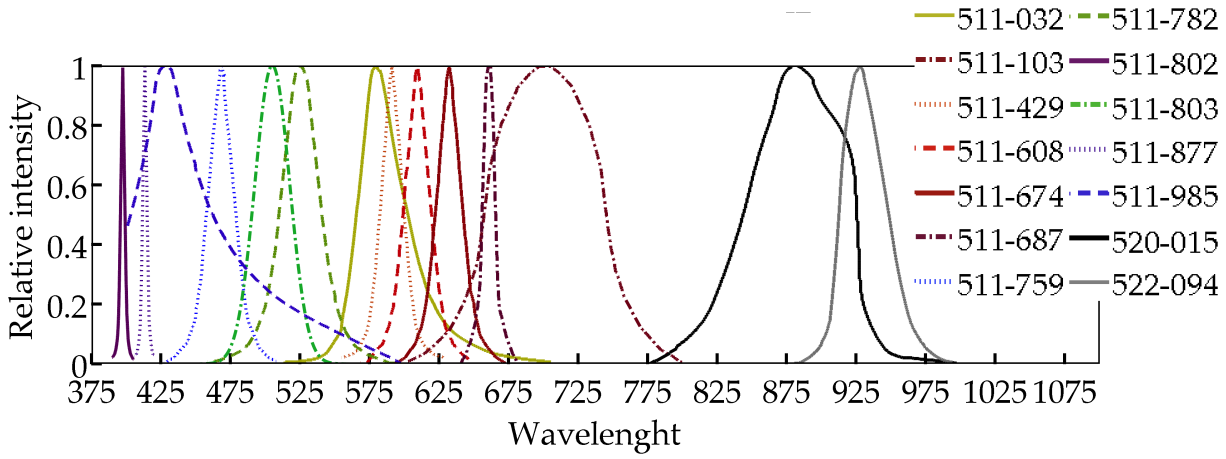


Fig. 1. Spectral relative intensities of used LEDs.

dedicated to public, and, of course, for the art conservation studies. Moreover, the advantage of our approach is that we do not limit the introduced solution to the hardware proposal. We describe the calibration and the evaluation of the system parameters to ensure the anticipated precision, which is very important step if we want to be sure about the meaning of the measured data. We demonstrate the applicability of the framework on the case study.

The proposed paper is organized as follows. The data hardware is described in Section 2. The proposed camera calibration system is described in Section 3. The Section 4 demonstrates the applicability of the method on the real data. Finally, Section 5 concludes our contribution.

II. Hardware for data acquisition

Proposed framework addresses the data acquisition in the interval from $380\,\mathrm{nm}$ up to $1200\,\mathrm{nm}$, covering the narrow part of the ultraviolet light (UV, till $400\,\mathrm{nm}$), visible light (VL, $400\,\mathrm{nm}$ up to $700nm$) and, finally, the infrared light (IR, $700\,\mathrm{nm}$ up to $1200\,\mathrm{nm}$). The most interesting and as well the most useful in the restorer practice is infrared (IR) band and ultraviolet fluorescence. Unlike the visible light, infrared radiation can pass through certain materials and this property is exploited in the art analysis - beginning stages of the artwork can be studied. First attempts to use the IR features for artwork investigation appeared around 1970 in the work of the Van Asperen De Boer [18]. However usage of the IR photography is still not yet as spread as it could be.

There are successful applications of IR imaging. Cornelis et al. [7] studied Gauguin paintings in thirteen high resolution spectral bands – nine in the visible domain, one in the near ultraviolet and three in the infrared domain. Anith et al. [1] used IR and other modalities to study van Gogh paintings, processing high resolution scans, too.

Usefulness of the visible light is apparent. UV imaging in the proposed system can capture wavelengths from the interval $380\,\mathrm{nm}$ - $400\,\mathrm{nm}$, however capturing of UV sub-bands can be limited by glass optics used on the camera. The UV fluorescence can uncover a condition of the varnish layer. A progress of restoration treatment (retouchings, over-paintings), or an identification of materials used for creation of the artwork can be studied in UV imaging.

In the proposed framework, we suggest a solution, which spectral and spatial resolutions are not as high as in the case of a special dedicated equipment, however our system is mobile, fast, easy to use, cheap, and easy and fast in the data postprocessing. The base unit of the system is a common digital camera (in our case Canon D500 or Canon D50) adjusted for capturing NIR wavelengths. Originally a light sensitive chip from the camera is equipped with IR cut filter (ICF). For our purpose ICF was removed. Such a camera adaptation broke color balance of a light sensitive chip, but its sensitivity is increased up to $1200\,\mathrm{nm}$ in the spectral domain. After this adjustment the camera is prepared for capturing wavelengths from $380\,\mathrm{nm}$ up to $1200\,\mathrm{nm}$. The acquired images are processed using the raw format to avoid mosaicing artifacts.

For filtering particular spectral sub-bands common photographic filters are applied: color filters (we have used red, orange, yellow, green, blue and sepia); IR cut-off filters ($> 680\,\mathrm{nm}$, $> 720\,\mathrm{nm}$, $> 760\,\mathrm{nm}$, $> 850\,\mathrm{nm}$, $> 950\,\mathrm{nm}$, and $> 1090\,\mathrm{nm}$), and an UV cut-off filter ($< 400\,\mathrm{nm}$). We have measured the transmittance of the filters to ensure higher precision (see tab. I). We recommend such evaluation for every used filter.

If the camera in use is not equipped with filter holder, instead of the filter application we propose to control light conditions to be able to capture specific spectral sub-bands. For such situation we suggest LEDs as a light source [10]. We have created the LED panel which is able to split the visual part of spectrum into eight sub-bands and two disjunctive IR sub-bands (see fig. 1). Filters and LEDs are shown in fig. 2.

A. Limitations

The proposed solution has many advantages such as its mobility, availability, and the price. However, there are some

All problems according to Preflight profile
Convert to PDF/A-2u

TABLE I
SPECTRAL SUB-BANDS ACHIEVABLE BY PROPOSED SOLUTIONS. THEY ARE REALIZED USING FILTERS AND LEDS.

spectral band	GME No.	**used filters/LED diods**
395-401nm	511-802	UV - 330MUV9C (limited with glas optics)
402-408nm	511-877	UV - 530MUV9C
400-470nm	511-985	L-53MBDL - BLUE
450-480nm	511-759	530PB6C - BLUE $3000/40\,\mathrm{deg}$ CREE
470-530nm	511-803	530PG0C - BLUEGREEN
500-550nm	511-782	540PG2C - PURE GREEN
550-580nm	511-032	L-HLMP-3950 - GREEN
560-610nm	511-429	540MY8C - YELLOW $3500/40\,\mathrm{deg}$
580-625nm	511-608	530MO0C - ORANGE
600-650nm	511-674	520MR2C - RED
650-670nm	511-687	L-53SRC-DW - RED
680-720nm		Filters: cut-off $720\,\mathrm{nm}$ minus cut-off $680\,\mathrm{nm}$
670-730nm	511-103	BL-BHG274 REG(GREAN)
720-760nm		Filters: cut-off $760\,\mathrm{nm}$ minus cut-off $620\,\mathrm{nm}$
760-850nm		Filters: cut-off $850\,\mathrm{nm}$ minus cut-off $760\,\mathrm{nm}$
825-925nm	520-015	SFH485-2 - IR
850-950nm		Filters: cut-off $950\,\mathrm{nm}$ minus cut-off $850\,\mathrm{nm}$
930-1000nm	511-094	LD271 - IR
950-1090nm		Filters: cut-off $1090\,\mathrm{nm}$ minus cut-off $950\,\mathrm{nm}$
1090-1200nm		XNite IR cut-off

drawbacks and limitations, which should be mentioned here.

The infrared imaging in the art conservation practice exploits wavelengths up to $2\mu m$[19], however the sensitivity of the standard CCD camera even after the ICF removal is cut off on $1200nm$. The camera optics is geometrically well balanced for the visible part of spectrum. Wavelengths from $700nm$ up to $1200nm$ require different focus setting than images taken in the visible light. The correct focus can be set for the visible or the IR part of the spectrum, respectively, by shifting the camera sensor. Therefore images from different modalities must be first geometrically aligned ([3]). In the proposed solution the geometrical alignment is achieved in the accordant software.

Reflections and light flares are very common defects visible on captured images especially in the IR spectrum, because the antireflection surface of the lens does not compensate these wavelengths. A varnish layer on the artwork makes the reflection problem even worse. An elimination of such reflections should start "in-situ", using direct light diffusion or by an exploitation of the polarizing filter on the camera.

Best results of the multispectral data acquisition are achieved with the uniform light source intensity. This is the most problematic part of the capturing "in-situ", where often uncontrolled light sources are present, such as windows. We recommend a creation of an auxiliary image for the light intensity balance. It captures a homogeneous color paper/canvas under the same light conditions as in the location of the captured artwork. Light conditions can be then normalized according to this auxiliary image (see Section 4 for more details).

Finally, we strongly recommend to photometrically calibrate the camera before any analysis of the pixel spectral response starts. Without an exact knowledge of the camera spectral response we cannot distinguish underdrawings or a specific paint material using only the captured data. The photometric camera calibration must be done according to the expert knowledge. Then an automatic post-processing and analysis of the acquired data can be realized.

III. PHOTOMETRIC CAMERA CALIBRATION

The goal of our approach is the utilization of the camera as a primitive spectroscope which is able to analyze the whole artwork. We will achieve a partially constant approximation of the spectral response of the artwork. This spectral approximation can be then used for the paint material identification. Knowledge of the camera sensitivity, see fig. 5, is necessary to achieve meaningful artwork representation. This can be find out by means of the photometric camera calibration. The calibration process as well helps to eliminate intensity values mixing due to the presence of CFA (color filter array).

The process of photometric calibration of a camera establishes the relation between pixel values produced by a given camera and photometric quantities such as SI light units. For the camera calibration it is necessary to have a calibrated light source, where we know the output light intensity for each wavelength sub-band, which we want measure. Well known light source is the Sun [17], however we used the calibrated light source HL2000 CAL-EXT (Ocean Optics, calibrated from $360\,\mathrm{nm}$ up to $1500\,\mathrm{nm}$) because of an easier setup for the measurement.

The calibration process will estimate the sensitivity of the camera $s(\lambda)$, where s is partially constant (for our purpose). We assume the same sensitivity function $s(\lambda)$ across the whole sensor.

All problems according to Preflight profile
Convert to PDF/A-2u

For the camera calibration we will use the following transmittance model:

$$I = g \int_{\lambda} l(\lambda) s(\lambda)\, \mathrm{d}\lambda, \tag{1}$$

where I is the captured intensity, $l(\lambda)$ represents a light intensity emitted from the light source. Finally, g function describes a nonlinear (in general) dependency between the light and the intensity on the captured photography. The function g is dependent on ISO, a white balance, a gamma correction and on other software intensity compensations. In accordance with our measurements we approximate the function g as

$$g(x) = ax + b, \tag{2}$$

with different a and b for each camera sensor (RGGB). The estimation of $s(\lambda)$ was realized in two ways. The first approach is based on a filter based intensity measurement, while the other makes use of a monochromatic measurement. Both methods are easily repeatable even under limited conditions.



Fig. 2. Constructed LED panel and used filters. All filters have common diameter 77mm.

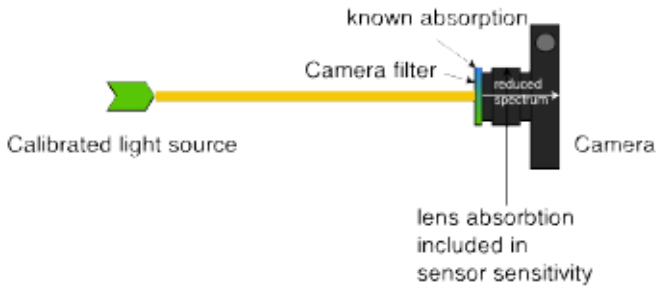


Fig. 3. Proposed scheme of the sub-band intensity measurement and the camera calibration.

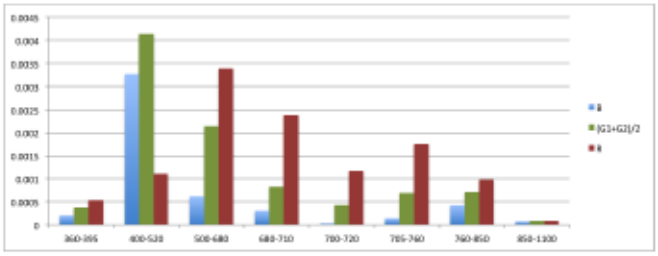


Fig. 4. Measured relative sensitivity of the camera segments (red, blue, green average). Horizontal axis contains 8 wavelength subbands. Vertical axis shows ratio between pixel response (measured intensity) and light intensity from particular subband. The sub-bands were constructed as a linear combination of the used filters.

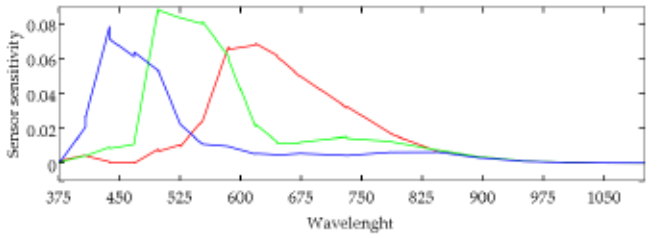


Fig. 5. The estimated sensitivity of camera segments. Values were measured for each 25nm, from 375 to 1050. Each step was captured twice with different camera ISO. The vertical skips in sensitivity curves correspond to multiple measurements in particular subband.

A. *Filter based intensity measurement*

The first approach to the camera calibration makes use of several filters and known calibrated light source. The light source is aimed directly into the camera. The camera is equipped consecutively with filters, used later for the artwork analysis (see fig. 3).

The formula (1) is now extended with $f_i(\lambda)$, which represents the transmittance of the filter i:

$$I_i = g \int_{\lambda} l(\lambda) f_i(\lambda) s(\lambda) d\lambda, \tag{3}$$

Measurements with different filters f_i and with a piecewise constant function s give us:

$$\begin{aligned} I &= A \times \vec{s} \\ s \approx \vec{s} &= A^{+} \times I, \end{aligned} \tag{4}$$

where A matrix contains in every row i-th values of $l(\lambda_j) f_i(\lambda_j)$. λ_j represents the interval, where s is approximated as a constant. Vector $\vec{s}$ therefore contains the sensitivity of the camera at intervals λ_j.

The discretization of the spectrum from 380 nm to 1200 nm was made according to the used filters. We obtain eight useful sub-bands (see fig. 4) in which we can measure the spectral response. These sub-bands were constructed as linear combinations of available measured filters (blue, green, orange, yellow, red, sepia and cut-off 680, 720, 760, 850).

B. *Monochromatic intensity measurement*

The second approach uses the same calibrated light source. In this case light spectrum was filtered to narrow sub-bands

All problems according to Preflight profile
Convert to PDF/A-2u

by a monochromator, the filters were not used. In contrast with the filter based estimation, the function s is measured for several wavelengths and then approximated by a polynomial.

Here, the model (1) must be extended with an extra light absorbance $D(\lambda)$ which reflects the reduction of the light intensity in the monochromator and with the parameter w, which reflects the function of the monochromator. The w function here is approximated by delta function. We neglect variance around filtered wavelength.

$$I = g \int_{\lambda} l(\lambda) s(\lambda) D(\lambda) w(\lambda) d\lambda \tag{5}$$

Then the narrowed light spectra is captured by an optical cable and is measured by the calibrated photodiode. The resulting intensity is evaluated in the camera, too. For each wavelength we evaluate the ratio of the camera-estimated intensity $g^{-1}(I)$ to the photodiode-estimated intensity I_p,

$$\frac{g^{-1}(I)}{I_p}. \tag{6}$$

The measurement was realized for 21 various wavelengths ranging from 317 nm up to 1103 nm, for each wavelength multiple times with various expositions. Results of the camera calibration process is demonstrated in fig. 5.

IV. Application

The applicability of the proposed solution for multispectral cultural data acquisition and preliminary analysis is demonstrated here. While studying the *Fruit festoon* painting (see fig. 6) we collected 12 spectral sub-bands - ($I_{captured}$) (see fig. 8). Each sub-band was normalized - (I_{norm}) - according to the shutter speed (T) and the LED panel average intensity. Individual spectral sub-bands were mutually aligned using weighted mean method [11] to remove possible geometrical differences, introduced during the acquisition process.

The LED panel intensity was captured separately for further normalization - (I_{canvas}). At the position of an artwork a white canvas was placed and its image was captured. An average intensity for the whole canvas was computed - $E(I_{canvas})$ - and used for the normalization of captured sub-bands

$$I_{norm} = \frac{I_{captured}}{T * E(I_{canvas})}. \tag{7}$$

Problematic scans 605 nm and 700 nm were dropped, because the values were out of the range of the camera sensitivity.

To verify realized measurements a virtual coloring was created (see fig. 6). The acquired data were used to evaluate the normalization and to demonstrate the quality of the proposed solution.

Spectral curves in fig. 7 show pixel responses in each sub-band, values are extracted directly from both the original and the generated image, respectively, in fig. 8. Values are relative to each other (according to shutter speed normalization and LED panel average intensity). Two types of blue were selected for the comparison. A significant dissimilarity appeared only around 500 nm.

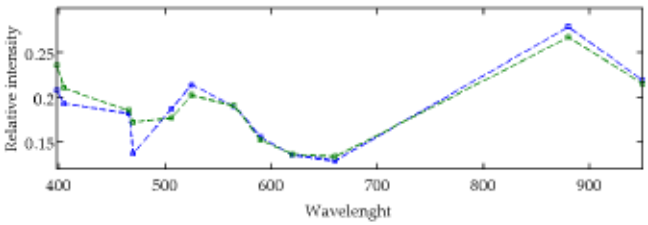


Fig. 7. Comparison of multispectral responses of two areas circled in fig. 6. Subband measurements were made by using LED light and camera RAW format normalized by shutter speed and segment sensitivity (in this case blue segment). Precision of the measurement can be influenced by used LED subbands and by the nonlinearity of the camera sensitivity. More significant dissimilarity appeared around 500nm.

V. Conclusions

We proposed an alternative approach to the multispectral data acquisition of the cultural heritage artifacts. The demonstrated solution is mobile and universal for any size of the artwork. It is based on the IR-modified camera with various filters or, if the camera is not equipped with filter holder, with the the LED panel, splitting the visual part of spectrum into eight sub-bands and two disjunctive IR sub-bands. The proposed solution is affordable and consists of commercial off-the-shelf products. Capturing of images is fast and does not require any special knowledge compared to other common documentation imaging. To ensure the requested accuracy, the photometric camera calibration was described. Two different approaches for the calibration were introduced, which could be chosen depending on the auxiliary tools availability. Both methods are easily repeatable even under limited conditions. Finally, we showed an exploitation of acquired images for the preliminary spectral analysis. The proposed methodology we successfully use in the art restoration practice.

We believe that the proposed system can spread the multispectral data analysis and made it available for general interested public. In the future, we plan to continue in the evaluation of the proposed system and to compare it to high-end systems.. We will concentrate on testing the calibration robustness and on comparison of the achieved spectral information to the results of the common spectrometer. Achieved experience will be utilized in the creation of the database of colors, pigments, and binding materials, where the spectral information will form the key entry in this database.

Acknowledgment

The authors would like to thank to Pavel Kvasnička for help with camera calibration. This work has been supported by Czech Science Fundation, (project no. P103/12/2211).

References

[1] Anila Anitha, Andrei Brasoveanu, Marco Duarte, Shannon Hughes, Ingrid Daubechies, Joris Dik, Koen Janssens, and Matthias Alfeld. Restoration of x-ray fluorescence images of hidden paintings. *Signal Process.*, 93(3):592–604, March 2013.

[2] Luca Poletto, Guido Maria Cortelazzo, Anna Paviotti, Filippo Ratti. Multispectral acquisition of large-sized pictorial surfaces. *EURASIP J. Image and Video Processing*, 2009.

All problems according to Preflight profile
Convert to PDF/A-2u



Fig. 6. (left) - Tomáš Tichý (2008), the copy of Fruit Festoon by Nicolaes van Gelder, oil on canvas - $65 \times 50\,\mathrm{cm}$. (right) - the reconstructed image, created from the scanned data in various sub-bands. The blue channel was taken from scans in $405\,\mathrm{nm}$, $466\,\mathrm{nm}$, and $470\,\mathrm{nm}$, respectively, the green one was taken from $506\,\mathrm{nm}$, $525\,\mathrm{nm}$, and $565\,\mathrm{nm}$, and, finally, the red band from $590\,\mathrm{nm}$, $620\,\mathrm{nm}$ and $660\,\mathrm{nm}$. Two circles contain points to be compared with the ground truth, see fig. 7

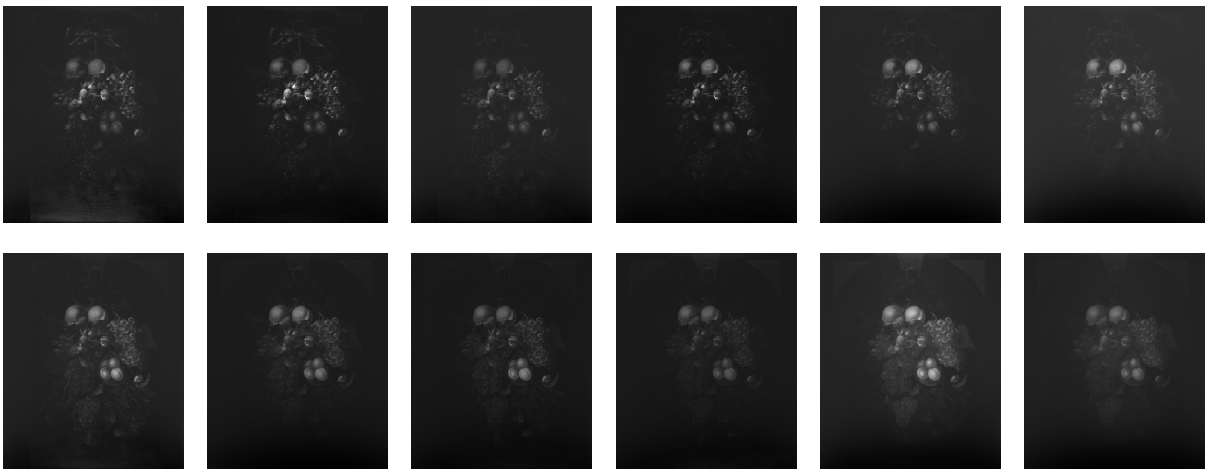


Fig. 8. Spectral responses in $398\,\mathrm{nm}$, $405\,\mathrm{nm}$, $466\,\mathrm{nm}$, $470\,\mathrm{nm}$, $506\,\mathrm{nm}$, $525\,\mathrm{nm}$, $565\,\mathrm{nm}$, $590\,\mathrm{nm}$, $620\,\mathrm{nm}$, $660\,\mathrm{nm}$, $880\,\mathrm{nm}$ and $950\,\mathrm{nm}$ (in the text order). In this case study the LED panel approach was used. Images are captured in camera RAW format, normalized by shutter speed and by segment sensitivity in particular subbands.

[3] Gianfranco Bianco, Fabio Bruno, and Maurizio Muzzupappa. Multispectral data cube acquisition of aligned images for document analysis by means of a filter-wheel camera provided with focus control. *Journal of Cultural Heritage*, 14(3):190 – 200, 2013.

[4] Franck S Marzani, Frank Boochs, Camille Simon Chane, and Alamin Mansouri. Integration of 3d and multispectral data for cultural heritage applications: survey and perspectives. *Image and Vision Computing*, 31:91–102, 2013.

[5] P. Carcagni, A. Della Patria, R. Fontana, M. Greco, M. Mastroianni, M. Materazzi, E. Pampaloni, and L. Pezzati. Multispectral imaging of paintings by optical scanning. *Optics and Lasers in Engineering*, 45:360367, 2007.

[6] R. Lahanier, C. Pitzalis, D. Colantoni, and P. Pillay. Analysis of multispectral images of paintings. *14th EuropeanSignal Processing Conference (EUSIPCO)*, pages 1–5, 2006.

[7] Bruno Cornelis, Ann Dooms, Frederik Leen, Adrian Munteanu, and Peter Schelkens. Multispectral imaging for digital painting analysis: a gauguin case study. pages 77980I–77980I–13, 2010.

[8] M. Caldon, M. Fedel, L. Poletto, N. Brusco, and G. Cortelazzo. Simultaneous acquisition of 3d shape and color texture from large frescoed areas. *Proc. SPIE: Optics for Arts, Architecture, and Archaeology*, (6618 O3A), 2007.

[9] M. Elias and P. Cotte. Multispectral camera and radiative transfer equation used to depict leonardo's sfumato in mona lisa. *Appl. Opt.*, (47):2146–2154, 2008.

[10] Laure Fauch. *Acquisition of Multispectral Color Images Using Light-Emitting Diodes*. PhD thesis, University of Eastern Finland, 2012.

[11] A. Ardeshir Goshtasby. *2-D and 3-D Image Registration: for Medical, Remote Sensing, and Industrial Applications*. Wiley-Interscience, 2005.

[12] K. Martinez, J. Cupitt, and D. Saunders. Methodology for art repro-

All problems according to Preflight profile
Convert to PDF/A-2u

duction in colour: the marc project. *Computers and the History of Art Journal*, 6(2):1–20, 1996.

[13] K. Martinez. High resolution digital imaging of paintings. the vasari project. *Microcomputers for Information Management*, 8(4):277283, 1991.

[14] Gianluca Novati, Paolo Pellegri, and Raimondo Schettini. An affordable multispectral imaging system for the digital museum. *International Journal on Digital Libraries*, 5(3):167–178, 2005.

[15] A. Pelagotti, A.D. Mastio, A.D. Rosa, and A. Piva. Multispectral imaging of paintings. *IEEE Signal Processing Magazine*, 25(4):27–36, 2008.

[16] A. Ribes, R. Pillay, F. Schmitt, and C. Lahanier. Studying that smile. *Signal Processing Magazine, IEEE*, 25(4):14–26, 2008.

[17] C. Riordan, D. Myers, M. Rymes, R. Hulstrom, W. Marion, C. Jennings, and C. Whitaker. Spectral solar radiation data base at {SERI}. *Solar Energy*, 42(1):67 – 79, 1989.

[18] J.R.J. van Asperen de Boer. Reflectography of paintings using an infrared vidicon television system. *Studies in Conservation*, 14:96–118, 1969.

[19] Elizabeth Walmsley, Catherine Metzger, John K. Delaney, and Colin Fletcher. Improved visualization of underdrawings with solid-state detectors operating in the infrared. *Studies in Conservation*, 39(4):pp. 217–231, 1994.

All problems according to Preflight profile
Convert to PDF/A-2u

M3art: A Database of Models of Canvas Paintings

Jan Blažek[1], Jindřich Soukup[1], Barbara Zitová[1], Jan Flusser[1], Janka Hradilová[2], David Hradil[2], and Tomáš Tichý[2],

[1] Dep. of Image Processing, UTIA AS CR, Pod Vodárenskou věží 4, 18208 Prague, Czech Republic
{blazek,soukupj,zitova,flusser}@utia.cas.cz
[2] ALMA Laboratory, Academy of Fine Arts in Prague, U Akademie 4, 170 22 Prague 7, Czech Republic
hradilovaj@volny.cz,hradil@iic.cas.cz,tomas.tichy@gmail.com

Abstract. M3art database contains data about colours behaviour in VIS and NIR spectral bands. The database is open, publicly available and should serve as the knowledge base for further study of optical properties of pigments, drawing materials and canvases. The content of database consists of FORS and digital camera data collected in range 400-1050nm. Measurements were made on up to three layer samples composed of canvas, underdrawing and colour layers. The colorants were selected to represent historical painting techniques in Gothic and Renaissance According to underdrawing acquisition ability four material categories were established.

Keywords: pigment database, FORS, underdrawing, penetration.

1 Introduction

The main issues for non-destructive and cost-effective evaluation of studied artwork are selection of an appropriate modality [1], of acquisition tools [2] and finally proper way of the measured data interpretation [3]. We focused on deep understanding of colour and behaviour of painting materials.

A few years ago we started with multimodal analysis of artworks (UV fluorescence, VIS - visible light spectrum and NIR - near infrared spectrum), thus we had to deal with the interpretation of measured data. In the literature [1] UV fluorescence is used for varnish repaintings and retouches (restoration intervention) detection and NIR for penetration of some pigment layers [4] of the artwork (especially for underdrawing visualization). Such optical effects were modelled for example in [5], [3], [6].

Description of layer based on reflected light only is insufficient in sense of its week conditioning. The unknown light absorption of top layers makes the interpretation of the measured data ambiguous. Observed high-value intensities may be caused by high reflectance of the top layer or high transmittance of the top layer combined with high reflectance of the bottom layer. These two effects cannot be distinguished without absorption/transmission measurement. Thus, our algorithms for automatic underdrawing detection has in such case many false positives in individual layer identification.

M. Ioannides et al. (Eds.): EuroMed 2014, LNCS 8740, pp. 176–185, 2014.
© Springer International Publishing Switzerland 2014

All problems according to Preflight profile
Convert to PDF/A-2u

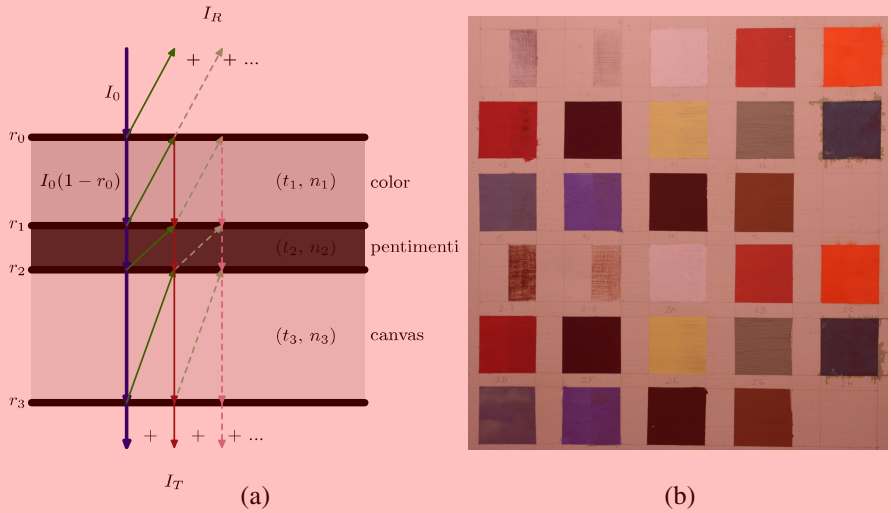


Fig. 1 (a) Model of painted layers. For particular layer boundary coefficient r denotes the reflection, for the layer (n, t) describe layer index of reflection and transmission coefficient I denotes light intensity (subscripts R - reflected, 0 - emitted and T - transmitted). (b) The canvas (Mock-up no.1) with model samples imitating Gothic to Renaissance Italian painting. First two samples in the first and fourth row (samples no. 1, 2, 16, 17) are only with underdrawing (graphite and red clay, respectively). Pigments follow (lead white, cinnabar, red lead, madder, indigo, lead-tin yellow, green earth, verdigris, azurite, ultramarine, bone black and umber raw). Right half of each pigment sample contains underdrawing according to sample no. 1 and no. 16. Sample numbering runs from left to right and from top to down.

For elimination of these problems we have designed a study, similar to one described in [7], leading to better understanding of the behaviour of simple material layers in sense of their transmittance [8]. We have studied 13 different pigments and dyes and 10 different drawing materials. The colour pallets were selected to reflect specific historical painting techniques; only small constraints regarding the experiment setup were accepted.

We prepare 11 representative canvas models, each consisting of set of 30 square samples (see Figure 1 (b)). Each sample was multiple-times measured by spectrometer (FORS) and also by digital camera (VIS+NIR). In this way the sample reflection and transmission for both of its parts (with and without underdrawing) were measured. The measurements database is the major output of our study [9]. We have started the evaluation of the measured data and conclusions enabled to formulate recommendations with respect to the interpretability of the used painting materials.

2 OpticalRepresentation

To be able to correctly interpret measured values we have to define appropriate physical model of the experiment setting (see Figure 1(a)). The painting is here understood as a set of certain number of colorant layers (similar to [10]).

All problems according to Preflight profile
Convert to PDF/A-2u

We represent layer optical behaviour by parameters: d - thickness, a - absorption coefficient and n - index of refraction. The vector (d, a, n) defines measured coefficients: t - layer transmission and r - reflection of the layer boundary (direct and scattered is included). The parameter r is dependent on neighbouring layers

On each layer boundary we expect reflection according to Shlick's approximation [11] of Fresnel law:

$$r = \left(\frac{n_i - n_j}{n_i + n_j}\right)^2 \tag{1}$$

where the subscript i assigns the parameter to the respective i-th layer. Note, that this equation is symmetric, r is equal for a ray going from layer i to layer j as well as for a ray going from layer j to layer i. Equation for t we describe as:

$$t = e^{-ad} \tag{2}$$

We have measured reflected and transmitted light intensities through different layer combinations (canvas, canvas-underdrawing, canvas-colour, canvas-underdrawing-colour). For each measurement we expect different thickness of the layers (samples are hand made) but constant absorption and index of refraction.

Measured values are:

I_0 – light intensity of the light source (equal to intensity falling on first layer)

r_M – reflection coefficient of calibration target (Munsell Colour Checker - white)

I_R, J_R, L_R, K_R – are light intensities reflected from canvas, canvas-underdrawing, canvas-colour and canvas-drawing-colour composites, respectively. These values are relative to the reflected light from calibration target ($I_0 * r_M$).

I_T, J_T, L_T, K_T – are light intensities passing through canvas, canvas-underdrawing, canvas-colour and canvas-drawing-colour composites, respectively. I_T is absolute value, J_T, L_T, K_T are measured relatively to I_T.

We assume the constant energy equation:

$$I_0 = I_R + I_T + I_A, \tag{3}$$

where I_A represents a light intensity absorbed in the artwork layers (mostly transformed to heat) and general energy loss. We reject from our model other energy transformations (i.e. creation or splitting of chemical bonds) during measurement. Similar energy equations are valid for all layer composites. As the index of refraction of the atmosphere was taken $n_0 = 1{,}00026$.

2.1 Limitations

Presented model assumes that all reflected and transmitted light was captured. Due to scattering (diffuse reflection) of light we are losing some intensity in spite of integration sphere usage. Basic correction is possible by a constant multiplication (according to an integration area) if the factor of scattering is constant across measurements.

All problems according to Preflight profile
Convert to PDF/A-2u

In fact the scattering depends on the size of pigment particles and the roughness of surface. Second deficiency is wavelength shifting (fluorescence and luminescence), where we assume error less than 1% (shifting of light wavelength above 1050nm is included in absorption coefficient).

3 Full-ScaleModelSamples(Mock-ups)

Respecting the period technology, 11 canvas full-scale models (mock-ups) have been prepared. On each of them, thirty 4 x 4 cm squares of different colours have been painted in regular matrix (see Figure 1(b)) using different pigments and binders and applied on grounds of various compositions. Each of these colour pallets corresponds to a specific historical painting technique, which, however, was modified having regard to specific conditions of the testing. Therefore, paints imitating Gothic panel painting technology were prepared on canvas support instead of wood to allow trans-luminiscence of the object from the backside. Further, instead of pure chalk (calcium carbonate), which is the most frequent material used in Gothic grounds north from the Alps in general, mixture of chalk with lead white (basic lead carbonate) has been applied imitating thus more likely Flemish and Netherlandish painting of the 16th to 17th century. These contextual "discrepancies" was guided by the effort to reduce the transparency of the white ground for infrared irradiation, which was necessary for the method calibration. In all squares, right half was under-painted by black and red brush drawing, respectively. Pigments used in paintings and drawings are listed in Tables 1 and 2.

Mock-ups number 1 to 4 imitate Gothic to Renaissance Italian painting, created on white ground prepared by mixing of 3 parts by volume of calcium sulphate (the so-called "Bologna chalk") (58100 Kremer Pigmente), 2 parts by volume of 7% aqueous solution of gelatine (Grac), 1 egg yolk and half-part by volume of polymerised linseed oil (3227 Umton). Similarly, mock-ups numbers 5-11 imitate Gothic to Renaissance painting of "north from the Alps" regions using calcium carbonate (chalk) instead of calcium sulphate (gypsum) in the ground. In our case, the original receipt was modified by addition of the lead white as follows: 2 parts by volume of calcium carbonate (chalk), (0100 Kittfort), 2 parts by volume of lead white, and 2 parts by volume of 7% aqueous solution of gelatine (Grac), 1 egg yolk and quarter-part by volume of polymerised linseed oil (3227 Umton).

For the underdrawing, following materials have been selected: graphite and red clay on the mock-ups 1 and 4, natural (vine or willow) and artificial charcoal on mock-up 2, iron Gall ink and sepia on the mock-ups 3 and 9, lead pencil and black chalk on the mock-up 5, graphite and galena (PbS) on the mock-up 6, red clay and lead pencil on the mock-up 7, natural vine black and black chalk on the mock-up 8, graphite, red clay, lead pencil, artificial charcoals, black chalk, vine black, sepia and iron Gall ink on the mock-up 10, and finally the silverpoint on the mock-up 11.

All problems according to Preflight profile
Convert to PDF/A-2u

Table 1 List of names respective producers/codes, and abbreviations of used pigments and dyes for painting and materials for drawing. KP stands for Kremer Pigmente, ICC stands for the Institute of Inorganic Chemistry of the AS CR, v.v.i., KNH stands for Koh-I-Noor Hardtmuth.

PIGMENTS AND DYES FOR PAINTING			MATERIALS FOR DRAWING		
Verdigris	g.r. Lachner	VG	Red clay (sinopia) RC	KNH	
Lead white	46000 KP	WL			
Cinnabar	10610 KP	CI	Graphite	12462 KP	GR
Red lead	Lachema Brno	RL	Natural willow charcoal	KNH	NC
Lead-tin yellow	10110 KP	LT	Artificial charcoal	KNH	SC
Green earth	17410 KP	GE	Iron Gall ink	own production	IG
Azurite	10210 KP	AZ	Sepia	12401 KP	SP
Ultramarine	10520 KP	UM	Lead pencil	ICC	LP
Umber raw	40730 KP	UR	Galena	10900 KP	GA
Bone black	47100 KP	BB	Black chalk	12450 KP	BC
Smalt	10000 KP	SM	Silverpoint	11348 KP	AG
Madder	37200-B KP	ML			
Indigo	36000-A KP	IG			

Table 2 Summary of prepared samples. Left table contains pigments and dyes used for the sample painting; right table provides information about the material used for underdrawing in the respective sample. Each mock-up (one double-row) contains two sets of 15 positions on the canvas (columns), corresponding to samples with 2 different underdrawing materials (upper row, no.1-15, and bottom row, no. 16-30, respectively). Used abbreviations are listed in Table 1.

Pigments and dyes

	1	2	3	4	5	6	7	8	9	10	11	12	13	14	15
P01			WL	CI	RL	ML	IN	LT	GE	VG	UM	AZ	BB	UR	
			WL	CI	RL	ML	IN	LT	GE	VG	UM	AZ	BB	UR	
P02			WL	CI	RL	ML	IN	LT	GE	AZ	AZ	UM	BB	UR	
			WL	CI	RL	ML	IN	LT	GE	AZ	AZ	UM	BB	UR	
P03			WL	CI	RL	ML	IN	LT	GE	VG	UM	AZ	BB	UR	
			WL	CI	RL	ML	IN	LT	GE	VG	UM	AZ	BB	UR	
P04			WL	CI	RL	ML	IN	LT	GE	UM	AZ	UM	BB	UR	
			WL	CI	RL	ML	IN	LT	GE	UM	AZ	UM	BB	UR	
P05			WL	CI	RL	ML	IN	LT	GE	IN	UM	AZ	BB	UR	SM
			WL	CI	RL	ML	IN	LT	GE	VG	UM	AZ	BB	UR	SM
P06			WL	CI	RL	ML	IN	LT	GE	VG	UM	AZ	BB	UR	SM
			WL	CI	RL	ML	IN	LT	GE	VG	UM	AZ	BB	UR	SM
P07			WL	CI	RL	ML	IN	LT	GE	VG	UM	AZ	BB	UR	SM
			WL	CI	RL	ML	IN	LT	GE	VG	UM	AZ	BB	UR	SM
P08			WL	CI	RL	ML	IN	LT	GE	VG	UM	AZ	BB	UR	SM
			WL	CI	RL	ML	IN	LT	GE	VG	UM	AZ	BB	UR	SM
P09			WL	CI	RL	ML	IN	LT	GE	VG	UM	AZ	BB	UR	SM
			WL	CI	RL	ML	IN	LT	GE	VG	UM	AZ	BB	UR	SM
P10	SM	SM	SM	SM	SM	SM	SM	SM	SM	SM	SM	SM	SM	SM	SM
	SM														
P11			WL	CI	RL	ML	IN	LT	GE	VG	UM	AZ	BB	UR	SM
			WL	CI	RL	ML	IN	LT	GE	VG	UM	AZ	BB	UR	SM

Drawing material

	1	2	3	4	5	6	7	8	9	10	11	12	13	14	15
P01	GR	GR	GR	GR	GR	GR	GR	GR	GR	GR	GR	GR	GR	GR	
	RC	RC	RC	RC	RC	RC	RC	RC	RC	RC	RC	RC	RC	RC	
P02	NC	NC	NC	NC	NC	NC	NC	NC	NC	NC	NC	NC	NC	NC	
	SC	SC	SC	SC	SC	SC	SC	SC	SC	SC	SC	SC	SC	SC	
P03	IG	IG	IG	IG	IG	IG	IG	IG	IG	IG	IG	IG	IG	IG	
	SP	SP	SP	SP	SP	SP	SP	SP	SP	SP	SP	SP	SP	SP	
P04	NC	NC	NC	NC	NC	NC	NC	NC	NC	NC	NC	NC	NC	NC	
	SC	SC	SC	SC	SC	SC	SC	SC	SC	SC	SC	SC	SC	SC	
P05	LP	LP	LP	LP	LP	LP	LP	LP	LP	LP	LP	LP	LP	LP	LP
	BC	BC	BC	BC	BC	BC	BC	BC	BC	BC	BC	BC	BC	BC	BC
P06	GR	GR	GR	GR	GR	GR	GR	GR	GR	GR	GR	GR	GR	GR	GR
	GA	GA	GA	GA	GA	GA	GA	GA	GA	GA	GA	GA	GA	GA	GA
P07	RC	RC	RC	RC	RC	RC	RC	RC	RC	RC	RC	RC	RC	RC	RC
	LP	LP	LP	LP	LP	LP	LP	LP	LP	LP	LP	LP	LP	LP	LP
P08	NC	NC	NC	NC	NC	NC	NC	NC	NC	NC	NC	NC	NC	NC	NC
	BC	BC	BC	BC	BC	BC	BC	BC	BC	BC	BC	BC	BC	BC	BC
P09	IG	IG	IG	IG	IG	IG	IG	IG	IG	IG	IG	IG	IG	IG	IG
	SP	SP	SP	SP	SP	SP	SP	SP	SP	SP	SP	SP	SP	SP	SP
P10	GR	GR	RC	RC	LP	LP	NC	NC	BC	BC	SP	SP	IG	IG	SC
	SC														
P11	AG	AG	AG	AG	AG	AG	AG	AG	AG	AG	AG	AG	AG	AG	AG
	AG	AG	AG	AG	AG	AG	AG	AG	AG	AG	AG	AG	AG	AG	AG

All problems according to Preflight profile
Convert to PDF/A-2u

Pigments in chromatic layers represent traditional "Old-Masters" palette with lead white ($2PbCO_3{\cdot}Pb(OH)_2$), cinnabar (HgS), red lead – minium (Pb_3O_4), lead-tin yellow type I ($PbSnO_4$), green earth (iron-rich clay minerals), azurite ($2CuCO_3.Cu(OH)_2$), ultramarine ($Na_{8-10}Al_6Si_6O_{24}S_{2-4}$), raw umber (Mn-rich clay), verdigris (copper acetate), bone black (calcium phosphate), smalt (Co-containing glass) and organic dyes madder and indigo. Principally, animal glue and oil were used as binders on the muck-ups numbered 1, 2, 3, 5, 10, and 4, 7, 8, 9, respectively. On the mock-up 6 both glue and oil were used in the way "half and half". On the mock-up 11 pure animal glue and emulsion containing glue and oil were combined. In cases lead white and indigo egg yolk was always added to the prevailing binder (either glue or oil) with the exception of mock-ups 6 and 7.

The surface of painting was left without any varnish, with the exception of mock-ups 6 and 11, where oil-resin varnish was applied to cover one half of each painted square. The composition of the varnish was as follows: 50g of dammar resin (60000 Kremer Pigmente), 7.5g of polymerised linseed oil (Stand Oil, 73201 Kremer Pigmente) and 150g of turpentine (70010 Kremer Pigmente).

4 Database of Measurements

Prepared samples were measured for their spectral transmission and reflection in range of visible light spectrum (VIS) and near infrared spectrum (NIR). Collected data are from 400nm up to 1050nm, each wavelength was measured separately.

4.1 Spectrometry

According to our optical model a layer is defined by (n, a, d) vector. In our samples the thickness of the layer d varies and therefore we have to take several independent measurements for each sample, more precisely for each sample half. For each sample half we took 4 measurements of reflection and two measurements of transmission (if it was possible[1]). In this way we obtained 8 reflection and 4 transmission measurements for the canvas (the left half of the samples 1 and 2 at each canvas) and for the canvas with drawing (the right half of those samples). The same was done for the colour on canvas (the left halves of the samples no. 3-15 and no. 18-30) and for the canvas-drawing-colour composite (the right halves).

The equipment used for the spectral measurement:

- Spectrometer USB 2000 [12] - Ocean Optics, range 428-1092nm
- Light source HL-2000-HP [13] - Ocean Optics, range 360-2400nm
- Optical fibres optimized for VIS, NIR
- 45° fibre holder for reflectance measurement and integrating sphere
- Collimating lenses for transmittance measurement
- X-Rite Munsell Colour Checker

Because of noise limitation useful range of spectrometer was from 440-1050nm.

[1] Transmission can be measured only on canvases 1-4 due to low power of light source.

All problems according to Preflight profile
Convert to PDF/A-2u

4.2 Normalization

Spectrometer was calibrated by HL-2000-CAL light source. Reflectance of Munsell Colour Checker (CC) white r_M was measured with HL-2000-CAL. The high power light source HL-2000-HP intensity I_0 was calibrated according to obtained r_M (see Figure 2), to avoid oversaturation of spectrometer by direct light. Measured data (J_R, I_R, K_R) were than measured relatively to I_0.* r_M, and this is the reason why reflectance can be higher than 100 % (see Figure 3). We select relation to the Munsell CC to achieve the repeatability of the measurement. The relative transmittance spectral data was normalized by the transmittance of the clear canvas. Thus we worked with the relative transmission measurements (J_T, I_T, K_T) to I_T. Data was collected from circle area of 0,5cm in diameter. The spectrometer sensor takes 2048 values in the range 428-1092nm. The step in the wavelength is therefore approx. 0,324nm.

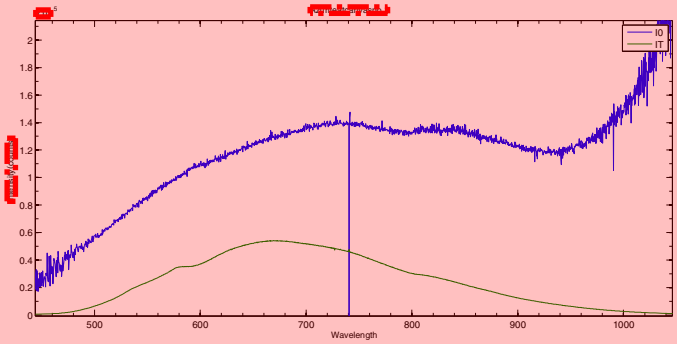


Fig. 2. Normalization of the spectrometer measurements. Blue (upper) curve denotes calibrated intensity of light source HL-2000-HP. Green (bottom) curve is average transmittance of canvas (canvas no. 1).

4.3 CameraPhotometry

Prepared samples were also documented by digital camera. Our camera Cannon iRebel D500 was modified for NIR photography by removing of ICF. The spectral resolution of camera was enhanced with using filters and LED diodes.

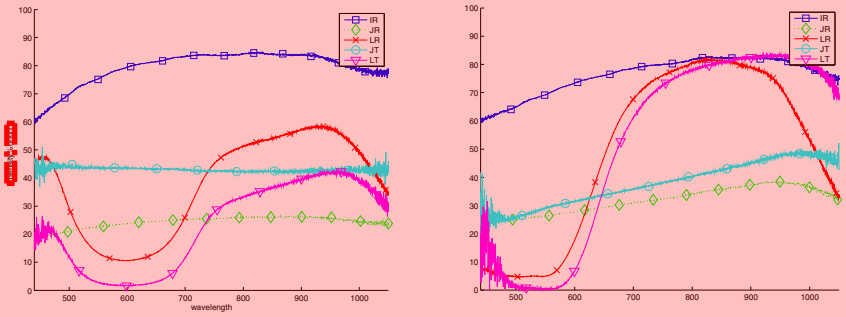
Forcameraphotometryweused:

- Canon iRebel D500
- Colour and IR filters – red, green, blue, yellow, orange, sepia and band pass filters 400-700nm, 680+, 720+, 760+, 850+ and 950+. Exact description can be found at [9].
- LED diodes with mean wavelength at – 398, 405, 466, 470, 506, 525, 565, 590, 605, 620, 660, 700, 880, 950nm. More detailed information can be found at [14].

The transmission of used filters and spectral characteristics of LED diodes can be found at [9], [15]. In spite of known characteristics data cannot be compared with the

All problems according to Preflight profile
Convert to PDF/A-2u

data from spectrometer. High temporal variance of emitted light intensity of LEDs or used light source affects interpretability of acquired values. These photos were used for evaluation of measured transparency of colours.



(a) (b)

Fig. 3. Measured transmittance and reflectance of azurite (a) on the canvas no. 1 and madder (b) on the canvas no. 5. IR denotes the reflectance of the canvas, LR and LT denote the reflectance and the transmittance of the canvas with azurite/madder layer, respectively and JR and JT denote the reflectance and the transmittance of the drawing on the canvas, respectively.

5 Results

The data from the proposed measurements in VIS and NIR spectral bands form the content of the m3art database of painting materials [9]. The m3art database should serve as the knowledge base for further study of optical properties of pigments, drawing materials and canvases.

For the underdrawing acquisition first conclusions were made. The Figure 3(a) shows results of measurement of (L_R, T_T) of azurite. The ratio of LR and LT curves determines ability for underdrawing detection by reflected or transmitted light. The higher reflectance (L_R) than transmittance (L_T) determines bad penetration ability of reflected light through azurite layer. Lower transmittance in general hardens penetration of layer also by transmitted light. Different behaviour of colour shows Figure 3(b), where (L_R, T_T) of madder were measured. Compared to azurite madder has lower ratio of reflectance/transmission. In other words, penetration of a madder layer is possible by the reflected light (in wavelengths above 700nm).

According to evaluation of the collected data we can split colour materials into four categories. First category contains materials whose transmission (LT curve, Figure 3) is almost zero and therefore they cannot be penetrated. In this category we put: bone black, verdigris and azurite.

Second category contains colours with high ratio of reflection/transmission. The reflected light cannot penetrate such (the reflection of top layer is in this case significantly higher than the reflection from bottom layer). For penetration of these colours and for the underdrawing discovery it is necessary to use a transmitted light. In this category we put lead white, lead-tin yellow and red lead.

All problems according to Preflight profile
Convert to PDF/A-2u

Third category contains colours with high transmission in NIR compared to VIS spectral band. These colours can be penetrated by reflected and also by transmitted NIR light. In this category we put smalt, ultramarine, indigo, madder and cinnabar.

Finally, fourth category contains colours with similar behaviour in NIR as in VIS. Penetration of such colours is possible only in special cases (good condition of artwork, usage of contrast underdrawing, etc.). This category contains green earth and umber raw from our collection.

Note that fifth category should be defined: the colours possible to be penetrated by the reflected light only. But, such colour must have low reflection and high transmission, in other words such colour would be transparent. Materials belonging to fifth category are varnishes, which were not included in presented study.

6 Conclusion

We proposed and implemented m3art database - the open database with collected data about colours and their behaviour in VIS and NIR spectral bands. We made this data set public and available through Internet [9]. All our measurements are repeatable and comparable because of the calibration.

We suggested base methods how to penetrate 8 colours from the representative Gothic/Renaissance set for underdrawing detection and identified the remaining 5 colours as the ones for which the penetration ability of NIR is poor or none. We define 4 categories of colours according to the possibility of their penetration in NIR spectrum. We conclude that transmission measurement is more universal than (more common) reflection measurement for underdrawing detection and should be used when possible (i.e. canvas paintings, sufficient light transmission).

Our following research will focus on the computation of optical properties of samples (n, a, d) and their stability in practice. We expect significant influence of different layer thickness, concentrations of binding media/pigment and age of the layer. We also focus on preparation of new mock-ups and their measurement, which enrich the m3art database.

Acknowledgments. We would like to acknowledge the Czech Science Foundation, which has supported this work (project no. P103/12/2211).

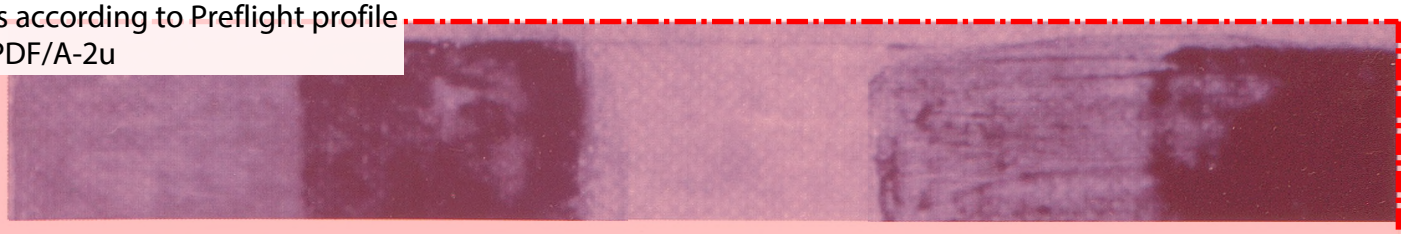
References

1. Douma, M.: Pigments through the Ages (2008), http://www.webexhibits.org/pigments
2. Cosentino, A.: Identification of pigments by multispectral imaging; a flowchart method. Heritage Science 2(1), 8 (2014)
3. Zhao, Y., Berns, R.S., Taplin, L.A., Coddington, J.: An Investigation of Multispectral Imaging for the Mapping of Pigments in Paintings. In: Computer Image Analysis in the Study of Art, vol. 6810 (2008)

All problems according to Preflight profile
Convert to PDF/A-2u

4. de Boer, J.A.: Reflectography of paintings using an infra-red vidicon television system. Studies in Conservation 14, 96–118 (1969)
5. Katayama, T., Toque, J.A., Murayama, Y., Ide-Ektessabi, A., Anders, J.: Estimation System for Pigments of Japanese Paintings, Department of Mechanical Engineering and Science, Graduate Schoolof Engineering, Kyoto University, Kyoto
6. Toque, J.A., Sakatoku, Y., Ide-Ektessabi, A.: Pigment identification by analytical imaging using multispectral images. In: 16th IEEE International Conference on Image Processing (ICIP), pp. 2861–2864 (2009)
7. Metzger, C., Delaney, J.K., Fletcher, C., Walmsley, E.: Improved Visualization of Underdrawings with Solid-State Detectors Operating in Infrared. Studies in Conservation 39, 217–231 (1994)
8. Picollo, M., Vervat, M., Cucci, C.: Trans-illumination and trans-irradiation with digital cameras: Potentials and limits of two imaging techniques used for the diagnostic investigation of paintings. Journal of Culture Heritage 13, 83–88 (2012)
9. Bartl, M., Jacko, J., Multispectral, V.: analysis of cultural heritage artefacts. Measurement Science Review 3(3), 9–12 (2003)
10. Schlick, C.: An Inexpensive BRDF Model for Physically-based Rendering. Computer Graphics Forum 13(3) (1994)
11. OceanOptics. Spectrometer USB 2000+datasheet (2012), http://www.oceanoptics.com/products/usb2000+.asp
12. OceanOptics. Lightsources - series HL-2000 datasheet (2012), http://www.oceanoptics.com/products/hl2000.asp
13. Blažek, J.: Database ofopticalpropertiesofpaintmaterials (2014), http://m3art.utia.cas.cz
14. Kuneš, M., Blažek, J.: Fieldof LED in 8x8 matrix, Institute of Information Theory and Automation of the ASCR, Department of Image Processing, Prague, Czech Republic (2014)
15. Blažek, J., et al.: Low-cost mobile system for multispectral cultural heritage data acquisition. In: Digital Heritage International Congress, Marseille, pp. 73–79 (2013)

All problems according to Preflight profile
Convert to PDF/A-2u



OPTICAL PROPERTIES OF HISTORICAL PAINT PIGMENTS UNDER NEAR INFRARED (NIR) RADIATION

Jan Blažek, Barbara Zitová
Institute of Information Theory
and Automation of the AS CR, v. v. i.
Pod Vodárenskou věží 8
182 08 Prague 8
Czech Republic
blazek@utia.cas.cz
zitova@utia.cas.cz

Tomáš Tichý, Vlasta Vasutová
Academy of Fine Arts in Prague
ALMA Laboratory
U Akademie 4
170 22 Prague 7
Czech Republic
tomas.tichy@gmail.com
vasutovavlasta@seznam.cz

ABSTRACT

The knowledge of paint pigments' optical characteristics enables the selection of an appropriate imaging methodology for non-invasive artwork investigation, i.e. optimising the visibility of preparatory layers using conventional photographic cameras modified for data acquisition in the near infrared wavelength range (700–950 nm). This contribution deals with the limits of this simple method in the analysis of selected common pigments used in prepared canvas mock-ups with typical structure including ground layer and underdrawings of various compositions. The monitored parameter was the visibility of the underdrawing. In this contribution, we suggest an optimisation of the procedure for the underdrawing visualisation based on the spectrometer transmittance measurements and reflectance of the studied samples. In the same time, we also quantify the probability of discovering the underdrawing in relation to the composition of the covering colour layer.

KEYWORDS: **transmittance, reflectance, non-invasive data acquisition, pigments and organic dyes**

Introduction

Visualisation of inner structure of painted work of art can be performed, apart from the advanced imaging methods, [1, 2] to a certain extent by commonly available instrumentation such as photography in NIR spectrum using conventional cameras with removed infrared ICF (internal cut) filter. Such modified camera is able to record data in the range of 400–1050 nm (this range of commonly available cameras may slightly differ). For removal of the visible part of the spectra (400–700 nm), either photographic filters (if the camera objective enables their installation), or infrared (IR) lamp illumination [3] are being used.

Based on our experience, the penetration ability of IR radiation is very important for the interpretation of NIR images, therefore, we have decided to quantify it. On the obtained images, the visibility of the preparatory layers largely differs. The most problematic cases are the ones with thick layers of paint or with the layers containing materials with high absorbance in the NIR range. Consequently, in certain cases, the visualisation of preparatory layers of painted work of art is not an easy task.

The advantage of the modified photographic cameras and compact VIS-NIR spectrometers is their availability and high mobility which enable routine screening. Moreover, it is possible to directly combine the imaging with reflection colour measurements, if it is meaningful in the particular case. Our goal was to evaluate the applicability and limits of the above-mentioned method in practice using empirical tests on prepared model samples with various types of colour layers and underdrawings.

The determination of proper methodology for non-invasive data acquisition or the complete exclusion of pointless imaging may often save precious time confined for analysis *in situ*. Under well-defined conditions, the automatic or semiautomatic identifi-

All problems according to Preflight profile
Convert to PDF/A-2u

cation of the underdrawings in NIR images obtained by non-invasive measurements may be obtainable through methods of digital image processing.

Our research relies on a long-term cooperation with ALMA laboratory, a joint workplace of the Academy of Fine Arts in Prague and the Institute of Inorganic Chemistry of the Academy of Sciences of the Czech Republic, and our experience with the processing of image documentation of analysis of works of art. [3–6] In practice, we have verified that the NIR spectrum radiation is often not able to penetrate the upper layer of the painting and to detect the underdrawings. The most common cause is the specific NIR-non-penetrable pigments or other components of the colour layer. Therefore, we have attempted to measure and quantify the impact of the employed pigments on the permeability in NIR on the artificially prepared samples. In the conservation/restoration practice, the spectral range of 700–950 nm is easily accessible by removal of ICF filter of a common photographic camera (more on the camera adjustment can be found at http://maxmax.com), therefore, we focused specifically on this interval.

Selection and preparation of representative samples (mock-ups)

During the first phase of the experiments, the pigments for mock-ups creation were selected with respect to the painting technique of the Gothic to Renaissance period. Purely for experimental purposes, a "transparent" support was used instead of wooden panels common in the Gothic period. Considering the required transparency of the support, thickness and composition of the ground layer were adjusted. The employed mixture of gypsum (calcium sulphate dihydrate) or chalk (calcium carbonate) and lead white (basic lead carbonate $Pb_2(CO_3)(OH)_2$) is compliant with the experimental requirements for reflection and transmission measurements. In the first case, the mixture was prepared using 3 vol. parts of calcium sulphate (Bologna chalk, 58100 Kremer Pigmente), which were mixed with 2 vol. parts of 7% aqueous solution of gelatine - Grac, 1 egg yolk and ¼ vol. part of polymerised linseed oil (Umton). In the second case, we used calcium carbonate (chalk) instead of calcium sulphate (gypsum), moreover, the original recipe was modified by addition of 2 vol. parts of lead white for 2 vol. parts of calcium carbonate (chalk) with the same amount of binder (2 vol. parts of 7% aqueous solution of gelatine – Grac, 1 egg yolk and ¼ vol. part of polymerised linseed oil). The pigments and dyes employed in the colour layer and underdrawing are summarised in Tables 1 and 2 (*Tab. 1, 2*). Individual pigments and dyes were mixed with glue and oil binding media.

The prepared model layers are depicted in Figure 1 (*Fig. 1*). For each combination of underdrawing and painting (colour), a 4 cm x 4 cm square was painted on the canvas with ground layer. One half of the square was prepared with underdrawing, while the other one was left without it. Finally, the whole square was covered with selected colour consisting of one particular pigment and binder. Thanks to this sample preparation technology, we were able to obtain information regarding the reflection and transmission of (i) the canvas itself (ground layer included), (ii) the canvas with the colour, and of (iii) the canvas, underdrawing and the colour, all these in two types of binders, i.e. resulting into six measured values.

If we assume constant thickness of all layers, the measured values sufficiently determine physical parameters of the layers – their index of refraction and absorbance. The measured physical parameters may be found in the literature (e.g. Pigment Compendium) [7], but the published values are only averages of the visible light spectrum.

The layers of the model samples were prepared using a classic painting technique; therefore, the assumption of constant layer thickness does not apply. This topic is covered in more detail in the Discussion of this paper. The thickness of colour layers was chosen in an empirical way to fully cover the underdrawing in visible light spectrum (400–700 nm). Since we assume a constant thickness of the layers in the course of the interpretation (within one colour or one underdrawing), the error of this simplification will propagate into the stated variances of measured values.

Measurement procedure

Reflection and transmission were measured on each prepared model sample. Both of these quantities were measured relatively to reflectance and transmittance of the canvas including the white ground layer. Reflection indicates the percentage of the light reflected by colour layer in contrast to the white canvas for given wavelength. By contrast, the transmission indicates the amount of the light absorbed by the colour layer and the percentage of light passing through the colour layer (100% represents the amount of the light that passed through the canvas with a ground layer to our studied layer). An output of such measurement is a spectral "fingerprint" of the employed colour.

The measurements were performed using FORS method (fibre-optics reflectance spectroscopy) by the means of mobile spectrometer OceanOptics USB2000+ working in the range of visible and near infrared radiation (VIS-NIR). The FORS in the UV-VIS or VIS-NIR range is in general used as

All problems according to Preflight profile
Convert to PDF/A-2u

Pigment	Producer/Supplier	Chemical structure/Origin
Verdigris	g.r. Lachner 30143-CP0	$(CH_3COO)_2Cu{\cdot}H_2O$ (99%)
Lead white	Kremer-Pigmente 46000	$Pb_3(CO_3)(OH)_2$
Cinnabar	Kremer-Pigmente 10610	HgS
Red lead	Lachema Brno	Pb_3O_4
Lead-tin yellow type I	Kremer-Pigmente 10110	Pb_2SnO_4
Green earth	Kremer-Pigmente 17410	celadonite from Cyprus (K, Mg, Fe silicate)
Azurite	Kremer-Pigmente 10210	$2CuCO_3{\cdot}Cu(OH)_2$
Ultramarine	Kremer-Pigmente 10520	$(Na, Ca)_8[(SO_4,S,Cl)_2(AlSiO_4)_6]$
Umber raw	Kremer-Pigmente 40730	natural earth from Cyprus, containing 50% iron hydo(oxides) + manganese oxides
Bone black	Kremer-Pigmente 47100	produced by charring of animal bones, main components: 57-80% $Ca_3(PO_4)_2$, 6-10% $CaCO_3$, [illegible] carbon
Smalt	Kremer-Pigmente 10000	potassium silicate glass containing Co and As
Madder	Kremer-Pigmente 37200-B	natural dye obtained from the root of the plant Rubia Tinctorum, main compounds: $C_{14}H_8O_5$ (purpurin) and $C_{14}H_8O_4$ (alizarin)
Indigo	Kremer-Pigmente 36000-A	$C_{16}H_{10}O_2N_2$

Tab. 1 Pigments and dyes employed in the model painting

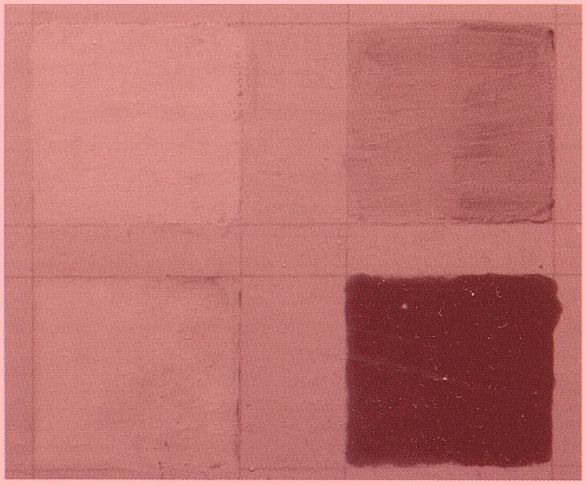
Underdrawing	Producer/Supplier
Red clay (sinopia)	KOH-I-NOOR HARDTMUTH
Graphite	Kremer-Pigmente 12462
Natural willow charcoal	KOH-I-NOOR HARDTMUTH
Artificial charcoal	KOH-I-NOOR HARDTMUTH
Iron Gall ink	Own production
Sepia	Kremer-Pigmente 12401
Lead pencil	Lead wire
Galena	Kremer-Pigmente 10 900
Black chalk	Kremer-Pigmente 12450
Silverpoint	Kremer-Pigmente 11348

Tab. 2 Materials employed for underdrawings

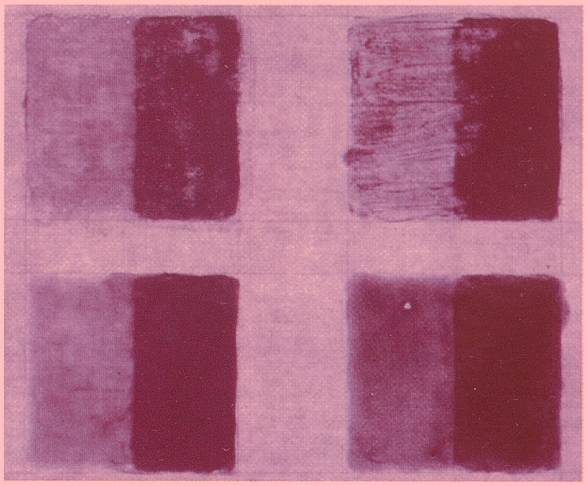
All problems according to Preflight profile
Convert to PDF/A-2u



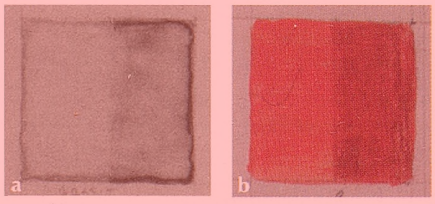
1 An example of canvas with emulsion ground containing chalk and lead white with samples in visible light (underdrawings were created with black chalk); first two samples do not have a covering layer (thick and thin underdrawing), they are followed by (from the left to the right and from the top to the bottom) lead white, cinnabar, minium, madder, indigo, lead-tin yellow, green earth, verdigris, ultramarine, azurite, bone black, umber raw and smalt; the binding media is glue; the left part of the sample (2 x 4 cm) is without any underdrawing (see *Fig. 2*); the right part has the underdrawing



2 The image of selected samples from the canvas in Figure 1 in NIR spectrum (720-950 nm, reflection) in the following order (from the left to the right and from the top to the bottom): lead white, cinnabar, lead-tin yellow, green earth; the underdrawing was made with black chalk, it is almost invisible in the right part of each sample due to high reflectance (lead pigments) or high absorbance (green earth) of the employed pigments, an exception is the cinnabar, where the underdrawing may be detected, but not with a high degree of certainty



3 The image of selected samples from the canvas in Figure 1 in NIR spectrum (700-950 nm, transmission) in the following order (from the left to the right and from the top to the bottom): lead white, cinnabar, lead-tin yellow, green earth; the underdrawing was made with black chalk, it is clearly discernible in the right part of each sample; in contrast to the reflection image, it contains artefacts, such as texture of the canvas and brush strokes (they are easily visible thanks to the differences in layer thickness in case of the cinnabar sample)



4 Complicating factors caused by drying and aging of the samples – the edge contour of the graphite underdrawing in areas of the fastest drying of the top smalt on canvas colour layer, in reflected light in the range of 700–950 nm (**a**), this effect appears especially in the samples with slowly drying oil binding media; penetration of the red clay underdrawing through the top minium layer after approx; 10 months after the sample creation in visible light (**b**)

All problems according to Preflight profile
Convert to PDF/A-2u

	700-950nm				colour (=100%)	canvas (=100%)
	avg(R)	std(R)	avg(T)	std(T)	contrast(R)	contrast(T)
lead white	87.7	9.3	51.2	0.3	5.3	41.3
cinnabar	53.2	7.8	33.4	6.8	12.3	26.9
minium	72.4	11.4	75.6	4.6	22.6	60.9
madder	57.9	17.0	63.9	13.6	34.1	51.4
indigo	32.8	11.2	23.9	19.1	27.2	19.2
lead-tin yellow	86.2	7.4	26.2	5.2	2.0	21.1
green earth	14.0	5.5	0.7	0.2	0.0	0.6
verdigris	5.5	2.3	1.5	1.1	1.0	1.2
azurite	32.7	12.4	22.6	4.0	12.8	18.2
ultramarine	16.8	11.5	7.5	7.5	9.7	6.1
bone black	3.9	1.3	0.3	0.1	0.0	0.2
umber raw	21.2	5.9	2.4	1.9	0.6	2.0
smalt	52.5	16.4	51.3	14.2	30.7	41.3
different underdrawings (average)	33.7	18.3	39.9	20.4		

Tab. 3 Results of measurements; all the measured values are in percentage; the columns avg(R) and avg(T) give the average reflectance and transmittance, respectively, of the colour layer in the 700-950 nm wavelength range; the columns std(R) and std(T) give the standard deviation from the average value for all measured samples; the column contrast(R) shows the maximal achievable contrast (under ideal conditions) between the underdrawing and the colour layer in reflected light; finally, the column contrast(T) gives the maximal achievable contrast of the underdrawing with respect to the lightest white colour on the image in transmitted light

a screening non-invasive method for pigment and dye identification of non-complicated paintings, such as illuminated manuscripts [8] or wall paintings [9]. Pigment identification is based on the comparison of obtained spectral "fingerprints" with the "fingerprints" of known pigments. The experiment setting had the following parameters: diameter of optical fibre - 0.6 μm; step - 0.31 nm; number of measurements - ca 800 in the 700–950 nm (NIR) range, the applicable overall range of the device is 435–950 nm and 428–1092 nm, respectively (2048 measurements in different wavelengths in total). Reflection was recorded under the 45 degrees angle and the transmittance under the 0 degrees angle from the perpendicular. Each individual measurement covers a circular area with 0.8 cm diameter.

Measurements were, for illustration, complemented with photos of canvases acquired with camera Canon iRebel D500 (in the Czech Republic marketed as Canon EOS 500D) adjusted for recording in NIR spectrum (more about this adjustment can be found at http://maxmax.com). Data acquisition in individual spectral ranges was regulated using optical filters (reflection) [10] or LED diods (transmission) [3, 11]. The employed IR-pass filters are commonly available; we have measured their transmittance (which is not significant for the imaging itself). It is necessary to know the value of transmission in order to obtain the spectral fingerprint using the camera. However, obtaining a spectral fingerprint with this methodology is more complicated and also more inaccurate. The employed monochromatic LED diodes are also commonly available; we have measured their spectral characteristics using the above-mentioned spectrometer. For the simulation of our measurement, neither LED diods, nor the photographic filters are essential. The obtained images are only complementary.

Results of measurements

Figures 2 (reflection) and 3 (transmission) depict complementary images obtained by camera in the 700–950 nm spectral range. Significant difference in the underdrawing visibility between these images demonstrates qualitative improvement caused by usage of transmission images. [12] In the reflected light, the underdrawing is more visible the darker the colour (with lower reflectivity in NIR) and the higher is its transparency (its transmission in NIR). The advantage of the transmission is its independence on the colour lightness (reflection in NIR).

All problems according to Preflight profile
Convert to PDF/A-2u

The qualitative measurements were performed with the spectrometer. For each of the prepared samples with the area of 4 x 4 cm, 8 reflection measurements (4 from the part with the underdrawing and 4 from the part without it) and 4 transmission measurements (2 and 2 from each half) were collected. Results are summarized in Table 3 (*Tab. 3*).

The reflection of the colour layer "avg(R)" is an average of 80 independent measurements realized on 10 samples with the same top layer (with different canvases and different underdrawings). The transmission "avg(T)" is an average of two measurements carried out on the sample part without the underdrawing. The last row in the table shows the average reflection and transmission of the underdrawing. The employed underdrawings (*Tab. 2*) were averaged all together to partly simulate real situations, when we do not know in advance the underdrawing's material composition. The column "contrast(R)" contains calculated maximal contrast (in percentage) of the top layer with the darkest possible underdrawing and without any underdrawing (only with the white ground layer) during the measurements in reflection; 100% represents the intensity of the top layer with the white ground layer without any underdrawing. If we express the transmission in a same way, the computed contrast will be 81% for all kinds of top layers (= 2 x standard deviation of the underdrawings). Therefore, in case of transmission, we prefer to state the relative contrast "contrast(T)", where 100% represents the intensity of the white colour and 0% is the intensity of the black one on the transmission image (i.e. the contrast is in the context of the whole image, not just of the coloured area). Variance of measured values is mostly caused by simplification of our calculation of the constant layer thickness. However, it does not affect our conclusions.

We found out that the pigments behaviour on the photographs corresponds to the expected behaviour based on our spectral measurements of transmission and reflection (*Tab. 3*). The observations are following:

Lead white has high reflectance (80–100%) of all wavelengths in the NIR spectrum range. This property prevents the identification of underdrawings in reflected light. The transmission of lead white is lower (30–50%) than its reflection. In this case, the transmission image is more suitable for underdrawing detection.

Cinnabar also has a significant difference between transmission and reflection, but not as immense as the lead white. The ground layer participation on the reflection intensity is about 10–15 % (in the best case). Also in case of cinnabar we suggest the usage of transmission images for the underdrawing detection. The achievable contrast in the reflected light may not be sufficient.

Minium has similar transmission and reflection (ca 75%). The underdrawing is well visible even in reflected light. On our samples, we have detected a sharp increase of absorbance with just a small increase of the layer thickness. Consequently, the underdrawings are detectable only under a thin layer of minium.

Madder has a similar behaviour to cinnabar, but its transmission and reflection is slightly higher (ca 60%). In ideal case, the reflection measurement should be sufficient (up to 34% of contrast). For thicker layers of paint, we still recommend to use primarily transmission measurements.

Indigo has a higher transmission (by ca 10 to 20%) than reflection, therefore reflected light may be used for underdrawing identification.

Lead-tin yellow behaves similarly to lead white due to its high reflectance and low transmittance. The transmission measurement can be recommended for the localisation of underdrawings which amount to 21% of contrast of the image. Such value is sufficient for the localisation.

Green earth has high absorbance and, therefore, is almost non-transparent. Underdrawings under the layer of green earth are not recognisable in NIR spectrum neither in reflectance images nor in the transmittance ones.

Verdigris has the same behaviour as the green earth. Underdrawings are not detectable.

Azurite allowed detection of underdrawings in reflected light in five out of ten model samples. Again, we can recommend the usage of transmission measurement for underdrawing detection. The reflection images were highly dependent on the thickness of the azurite layer and on the underdrawing material (lead pencil and silverpoint were not recognisable at all).

Ultramarine behaves similarly to azurite. The reflection images do not guarantee successful underdrawing localisation (only in two cases out of ten samples). The maximal reachable contrast measured in reflection was 9.6 % of ultramarine intensity – this value is, in practice, almost inapplicable, the pigment itself is relatively dark. We cannot recommend collection of NIR-reflected images for underdrawing localisation under ultramarine layer. The detection of underdrawings in transmitted light is possible (up to 6% of the image contrast, depending on the darkness of the underdrawing) but not guaranteed.

Bone black, due to its almost absolute absorbance, does not allow the underdrawing detection in NIR spectrum.

Umber raw has also high absorbance preventing underdrawing detection, even in the case of trans-

All problems according to Preflight profile
Convert to PDF/A-2u

mission imaging. It has the same behaviour as bone black or green earth.

Smalt requires further research. According to our measurements, there is strong dependence between the granularity of underdrawings and its transmission in NIR. The the particles of underdrawing (e.g. iron gall ink), the higher is the transmittance, the coarser the particles (e.g. black chalk), the lower is the transmittance. In our study, the reflection images were sufficient for underdrawing identification.

Discussion

During the preparation of model samples, "faithfulness to the original" was maintained, the historical recipe and the period painting technique were abided. In ite of our effort to reduce the inhomogeneity of ground layer in course of its preparation, we were not able to achieve a fully homogeneous surface. The same problem appeared in the se of colour layers. The surface inhomogeneity of the layers or dissimilar granularity and/or thickness may slightly affect the results of experiment measurements.

An example of inhomogeneity is the concentration of pigment particles at the quickly drying edges of the painting or drawing (*Fig. 4a*). This effect is multiplied by the duration of the drying process – the most affected samples are those with slowly drying oil binding media. In our study, we do not focus on the inhomogeneity problem, since for the spectroscopic measurements, we have selected homogeneous areas located in the centre of the painted surface. The effect of drying and the preparation process of the colour in context of its interaction with underdrawing requires further research.

Another effect that manifested itself on sample is related to aging, which resulted in an increased transparency of the top layer (*Fig. 4b*). While the thickness of the colour layer was sufficient to cover the underdrawings when the samples were created, after several months, the underdrawings started to be visible through the colour layer. This effect is common also in se of Gothic paintings, therefore can be perceived as authentic. In ur se, it was probably caused by the change of index of refraction of the employed tempera paints during aging. Oil painting index can increase in a similar way. [13]

As it has been already said, the paints were applied by brush, therefore, the thickness of the layers was not constant. Since the absorption of the layer depends on the thickness exponentially [14], we can estimate the shape of this exponential according to the results of multiple measurements (in different parts of the sample). The more measurements we perform the more precise absorption curve we obtain. However, in the presented study, an assumed constant thickness was sufficient, because the variances of the measured data were acceptable (*Tab. 3*).

It is also necessary to not that the stated maximal achievable underdrawing contrast depends on its employed material (*Tab. 3*), and can be reached only in an ideal se, when the dark underdrawing was u d. For example, the underdrawings made by silverpoint or lead pencil on the white ground layer could not be detected in the NIR spectrum at all. For the study of these underdrawings, it is necessary to employ a different visualisation method/approach. The possibility of their localisation is out of scope of this paper.

Finally, the last factor which can influence the outcome of the underdrawing detection is the presence of artefacts appearing in the transmission images. The canvas textu , brush strokes, differences in colour layer thickness as well as inhomogeneities in colour layer may be visible. The removal of canvas textu from the transmission images is the subject of our previous work. [6]

Conclusions

We have tested fourteen old master pigments and ten different underdrawing materials. For these pigments, we can define three categories according to the possibility of underdrawing detection, based on the results of performed experiments:

- the underdrawing is invisible due to the negligible transmittance of NIR radiation (green earth, verdigris, bone black, umber raw);
- the underdrawing is recognisable in reflected light due to the material low reflectivity and high transmittance (madder, smalt, indigo, minium, azurite, cinnabar);
- the underdrawing is not recognisable in reflected light (the lightness of the reflected light is too high), but it is recognisable in transmitted light (lead white, lead-tin yellow, cinnabar, azurite).

In se of azurite and cinnabar, there is an evident dependence on the thickness of the layer. Generally, for underdrawing detection, it is always advantageous to use images acquired with transmitted light. We have confirmed that the underdrawings made by silverpoint or by lead pencil on white ground layer (u d in our experiments, a mixture of chalk and lead white) are invisible in the 700–950nm wavelength band.

Acknowledgement

We would like to thank Janka Hradilová and David Hradil from ALMA laboratory for their expert knowledge necessary for creation and analysis of prepared samples, for data provision and for their objective remarks. This work has been supported by Czech Science Foundation, project No. P103/12/2211.

All problems according to Preflight profile
Convert to PDF/A-2u

References

[1] Ambrosini D., Daffara C., Di Biase R., Paoletti D., Pezzati L., Bellucci R., Bettini F.: Integrated reflectography and thermography for wooden paintings diagnostics. *Journal of Culture Heritage* 11 (2010), 196–204.

[2] Carcagni P., Patria A. D., Fontana R., Greco M., Mastroianni M., Materazzi M., Pampaloni E., Pezzati L., Piccolo R.: Spectral and colorimetric characterization of painted surfaces: A scanning device for the imaging analysis of paintings. In Salimbeni R., Pezzati L. (eds.): SPIE Proceedings Vol. 5857: Optical Methods for Arts and Archaeology, 58570T (12 August 2005); doi: 10.1117/12.612565.

[3] Blažek J., Soukup J., Tichý T., Zitová B., Hradilová J., Flusser J.: Low-cost mobile system for multispectral cultural heritage data acquisition. In Digital Heritage International Congress 1 (2013), 73–79.

[4] Blažek J., Hradilová J., Kamenická J., Zitová B.: Detection of copies using mathematical processing of images I. Theoretical basis and methodology. In Hradil D., Hradilová J. (eds.): Acta Artis Academica 2012,141–152.

[5] Hradilová J., Valchařová B., Velíšek M., Blažek J.: Detection of copies using mathematical processing of images II. Story of a painting on canvas of a boy petting a bird. In Hradil D., Hradilová J. (eds.): Acta Artis Academica 2012, 153–162.

[6] Beneš M., Zitová B., Blažek J., Hradilová J., Hradil D.: Removing the Artifacts from Artwork Cross-section Images. In Proceedings of the 18th IEEE International Conference on Image Processing 2011, 3598–3601.

[7] Eastaugh N., Walsh V., Chaplin T.: Pigment Compendium: Optical Microscopy of Historical Pigments. Elsevier Butterworth-Heinemann, Oxford UK 2005.

[8] Aceto M., Agostino A., Fenoglio G., Idone A., Gulmini M., Picollo M., Ricciardie P., Delaney J.K.: Characterisation of colourants on illuminated manuscripts by portable fibre optic UV visible-NIR. Analytical Methods 6 (2014), 1488–1500.

[9] Cheilakou E., Troullinos M., Koui M.: Identification of pigments on Byzantine wall paintings from Crete (14th century AD) using non-invasive Fiber Optics Diffuse Reflectance Spectroscopy (FORS). Journal of Archaeological Science 41 (2014), 541–555.

[10] Hollaus F., Gau M., Sablatnig R.: Multispectral image acquisition of ancient manuscripts. In Progress in Cultural Heritage Preservation 2012, 30–39.

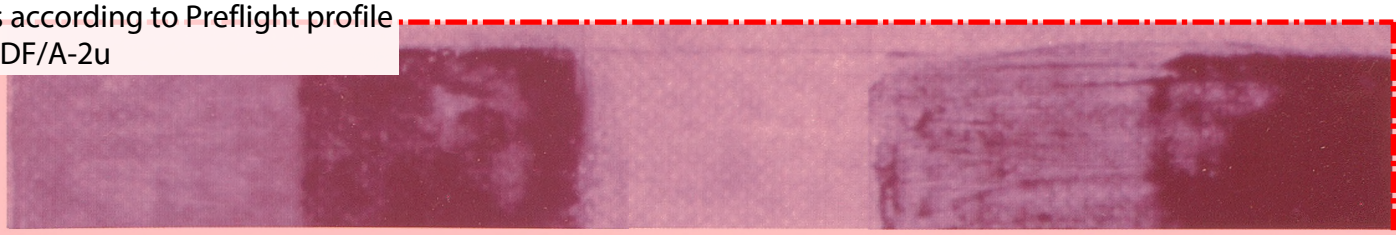
[11] Kunecký M., Blažek J.: LED field in the 8x8 matrix. Technical documentation of the Department of Image Information Processing of the IITA AS CR (2012), http://www.utia.cas.cz/ZOI-publications

[12] Cucci C., Picollo M., Vervat M.: Trans-illumination and trans-irradiation with digital cameras: Potentials and limits of two imaging techniques used for the diagnostic investigation of paintings. *Journal of Culture Heritage* 13 (2012), 83–88.

[13] Slánský B.: Painting technique. Part I. Painting and conservation materials /in Czech/. Státní nakladatelství krásné literatury, hudby a umění, Praha 1953.

[14] Houghton J. T.: The Physics of Atmospheres (2nd ed.). Cambridge University Press 2002, Chapter 2.

All problems according to Preflight profile
Convert to PDF/A-2u



OPTICKÉ VLASTNOSTI HISTORICKÝCH MALÍŘSKÝCH PIGMENTŮ V BLÍZKÉM INFRAČERVENÉM (NIR) ZÁŘENÍ

Jan Blažek, Barbara Zitová
Ústav teorie informace a automatizace AV ČR, v.v.i.
Pod Vodárenskou věží 8
182 08 Praha
blazek@utia.cas.cz
zitova@utia.cas.cz

Tomáš Tichý, Vlasta Vasutová
Akademie uměleckých umění v Praze
Laboratoř LAMA
U Akademie 4
170 22 Praha 7
tomas.tichy@gmail.com
vasutovavlasta@seznam.cz

ABSTRAKT

Znalost optických charakteristik malířských pigmentů umožňuje volit techniku snímání malby při jejím neinvazívním průzkumu tak, aby byla optimalizována viditelnost podpravných vrstev, a to s využitím běžných fotoaparátů upravených pro snímání v blízké infračervené oblasti (700–950nm). Práce se zabývá limity této jednoduché metody pro vybrané běžné pigmenty použité v modelových malbách na plátně s klasickou výstavbou včetně podkladu (štěpsu) a podkresby různého složení. Právě viditelnost podkresby byla sledovaným parametrem. Na základě spektrometricky naměřené propustnosti a odrazivosti světla studovaných vzorků navrhujeme v této práci optimalizaci postupu pro vizualizaci podkresby. Zároveň kvantifikujeme pravděpodobnost, s jakou je možné podkresbu v závislosti na složení překryvné barevné vrstvy odhalit.

KLÍČOVÁ SLOVA: **propustnost, odrazivost, neinvazivní snímání, pigmenty a organické barviva**

Úvod

K vizualizaci vnitřní struktury malířského díla lze vedle pokročilých prozařovacích metod [1, 2] do určité míry využít i zařízení běžně dostupná jako je snímkování v NIR spektru pomocí běžných fotoaparátů, kterým je odstraněn infračervený filtr (ICF) ze snímače. Takto upravený fotoaparát poskytuje snímky v rozsahu cca 400–1050nm (tento rozsah se u běžně dostupných fotoaparátů může nevýznamně lišit). Pro odfiltrování viditelné části spektra (400–700nm) se používají buď fotografické filtry (pokud objektiv umožňuje jejich instalaci), anebo světlo z infračervených lamp [3].

Naše dosavadní zkušenost ukazuje, že pronikavost infračerveného záření je pro interpretaci NIR snímků podstatná, proto jsme se ji rozhodli kvantifikovat. Viditelnost podpravných vrstev se na námi pořízených snímcích značně liší. Problémem se jeví zejména silné vrstvy maleb a případné materiály s vysokou absorbancí v NIR oblasti. Rozpoznání podpravných vrstev malby tedy v některých případech není snadné.

Výhodou fotoaparátů a kompaktních VIS-NIR spektrometrů je snadná dostupnost a vysoký stupeň mobility umožňující rutinní screening. Navíc lze přímo kombinovat prozařování s reflexním měřením barevnosti, pokud je to v daném případě smysluplné. Naším cílem bylo pomocí empirických testů na modelových vzorcích s různými typy barevných vrstev a podkreseb ověřit, je-li výše uvedená metoda v praxi použitelná, do jaké míry a za jakých předpokladů. Určení správné metodiky pro neinvazivní snímání a úplné vyloučení neúčelného snímkování může často ušetřit drahocenný čas určený pro analýzu *in situ*. Za dobře definovaných podmínek by pak byla možná i automatická a poloautomatická identifikace podkreseb na NIR snímcích získaných neinvazivním měřením s využitím metod matematického zpracování obrazu.

Náš výzkum se opírá o víceletou spolupráci s ALMA laboratoří a zkušenost se zpracováním obrazové dokumentace z analýz uměleckých děl. [3–6] V praxi jsme ověřili, že paprsky světla v NIR

All problems according to Preflight profile
Convert to PDF/A-2u

spektru často nedokáže "proniknout" skrze vrchní vrstvu malby a zaznamenat podkresby. Nejčastěji používanou jsou konkrétní "NIR-neprostupné" pigmenty či jiné složky barevné vrstvy. Dopad použitého pigmentu na propustnost v NIR jsme se tedy pokusili změřit a kvantifikovat na umělých připravených vzorcích. V restaurátorské praxi je rozsah vlnových délek 700–950nm snadno dostupný odstraněním ICF filtru ze snímače běžného fotoaparátu (více o úpravě fotoaparátu lze najít na http://maxmax.com), proto jsme se zaměřili právě na tuto oblast.

Výběr a příprava reprezentativních vzorků

Při přípravě simulačních vzorků pro první fázi experimentu jsme pigmenty vybírali s ohledem na technologii malby v období gotiky a renesance. Čistě z experimentálních důvodů byla ale použita "průsvitná" podložka – tedy plátno místo v gotice běžných dřevěných panelů. Vzhledem k tomu byl uzpůsoben i svrchní podklad – tedy, a to jak tloušťkou, tak složením. Finálně použitá směs sádry (síran vápenatý dihydrát) nebo přírodní křídy (uhličitan vápenatý) a olovnaté běloby (bazický uhličitan olovnatý - $Pb_2(CO_3)(OH)_2$) splňuje experimentální požadavky pro měření odrazivosti a propustnosti. V prvním případě byla použita směs připravená s 3 obj. dílů bolonské křídy (58100 Kremer Pigmente), 2 obj. díly 7% želatiny – Grac, ¼ dílu polymerovaného lněného oleje (Umton), 1 doutek. V druhém případě jsme použili namísto síranu vápenatého uhličitan [vápenatý], původní recept byl navíc modifikován přidáním 2 dílů olovnaté běloby na 2 díly plavené křídy se stejným poměrem pojiva (2 obj. díly 7% želatiny – Grac, ¼ dílu polymerovaného lněného oleje (3227 Umton), 1 doutek). Použité pigmenty a barviva v barevné vrstvě a podkresbě shrnují tabulky 1 a 2 (*tab. 1, 2*). Jednotlivé pigmenty a barviva byly míchány v klihovém a olejovém pojivu.

Připravené modelové vrstvy jsou znázorněny na obrázku 1 (*obr. 1*). Pro každou kombinaci podkresba - malba (barva) byl na napůsobovaném plátně namalován čtverec 4x4cm, kde polovina čtverce byla opatřena podkresbou a druhá polovina zůstala bez podkresby. Celý čtverec byl pak překryt zvolenou barvou obsahující jediný pigment a pojivo. Díky této technologii přípravy vzorku jsme získali informaci o propustnosti a odrazivosti (i) samotného plátna, (ii) plátna a barvy, (iii) plátna, podkresby a barvy, vše v obou typech pojiva, tj. celkem šest naměřených hodnot. Při zjednodušení, že tloušťka vrstev je konstantní, naměřené hodnoty dostatečně určují fyzikální parametry vrstev - index lomu a absorbanci. Naměřené fyzikální parametry je těchto mnoho nalézt v literatuře (např. Pigment Compendium) [7], ovšem zde uváděné hodnoty jsou průměrem ve viditelném spektru.

Při přípravě modelových vzorků byly vrstvy nanášeny klasickou malířskou technikou, neplatí tedy zjednodušení našeho modelu pro konstantní tloušťku vrstev. Více se této problematice věnujeme v diskusi tohoto článku. Tloušťka barevných vrstev byla empiricky volena tak, aby byla dostatečná k úplnému překryvu podkresby ve viditelném spektru (400–700 nm). Protože při vyhodnocení předpokládáme tloušťku vrstev konstantní (v rámci jedné barvy a jedné podkresby), promítne se nám chyba tohoto zjednodušení v uvedeném rozptylu naměřených hodnot.

Postup měření

U připravených vzorků byla měřena odrazivost a propustnost. Obě tyto veličiny byly měřeny relativně k odrazivosti a propustnosti plátna opatřeného bílým podkladem. Odrazivost nám říká, kolik procent světla barevná vrstva odráží oproti bílému plátnu v dané vlnové délce. Naproti tomu propustnost podává informaci o tom kolik světla bylo absorbováno barevnou vrstvou a kolik světla barevnou vrstvou prošlo (100% reprezentuje množství světla, které prošlo podkladovou vrstvou - odpovídá k námi naměřené vrstvě). Výstupem takovéhoto měření je spektrální „otisk" použité barvy.

Měření bylo provedeno metodou FORS ("fibre-optics reflectance spectroscopy" - spektrometrie využívající optických vláken) s přenosným spektrometrem OceanOptics USB2000+ pracujícím v oboru viditelného a blízkého infračerveného záření (VIS-NIR). FORS, a to v rozsahu UV-VIS nebo VIS-NIR se používá jako screeningová neinvazivní metoda k identifikaci pigmentů a barviv na nekomplikovaných malbách, typicky například iluminovaných rukopisech [8], nebo i nástěnných malbách [9]. Identifikace probíhá pomocí porovnání zjištěných „otisků" s „otisky" známých pigmentů. Použitá konfigurace měla následující parametry: průměr optického vlákna 0,6 μm, krok: 0,31nm, počet měření cca 800 v rozsahu 700–950nm (NIR), použitelně respektive celkový rozsah přístroje je potom 435–950nm, respektive 428–1092nm (celkem 2048 měřených vlnových délek). Reflexe byla snímána pod úhlem 45° a propustnost v úhlu 0° od kolmice. Jednotlivé měření pokrývá kruhovou plochu o průměru 0.8cm.

Měření bylo pro lepší představu doplněno ilustrativními snímky pláten pořízenými fotoaparátem Canon (Kréwl D500 (na českém trhu označován jako Canon EOS 500D) upraveným pro snímání v NIR spektru (více o této úpravě lze nalézt na http://maxmax.com). Snímání jednotlivých spektrálních pásem probíhalo za pomoci optických filtrů (reflektance) [10] a LED diod (transmise) [3,11]. Použity byly běžně dostupné IR-pass filtry, u kterých jsme proměřili jejich propustnost (pro snímkování samotné

All problems according to Preflight profile
Convert to PDF/A-2u

Pigment	Výrobce/dodavatel	Chemické složení/původ
M[illegible]ka	g.r. Lachner[illegible]	$(CH_3COO)_2Cu \cdot H_2O$ (99%)
Olovnatá b[illegible]oba	Kremer-Pigmente 46000	$Pb_3(CO_3)(OH)_2$
Rum[illegible]ka	Kremer-Pigmente 10610	HgS
Minium	Lachema Brno	Pb_3O_4
Olovnato-cíni[illegible]	Kremer-Pigmente 10110	Pb_2SnO_4
Zem zelená	Kremer-Pigmente 17410	seladonit z Kypru (K, Mg, Fe silikát)
Azurit	Kremer-Pigmente 10210	$2CuCO_3 \cdot Cu(OH)_2$
Ultramarín	Kremer-Pigmente 10520	$(Na, Ca)_8[(SO_4,S,Cl)_2(AlSiO_4)_6]$
Umbra	Kremer-Pigmente 40730	p[illegible] hlinka z Kypru, obsahující 50% hydro(oxidů) Fe + oxidy Mn
Kostní [illegible]	Kremer-Pigmente 47100	zuhelnatělé zvířecí kosti, hlavní složky: 57-80% $Ca_3(PO_4)_2$, 6-10% $CaCO_3$, [illegible] carbon
Smalt	Kremer-Pigmente 10000	draselné kobaltité sklo s obsahem Co a As
Kraplak	Kremer-Pigmente 37200-B	přírodní barvivo získané z kořenů Rubia Tinctorum, hlavní složky: $C_{14}H_8O_5$ (purpurin) a $C_{14}H_8O_4$ (alizarin)
Indigo	Kremer-Pigmente 36000-A	$C_{16}H_{10}O_2N_2$

Tab. 1 Pigmenty a barviva použitá v modelové malbě

Podkresba	Výrobce/dodavatel
Červená rudka	KOH-I-NOOR HARDTMUTH
Grafit	Kremer-Pigmente 12462
P[illegible]ový uhel	KOH-I-NOOR HARDTMUTH
Um[illegible]uhel	KOH-I-NOOR HARDTMUTH
Dub[illegible]kovýinkoust	vlastní prodkuce
Sépie	Kremer-Pigmente 12401
Ol[illegible]vko	olověný drát
Ol[illegible]vko prá[illegible]k	Kremer-Pigmente 10 900
Černá k[illegible]da	Kremer-Pigmente 12450
St[illegible]borná tu[illegible]ka	Kremer-Pigmente 11348

Tab. 2 Materiály podkreseb

není propustnost podstatná). Propustnost je třeba znát pro získání spektrálního otisku pomocí fotoaparátu. Získání spektrálního otisku pigmentu touto cestou je ovšem složitější a nepřesnější. Monochromatické LED diody jsou opět běžně dostupným zbožím, v našem případě jsme měřili jejich spektrální vlastnosti pomocí výše uvedeného spektrometru. Pro simulaci našeho měření LED diody ani fotografické filtry nejsou podstatné. Snímky takto pořízené jsou pouze doplňkem pro lepší představivost.

All problems according to Preflight profile
Convert to PDF/A-2u

	700-950nm				barva (=100%)	plátno (=100%)
	avg(R)	std(R)	avg(T)	std(T)	contrast(R)	contrast(T)
olovnatá běloba	87,7	9,3	51,2	0,3	5,3	41,3
rumělka	53,2	7,8	33,4	6,8	12,3	26,9
minium	72,4	11,4	75,6	4,6	22,6	60,9
kraplak	57,9	17,0	63,9	13,6	34,1	51,4
indigo	32,8	11,2	23,9	19,1	27,2	19,2
olovnato-cínitá žluť	86,2	7,4	26,2	5,2	2,0	21,1
zemzelená	14,0	5,5	0,7	0,2	0,0	0,6
modřanka	5,5	2,3	1,5	1,1	1,0	1,2
azurit	32,7	12,4	22,6	4,0	12,8	18,2
ultramarín	16,8	11,5	7,5	7,5	9,7	6,1
kostní černě	3,9	1,3	0,3	0,1	0,0	0,2
umbra	21,2	5,9	2,4	1,9	0,6	2,0
smalt	52,5	16,4	51,3	14,2	30,7	41,3
různé podkresby (průměr)	33,7	18,3	39,9	20,4		

Tab. 3 Výsledky měření; všechny naměřené hodnoty jsou v procentech. Sloupec avg(R) respektive avg(T) udává průměrnou odrazivost respektive propustnost barevné vrstvy v pásu 700-950nm; sloupce std(R) a std(T) udávají směrodatnou odchylku od průměrné hodnoty na naměřených vzorcích; sloupec contrast(R) udává maximální dosažitelný kontrast (za ideálních podmínek) podkresby vůči barevné vrstvě v odraženém světle; sloupec contrast(T) pak udává maximální dosažitelný kontrast podkresby vůči nejsvětlejší bílé barvě na snímku propuštěného záření

Výsledky měření

Doplňkové snímky z fotoaparátu v pásmu 700–950nm ukazuje obrázek 2 - reflektance (*obr. 2*) a obrázek 3 - transmise (*obr. 3*). Zřetelný rozdíl ve viditelnosti podkresby na těchto snímcích ukazuje kvalitativní zlepšení při použití transmisních snímků [12] V odraženém světle je podkresba tím viditelnější, čím je barva tmavší (nižší odrazivost v NIR) a čím má vyšší propustnost (transparentnost v NIR). Výhodou transmise je, že světlost barvy (odrazivost v NIR) není pro výsledek podstatná.

Kvalitativní měření bylo provedeno spektrometrem, kdy z každého natřeného vzorku v ploše 4x4 cm bylo pořízeno celkem 8 měření odrazivosti (4 z části bez podkresby a 4 z části s podkresbou) a 4 měření propustnosti (2+2 z každé poloviny). Výsledky shrnuje tabulka 3 (*tab. 3*).

Odrazivost barevné vrstvy „avg(R)“ je průměrem 80 nezávislých měření na 10 vzorcích se stejnou svrchní vrstvou (různým plátnem a různou podkresbou). Propustnost „avg(T)“ je průměrem dvou měření na plátně v části vzorku, kde podkresba není. Poslední řádek v tabulce udává průměrnou odrazivost a propustnost podkresby. Zde byly průměrovány všechny použité podkresby (*tab. 2*) dohromady (tím chceme alespoň částečně simulovat případy, kdy dopředu neznáme použitou podkresbu). Sloupec “contrast(R)” představuje vypočtený maximální kontrast svrchní vrstvy s nejtmavší možnou podkresbou a bez podkresby (s bílým podkladem) při měření odrazem v procentech; 100% potom odpovídá intenzitě svrchní vrstvy bez podkresby s bílým podkladem. Pokud bychom transmisi vyjádřili obdobně, byla by hodnota 81% pro všechny typy svrchních vrstev (=2 x směrodatná odchylka podkladu). Při transmisi raději udáváme relativní kontrast „contrast(T)“, kde 100% odpovídá bílé barvě a 0% naprosto černé barvě (jedná se tedy o kontrast v rámci celého snímku, nikoli pouze v rámci barevné oblasti). Rozptyl hodnot u naměřených veličin je z velké míry způsoben zjednodušením našeho výpočtu pro konstantní tloušťku vrstvy. Pro ověření našich závěrů je ale postačující.

Zjistili jsme, že chování pigmentů na fotografiích odpovídá předpokládanému chování dle naměřených propustností a odrazivostí ze spektrometru (*tab. 3*). Je následující:

Olovnatá běloba má velkou odrazivost (80–100%) v celých vlnových délek v rozsahu NIR, což znemožňuje identifikovat podkresbu v odraženém světle. Propustnost olovnaté běloby je nižší (30–50%) než odrazivost. V tomto případě se tedy ukazuje jako vhodný způsob identifikace podkreseb snímek transmise záření.

Rumělka vykazuje také rozdíl mezi propustností a odrazivostí, není však tak propastný jako u olovnaté běloby. Počítá se na naměřené hodnoty intenzity podílí asi 10–15% při měření odraženého světla (v nejlepším případě). I zde je tedy vhodnější pou-

All problems according to Preflight profile
Convert to PDF/A-2u

ut transmisi pro identifikaci podkreseb. Kontrast v odraženém světle nemusí být dostatečný.

Minium má propustnost i odrazivost podobnou (cca 75%). Podkresba je tedy dobře patrná i v odraženém světle. Na našich vzorcích jsme navíc zjistili rychlý nárůst absorbance při malém zvýšení tloušťky vrstvy. Podkresby jsou tedy detekovatelné pouze pod slabou vrstvou minia.

Kraplak má obdobné chování jako rumělka, propustnost i odrazivost je však nepatrně vyšší (kolem 60%). V ideálním případě by reflexní měření mělo stačit (až 34% kontrastu). Při silnější vrstvě barvy ale stále doporučujeme zvolit primárně transmisní měření.

Indigo vykazuje propustnost světla vyšší o cca 10–20% než odrazivost, při identifikaci podkresby lze tak použít jít odražené světlo.

Olovnato-cínitá žluť se díky vysoké odrazivosti a nízké propustnosti chová obdobně jako olovnatá běloba. Vhodným způsobem pro lokalizaci podkreseb je měření transmise, kde podkresba dosahuje až 21% kontrastu snímku. Tato hodnota je pro bezpečnou lokalizaci dostačující.

Zem zelená je se svou vysokou absorbancí reálně neprůsvitná. Podkresby pod vrstvou země zelené není možné odhalit v NIR spektru na snímcích odraženého ani propuštěného světla.

Modřanka vykazuje totožné chování jako zem zelená. Podkresby jsou neodhalitelné.

Azurit umožnil rozpoznání podkresby v odraženém světle v pěti z celkem deseti vytvořených vzorků. Opět tedy lze doporučit měření transmise pro odhalení podkreseb. U reflexe velmi závisí na tloušťce vrstvy a použitém materiálu podkresby (olůvko a stříbro nelze rozpoznat vůbec).

Ultramarín vykazuje podobné chování jako azurit. Při lokalizaci podkreseb v odraženém světle úspěch není zaručen (v našem případě pouze ve dvou z deseti vzorků). Zjištěný maximální dosažitelný kontrast při měření reflexe je 9,6% intenzity ultramarinu - toto je v praxi téměř nepoužitelná hodnota, pigment je sám o sobě poměrně tmavý. Pořizování NIR-reflexivních snímků pro odhalení podkreseb pod vrstvou ultramarinu tedy nelze doporučit. Lokalizace podkresby v propuštěném světle možná je (až 6% kontrastu snímku, dle tmavosti podkresby), ale není zaručená.

Kostní černi neumožňuje odhalit podkresbu v NIR spektru vůbec, a to díky téměř absolutní absorbanci podkresby pod barevnou vrstvou.

Umbra rovněž díky vysoké absorbanci znemožňuje detekci podkresby, a to i při snímání transmise. Jde o chování totožné jako v případě země zelené i kostní černi.

Smalt vyžaduje další výzkum. Zatím se zdá, že jeho propustnost v NIR oblasti silně závisí na zrnitosti podkresby. Čím je podkresba jemnější (např. dubovkový inkoust) tím je propustnost vyšší, čím je hrubší (např. černá křída), tím je propustnost menší. V naší studii pro identifikaci podkreseb postačilo pouze měření odraženého záření.

Diskuse

Při přípravě modelových vzorků byla zachovávána "věrnost vůči předloze", tedy historickému receptu a dobové malířské technice. I když jsme se snažili nehomogenitu povrchu podkladové vrstvy znatelně omezit při přípravě křídy, nebylo možné ji ideálně dodržet. Ani v případě barevných vrstev nebyly parametry technické ideální. Nehomogenita vrstev v ploše, nestejnoměrná zrnitost a tloušťka jsou patrně vlivy, které mohly, byť minoritně, ovlivnit výsledky měření.

Příkladem nehomogenity je koncentrace pigmentových částic u rychleji schnoucích okrajů malby nebo kresby (*obr. 4a*). Tento efekt se násobí délkou vysychání - nejvíce postižené jsou vzorky, kde byl jako pojivo použit pomalu schnoucí olej. Problému nehomogenit se naše studie dále nevěnuje - pro měření spektrometrem byly vybrána místa homogenní, uvnitř namalované plochy. Efekt vysychání a přípravy samotné barvy v kontextu interakce s podkresbou vyžaduje další výzkum.

Dalším jevem, který se na našich modelových vzorcích projevil, je zprůhlednění malby v průběhu stárnutí (*obr. 4b*). Zatímco při přípravě vzorků byla tloušťka barevné vrstvy dostačující pro zakrytí podkresby, po několika měsících podkresba začala prosvítat skrze barevnou vrstvu. Tento jev je častý i u gotických maleb, lze jej považovat za autentický. V našem případě jde nejspíše o změnu indexu lomu temperové malby v průběhu stárnutí podobně dochází ke zvýšení indexu lomu u olejomalby.[13]

Jak již bylo řečeno, barvy byly nanášeny štětcem, a tedy tloušťka vrstev nebyla konstantní. Jelikož absorpce vrstvy na tloušťce závisí exponenciálně [14] můžeme opakováním měření v různých místech vzorku odhadnout tvar této exponenciální křivky. Čím více měření je provedeno, tím přesnější absorpční křivku dostáváme. Pro tuto studii však postačil předpoklad konstantní tloušťky, protože statistické odchylky naměřených dat nepřesáhly únosnou míru (*tab. 3*).

Dále je třeba zmínit, že námi uváděný maximální kontrast podkreseb (*tab. 3*) je ovlivněn materiálem, který byl k jejich přípravě použit a platí pouze v ideálním případě kterým je tmavá podkresba. Například podkresby provedené stříbrnou tužkou nebo olůvkem nebylo možné na bílém podkladu v NIR

All problems according to Preflight profile
Convert to PDF/A-2u

spektru identifikovat vůbec. Pro studium těchto podkreseb je proto třeba zvolit jiný postup. Možnost jejich lokalizace je nad rámec této studie.

Posledním komplikujícím faktorem jsou artefakty způsobené při infračervené transmisi. Zde se zřetelně projevuje textura plátna v pořízeném snímku nebo viditelné tahy štětcem v místech s různou tloušťkou barevné vrstvy, v neposlední řadě u reálných maleb pak i nehomogenity v barevné vrstvě. Problematikou odstranění textury se zabývá naše další práce. [6]

Závěry

Testovali jsme patnáct staromistrovských pigmentů a deset různých podkreseb. U těchto pigmentů můžeme definovat tři kategorie podle možnosti identifikace podkresby:

- podkresba vidět není z důvodu zanedbatelné propustnosti NIR záření (zem zelená, modřanka, kostní čerň, umbra)
- podkresbu je možné identifikovat v odraženém světle díky nízké odrazivosti a velká propustnosti (kraplak, smalt, indigo, minium, azurit, rumělka)
- podkresbu není možné identifikovat v odraženém světle (odražené světlo má příliš velký jas a intenzita světla odraženého podkresbou zanikne v šumu), ale je možné ji identifikovat v propuštěném světle, tj. v transmisi (olovnatá běloba, olovnato-cínová žluť rumělka, azurit).

U azuritu a rumělky lze dobře vysledovat závislost na tloušťce barevné vrstvy. Obecně je vždy výhodnější pro identifikaci podkreseb použít snímek propuštěného světla (transmisi).

Ověřili jsme, že podkresby stříbrnou tužkou a olůvkem nelze identifikovat v pásu 700–950nm na námi použitém bílém podkladu (smalt, kraplak a olovnaté běloby).

Poděkování

Děkujeme Janě a Davidovi Hradilovým z laboratoří ALMA za odbornou pomoc při tvorbě a analýze připravených vzorků, poskytnutá data a věcné připomínky. Tato práce byla podpořena projektem GAČR P103/12/2211.

Literatura

[1] Ambrosini D., Daffara C., Di Biase R., Paoletti D., Pezzati L., Bellucci R., Bettini F.: Integrated reflectography and thermography for wooden paintings diagnostics. *Journal of Culture Heritage* 11 (2010), 196–204.

[2] Carcagni P., Patria A., Fontana R., Greco M., Mastroianni M., Materazzi M., Pampaloni E., Pezzati L., Piccolo R.: Spectral and colorimetric characterization of painted surfaces: A scanning device for the imaging analysis of paintings. In Salimbeni R., Pezzati L. (eds.): SPIE Proceedings Vol. 5857: Optical Methods for Arts and Archaeology, 58570T (12 August 2005); doi: 10.1117/12.612565

[3] Blažek J., Soukup J., Tichý T., Zitová B., Hradilová J., Flusser J.: Low-cost mobile system for multispectral cultural heritage data acquisition. In Digital Heritage International Congress 1 (2013), 73–79.

[4] Blažek J., Hradilová J., Kamenický J., Zitová B.: Odhalování kopií pomocí matematického zpracování obrazu I. Teoretická východiska a princip metody. In Hradil D., Hradilová J. (eds.): Acta Artis Academica 2012, 141–152.

[5] Hradilová J., Valchařová B., Velíček M., Blažek J.: Odhalování kopií pomocí matematického zpracování obrazu II. Případ malby na plátně s námětem chlapce hladícího ptáčata". In Hradil D., Hradilová J. (eds.): Acta Artis Academica 2012, 153–162.

[6] Beneš M., Zitová B., Blažek J., Hradilová J., Hradil D.: Removing the Artifacts from Artwork Cross-section Images. In Proceedings of the 18th IEEE International Conference on Image Processing 2011, 3597–3601.

[7] Eastaugh N., Walsh V., Chaplin T.: Pigment Compendium: Optical Microscopy of Historical Pigments. Elsevier Butterworth-Heinemann, Oxford UK 2005.

[8] Aceto M., Agostino A., Fenoglio G., Idone A., Gulmini M., Picollo M., Ricciardie P., Delaney J.K.: Characterisation of colourants on illuminated manuscripts by portable fibre optic UV-visible-NIR. *Analytical Methods* 6 (2014), 1488–1500.

[9] Cheilakou E., Troullinos M., Koui M.: Identification of pigments on Byzantine wall paintings from Crete (14th century AD) using non-invasive Fiber Optics Diffuse Reflectance Spectroscopy (FORS). *Journal of Archaeological Science* 41 (2014), 541–555.

[10] Hollaus F., Gau M., Sablatnig R.: Multispectral image acquisition of ancient manuscripts. In Progress in Cultural Heritage Preservation 2012, 30–39.

All problems according to Preflight profile
Convert to PDF/A-2u

[11] Kunc M., Blažek J.: Pole LED v matici 8x8. Technická dokumentace odd. Zpracování obrazové informace ÚTIA AV ČR (2012), http://www.utia.cas.cz/ZOI-publications

[12] Cucci C., Picollo M., Vervat M.: Trans-illumination and trans-irradiation with digital cameras: Potentials and limits of two imaging techniques used for the diagnostic investigation of paintings. *Journal of Culture Heritage* 13 (2012), 83–88.

[13] Slánský B.: Technika malby. Díl I. Malířská a konzervační materiál., Státní nakladatelství krásné literatury, hudby a umění, Praha 1953.

[14] Houghton J. T.: The Physics of Atmospheres (2nd ed.). Cambridge University Press 2002, Chapter 6.

Seznam obrázků

1 Ukázka plátna s emulzním podkladem (olovnatá běloba a uhličitan vápenatý) se vzorky ve viditelném světle (s podkresbou vytvořenou černou kružidlou); první dva vzorky jsou bez krycí vrstvy (hustá a tenká podkresba), následuje (zleva-doprava, shora-dolů) olovnatá běloba, rumělka, minium, kraplak, indigo, olovnato-cíniitá žluť, zeleň, malachit, ultramarín, azurit, kostní černá, umbra a smalt; pojivo je klihové; levá část vzorku (2x4cm) je ponechána bez podkresby (viz obrázek 2), pravá část je s podkresbou

2 Snímek vybraných vzorků z plátna dle obrázku 1 v NIR spektru (zde 720–950nm, reflexe) v pořadí (zleva-doprava, shora-dolů) olovnatá běloba, rumělka, olovnato-cíniitá žluť, zeleň; podkresba černou kružidlou, v pravé části každého vzorku není patrná díky velké odrazivosti (olovnaté pigmenty) nebo vysoké absorbanci (zeleň) použitých pigmentů; výjimkou je zde rumělka, kde lze podkresbu odhalit ovšem s nevelkou určitostí

3 Snímek vybraných vzorků z plátna dle obrázku 1 v NIR spektru (zde 700–900nm, transmise) v pořadí (zleva-doprava, shora-dolů) olovnatá běloba, rumělka, olovnato-cíniitá žluť, zeleň; podkresba černou kružidlou, v pravé části každého vzorku, je velmi dobře patrná; narozdíl od snímání reflexe, snímek obsahuje artefakty v podobě textury plátna a tahů štětcem, (dobře viditelné díky různé tloušťce vrstvy v různých místech vzorku s rumělkou

4 Komplikující faktory vlivem schnutí a stárnutí vzorků - okrajová kontura grafitové podkresby v oblastech nejrychlejšího schnutí svrchní barevné vrstvy smaltu na plátně v odraženém světle v rozsahu 700–950nm (**a**), tento efekt se vyskytuje zejména ve vzorcích pomalu schnoucích s olejovým pojivem; a prostup podkresby provedené červenou rudkou svrchní vrstvou minia po cca 10 měsících od vytvoření vzorku, ve viditelném světle (**b**)

All problems according to Preflight profile
Convert to PDF/A-2u

Research article

Journal of RAMAN SPECTROSCOPY

Received: 15 September 2014 Revised: 23 October 2014 Accepted: 4 November 2014 Published online in Wiley Online Library

(wileyonlinelibrary.com) DOI 10.1002/jrs.4627

Naturally irradiated fluorite as a historic violet pigment: Raman spectroscopic and X-ray diffraction study

Zdeňka Čermáková,[a,b,c]* Petr Bezdička,[a,b] Ivan Němec,[d] Janka Hradilová,[b] Vladimír Šrein,[e] Jan Blažek[f] and David Hradil[a,b]

Naturally irradiated violet fluorite, a cubic CaF_2 mineral, is a rare historic pigment. Its documented usage in Europe stretches from ca. 1450 to ca. 1550. The intensely coloured violetish black naturally irradiated fluorite is commonly called antozonite, which is only vaguely defined based on its dark colour and specific odour emanated during grinding. In the published literature, there have been some discrepancies about its Raman spectrum. Therefore, sixteen samples of antozonite were analysed by Raman (micro-)spectroscopy using five different excitation laser wavelengths (445, 532, 633, 780 and 1064 nm), which revealed specific bands located below 500 cm^{-1} probably related to radiation-caused defects. Their intensity increased with increasing violet colour saturation, thus providing a specification for antozonite's definition. Spectra excited at 445 and 780 nm contained also numerous broad bands above 500 cm^{-1}, which seem to be caused by the presence of rare earth elements. The structural damage of antozonite samples has been assessed by X-ray diffraction and related to their lightness using analysis of image histograms. The obtained results have been applied in the analysis of micro-samples of a Late Gothic altarpiece located in an Italian Court in UNESCO city Kutná Hora, Czech Republic, which contained exceptionally large grains of deep violet fluorite identified as antozonite. Copyright © 2015 John Wiley & Sons, Ltd.

Supporting information may be found in the online version of this article at the publisher's web site.

Keywords: fluorite; pigment; fluorescence bands; diffraction lines broadening; irradiation

Introduction

Fluorite is a cubic mineral with ideal composition CaF_2. In nature, it most commonly forms granular to massive aggregates or cubic crystals. Its colour is variable: from colourless, white, yellow to orange, pink to purple–red, purple to violet, blue, pale green, brown or violet–black.[1] These colours are usually pale; the only truly intense colour is the violet–black one which forms due to the influence of radioactivity on fluorite's crystal structure causing structural dislocations. The irradiation is caused by uranium or thorium-rich minerals coexisting with fluorite in certain geological settings.[2] This type of irradiated fluorite is commonly called antozonite, or fetid fluorite (derived from the specific odour that antozonite emanates when crushed). The nature of the odour has been discussed by several authors; while Vochten *et al.* (1977)[3] reported that the enclosed gases comprised of SO_2, SOF_2, S_2F_2, H_2S and Ar, the most recent study by Schmedt auf der Günne *et al.* (2012)[2] showed that based on olfactory testing and magic-angle-spinning nuclear magnetic resonance (MAS-NMR) spectroscopy analysis, the odour is caused by elemental difluorine. These intensely coloured fluorites are often banded with less-saturated or almost colourless parts. Still, the radioactively damaged violet–black fluorite is the only one that has sufficient colouring power even in the form of small particles suitable for the usage as a painting pigment, as proved, e. g. by Richter *et al.* (2001).[4]

Violet to purple historical pigments are rare; these hues were usually obtained by mixing blue and red pigments. Besides natural fluorite, historical inorganic violet–purple painting pigments include, e.g. the artificially-prepared Han purple;[5] modern synthetic pigments, introduced in the 19th century, encompass dark and light cobalt violet, or ultramarine violet.[6–8]

The documented usage of violet to purple fluorite in European art stretches from ca. 1450 to ca. 1550, which is a rather narrow time interval.[9–13] Originally, violet fluorite was thought to be used exclusively in Switzerland and Germany due to the first identifications of this pigment in the artworks originating in these countries (the first one took place in 1980s). Later on, the research of various types of artworks (panel paintings, polychromy on

* *Correspondence to: Zdeňka Čermáková, Institute of Inorganic Chemistry of the AS CR, v.v.i., ALMA laboratory, Husinec-Řež 1001, 250 68 Řež, Czech Republic. E-mail: cermakova@iic.cas.cz*

a *Institute of Inorganic Chemistry of the AS CR, v.v.i., ALMA laboratory, Husinec-Řež 1001, 250 68 Řež, Czech Republic*

b *Academy of Fine Arts in Prague, ALMA laboratory, U Akademie 4, 170 22 Prague 7, Czech Republic*

c *Institute of Geochemistry, Mineralogy and Mineral Resources, Faculty of Science, Charles University in Prague, Albertov 6, 128 43 Prague 2, Czech Republic*

d *Department of Inorganic Chemistry, Faculty of Science, Charles University in Prague, Hlavova 8, 128 00 Prague 2, Czech Republic*

e *Czech Geological Survey, Klárov 3, 118 21 Prague 1, Czech Republic*

f *Institute of Information Theory and Automation of the AS CR, v.v.i., Pod Vodárenskou věží 4, 182 08 Prague 8, Czech Republic*

Copyright © 2015 John Wiley & Sons, Ltd.

All problems according to Preflight profile
Convert to PDF/A-2u

wooden/stone sculptures and wall paintings) proved that violet fluorite was used also throughout the Central European region (Czech Republic, Slovakia, Austria, Poland-Lower Silesia and Hungary) as well as in The Netherlands and Belgium. Some of the reported fluorites are rather light coloured; others have deep violet to purple colour consistent with the intensively irradiated antozonite.[9–13] The list of the works with violet fluorite may not be final—so far, this pigment was identified in only about 40 works of art.

The dating and geographical spread of the dark violet fluorite pigment usage seem to be connected with its period extraction. Šrein *et al.* (2010)[14] studied dark violet fluorite samples (antozonites) from several localities in the Czech Republic, Germany and Poland. They identified Wölsendorf in Bavaria, Germany, as the most likely source of suitable fluorite pigment material based on observations of the material as well as historic data: the ground samples from Wölsendorf contained the highest amount of dark-coloured grains, the time of fluorite's usage coincide with the time of the extraction of silver ores (the locality has been discovered around 1450, the mining activities were abandoned after 1520–1550) and after extraction of the most prolific upper parts, the silver ores were mined from the fluorite-rich veins. Spring (2000)[13] suggests that in case of The Netherlands, Belgium and north-western part of Germany, the violet fluorite was extracted in several places in Ardennes, which were, in that period of time, mined for zinc ore used for brass production.

The identification of fluorite in micro-samples of painted works of art is facilitated by its unique elemental composition, comprising calcium and fluorine. Therefore, unambiguous identification can be performed using scanning electron microscopy–energy dispersive spectroscopy (SEM-EDS). However, using SEM-EDS, it is not possible to identify the structural damage present in intensely irradiated samples. The structural information supporting the elemental analysis may be obtained by micro-X-ray diffraction (if the concentration of fluorite in the sample is sufficient), or by vibrational spectroscopies; it seems that for the identification of violet fluorite in painted work of art, Raman spectroscopy has been used, so far, only once.[15]

Dill and Weber (2010)[16] published Raman spectra of natural samples of fluorites with various colours (including antozonite). They reported that the appearance of the spectrum of antozonite was 'rather degraded'. However, the problem of these presented spectra is that they are not actually Raman bands of fluorite—fluorite as a cubic compound has a very simple Raman spectrum with a sharp band at the position of 322 cm^{-1}.[17] The spectra published by Dill and Weber (2010)[16] encompass the 400 to 2400 cm^{-1} part of the spectrum, i.e. excluding the only Raman band of fluorite.

X-ray diffraction patterns of antozonite were studied, e.g. by Vlček *et al.* (2012)[18] and Berman (1957).[19] They showed that the patterns contain broadened diffraction lines, and the value of the cell parameter a increases compared to the synthetic standard. The reported change of the latter is rather small.

Based on the discrepancies in published Raman spectra of antozonite, the authors decided to perform a Raman spectroscopic study which would show whether the radioactively damaged fluorite has a specific Raman spectrum, how it relates to the structural damage observable by X-ray diffraction and the relation of these structural effects on the colour of the fluorite pigment. The results of the study were applied in the analysis of micro-samples of Late Gothic altarpiece located in an Italian Court in UNESCO city Kutná Hora, Czech Republic.

Samples

Sixteen samples of naturally irradiated fluorite designated as antozonites (based on the dark violet to black colour and specific odour emanated during grinding) originating from different localities were selected for Raman spectroscopic and X-ray diffraction study, including antozonites from Wölsendorf, Germany, a supposed historic source of dark violet fluorite pigment.[14] White synthetic fluorite produced by Sigma Aldrich served as a standard, and three fluorites with different colours (yellow, bluish and green) were counter-tested by Raman spectroscopy. All the analysed samples and their localities are summarised in Table 1.

The results of the study with natural samples were applied on two micro-samples (J1325-1hv and J1325-U) obtained from an altarpiece of the *Triptych with St. James the Lesser and St. Philip* located in the chapel of St. Wenceslas and Ladislaus in Italian Court, Kutná Hora, Czech Republic. The altarpiece was created in 1497. In 1906, it was conserved/restored and partially overpainted. Sample J1325-1hv represents only the original layers; it was taken from the blue drapery of St. Ladislaus, where fluorite forms an underpainting of blue azurite and modern overpainting. Sample J1325-U comes from the red fringe of the painted background, where fluorite is applied over gilding and covered by red glaze, varnish and overpainting. The cross-sections of the samples are depicted in Figure 1. The dark violet grains of fluorite present in the micro-samples have exceptional dimensions (up to 70 μm).

Table 1. Source localities and colour of the studied fluorite samples

Sample	Colour	Locality
1	Black	Jáchymov, Czech Republic
2	Black	Jáchymov, Czech Republic
3	Violetish black	Vlastějovice, Czech Republic
4	Violetish black	Vlastějovice, Czech Republic
5	Violetish black	Nabburg, Bavaria, Germany
6	Black	Nabburg, Bavaria, Germany
7	Black	Nabburg, Bavaria, Germany
8	Black	Johanneschacht, Wölsendorf, Bavaria, Germany
9	Black	Johanneschacht, Wölsendorf, Bavaria, Germany
10	Black	Johanneszeche, Wölsendorf, Bavaria, Germany
11	Black	Johanneszeche, Wölsendorf, Bavaria, Germany
12	Black	Marienschacht, Wölsendorf, Bavaria, Germany
13	Black	Marienschacht, Wölsendorf, Bavaria, Germany
14	Very deep violet	Melchor Múzquiz, Múzquiz Municipality, Coahuila de Zaragoza, Mexico
15	Black	Krzyżatka, Poland
16	Black	Krzyżatka, Poland
17	Bluish	Yaogangxian, Hunan Province, China
18	Green	Harrachov, Czech Republic
19	Yellow	Vrchoslav, Krupka, Czech Republic
S. A.	White	- (synthetic fluorite from Sigma Aldrich)

Copyright © 2015 John Wiley & Sons, Ltd.

All problems according to Preflight profile
Convert to PDF/A-2u

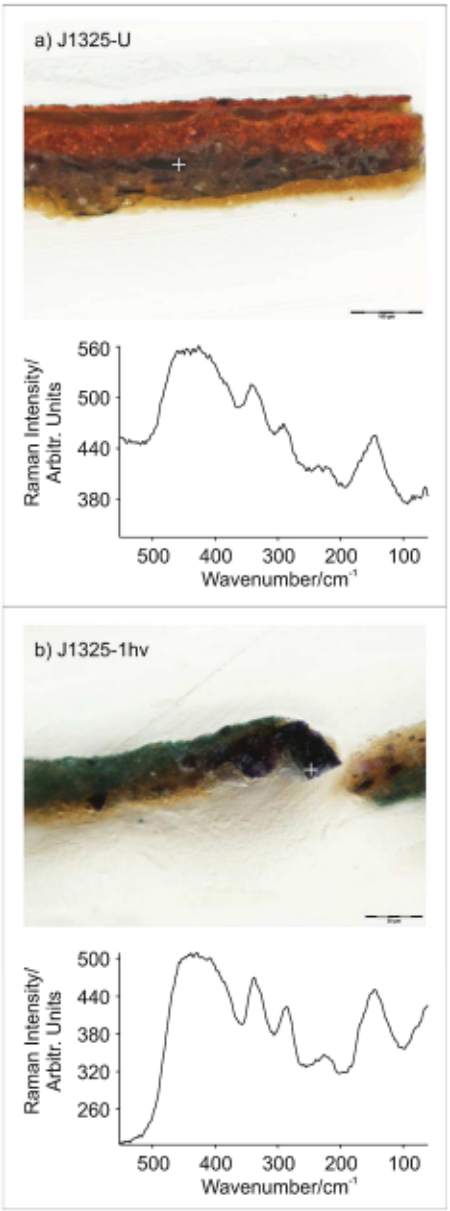


Figure 1. Photographs of micro-samples together with Raman spectra (532 nm laser) obtained in dark violet angular grains (analyses locations marked by white crosses): a) J1325-U, b) J1325-1hv. Photo: J. Hradilová. This figure is available in colour online at wileyonlinelibrary.com/journal/jrs.

Methods

Optical microscopy, photography

The micro-samples from the altar were embedded in polyester resin Neukadur PE 45 and polished in cross-section. Subsequently, they were observed by Axio Imager A.2 light microscope (Zeiss) in reflected visible and UV light (365 and 470 nm) and photographed using digital microscope camera Olympus DP 75. The fragment of a crystal from fluorite 14 was observed and photographed by Olympus BX 40 microscope equipped with DP 10 camera.

Scanning electron microscopy–energy dispersive spectroscopy (SEM-EDS)

The micro-samples embedded in the resin were analysed by Jeol JSM6510 scanning electron microscope equipped with energy-dispersive spectrometer INCA (Oxford Instruments) with SDD detector allowing detection of elements heavier than Be ($Z > 4$) at 125 eV resolution. Measurements were carried out in a low vacuum mode under the pressure of 30 Pa and accelerating voltage of 25 kV; backscattered electrons were detected. Low vacuum mode allowed analysis of samples without conductive coating of their surface.

UV–VIS spectrophotometry and analysis of image histograms

Two naturally irradiated fluorite samples (14 and 16—as representatives of light and dark coloured samples) were measured by UV–VIS spectrophotometer Cary 4000 UV–vis (Agilent) equipped with an integration sphere. The measurement has been performed in diffuse reflectance mode to minimize light scattering. Since the dark coloured sample exhibited complete absorption and it was not desirable to dilute the samples in order to prevent the contamination for following analyses, the evaluation of the samples' lightness has been performed by the analysis of image histograms. Each ground naturally irradiated antozonite sample was applied in a continuous flat layer on glass slide and photographed by Canon D500 Rebel camera under controlled light (D65 light source). Position of the sample, camera and light source were fixed and the camera parameters (shutter speed, aperture, objective, focus and white balance) were kept the same. These constant conditions ensured that the histograms of the photographs were comparable.

X-ray diffraction (XRD)

Natural samples of antozonites and of the white fluorite standard were each ground in an agate mortar in suspension with cyclohexane. Each sample of antozonite emanated a strong specific odour during grinding. The sample suspension was transferred on top of a mylar foil on a transmission sample holder. After evaporation of the solvent, thin layer of the sample was covered by another mylar foil.

Diffraction patterns were collected using a PANalytical X'Pert PRO diffractometer equipped with a conventional X-ray tube ($Cu_{K\alpha}$ 40 kV, 30 mA, line focus) in transmission mode. An elliptic focusing mirror, a divergence slit 0.5°, an anti-scatter slit 0.5° and a Soller slit of 0.02 rad were used in the primary beam. A fast linear position sensitive detector PIXcel with an anti-scatter shield and a Soller slit of 0.02 rad were used in the diffracted beam. All patterns were collected in the range of 22 to 88° 2-Theta with the step of 0.013° and 900 s/step resulting in a scan of about 5 h.

Qualitative analysis has been performed using HighScorePlus software package (PANalytical, The Netherlands, version 3.0e), Diffrac-Plus software package (Bruker AXS, Germany, version 8.0) and JCPDS PDF-2 database.[20] Unit cell refinement has been performed by the least squares method, as implemented in the HighScorePlus software and AFPAR programme.[21]

Raman spectroscopy

Micro-Raman spectra of the samples were obtained on a Thermo Scientific DXR Raman Microscope with Peltier-cooled CCD detector interfaced to an Olympus microscope (10× and 50× objective lens) in the 50–3400 cm^{-1} spectral region with 4 cm^{-1} resolution. The spectrometer was calibrated by software-controlled calibration procedure using multiple neon emission lines (wavelength calibration), multiple polystyrene Raman bands (laser wavenumber calibration) and standardized white light sources (intensity calibration).

The spectra of micro-samples were collected using 532-nm laser with 0.1 to 0.2 mW laser power, 32 scans and 2 s exposure time,

Copyright © 2015 John Wiley & Sons, Ltd.

All problems according to Preflight profile
Convert to PDF/A-2u

50× objective lens. For the analysis of natural samples, four lasers of different wavelengths were used: 445, 532, 633 and 780 nm. Typical analytical conditions were following: 10× objective lens, 64 scans, 2 s exposure time, 10 mW laser power.

Two of the naturally irradiated fluorites (fluorite 3 and 13) were measured also by FT Raman spectrometer Thermo Nicolet 6700 FTIR equipped with a Nexus FT Raman module (1064-nm Nd:YVO4 laser excitation, Happ–Genzel apodization, 4 cm^{-1} resolution, 3700–150 cm^{-1} range); however, the samples exhibited strong fluorescence.

Results and discussion

Natural samples

X-ray diffraction and analysis of image histograms

All sixteen samples of naturally irradiated fluorites—antozonites, as well as the white synthetic fluorite standard were measured by X-ray diffraction in transmission mode to observe and compare the effect of irradiation on the structure. Table 2 summarises the calculated characteristics of the studied samples.

According to Vlček *et al.* (2012),[18] natural radiation causes dislocation loops and subsequent defect clustering in the fluorite's structure. Such structural disorder should be expressed in the diffraction pattern by increased full-width half-maximum (FWHM) of the diffraction lines (i.e. their broadening). Vlček *et al.* (2012)[18] also reported an increase of the unit cell volume (up to 0.26%). In agreement to the already published data,[18,19] the majority of antozonites showed broadening of their diffraction lines in comparison to synthetic standard (Table 2). The increase of FWHM corresponds to the decreasing colour lightness of the ground samples; they ranged from light violet (fluorite 14) to completely black (fluorite 13), while the FWHM of the 111 diffraction line ranged from 0.054 (fluorite 14) to 0.114° 2-Theta (fluorite 13). The difference of FWHMs represents an increase of 111.11%. The diffraction patterns of fluorites 3, 5 and 14 with light violet colour (as ground samples) were similar to the white synthetic standard.

To objectively compare the colour (with special attention to lightness, possibly related to the structural damage) and the FWHM of antozonites, UV/VIS spectrophotometry was thought to be a suitable method. It has been tested on two selected ground samples—fluorite 14 (light violet) and 16 (violetish black). In the 350 to 750 nm region, fluorite 14 exhibited one broad band with the maximum positioned at approx. 580 nm. Bill and Calas (1978)[22] have observed similar spectra in samples with intense blue and deep purple colours, and ascribe it to the presence of calcium colloids, which form due to irradiation. In case of fluorite 16, its very dark colour resulted in total absorption, and as it was not desirable to dilute the dark-coloured samples and contaminate them for following analyses, a different approach for the comparison of their lightness has been taken. All 16 ground antozonite samples were photographed under constant lighting and with constant camera setting. Histogram of each of the images has been averaged; the averages represent the overall relative lightness of the samples. Figure S1 (Supporting Information) shows two representative photographs of the samples. It can be clearly seen that the lighter-coloured samples are actually mixtures of dark violet and violet grains together with white grains, while the dark-coloured samples are composed almost singularly of dark violet grains. The composition of the lighter-coloured samples is predominantly not caused by inaccurate manual separation, but rather by different 'density' of the radioactive damage within fluorite. Figure 2 depicts the averages of photographs' histograms plotted against the FWHMs (111 diffraction lines). The coefficient of determination R^2 of the presented data (using linear regression) is 0.7208. The R^2 values above 0.8 are perceived to indicate strong correlation, while values below 0.5 indicate weak correlation. Therefore, the correlation is rather strong.

On the other hand, according to the results of this study, the reported increase of the unit cell parameter a (resulting in an increase of the unit cell volume)[18] is not straightforward. The differences between the parameters are very small, and the values are dependent on the programme with which they were calculated (in this case HighScorePlus vs. AFPAR programmes). The values of parameter fluctuate, and if the linear regression is applied on parameter vs.

Table 2. Parameters of studied naturally irradiated fluorites—antozonites and of the white synthetic fluorite calculated from their X-ray diffraction patterns

Sample	Colour of the ground sample	Parameter a [Å]		FWHM [°2-Theta]				Unit cell volume [Å^3]	
		Afpar	HS+	111	220	400	422	Afpar	HS+
13	Black	5.4646	5.4647	0.114	0.167	0.198	0.383	163.1867	163.1920
12	Black	5.4645	5.4648	0.112	0.163	0.193	0.385	163.1714	163.2010
2	Violetish black	5.4652	5.4650	0.101	0.143	0.171	0.330	163.2368	163.2189
1	Violetish black	5.4639	5.4645	0.095	0.128	0.158	0.296	163.1240	163.1741
16	Violetish black	5.4634	5.4639	0.084	0.109	0.137	0.225	163.0783	163.1204
9	Deep violet	5.4634	5.4639	0.084	0.109	0.137	0.225	163.0783	163.1204
15	Violetish black	5.4645	5.4645	0.081	0.106	0.129	0.221	163.1768	163.1741
6	Deep violet	5.4637	5.4639	0.065	0.080	0.099	0.150	163.1052	163.1204
8	Deep violet	5.4641	5.4642	0.063	0.078	0.094	0.145	163.1374	163.1473
7	Deep violet	5.4638	5.4639	0.063	0.078	0.099	0.143	163.1105	163.1204
10	Deep violet	5.4634	5.4636	0.061	0.075	0.094	0.139	163.0756	163.0935
4	Light violet	5.4627	5.4628	0.061	0.077	0.094	0.132	163.0093	163.0219
11	Deep violet	5.4632	5.4635	0.060	0.075	0.091	0.140	163.0604	163.0846
S. A.	White	5.4645	5.4642	0.057	0.069	0.081	0.116	163.1741	163.1481
5	Light violet	5.4630	5.4633	0.057	0.069	0.080	0.120	163.0416	163.0666
3	Light violet	5.4630	5.4633	0.056	0.066	0.082	0.114	163.0398	163.0666
14	Light violet	5.4640	5.4637	0.054	0.064	0.077	0.102	163.1311	163.1052

Copyright © 2015 John Wiley & Sons, Ltd.

All problems according to Preflight profile
Convert to PDF/A-2u

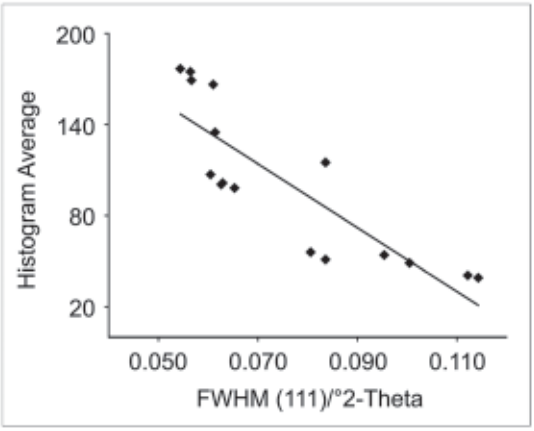


Figure 2. Histogram averages of the ground antozonite samples' photographs plotted against the full-width half-maximum (FWHM) values of their 111 diffraction line. The linear regression has a coefficient of determination $R^2 = 0.7208$ indicating a good level of correlation..

FWHM (111) values, the correlation coefficient R^2 for HighScorePlus data is 0.6104 and 0.3555 for AFPAR data. Nevertheless, fluorite 2 with the highest value of unit cell parameter has also one of the highest values of FWHM (111 diffraction line: 0.101).

The results show that the structural disorder of antozonites caused by natural irradiation may be expressed by the level of broadening of their diffraction lines and the low lightness of their dark violet to almost black colour; the increase of the unit cell parameter and volume has been observed only in some of the studied samples.

Raman spectroscopy

All the studied natural fluorites (antozonites and yellow, bluish and green samples) as well as white synthetic fluorite standard (Table 1) were analysed by Raman spectroscopy. As the photographs of the ground samples have already indicated, the antozonite samples are not homogenous; this forms a challenge for data comparison with X-ray diffraction, which is an analysis encompassing the whole sample. If applicable, the authors attempted to obtain Raman spectra on both violet/violetish black as well as colourless fluorite grains.

First, all the samples were measured with 532 nm excitation. Interestingly, all sixteen samples of antozonite (deep violet, violetish black and almost black grains) showed almost similar spectra

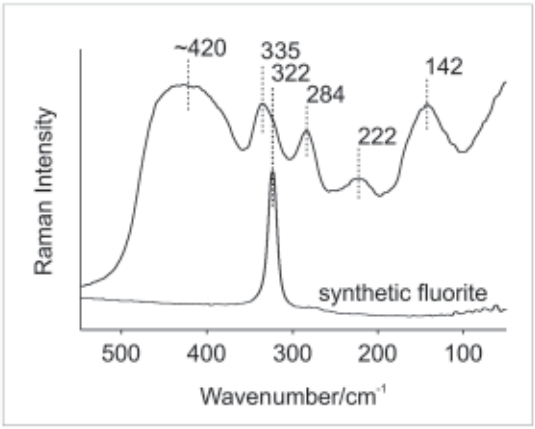


Figure 3. Raman spectrum (532 nm) of fluorite 8, representative of all antozonite samples, together with spectrum of white synthetic fluorite (collected with the same excitation wavelength) for comparison..

(Figure 3), which completely differed from the one reported by Dill and Weber (2010)[16] and of that of the white synthetic standard. The spectra were measured in full range covering 50 to 3400 cm^{-1}, and the only present bands were five broad ones in the region below 500 cm^{-1} with following approximate positions: 420, 335, 284, 222 and 142 cm^{-1}, and one broad low intensity one at ca. 910 cm^{-1}. As the only band ascribable to the fluorite's ideal structure is positioned at 322 cm^{-1}, the 335 cm^{-1} is formed by two overlapping bands. This is documented by Figure 4, which represents measurements of a fragment of a crystal from fluorite 14. This sample is formed by colourless fluorite covered by a few-millimetres-deep layer of violetish black colour, thus representing a transition from common fluorite to antozonite. Figure 4 shows the Raman spectrum of the colourless part adjacent to the violet layer and documents the increasing intensity of the above-mentioned bands in the Raman spectra with increasing violet colour saturation towards the surface of the sample. Interestingly, also the colourless fluorite spectrum exhibited the above-mentioned bands, but their intensity was much lower compared to the 322 cm^{-1} band. A spectrum of the colourless fluorite not adjacent to the layer showed only the band at 322 cm^{-1} and three unassigned bands at 484 cm^{-1} (strong), 1465 (weak) and 1527 cm^{-1} (weak).

The relative intensity of the 335 and 322 cm^{-1} bands has varied in all antozonite Raman spectra depending on the saturation of their colour, from lighter violet (discernible 322 cm^{-1} band) to deep violet or almost black colour of the grains (the 335 cm^{-1} band completely overlaps the 322 cm^{-1} one, or is even of higher intensity). The spectra varied among the grains of each sample depending on their colour saturation, but, generally, the more there was of structural damage indicated by X-ray diffraction, the more pronounced and frequent was the spectrum with stronger 335 cm^{-1} band.

Since Dill and Weber (2010)[16] present spectra excited by 795 nm laser, all antozonite samples and white fluorite synthetic standard were measured using 780 nm excitation in order to obtain comparable results. Unexpectedly, the spectra differed from the ones collected with 532 nm excitation. They contained similarly positioned bands below 500 cm^{-1}, but also other numerous broad bands (Figure 5). The antozonites' spectra (in the region above 500 cm^{-1}) slightly differed among each other, and also still differed from the spectra of Dill and Weber (2010).[16]

To assess the effect of the excitation laser wavelength on the measurements, five selected antozonites from different localities (3, 8, 13, 14 and 16) and the white fluorite standard were measured also by 445 and 633 nm lasers. The spectra excited at 633 nm were similar to the ones obtained by 532 nm laser; however, the spectra excited at 445 nm contained, again, numerous bands (Figure 5). The measurements using 1064 nm laser were completely hindered by fluorescence and no bands could be resolved.

All obtained spectra of antozonites, regardless of the excitation laser wavelength used, contained the bands in the region below 500 cm^{-1} described above (Figure 5). Their intensity and broadness varied, but their position remained the same. Poklonskaya and Khomich (2013)[23] published Raman spectra of artificially irradiated diamonds, and similarly to antozonites, the spectra contained also broad bands in the region below 500 cm^{-1}. The authors ascribe them to the local vibrations of complexes of radiation-induced point defects. It seems probable that the Raman bands of antozonites also relate to these radiation-induced defects.

The bands above 500 cm^{-1} that occurred only in the spectra measured by 780 nm laser and the ones obtained by 445 nm laser are of different nature. It is demonstrated in Figure 4, which depicts Raman spectra of the fragment of a crystal of fluorite 14 (with

Copyright © 2015 John Wiley & Sons, Ltd.

All problems according to Preflight profile
Convert to PDF/A-2u

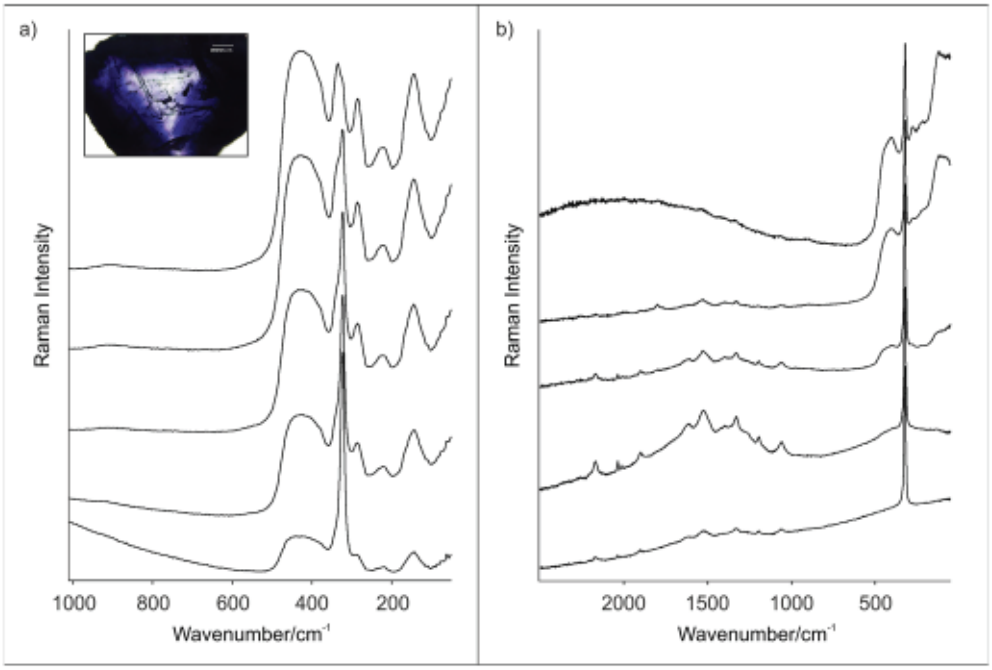


Figure 4. Raman spectra of fragment of a crystal from fluorite 14 (its photograph is in the inset) indicating the increase of the bands below 500 cm^{-1} with increasing violet colour saturation (colourless—spectrum at the bottom, very deep violet—spectrum at the top): a) 532 nm laser, b) 780 nm laser—the bands above 500 cm^{-1} most probably relate to the content of REE different at respective measurement positions. Photo: Z. Čermáková. This figure is available in colour online at wileyonlinelibrary.com/journal/jrs.

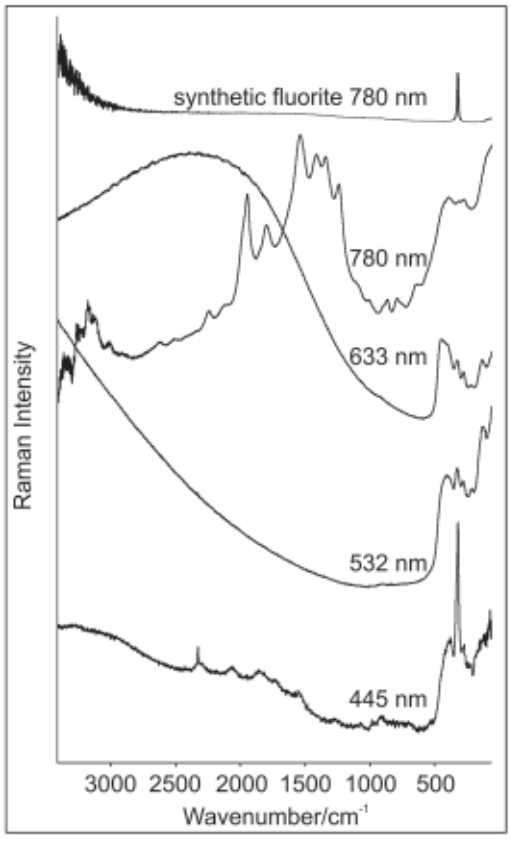


Figure 5. Comparison of Raman spectra of fluorite 16 obtained with different laser wavelengths; below 500 cm^{-1}, the spectra contain bands with similar positions, while above 500 cm^{-1} the spectra differ probably due to REE-related fluorescence bands. Raman spectrum of white synthetic fluorite (780 nm) is depicted at the top..

gradual coloration from colourless to deep violet) obtained with 780 nm laser. While the intensity of the bands below 500 cm^{-1} gradually increases, the intensity of the bands above 500 cm^{-1} fluctuates regardless of the coloration.

The most plausible explanation of the bands above 500 cm^{-1} is that they are fluorescence bands—they are quite broad, which is atypical for normal Raman bands, and they occur only during measurements with certain laser wavelengths. As Aminzadeh (1997)[24] notes, the presence of fluorescence bands is an effect known mainly in the measurements made by FT-Raman instruments equipped with 1064 nm laser, but Chen and Stimets (2014)[25] showed that the fluorescence bands may be excited also by a 785 nm laser. The presence of rare earth elements (REE) is known to cause fluorescence in several Ca-minerals,[24] and Chen and Stimets (2014)[25] showed it specifically on Dy^{3+}-doped fluorites with Nd^{3+}-related fluorescence. It is probable that similar fluorescence may occur also in natural fluorites, as they are known to easily incorporate various amounts of REE.[18,22,26] Chen and Stimets (2014)[25] describe that the transition energy produced by a 785 nm laser is close to particular 4f energy levels of trivalent rare-earth ions, and as the crystal field of the host fluorite split the 2J + 1 degenerate levels of the ionic multiplet by an amount of up to a few hundred cm^{-1}, several fluorescence bands may occur in the spectrum. The transition strengths of some of the bands are weak; therefore, not all of them will be observed. Raman spectrum of the Dy^{3+}-doped fluorite measured at room temperature showed five fluorescence bands in the 1000–2500 cm^{-1} region (1137, 1234, 1343, 1775 and 1877 cm^{-1}). The position of the reported bands is different from the ones observed in case of the studied antozonites, but they may be caused by different REE-related fluorescence. This is supported by slightly different spectra of antozonites which come from six different localities with different geological conditions, which suggests their different trace elemental composition. However, it is not well-studied which

Copyright © 2015 John Wiley & Sons, Ltd.

All problems according to Preflight profile
Convert to PDF/A-2u

elements cause which fluorescence bands, and depending on the elements' energy levels and the transition energy produced by the laser, only the presence of certain elemental impurities will be exhibited in the studied spectral region. Therefore, even different overall trace elemental composition may result in the same Raman/fluorescence spectrum. Still, Raman studies of antozonites may lead to characteristics related to their trace-elemental composition and, possibly, to pigment provenance analysis. However, this topic exceeds the scope of this paper and will be a subject of further research.

To check whether the spectra of antozonites in the region below 500 cm^{-1} are truly specific, three samples of fluorites of different colour (17, 18 and 19) were also measured using the 532 and 780 nm lasers. Figure S2 (Supporting Information) depicts their Raman spectra with a wide range of broad bands, but neither of them had the spectrum similar to antozonites (below 500 cm^{-1}). Interestingly, some of the spectra of the colourless grains present in antozonite samples are almost similar to the yellow/green as well as bluish fluorite's spectra; therefore, they should not be seen as specific for the respective colour type of fluorite, but rather representing the presence of certain REEs.

Micro-samples of the altarpiece

Scanning electron microscopy–energy dispersive spectroscopy (SEM-EDS)

Polished cross sections of the micro-samples were first analysed by SEM-EDS to determine the elemental composition of the paint layers. The deep violet angular grains were indeed found to be fluorite—composed of calcium and fluorine, and a small amount of yttrium. The analysis of other rare earth elements was ruled out by the detection limit of the method (around 0.5 wt. %).

Raman spectroscopy

As it can be seen in Figure 1, the micro-samples' cross sections are quite thin (70 and 140 μm), which indicates that the analysis by micro-X-ray diffraction would be hindered by the signal from the amorphous embedding resin. Furthermore, micro-X-ray diffraction, despite its versatile applicability on micro-samples, has its limitations compared to standardised transmission measurements; the precision of the analysis is not sufficient for reliable calculations of diffraction lines' FWHMs and of the unit cell parameters.

Therefore, the method of choice to confirm the presence of antozonite was Raman micro-spectroscopy. The analysis of natural antozonite samples showed that for the distinction of bands caused by radiation-induced damage, it is best to use the 532 nm laser, which does not excite the fluorescence bands. Figure 1 depicts the Raman spectra obtained on two micro-samples, which are completely similar to the spectra measured on natural antozonites with higher structural damage. The spectral manifestations of the micro-samples collected with 780 nm excitation were rather hindered by overall fluorescence.

It seems that the only other Raman spectroscopic study of fluorite pigment present in colour layer of an artwork has been performed by Banerjee *et al.* (2000),[15] who identified light violet fluorite in the polychrome colour layers of a sculpture originating in the end of the 15th century using 514.5 nm laser. They observed 321 cm^{-1} fluorite band and one unassigned band positioned at 840 cm^{-1}. Interestingly, no radiation-related bands below 500 cm^{-1} were detected, which suggests that the radiation-induced damage is observable by Raman spectroscopy only from a certain level. This should prompt a more thorough discussion about the definition of antozonite, and incorporate not only the specific colour and odour during grinding, but also specific Raman spectrum.

Conclusions

The X-ray diffraction study of antozonite confirmed that the structural disorder caused by natural irradiation may be expressed by broadening of its diffraction lines. The higher is their full-width half-maxima, the lower is the sample's lightness. On the other hand, the reported increase of antozonite's unit cell parameter (and the unit cell volume) is not so straightforward. The studied antozonite samples did not exhibit positive correlation of the parameter and the observed increase of the FWHMs. Still, the sample with the highest full-width half-maxima had also one of the highest values of the unit cell parameter.

The Raman spectroscopic study showed that antozonites have a specific spectrum—several broad bands below 500 cm^{-1} seem to be related with the radiation-induced damage and were observable in all four laser wavelengths successfully applied for the analyses. The bands above 500 cm^{-1} that were observed in case of 445 and 780 nm excitation are probably related to the presence of rare earth elements. Since the spectra excited at 532 nm contained only antozonite-specific bands, it was the laser wavelength of choice for the analysis of the micro-samples of works of art.

The definition of antozonite is rather vague, and it would be beneficial to enrich it by a specific Raman spectrum. Other studies showed that light violet fluorite grains in colour layers of artworks may have a normal fluorite spectrum. Therefore, the Raman spectroscopy can confirm the presence of intensely naturally irradiated fluorite—antozonite, and offers a possibility for provenance-related studies.

Acknowledgements

The authors would like to thank Petr Henke (Faculty of Science, Charles University in Prague) for performing the UV/VIS spectrophotometry. Silvie Švarcová and Vlasta Vašutová (ALMA laboratory, Institute of Inorganic Chemistry of the AS CR, v.v.i., and Academy of Fine Arts in Prague) are gratefully acknowledged for their versatile cooperation. Thanks belong also to Irena Matulková (Faculty of Science, Charles University in Prague) for her help during Raman micro-spectroscopic measurements. This study has been supported by Czech Science Foundation, project no. P103/12/2211, and by RVO 61388980.

References

[1] J. H. Bernard, J. Hyršl, *Minerals and their Localities*, Granit, Prague, **2006**.
[2] R. Vochten, E. Esmans, W. Vermeirsch, *Chem.Geol.* **1977**, *20*, 253–263.
[3] J. Schmedt auf der Günne, M. Mangstl, F. Kraus, *Angew. Chem. Int. Ed.* **2012**, *51*, 7847–7849
[4] M. Richter, O. Hahn, R. Fuchs, *Stud. Conserv.* **2001**, *46*, 1–13.
[5] X. Cheng, Y. Xia, Y. Ma, Y. Lei, *J. Raman Spectrosc.* **2007**, *38*, 1274–1279.
[6] F. Casadio, A. Bezúr, I. Fiedler, K. Muir, T. Trad, S. Maccagnola, *J. Raman Spectrosc.* **2012**, *43*, 1761–1771.
[7] M.-C. Corbeil, J.-P. Charland, E. A. Moffatt, *Stud. Conserv.* **2002**, *47*, 237–249.
[8] D. Oltrogge, *Research Project Painting Techniques of Impressionism and Postimpressionism*, online-edition, Museen, Köln, **2008**.
[9] Š. Chlumská, D. Pechová, R. Šefců, A. Třeštíková, in *Acta Artis Academica*, (Eds: D. Hradil, J. Hradilová), Academy of Fine Arts in Prague, Prague, **2010**, pp. 165–188.
[10] M. Spring, *Making Art in Tudor Britain, Abstracts from Academic Workshops*, National Gallery, London, **2007**, 8.

Copyright © 2015 John Wiley & Sons, Ltd.

All problems according to Preflight profile
Convert to PDF/A-2u

[11] J. Želinská, Proceedings of the Forum for conservationists-restorers, Brno, **2012**, 18–27. (in Slovak)
[12] A. Kosinova, *V&A Conservation Journal*, **2002**, *42*, 6–8.
[13] M. Spring, *National Gallery Technical Bulletin*, **2000**, *21*, 20–27.
[14] V. Šrein, B. Šreinová, J. Hradilová, 2010 in *Acta Artis Academica*, (Eds: D. Hradil, J. Hradilová), Academy of Fine Arts in Prague, Prague, **2010**, pp. 213–225.
[15] A. Banerjee, L. Nasdala, A. Wähning, *Arbeitsblätter für Restauratoren*, **2000**, *33*, 243–246. (in German)
[16] H. G. Dill, B. Weber, *Ore Geol. Rev.*, **2010**, *37*, 65–86.
[17] H. Shwastava, H. V. Lauer, L. L. Chase, W. E. Bron, *Phys. Lett.*, **1971**, *36A*, 333–334.
[18] V. Vlček, R. Skála, V. Goliáš, J. Drahokoupil, J. Čížek, L. Strnad, J. Ederová, *J. Geosci.*, **2012**, *57*, 45–52.
[19] R. Berman, *Am. Mineral.*, **1957**, *42*, 191–203.
[20] JCPDS PDF-2 database, International Centre for Diffraction Data, Newtown Square, PA, U.S.A. release 54, **2004**.
[21] B. Lestienne, *AFPAR Programme*, LCS CNRS, Talence, France, **1990**.
[22] H. Bill, G. Calas, *Phys. Chem. Minerals.*, **1978**, *3*, 117–131.
[23] O. N. Poklonskaya, A. A. Khomich, *J. Appl. Spectrosc.*, **2013**, *80*, 715–720.
[24] A. Aminzadeh, *Spectrochim. Acta, Part A*, **1997**, *53*, 693–697.
[25] H. Chen, R. W. Stimets, *Am. Mineral.*, **2014**, *99*, 332–342.
[26] H. G. Dill, B. T. Hansen, B. Weber, *Ore Geol. Rev.*, **2011**, *40*, 132–148.

Supporting information

Additional supporting information may be found in the online version of this article at the publisher's web site.

Copyright © 2015 John Wiley & Sons, Ltd.

All problems according to Preflight profile
Convert to PDF/A-2u

Spectrochimica Acta Part A: Molecular and Biomolecular Spectroscopy 140 (2015) 101–110

Contents lists available at ScienceDirect

Spectrochimica Acta Part A: Molecular and Biomolecular Spectroscopy

journal homepage: www.elsevier.com/locate/saa

Temperature-related degradation and colour changes of historic paintings containing vivianite

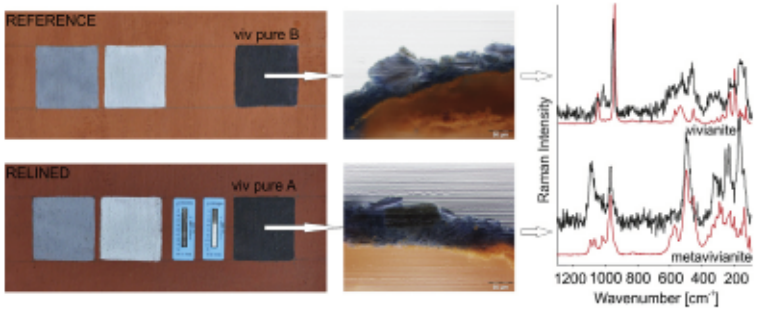
Čermáková Zdeňka [a,b,c,*], Švarcová Silvie [a], Hradilová Janka [b], Bezdička Petr [a,b], Lančok Adriana [a], Vašutová Vlasta [b], Blažek Jan [d], Hradil David [a,b]

[a] Institute of Inorganic Chemistry of the AS CR, v.v.i., ALMA Laboratory & Laboratory of Low Temperatures, Husinec-Řež 1001, 250 68 Řež, Czech Republic
[b] Academy of Fine Arts in Prague, ALMA Laboratory, U Akademie 4, 170 22 Prague 7, Czech Republic
[c] Institute of Geochemistry, Mineralogy and Mineral Resources, Faculty of Science of Charles University in Prague, Albertov 6, 128 43 Prague 2, Czech Republic
[d] Institute of Information Theory and Automation of the AS CR, v.v.i., Pod Vodárenskou věží 4, 182 08 Prague 8, Czech Republic

HIGHLIGHTS

- Temperature-related degradation of vivianite is presented.
- Already temperatures around 70 °C are harmful, 90 °C start vivianite's oxidation.
- At 80 °C, ground natural vivianite paint layer sample turns from blue to grey.
- The colour change corresponds with the one described in works of art.
- Conservation treatments using heat (like relining) should be performed with care.

GRAPHICAL ABSTRACT



ARTICLE INFO

Article history:
Received 26 June 2014
Received in revised form 24 November 2014
Accepted 17 December 2014
Available online 25 December 2014

Keywords:
Vivianite
Degradation
High-temperature X-ray diffraction
Mössbauer spectroscopy
Model experiments

ABSTRACT

Temperature-related degradation of pure synthetic as well as partly oxidised natural vivianite has been studied by high-temperature X-ray diffraction (HT-XRD) covering the whole extent of the temperature-related stability of its structure. While temperatures around 70 °C are already damaging to vivianite, exposition to 160 °C results in complete amorphisation of both the vivianite and its oxidation products. As indicated by Mössbauer spectroscopy, temperature-induced oxidation of vivianite starts at 90 °C. To study the occurring structural as well as accompanying colour changes in more detail, model vivianite paint layer samples with different historic binders were prepared and subjected to increased temperatures. Exposition to 80 °C caused pronounced colour changes of all the samples: ground natural blue vivianite became grey – a colour change which has been described in actual works of art. Regarding the binders, the oil seemed to facilitate the transfer of heat to vivianite's grains. To simulate conditions of conservation treatment under which the painting is exposed to increased temperatures, oil-on-canvas mock-ups with vivianite were prepared and relined in a traditional way using iron. The treatment affected preferentially larger grains of vivianite; the micro-samples documented their change to grey, and their Raman spectra showed the change from vivianite to metavivianite.

© 2014 Elsevier B.V. All rights reserved.

* Corresponding author at: Institute of Inorganic Chemistry of the AS CR, v.v.i., ALMA Laboratory & Laboratory of Low Temperatures, Husinec-Řež 1001, 250 68 Řež, Czech Republic. Tel.: +420 266 173 115.
E-mail address: cermakova@iic.cas.cz (Z. Čermáková).

http://dx.doi.org/10.1016/j.saa.2014.12.082
1386-1425/© 2014 Elsevier B.V. All rights reserved.

All problems according to Preflight profile
Convert to PDF/A-2u

Introduction

Vivianite is a phosphate mineral ($Fe_3(PO_4)_2{\cdot}8H_2O$) with monoclinic crystal structure. In nature, it is found either in the form of crystals or various types of aggregates, commonly the earthy ones [1]. The colour of the crystals is often very dark with strong pleochroism [2], earthy vivianite ranges from light greyish green to saturated blue, frequently being light blue.

Vivianite has been used as a pigment for several centuries (documented usage in Europe ranges from 1050 to 1780) in various types of artworks: from polychromy on wood and stone to wall paintings, as well as paintings executed on wooden panels and canvases. The resulting colour of the paint with vivianite was usually blue (commonly in mixture with lead white, sometimes also with other blue pigments like azurite, smalt or ultramarine), more rarely green (e.g., in complex mixtures of pigments including yellow lake and yellow earth) [3].

Vivianite is a rare pigment and, so far, has been identified in only about eighty artworks; the majority of them originate in Germany and Austria. However, in the 17th century, the predominant country of origin of works with identified vivianite is The Netherlands, where this pigment was used e.g. in the famous workshops of Rembrandt van Rijn, Aelbert Cuyp or Jan Vermeer. Other documented works come from the Czech Republic (recently, vivianite was identified as a constant part of Jean George de Hamilton's palette – in seven of his canvas paintings), United Kingdom, Switzerland, Norway, Sweden, Lithuania and Romania [3–7].

In some of the artworks, vivianite has degraded and changed its colour to grey or yellowish brown. A pronounced colour change is described e.g., by van Loon [8] on the 17th century paintings located in the Oranjezaal in the Royal Palace of Huis ten Bosch (The Hague, The Netherlands) or by Spring and Keith [9] in the oil-on-canvas painting "The Large Dort" by Aelbert Cuyp (c. 1650).

So far, the external causes of the degradative changes of vivianite in the paintings have not been studied. It is known that the colour stability of vivianite is endangered by its tendency to oxidative degradation.

The current knowledge about vivianite's mineralogical oxidation series is following: vivianite (monoclinic) – metavivianite (triclinic) – Fe^{3+}-rich "metavivianite" (triclinic with different cell dimensions) – santabarbaraite (amorphous) [10]. This degradation is known to be accompanied by colour change from white to blue to, finally, yellowish brown; while white vivianite in pristine state in contact with air almost immediately starts to change to blue, it seems that the change to yellowish brown is a much longer process. The colour change can also be triggered by external conditions, e.g. increased temperature.

The temperature-related oxidation of vivianite can be profitably monitored by Mössbauer spectroscopy. One of the studies regarding vivianite as a pigment [11] describes the structural, colour and oxidation changes at the temperatures of 200, 300 and 800 °C. A more profound Mössbauer study of vivianite's oxidation by increased temperatures was performed by Hanzel et al. [12]. However, it is not clearly stated at which temperature vivianite starts to oxidise by temperature influence, a graph suggests value around 105 °C.

The structural changes of vivianite under increased temperatures were monitored e.g., by Tien and Waugh [13] in an X-ray diffraction (XRD) study of thermally treated vivianite. A high-temperature XRD (HT-XRD) study was undertaken by Poffet [14] in her thesis – she described the loss of intensity of the lines of vivianite diffraction pattern during storage at certain temperatures.

Based on the above-stated published data, it seems that temperatures around 70 °C may already be harmful for vivianite. Historic paintings containing this pigment can be exposed to such conditions, especially when inappropriately positioned on direct sunlight, or during relining – a common conservation treatment of canvas paintings, which consists of ironing a new canvas to the painting's degraded one from the back using, e.g., a mixture of wax and resin [15,16]. The wax-resin method has been widely used up to 1970s; since this period of time, the most wide-spread method of relining employed modern materials like BEVA 371 (a complex mixture of copolymers, synthetic resin and wax) or acrylic adhesives [17,18]. Nowadays, the traditional wax–resin or glue–paste relining whose side-effects may include canvas shrinkage (glue–paste) or darkening of the paintings (wax–resin) is applied more scarcely and in cases when the paintings have been previously relined by this method [18]. Unlike the hand irons, modern relining tables enable temperature control; however, earlier conservation treatments could exceed recommended temperatures. Furthermore, 70 °C is generally considered to be a safe temperature for the procedure [Igor Fogaš, restorer, pers. comm.].

To clarify the temperature-related behaviour of vivianite especially during the initial state of the changes, a high-temperature X-ray diffraction study was performed; the full range of the vivianite's structure temperature-stability is published for the first time. For this purpose, a synthetic vivianite was prepared by an adapted procedure. Subsequently, the damaging effect on vivianite of relatively low temperatures has been monitored by Mössbauer spectroscopy. Afterwards, experiments with vivianite model paint layer samples were carried out in order to study the dependence of changes of colour on structural changes that take place in the temperature interval up to 200 °C. To test and simulate the actual conditions that may cause vivianite's temperature degradation in works of art, oil-on-canvas mock-ups were prepared, and subsequently, relined in a traditional way. The changes were monitored by analysis of image histograms and micro-Raman spectroscopy.

Samples

Synthesis and reference vivianites

Synthetic vivianite for the experiments was prepared by a precipitation reaction. Since the reported procedures [19] led to multicomponent products (e.g., the recommended method of Evans resulted in a mixture of vivianite and spheniscidite, $(Fe_2(NH_4)(OH)(PO_4)_2{\cdot}2H_2O)$, the method has been adapted.

The precipitation reaction was carried out according to a general principle:

$$3Fe^{2+} + 3HPO_4^{2-} \rightarrow Fe_3(PO_4)_2 + 3H^+ + PO_4^{3-}$$

An appropriate amount of $FeSO_4{\cdot}7H_2O$ p.a. (Lachema Neratovice) was dissolved in 5 wt.% solution of H_3PO_4 (Merck) with a final molar concentration of Fe being 0.28 mol/l. A stoichiometric quantity of $Na_2HPO_4{\cdot}12H_2O$ p.a. (Lachema Neratovice) was dissolved in distilled water and added drop by drop by peristaltic pump (ca 3 ml/min) into the solution of $FeSO_4$ and H_3PO_4 under continuous magnetic stirring. The resulting mixture was then stirred until the following day under laboratory conditions. Subsequently, the bluish grey precipitate was left to settle for 24 h. The resulting product was separated by centrifugation and washed by distilled water. The centrifugation showed that the product is formed by whitish and blue precipitates with different density, therefore, they were separated by the centrifugation process. The final blue precipitate was left to dry on air under laboratory conditions and checked by X-ray diffraction as well as Mössbauer spectroscopy, which showed that it is phase pure vivianite with 15% of Fe^{3+}. The whitish by-product was found to be amorphous phosphate with 94% of Fe^{3+}.

All problems according to Preflight profile
Convert to PDF/A-2u

To verify that there is no significant difference of behaviour between the powdery synthetic vivianite and natural vivianite, vivianite crystals from Bolivia (Tomokoni Mine, Colavi District, Potosí Department) (Fig. 1) (bought from Minerály Jiří Špalek, Czech Republic) were also used for the experiments. They were first cleaned of the iron-rich matrix and then powdered in an agate mortar. The phase composition of the natural powdered vivianite was determined by X-ray diffraction.

For the HT-XRD study, a Kremer Pigmente vivianite (which was reportedly prepared by grinding crystals originating from Colombia [Georg Kremer, pers. comm.]) was used as well, since it contained a higher amount of oxidative degradation products (metavivianites) than the above-stated vivianite crystals from Bolivia.

Model paint layer samples

The synthetic vivianite was mixed with four main historic binders, i.e., oil (linseed stand oil Kremer Pigmente), egg yolk (egg from bio-farming, egg yolk separated from egg white and pierced through gauze to ensure that no egg membrane enters the paint), glue (5% solution of rabbit glue Graz in distilled water, gently heated to 60 °C) and water (distilled). The powdered natural sample was mixed only with distilled water.

Vivianite with each separate binder was ground in an agate mortar so the pigment would sufficiently bind with the binder and thus create a resulting paint of good quality. The binders were added in such amount that a paint of satisfactory density was prepared (consulted with restorer). Two samples of each type of paint (one for the experiment and one as a reference) were created and applied on glass slides. After that, the samples were kept in dark. Vivianite with oil was prepared as the first type of model samples and was left to dry for 7 months. Other mixtures were dry in less than a week.

Oil-on-canvas mock-ups

In order to test the actual effect of relining on canvas paintings, two small canvases were created; the employed painting technique was inspired by the one used e.g., by Jean George de Hamilton [4], a painter of the end of the 16th and the beginning of the 17th century active (among others) in the region of today's Czech Republic.



Fig. 1. Natural crystals of vivianite from Bolivia, which were, subsequently, cleaned of the iron-rich matrix and ground for the creation of model paint layer samples as well as oil-on-canvas mock-ups. The length of the crystal in the front = 5 cm.

First, a ground was prepared using iron-rich earths (Red Bole, Kremer Pigmente + glue solution + linseed stand oil Kremer Pigmente + beeswax). Then, on both canvases, three squares of oil paint were applied, freshly ground-up natural vivianite crystals (described above) with:

(1) oil (linseed stand oil UMTON) and a few drops of turpentine (balsam turpentine Kremer Pigmente),
(2) oil, a few drops of turpentine and lead white (Kremer Pigmente, Kremser White 46,000) (vivianite:Pb white approx. 40:60),
(3) oil, a few drops of turpentine and lead white (vivianite:Pb white approx. 10:90).

After relining, micro-samples were obtained from both the relined and the reference oil-on-canvas mock-ups. They were embedded in polyester resin Neukadur PE 45, ground and polished in cross-section.

The designation of all model samples together with their composition is summarised in Table 1.

Methods

Optical microscopy, photography

Optical studies of samples on glass heated to different temperatures were undertaken using Olympus BX 40 microscope equipped with DP 10 camera. The micro-samples of oil-on-canvas mock-ups were observed by Axio Imager A.2 light microscope (Zeiss) in reflected visible and UV light (365 and 470 nm). The cross-sections were photographed using digital microscope camera Olympus DP 75.

The macro-photographs of the model paint layer samples and oil-on-canvas mock-ups were taken together with a standard grey plate, which was later on used to refine the colours in Adobe Photoshop Lightroom, therefore, their colouring is accurate and comparable to each other.

Fourier-transform infrared spectroscopy (FTIR) and Raman spectroscopy

The FTIR measurements in transmission mode were performed using Thermo Scientific Nicolet NEXUS 670 FT-IR. The samples were analysed in KBr pellets. The amount of the sample for the analysis was ranging from 1.4 to 1.5 mg/300 mg KBr. The acquisition of the spectra comprised 64 scans in the range of 4000–400 cm^{-1}, resolution being 4 cm^{-1}.

Micro-Raman spectra were obtained on a Thermo Scientific DXR Raman Microscope with Peltier-cooled CCD detector interfaced to an Olympus microscope (50× objective lens) in the 50–3400 cm^{-1} spectral region with 4 cm^{-1} resolution and 32 scans. The spectrometer was calibrated by software-controlled calibration procedure using multiple neon emission lines (wavelength calibration), multiple polystyrene Raman bands (laser wavenumber calibration) and standardised white light sources (intensity calibration). The spectra were collected using diode-pumped solid state laser (532 nm) with the 0.1 to 0.2 mW laser power.

X-ray diffraction (XRD)

Diffraction patterns were collected on PANalytical X'Pert PRO diffractometer equipped with conventional X-ray tube (Co_{K_α}

All problems according to Preflight profile
Convert to PDF/A-2u

Table 1
Summary of the analysed samples.

Sample designation	Composition
viv-cryst-A	Ground natural vivianite + distilled water
290-w-A	Synthetic vivianite + distilled water
290-g-A	Synthetic vivianite + rabbit glue in distilled water
290-ey-A	Synthetic vivianite + egg yolk
282-G	Synthetic vivianite + linseed stand oil
viv pure A	Ground natural vivianite + oil + few drops of turpentine (after relining)
viv pure B	Ground natural vivianite + oil + few drops of turpentine (reference sample)
viv-Pb white (40:60) A	Ground natural vivianite + oil + few drops of turpentine + lead white (vivianite: lead white = 40:60) (after relining)
viv-Pb white (40:60) B	Ground natural vivianite + oil + few drops of turpentine + lead white (vivianite: lead white = 40:60) (reference sample)
viv-Pb white (10:90) A	Ground natural vivianite + oil + few drops of turpentine + lead white (vivianite: lead white = 10:90) (after relining)
viv-Pb white (10:90) B	Ground natural vivianite + oil + few drops of turpentine + lead white (vivianite: lead white = 10:90) (reference sample)

radiation, 40 kV, 30 mA, line focus) and a multichannel detector X'Celerator with an anti-scatter shield. X-ray patterns were measured in the range of 6–110° 2Theta with the step of 0.0167° and 120 s counting per step (total time of the scan: approx. 1.75 h), using conventional Bragg–Brentano geometry. XRD patterns were not pre-treated before interpretation as no background correction was needed. Qualitative analysis was performed using HighScore-Plus software package (PANalytical, The Netherlands, version 3.0.5) and JCPDS PDF-2 database (2004) [20].

Mössbauer spectroscopy

Mössbauer spectroscopy was used to determine the ratio of Fe^{2+} and Fe^{3+} in the synthesised vivianite and the ground vivianite crystals from Bolivia. The Mössbauer spectra measurement was carried out in transmission mode with ^{57}Co diffused into a Rh matrix as a source moving with constant acceleration at room temperature. The spectrometer (Wissel) was calibrated using a standard α-Fe foil, and the isomer shift was expressed with respect to this standard at 293 K. The fitting of the spectra was performed in CONFIT program [21]. This program utilizes a convolution algorithm in the fitting of the overlapped Mössbauer spectra. The program also integrates the fitting of the ratio of Fe^{2+} and Fe^{3+} atoms. It is able to work with 1024 experimental points per spectrum; the number of fitted parameters must not exceed 105 and the number of spectrum components must be less than or equal to 99.

To monitor the oxidation changes with increasing temperature, vivianite sample (ground crystals from Bolivia) was heated in separate steps to 60, 80, 90, 100, 110, 120 and 130 °C. Each heating step took 30 min; after the sample cooled down to room temperature, Mössbauer analysis has been performed.

UV–VIS spectrophotometry and analysis of image histograms

The model paint layer samples were measured by UV–VIS spectrophotometer Lambda 35 from Perkin Elmer Instruments using an integrating sphere. The samples of synthetic vivianite with oil (whose layer was very thin) were, during measurement, underlaid by a black pad to ensure that no incoming radiation pass through the sample and the glass. The obtained reflectance results were transformed into CIE L^*a^*b 1964 space using the Color program.

For the evaluation of the colour change of oil-on-canvas mock-up after relining, which is too large to fit into the above-stated UV–VIS spectrophotometer, photographs of the vivianite paints were obtained using Canon D500 Rebel camera under controlled light (D65 light source). Position of the oil-on-canvas mock-ups, camera and light source were fixed and the camera parameters (shutter speed, aperture, objective, focus, white balance) were kept the same. These constant conditions ensured that the RGB coordinates of the photographs' pixels were comparable. The size of the taken photos was 417 × 433 for the reference mock-up and 427 × 446 for the relined one. This number of pixels resulted in more than 180,000 point measurements of RGB coordinates.

High temperature X-ray diffraction (HT-XRD) experiment (in situ)

High temperature diffraction patterns were collected using the same diffractometer and setting as for the normal room temperature measurements (see above) together with high temperature chamber (HTK 16, Anton Paar, Graz, Austria). X-ray patterns were measured at 25 °C and between 40 and 200 °C with a step of 10 °C in the range of 10–50° 2Theta (step of 0.0334° and 100 s counting per step yielding a scan of ca 16 min) using conventional Bragg–Brentano geometry. The measurements were performed while the sample was heated to the designated temperature, i.e., in situ.

Temperature experiments (ex situ)

The model paint layer samples (both the ones to be heated and the reference ones) were, before the heating experiments started, measured by UV–VIS spectrophotometry, FTIR spectrometry, XRD and analysed by optical microscopy. Then, one set of the model paint layer samples was inserted into the oven and heated in separate steps to 60, 80, 100, 120, 160 and 200 °C. After every heating step, the samples were measured by UV–VIS spectrophotometry and photographed. After every second step (80, 120, 200 °C), all the following analyses were performed on all the heated samples: UV–VIS, FTIR, XRD and optical microscopy. The measurements were performed after the samples were exposed to heating, i.e., ex situ.

For the heating, a Memmert oven was used enabling a very precise programming of the heating process. The samples were inserted into the oven and the desired temperature was input. The heating until the desired temperature was set to full power; after the input temperature was achieved, it was held for 30 min. Then, the fan was programmed to 100% while the heating was turned off and the cooling took place during 10 min. After that, the samples were removed from the oven and let cool down to room temperature.

Conservation technique – relining

For the execution of the traditional relining, bleached beeswax and damar resin (both from art materials supplier Zlatá Lod', Prague, Czech Republic) were used. 50 ml of damar resin was mixed with 100 ml of beeswax and 30 ml of turpentine (Kremer Pigmente fir turpentin) and heated. For the monitoring of temperature to which the vivianite-containing paint is exposed during the procedure, two types of irreversible temperature indicators (Testoterm, Testo AG, Lenzkirch) were employed, one type covering the temperature range from 37 to 65 °C, the other from 71 to 110 °C, both with steps of 3–6 °C. These were applied before the relining

All problems according to Preflight profile
Convert to PDF/A-2u

to the painted side of the canvas. During the relining, the temperature was also monitored by an infrared thermometer Voltcraft IR-364 (optics: 30:1).

The relining was performed in a traditional way using iron [15,16].

Results and discussion

High-temperature X-ray diffraction

The first technique applied on synthetic vivianite in order to study its temperature-related behaviour was high temperature-X-ray diffraction (HT-XRD). Fig. 2 shows that already at 60 °C, the most intense diffraction line of vivianite subtly decreases. A more pronounced decrease can be clearly seen at 70 °C; this process gradually continues up to 160 °C, when vivianite loses its structure and becomes completely amorphous. The resulting product has a brownish orange colour, but it is not, as one might expect, santabarbaraite, a naturally occurring end-member of the vivianite degradation series, but a different amorphous iron phosphate. It is documented by its FTIR spectrum depicted in Fig. 3 (compared to data stated in [10] for santabarbaraite). The main difference lies in the shift of the main phosphate band from 1021 to 1061 cm^{-1}, and in distinctly lower intensity of the bands related to the presence of water and hydroxyl groups caused by the applied high temperature treatment.

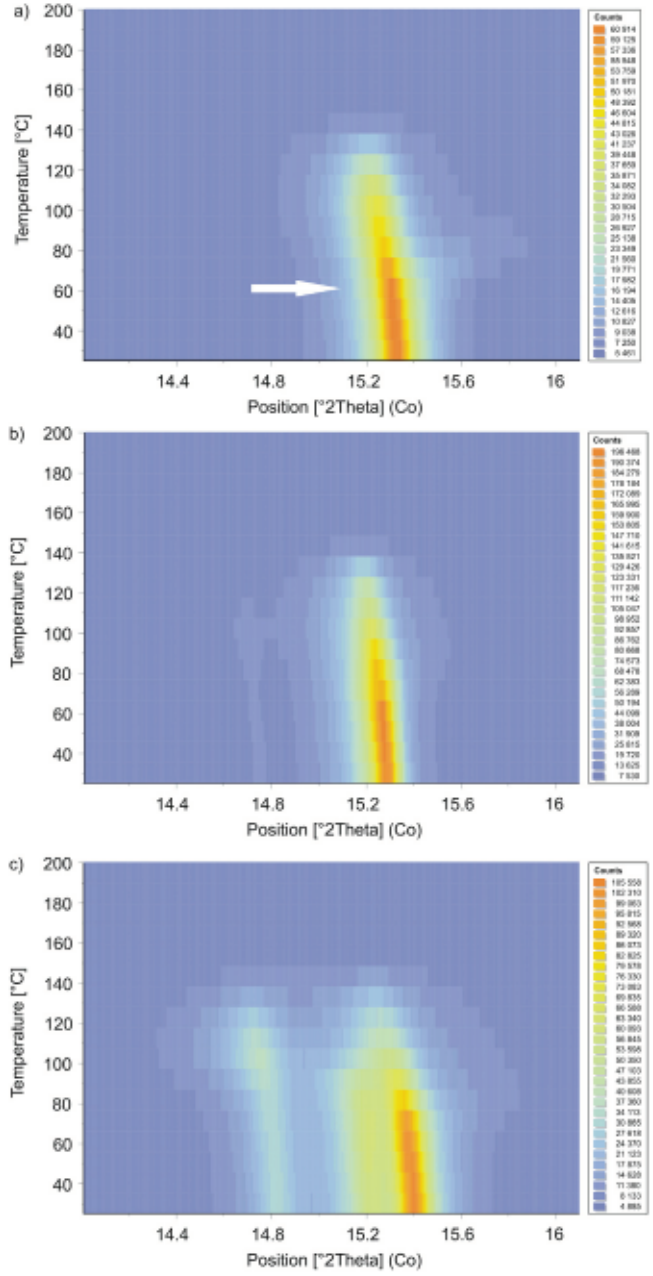


Fig. 2. HT-XRD patterns of (a) synthetic vivianite, (b) ground natural vivianite crystals used for the model samples, (c) Kremer Pigmente vivianite (with higher amount of oxidative degradation products). The "drift" of the diffraction lines to the left with increasing temperature is caused by the temperature-related expansivity of the unit cell of the present minerals. The white arrow indicates the first subtle decrease of the vivianite's diffraction line at 60 °C. Position of the diffraction lines: metavivianite = 14.8° 2Theta, Fe^{3+}-rich "metavivianite" = 15.2° 2Theta, vivianite = 15.35° 2Theta.

The HT-XRD was performed also on vivianite pigment from Kremer Pigmente, which (apart from vivianite) contained also metavivianite and the Fe^{3+}-rich "metavivianite", the vivianite's two oxidative degradation products. As it can be clearly seen in Fig. 2, the amount of metavivianite (diffraction line on 14.8° 2Theta) slightly increases at 90 °C up to 110 °C; at 120 °C, it starts to decompose and, similarly to vivianite, becomes completely amorphous at 160 °C. The amount of Fe^{3+}-rich "metavivianite" (diffraction line on 15.2° 2Theta) seems to remain stable up to 100 °C, when it starts to decompose and, again, becomes amorphous at 160 °C. Fig. 2 depicts also the HT-XRD pattern of the ground natural crystals from Bolivia, which were used for the creation of model samples. They are only partly oxidised and represent an intermediate stage between pure synthetic vivianite and vivianite pigment from Kremer Pigmente.

This is the first published X-ray study of the in situ temperature-related behaviour of pure synthetic vivianite covering the whole extent of the stability of vivianite's structure, as well as of the vivianite with its oxidative degradation products. A temperature-related degradation study (ex situ) of synthetic vivianite has been performed by Piña et al. [11], but the heating steps were quite high: 200, 300 and 800 °C. At 200 °C, vivianite has already lost its crystal structure and the iron was completely oxidised to its trivalent state.

In the study of Tien and Waugh [13], who preformed ex situ X-ray diffraction temperature experiments on natural sample of earthy vivianite (it seems that the sample was heated in several steps to 175, 200, 250, 275, 305 °C and more), the structure of vivianite has been maintained up to 300 °C. They do not mention for how long they heated their studied sample, which may be the

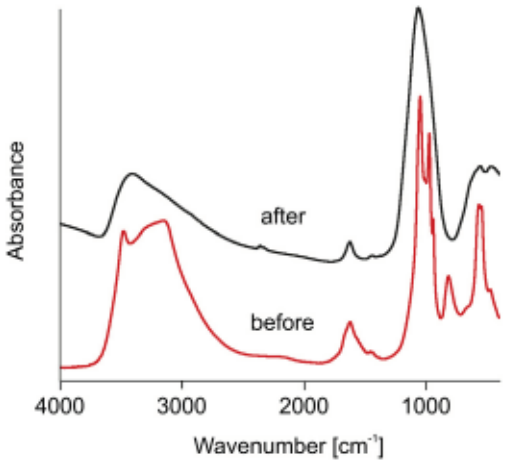


Fig. 3. The FTIR spectra of synthetic vivianite before and after HT-XRD analysis. After the HT-XRD measurements which exposed the sample to temperatures up to 200 °C, vivianite changed to amorphous hydrated iron phosphate.

All problems according to Preflight profile
Convert to PDF/A-2u

reason of the discrepancy between their results and this study. As Poffet [14] shows, temperature degradation of vivianite is time-dependent – the longer the vivianite is exposed to a certain temperature, the more it is degraded. Her analyses indicate that at 85 °C, the amount of crystalline vivianite (from sewage sludge) decreases approx. two times after one hour. At 75 °C, the results show fluctuation and at 65 °C vivianite seems to be stable. The results partly contrast with this study which shows a clear decrease of the intensity of X-ray diffraction lines of vivianite already at 70 °C.

The individual HT-XRD measurements performed in this study took about 16.5 min each. However, the degradation was monitored on the diffraction line of the highest intensity, which is positioned at 15.35° 2Theta (Co radiation); therefore, this line has been recorded already after approx. 2.2 min of each heating step, and the results show that this relatively short time is sufficient to cause damage.

It is interesting to note that a process in some of the syntheses recommends gentle heating of the resulting product with vivianite above 70 °C in order to get rid of a synthesis by-product or to digest it [11,19,22]. According to the results of this HT-XRD study, it would already have a harmful effect on the structure of the synthesised vivianite.

Mössbauer spectroscopy

To study in more detail the harmful oxidative effect of even lower temperatures on vivianite, the ground natural crystals of vivianite used for the model samples were first measured at room temperature, then heated to 60 °C for 30 min, measured again, and this process was repeated for 80, 90, 100, 110, 120 and 130 °C. The heating steps were chosen based on the results of HT-XRD. The amount of Fe^{3+} at room temperature was 35%; it remained the same up to 80 °C. The first signs of oxidation took place after the heating to 90 °C (again for 30 min), which contrasts with the data stated by Hanzel et al. [23], whose graph suggests that the oxidation starts from around 105 °C. Fig. 4 shows the evolution of Mössbauer spectra with increasing temperature, and Table 2 summarises the amounts of Fe^{2+} and Fe^{3+} after each heating step. The heating was performed on air in order to enable the diffusion of oxygen into the vivianite lattice from the surrounding atmosphere. Hanzel et al. [12] describe that the oxidation is caused not only by the oxygen diffusion, but also by autooxidation by crystal water (proven by experiments made in vacuum). The results of Mössbauer spectroscopy correspond with the results of HT-XRD – the observed increase of the amount of metavivianite, the first oxidative degradation product of vivianite, during the analysis of this sample by HT-XRD took place at 90 °C. However, distinct changes could be seen on the HT-XRD patterns already at 70 °C, therefore, following experiments have been performed.

Temperature experiments

To study the temperature-related behaviour (i.e., colour and structural changes) of vivianite in more detail, and not only in its pure synthetic or natural form, but also in the systems comparable to historic paints, model paint layers of synthetic vivianite with four different historic binders (skin glue, egg yolk, linseed oil, water) and of natural ground vivianite crystal with water were heated in an oven in several steps. The heating procedure is comparable with the one used for the Mössbauer spectroscopy measurements. The heating steps were following: 60, 80, 100, 120, 160 and 200 °C. Fig. 5 shows a composite photograph of reference samples and the heated samples. The occurring colour changes were accurately measured by UV–VIS spectrophotometry; the results converted into CIE L^*a^*b colour space are depicted in Fig. 6.

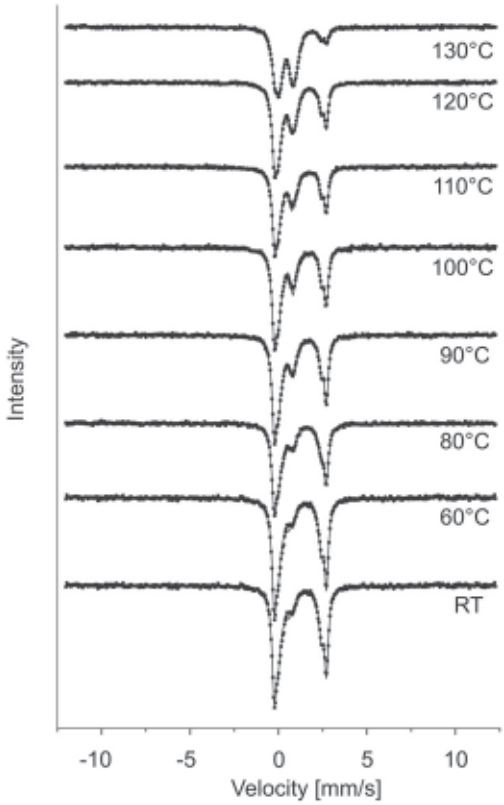


Fig. 4. Mössbauer spectra of ground natural vivianite crystals used for the model samples after exposition to a series of heating steps.

Table 2
Results of Mössbauer spectroscopy after each heating step.

Heating step	Fe^{2+} (%)	Fe^{3+} (%)
Room temperature	65	35
60 °C	65	35
80 °C	64	36
90 °C	55	45
100 °C	54	46
110 °C	48	52
120 °C	41	59
130 °C	20	80

From the art point of view, the most important aspect of the degradation is the colour change. After heating to 60 °C, the occurring colour changes on all the model paint layer samples were minimal and almost imperceptible to the human eye. However, at 80 °C, all the samples started to change. The process of colour change across the whole tested temperature range was comparable in case of natural ground vivianite crystal with water (viv-cryst-A), synthetic vivianite with water (290-w-A) and skin glue (290-g-A). A distinctly different course of the colour change took place in case of synthetic vivianite with egg yolk (290-ey-A) and oil (282-G).

After 80 °C, the most striking difference (among the paint layer samples with water and glue) was observed in case of natural vivianite (viv-cryst-A) – its bluish component decreased significantly, the greenish slightly increased and it became lighter. The position in the colour space got closer to the centre and the overall colour perception of the sample changed to grey. Similar colour trends occurred in case of synthetic vivianite with water and glue (290-w-A and 290-g-A) (Fig. 6), but they were not so pronounced. This type of colour change under relatively low temperatures is an important finding, since the colour degradation described in some of the historic paintings consisted of the vivianite's change from

All problems according to Preflight profile
Convert to PDF/A-2u

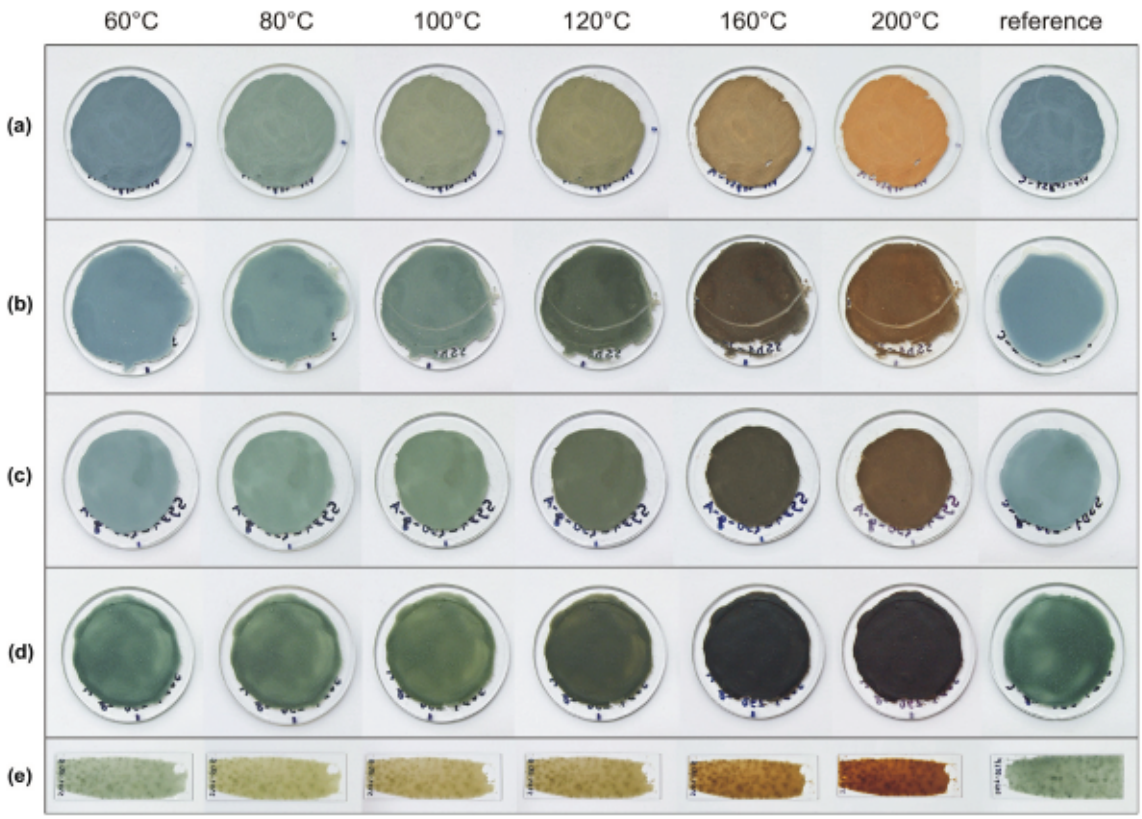


Fig. 5. Composite photograph of model paint layer samples after each heating step together with reference samples: (a) ground natural crystals + water (viv-cryst-A), (b) synthetic vivianite + water (290-w-A), (c) synthetic vivianite + glue (290-g-A), (d) synthetic vivianite + egg yolk (290-ey-A) and (e) synthetic vivianite + oil (282-G).

blue to grey or greenish grey [8,24]. With increasing temperatures of the experiment, yellow and red components of the model paint layers started to grew stronger with most pronounced values in case of natural vivianite viv-cryst-A, and after final heating to 200 °C, 290-w-A and 290-g-A ended as orangey brown, while viv-cryst-A as bright orange.

To monitor not only the colour changes, but also the accompanying structural ones, the samples were checked by XRD and FTIR after 80, 120 and 200 °C heating steps.

The XRD, as expected after performing HT-XRD, showed gradual amorphisation of the samples. In case of natural vivianite (viv-cryst-A), XRD determined that it contains, apart from vivianite as a main component, also metavivianite and a small amount of Fe^{3+}-rich "metavivianite", the two triclinic phases of vivianite's oxidation series.

The FTIR spectra also documented the process of amorphisation – the bands of the samples 290-w-A and 290-g-A were gradually becoming wider. The FTIR spectrum of viv-cryst-A (before the heating) contained more bands due to the presence of metavivianites. One of them was a band at 1010 cm^{-1} in the region of phosphate ions, which is not, so far, ascribed to any of the present phases. It was suggested [4] that it belongs to a not well-studied Fe^{3+}-rich "metavivianite". However, in the present experiments, the bands (including the one at 1010 cm^{-1}) almost disappear after exposition to 80 °C, and only those of vivianite remain (Fig. 7). It contrasts with the results of XRD, where no structural change could be seen (except of the overall decrease of the diffraction lines' intensity). Another band that disappeared after exposition to 80 °C was positioned at 770 cm^{-1}, and it has been ascribed by Chukanov et al. [10] to the vibrations of FeOH group (and the presence of metavivianite). It is possible that this 1010 cm^{-1} band may also correspond to the FeOH vibrations. This may be supported also by the FTIR spectrum of synthetic vivianite which was kept in laboratory conditions for one year, in which the band at 1010 cm^{-1} started to occur. It seems to be the first sign of degradation which corresponds with the deepening of vivianite's blue colour. Since the oxidation of iron has to be accompanied by the transition of water molecules to hydroxyl groups in order to maintain the electroneutrality of the molecule, it seems probable that this band is related to the presence of hydroxyl groups. Together with the above-stated results of Mössbauer spectroscopy, which indicate that the oxidation starts only above 90 °C, the FTIR results suggests that the changes occurring up to 90 °C are triggered by a different mechanism than oxidation, most probably by the effect caused by increased temperatures on hydroxyl molecules present in vivianite.

Up to 100 °C, a similar trend of colour change as the above-described samples with glue and water was observed in case of the sample with synthetic vivianite and egg yolk (290-ey-A), even though it started as more greenish due to the effect of the intense yellow colour of the binder. However, Figs. 5 and 6 show that after exposition to 120 °C, the sample starts to move closer towards the centre of the *a* and *b* coordinates of the colour space, while the lightness of the sample gradually decreases, and after 200 °C, the sample becomes black in the overall colour perception. The XRD measurements show gradual amorphisation of vivianite. In the sample exposed to the highest temperature (200 °C), vivianite is no more discernible, however, a new, not very well-crystalline phase has been created. Interestingly, based on the reference diffraction patterns, the new phase is tetragonal magnesium sulphate hydroxide. The black colour of the sample is due to the combustion products of the employed binder.

A very different course of the colour change has been observed in case of synthetic vivianite with oil (282-G), which exhibited the

All problems according to Preflight profile
Convert to PDF/A-2u

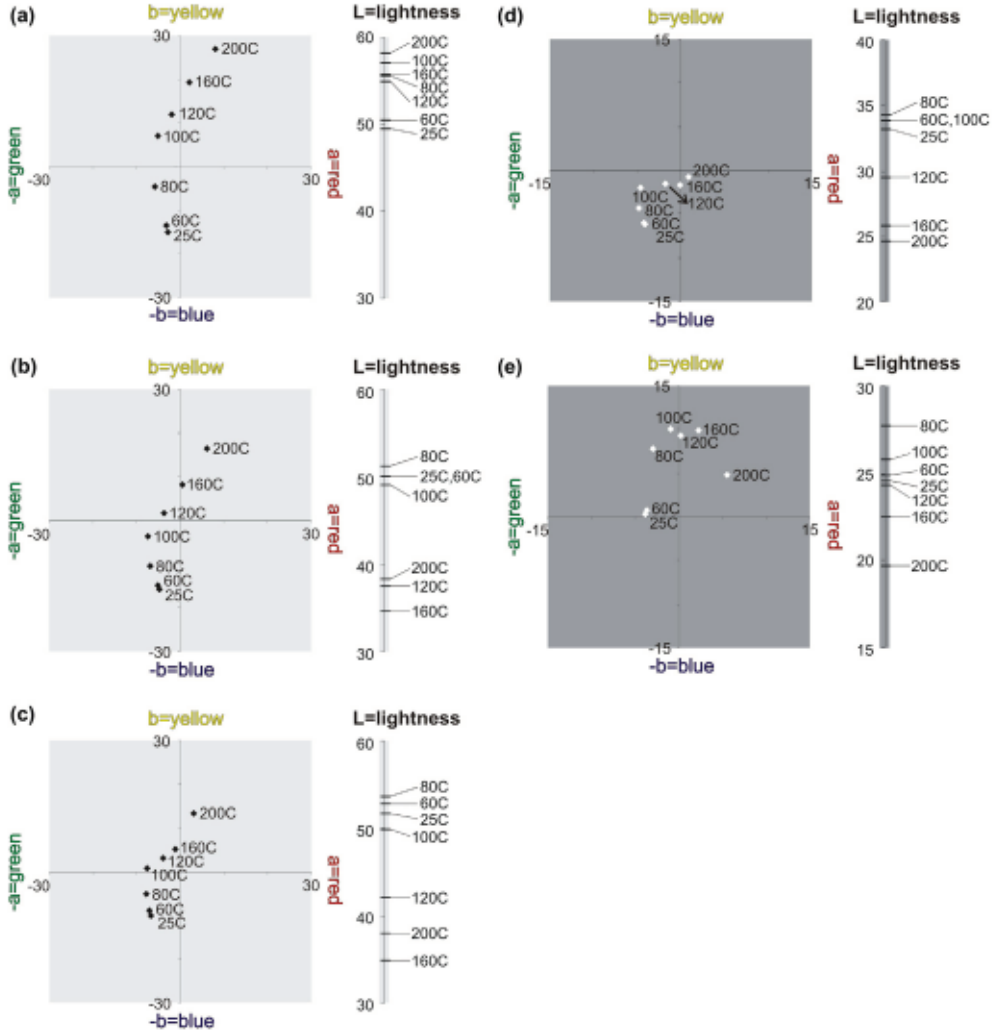


Fig. 6. The colour changes of model paint layer samples after each heating step displayed in CIE *L*a*b* colour space: (a) ground natural crystals + water (viv-cryst-A), (b) synthetic vivianite + water (290-w-A), (c) synthetic vivianite + glue (290-g-A), (d) synthetic vivianite + egg yolk (290-ey-A) and (e) synthetic vivianite + oil (282-G). Please note the change of the axes' range between (a–c) and (d–e).

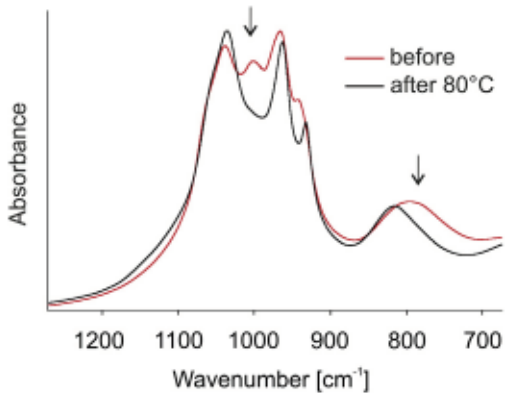


Fig. 7. The FTIR spectra of the viv-cryst-A before the temperature experiment and after exposition to 80 °C. The bands positioned at 770 and 1010 cm^{-1} (marked by arrows) are related most probably to the vibrations of FeOH group.

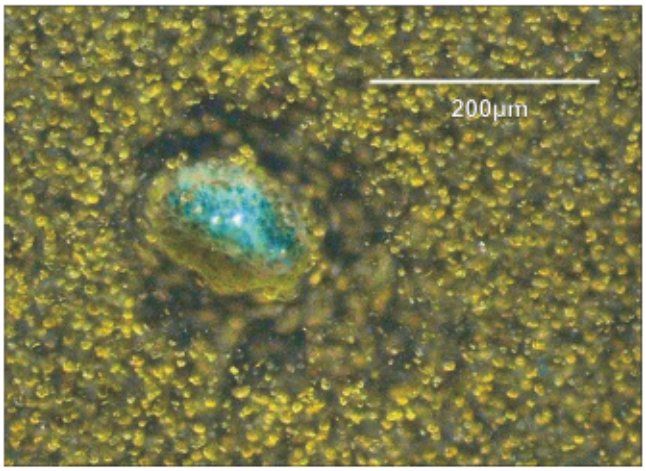


Fig. 8. Micro-photograph of the sample 282-G after exposition to 100 °C. The grains of vivianite dispersed in oil are completely degraded, while the "lump" still contains bluish grains. The photograph is a composite of two due to the depth of field.

most pronounced change of all the samples after exposition to 80 °C. This is partly caused by the thinness of the layer – the dominant effect on colour has the temperature-related change of the oil binder. Red and yellow components of the colour increased with the temperature and at the end of the temperature experiments, the sample became deep orange. Fig. 8 depicts the influence of the binder and the thinness of the paint layer – after exposition to 100 °C, the grains of vivianite which are completely

All problems according to Preflight profile
Convert to PDF/A-2u

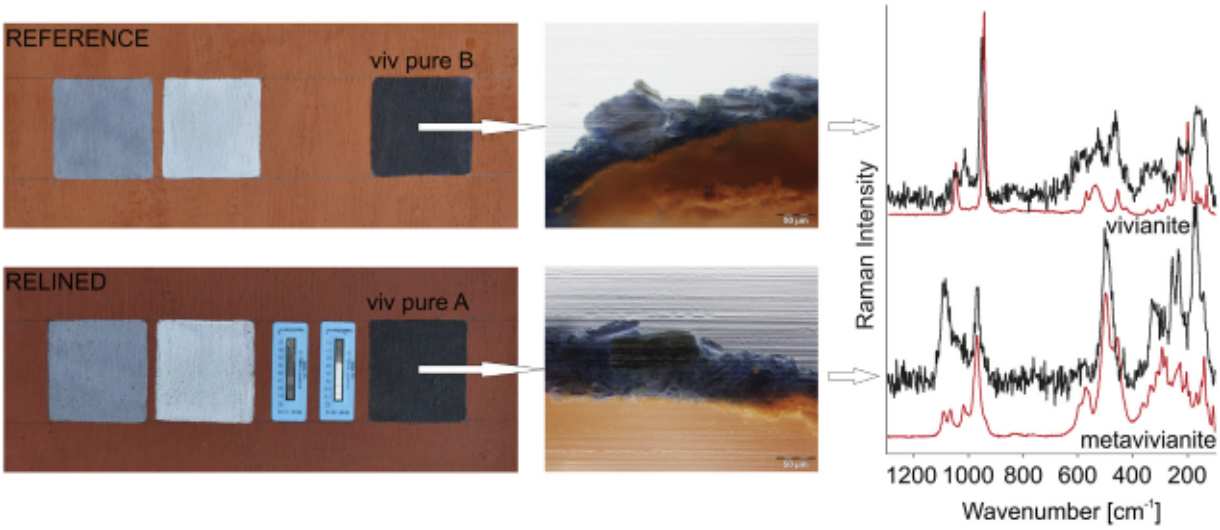


Fig. 9. Reference and relined oil-on-canvas mock-ups together with micro-photographs of micro-samples obtained from the pure vivianite oil paints. The micro-Raman spectra were obtained on selected grains of (meta)vivianite of the micro-samples, and are accompanied by reference spectra of respective minerals (in red). (For interpretation of the references to colour in this figure legend, the reader is referred to the web version of this article.)

surrounded by the binder are all yellow and degraded, while a lump of accumulated vivianite grains still contain bluish particles; the oil most probably facilitated the transfer of heat. The oil samples were prepared almost one year before the others, and it took them 7 months to get completely dry. During this period of time, according to the XRD measurements, the vivianite remained unchanged (no metavivianites were detected); however, an unknown organic phase was created in the sample. The XRD shows that it has been destroyed by the 80 °C temperature (but the XRD was performed only after 80, 120, and 200 °C heating steps, so it cannot be excluded that already 60 °C, the first step of the temperature experiments, caused its decomposition).

The FTIR spectra of both the 290-ey-A and the 282-G are dominated by the bands of the binders, and there is no significant change in the 80 and 120 °C steps. However, both spectra exhibit a certain amount of deterioration after 200 °C.

Relining of oil-on-canvas mock-ups

The temperature experiments with model paint layers showed that the most "risky" binder regarding the temperature-related colour change of the paint is oil, as it facilitates the transfer of heat. In addition, the described colour changes of historic paintings containing vivianite often take place in oil paintings [8,9,24]. Therefore, the canvas mock-ups were prepared using oil as a binder and one of them was subjected to relining, i.e., the application of a new canvas on the back of the painting using organic matters and heat. The oil paints were prepared from ground natural crystals of vivianite, as it showed the most pronounced colour change during temperature experiments. Fig. 9 depicts the reference canvas mock-up together with the canvas mock-up after relining.

The temperature reached by the process was monitored in two ways – by an infrared non-contact thermometer (from the reverse side of the canvases) and by irreversible temperature indicators applied on the front of the relined canvas.

Firstly, the relining was performed using the lowest possible temperature while maintaining the efficacy of the process. The ironing took approx. 10 min., and the highest temperature measured by the non-contact infrared thermometer was 51 °C, while the irreversible indicator showed that it was exposed to temperature at least 54 °C (but less than 60 °C). Almost no colour change of the vivianite paints (except of the darkening of the whole canvas due to the saturation by the wax–resin mixture) was observable by naked eye. In the second step, the temperature was increased. The heat was applied again by ironing the canvas, this time for approx. 15 min. The highest temperature measured by non-contact infrared thermometer was 95.3 °C, but the temperature most commonly fluctuated around 76 °C. The irreversible indicator showed that the temperature reached an interval of 82–88 °C. This time, it was possible to observe a slight colour change, especially in case of the pure vivianite paint – even though the whole canvas grew darker, the paint seemed to be slightly greyer. The relined oil-on-canvas mock-up as well as the reference one were photographed and the relative RGB coordinates of the photos were analysed. The results show the darkening of the paints (caused by the saturation by the wax-resin mixture), while the width of the RGB parameters decreased, suggesting the disappearance of subtle modelling. While these effects can be ascribed to the effect of the saturation by the relining medium, a detailed study of the photographs showed that the larger grains of vivianite became lighter.

To further document the occurring changes of vivianite, micro-samples were taken from both the reference and the relined canvas. Fig. 9 show the micro-samples taken from relined and reference pure vivianite paints and the micro-Raman spectra obtained on selected grains. Micro-Raman was applied instead of micro-FTIR measurements due to its better spatial resolution as well as better optics enabling proper localisation of the grains. The grey grain in the sample of the pure vivianite oil paint after relining shows signs of degradation – the spectrum enabled its identification as metavivianite, while the spectra of untreated samples show only the spectrum of vivianite. It remains unclear why this grain was degraded more than the surrounding ones, but the above-stated macro-scale eye-observations indicate that larger grains were preferentially affected by the relining.

These results highlight the importance of (1) precise material investigation of historic paintings before conservation treatment and (2) careful application of such treatment in case of the presence of sensitive materials like vivianite.

Conclusions

A high-temperature X-ray diffraction study of pure synthetic (as well as partly oxidised) vivianite covering the whole extent of the

All problems according to Preflight profile
Convert to PDF/A-2u

temperature-related stability of its structure is being published for the first time. The results show that already temperatures around 70 °C are damaging to vivianite, therefore, some of the recommended procedures during vivianite's synthesis including digestion under increased temperatures should be avoided. The HT-XRD of oxidised vivianite indicates that while vivianite gradually becomes amorphous with increasing temperatures, the amount of metavivianite, the first oxidative degradation product, increases from 90 °C up to 110 °C; then it starts to decompose as well. Exposition to 160 °C causes complete amorphisation of both the vivianite and its oxidation products.

Mössbauer spectra demonstrated that the temperature-induced oxidation of vivianite starts at 90 °C, which corresponds with the increase of the amount of metavivianite. Since the structural changes of the samples in the HT-XRD study have been clearly observed at 70 °C, they were studied in more detail in model vivianite paint layer samples with different historic binders. After exposition to 80 °C, the colour changes of all types of model paint layer samples were pronounced. Regarding the pigment, the most distinct colour change took place in case of paint layer sample prepared from ground natural vivianite crystals with water, which changed from blue to grey. It is an important finding, since such colour change has been described in actual works of art. Its FTIR spectra indicated the loss of hydroxyl molecules, while its phase composition analysed by XRD remained the same (except the slight decrease of diffraction lines' intensity). Regarding the binder, the most pronounced influence has been observed in the model paint layer sample of vivianite with oil – the grains of the pigment which were fully encompassed by oil were more prone to temperature-related degradation as the oil facilitated the transfer of heat.

To simulate the actual conditions under which a work of art containing vivianite paint layer may be degraded, oil-on-canvas mock-ups were created and relined in a traditional way using iron. The temperature fluctuated around 76 °C. It seems that larger grains were preferentially affected by the process; the obtained micro-samples documented the change of the larger grains to grey. While the reference micro-sample showed only the Raman spectrum of vivianite, the grey grain in the relined micro-sample showed the spectrum of metavivianite.

Acknowledgements

The authors express their thanks to Ivan Němec (Faculty of Science, Charles University in Prague) for his help with the micro-Raman spectroscopic analysis, to Kamil Lang (Institute of Inorganic Chemistry, AS CR, v.v.i.) for his help with the UV–VIS spectrophotometry, and Jitka Večerníková (Institute of Inorganic Chemistry, AS CR, v.v.i.) for the performance of FTIR measurements in transmission mode. The cooperation of Pavla Bauerová (Academy of Fine Arts in Prague, ALMA Laboratory) during the preparation of model paint layer samples with oil and of painter and restorer Tomáš Tichý (Academy of Fine Arts in Prague, ALMA laboratory) during the execution of oil-on-canvas mock-ups and relining experiments is gratefully acknowledged. Thanks also belong to Igor Fogaš (Moravian Gallery in Brno) for the fruitful discussion about relining. The study has been supported by Czech Science Foundation, project No. P103/12/2211, and by RVO 61388980.

References

[1] J.H. Bernard, R. Rost, Encyclopaedia of minerals [in Czech], Academia, Praha, 1992.
[2] M. O'Donoghue, Gems: their sources, descriptions and identification, Butterworth-Heinemann, 2006.
[3] M. Richter, Shedding some new light on the blue pigment 'vivianite' in technical documentary sources of northern Europe, Art Matters Neth. Tech. Stud. Art 4 (2007) 37–53.
[4] Z. Čermáková, J. Hradilová, J. Jehlička, K. Osterrothová, A. Massanek, P. Bezdička, D. Hradil, Vivianite's identification in painted works of art and its significance for provenance and authorship studies, Archaeometry 56 (Suppl. 1) (2014) 148–167.
[5] S. Castro, A. Reden, U. von Baumer, P. Dietemann, H. Stege, I. Fiedler, C. Tilenschi, J. Klaas, Examinations of two 17th century Dutch paintings with respect to colour alteration and the greyish appearance of the paint layers, Zeitschrift für Kunsttechnologie und Konservierung 23 (2) (2009) 177–195.
[6] D. Karl, Technological examination of the romanesque triumph-crucifix from the Holy cross church in Klöden, Zeitschrift für Kunsttechnologie und Konservierung 23 (1) (2009) 140–159.
[7] L. Sheldon, Blue and yellow pigments – the hidden colours of light in Cuyp and Vermeer, Art Matters Neth. Tech. Stud. Art 4 (2007) 97–102.
[8] A. van Loon, Color changes and chemical reactivity in seventeenth-century oil paintings. Dissertation thesis, Faculty of Science, University of Amsterdam, The Netherlands, (2008).
[9] M Spring, L. Keith, Aelbert's Cuyp large Dort: colour change and conservation, National Gallery Technical Bulletin 30th Anniversary vol., 2009.
[10] N.V. Chukanov, R. Scholz, S.M. Aksenov, R.K. Rastsvetaeva, I.V. Pekov, D.I. Belakovskiy, K. Krambrock, R.M. Paniago, A. Righi, R.F. Martins, F.M. Belotti, V. Bermanec, Metavivianite, $Fe^{2+}Fe^{3+}_2(PO_4)_2(OH)_2{\cdot}6H_2O$: new data and formula revision, Mineral. Mag. 76 (3) (2012) 725–741.
[11] C. Piña, H. Arriola, N. Nava, Mössbauer spectroscopy of iron phosphate. $Fe_3(PO_4)_2(H_2O)_n$ pigments, J. Phys: Conf. Ser. 217 (2010) 1–4.
[12] D. Hanzel, W. Meisel, D. Hanzel, P. Gütlich, Mössbauer effect study of the oxidation of vivianite, Solid State Commun. 76 (3) (1990) 307–310.
[13] P.-L. Tien, T.C. Waugh, Thermal and X-ray studies on earthy vivianite in Graneros shale (upper cretaceous), Kansas, Am. Mineral. 54 (9–10) (1969) 1355–1362.
[14] M.S. Poffet, Thermal runaway of the dried sewage sludge in the storage tanks: from molecular origins to technical measures of smouldering fire prevention. Dissertation thesis, Faculty of Science, University of Fribourg, Switzerland, (2007).
[15] P.B. Boissonnas, A.K. Diethelm, Some problems affecting choice, formulation and application of materials in restoration and lining. Paris: International Council of Museums, in: 6th Triennial Meeting/ICOM Committee for Conservation, Ottawa, September 21–25, 1981.
[16] P.-P. Westby, The lining cycle: fundamental causes of deterioration in painting on canvas: materials and methods of impregnation and lining from the 17th century to the present day, Conference on Comparative Lining Techniques, April, 1974.
[17] S. Hackney, Paintings on canvas: lining and alternatives. Tate Papers 2 (2004).
[18] P. Ackroyd, The structural conservation of canvas paintings: changes in attitude and practice since the early 1970s, Rev. Conserv. 3 (2002) 3–14.
[19] E. Mattievich, J. Danon, Hydrothermal synthesis and Mössbauer studies of ferrous phosphates of the homologous series $Fe^{2+}_3(PO_4)_2(H_2O)_n$, J. Inorg. Nucl. Chem. 39 (1977) 569–580.
[20] JCPDS PDF-2 Database, International Centre for Diffraction Data, Newtown Square, PA, U.S.A. release 54, 2004.
[21] T. Žák, Y. Jirásková, CONFIT: Mössbauer spectra fitting program, Surf. Interface Anal. 38 (2006) 710–714.
[22] R.L. Frost, M.L. Weier, W. Martens, J.T. Kloprogge, Z. Ding, Dehydration of synthetic and natural vivianite, Thermochim. Acta 401 (2003) 121–130.
[23] D. Hanzel, W. Meisel, D. Hanzel, P. Gütlich, Conversion electron Mössbauer study of vacuum and thermally treated vivianite, Hyperfine Interact. 57 (1–4) (1990) 2201–2207.
[24] Stege H., C. Tilenschi, A. Unger, Known and unknown. New research in Vermeer's palette in the Procuress, in: U. Neidhardt, M. Giebe (Eds.), Johannes Vermeer. Bei der Kupplerin, Exhibition Catalogue, Staatliche Kunstssammlungen Dresden [in German], Dresden, 1990, pp. 77–82.

All problems according to Preflight profile
Convert to PDF/A-2u

Contents lists available at ScienceDirect

www.elsevier.com/locate/dsp





ARTICLE INFO

ABSTRACT

All problems according to Preflight profile
Convert to PDF/A-2u

- To demonstrate a new method of digital image processing that improves the visibility of concealed features in NIR reflectograms and thus improves the comprehensibility of the collected multispectral data set.
- To suggest an algorithm following the proposed method.
- To quantitatively describe NIR and VIS separability limitations.

In published papers a similar task has already been addressed, for example by means of VIS-NIR multispectral analysis or Raman and XRF imaging, solving the identification of painted layers [19,20] and used pigments [21], performing pigment segmentation [22,23] and classification [24–26], layer separation [27] by difference visualization [28] or by image enhancement methods [29], or composition change detection [19]. In general digital image processing methods (DIP) can produce more comprehensible images providing the art investigator with better insight into a painting.

2. Samples and artworks

2.1. Samples

A set of 132 mock-ups, either on wooden or canvas support, was used for this research. In specific, series of mock-ups simulating paintings on wooden desk were prepared in 1994 in the Opificio delle Pietre Dure and therefore properly naturally aged. The pigments, purchased as powders from Zecchi (Italy), were applied with egg tempera (50% egg yolk, 25% egg white, 25% vinegar) and oil binding medium on wooden panels with a preparation layer composed of gypsum and animal glue (rabbit skin glue dissolved in water in 1:16 ratio). Furthermore, all the mock-ups included underdrawings [30].

Additional mock-up samples were chosen from the M3art database [31], prepared to imitate gothic to baroque Italian paintings. The 4×4 cm squares of different colors were painted on white canvas using animal glue as a binding medium for the gothic to renaissance period. The composition of the color layer was constant for all mock-ups: 2 g of pigment for 10 drops of 5% solution of animal glue, 5 drops of turpentine, 3 drops of egg yolk and 1 drop of ethanol. The white canvas was prepared by mixing 3 volume parts of Bologna chalk (calcium sulfate), 2 volume parts of 7% aqueous solution of gelatin, 1 egg yolk and $\frac{1}{4}$ volume parts of polymerized linseed oil. The right half of each square color sample contained underdrawings.

2.2. Artworks

A brief description of the three case studies, on which the developed algorithm was tested, is given.

The first one is a non-assigned gothic painting of Golgotha. It is a tempera painting on wood. Size of the processed area is about 6×6 cm. The processed image was captured by a standard digital single lens reflective (DLSR) camera Canon D500 with removed infrared filter covering the CCD. Color depth was 8 bits. Range of NIR spectral window was $\langle 720, 1050 \rangle$ nm.

The second one is a 'Still life' from the Fine Arts Museum of Asturias, in the north of Spain. It is an early 20th century anonymous oil on canvas painting (23.4×28.4 cm). It represents a series of pottery, in a very centered composition, made with three different ceramic techniques: the first with a green tone, the second very glossy and the third on the part in the left side, in satinated brown. The background is plain to highlight the figures acting as protagonists on the canvas. Analysis with IRR reflectography revealed the top layer to be painted with red ochre, green earth, and lead white pigments. The presence of underpainting and underdrawings was discerned as well.

The third example subjected to feed forward ANN testing is the 'Madonna dei Fusi' (Madonna of the Yarnwinder). It is an oil on panel painting, realized between the years 1501–1507, attributed to Leonardo da Vinci, possibly with the contribution of one of his pupils. The painting is privately owned. It was restored at least twice, however previous attempts cannot be excluded. IRR revealed different pentimenti in the preparatory drawing.

Reflectographic images on the 20th and 16th century paintings, as well as on mock-ups, were recorded by means of the VIS-NIR multispectral scanner with a single point measurement of reflectance with perfect registration of each pixel as a function of wavelength. The instrument was described in detail elsewhere [5,32]. In brief, the detecting system consists of Si (for $\langle 380, 1000 \rangle$ nm range) and InGaAs (for $\langle 1050, 2500 \rangle$ nm range) detectors equipped with interferential filters yielding 32 channels (16 channels in the VIS range $\langle 380, 780 \rangle$ nm and 16 channels in the NIR range $\langle 750, 2500 \rangle$ nm). The spectral resolution, determined by the filter FWHM, is 20–30 nm and 60–120 nm in the VIS and NIR range, respectively. As a result, 32 spatially registered images at different wavelengths $\langle 400, 2500 \rangle$ nm were collected completing a hypercube of spectral and spatial information.

3. Method

The fundamental idea justifying our method development is based on the fact that some information content of the NIR reflectogram cannot be estimated from the VIS reflectogram. We assume a match of such estimated NIR values and measured NIR values, indicating the absence of any additional *layer*. Contrarily, when the estimation does not match the measured values, the resultant error is assigned to an extra *layer* affecting the response in the NIR.

3.1. Definitions

Due to the terminology interference between art and IT experts we start with definitions of terms used in this paper.

Definition 1. As a *spectral window* centered in wavelength λ with defined width w we understood a radiometric sub-band where density of radiation wavelengths in range $\langle \lambda - w, \lambda + w \rangle$ is significantly higher than density of other wavelengths. Moreover, density function is increasing at $\langle -\infty, \lambda \rangle$ and decreasing at $\langle \lambda, +\infty \rangle$.

For our purpose it is not necessary to define "significantly higher" in practice this parameter is defined by screening equipment (filter transmittance, sensor sensitivity, light source radiation density function).

Definition 2. A *layer* is a continuous volume of paint material (color, varnish, support, etc.), homogeneous in the sense of its optical properties.

Such *layer* does not necessarily correspond to the material used. We track the optical homogeneity which can vary in one material due to particle size, chemical modification on its volume border, cracks or other inhomogeneities.

In the following text we distinguish between VIS and NIR reflectogram information content and their difference. Corresponding terminology – *visible cover* of a painting and the *information gain* – was defined as follows:

Definition 3. A *visible cover* for a given pixel is set of *layers* which contribute to the reflectance measured in visible spectrum.

All problems according to Preflight profile
Convert to PDF/A-2u

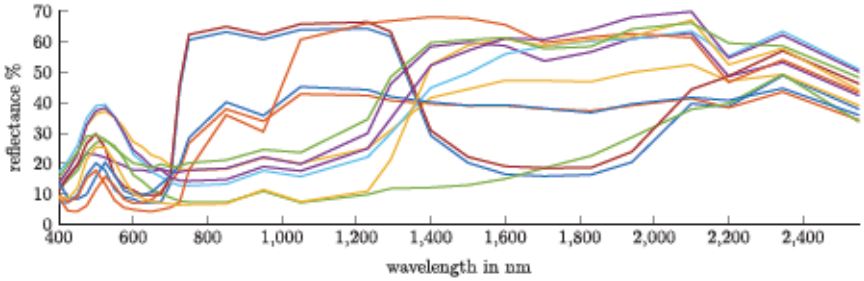


Fig. 1. Spectral responses of several green pigments in oil and egg tempera binding media. In the visible spectral range reflectance curves are very similar, whereas they vary much more in the near infrared range.

Thus the visible cover can contain for a given pixel more than one layer due to semi-transparency of the upper layer(s). This definition is not very intuitive but well describes reality where (in VIS) transparent, semi-transparent and opaque *layers* can be combined.

Definition 4. The *information gain* for a certain *spectral window* and a given pixel is the change in captured radiation caused by *layers* not included in the *visible cover*.

The *visible cover* affects the measured intensity the most because the level of absorption of upper *layers* weakens every effect of the *layers* below. In order to obtain *information gain* we need to suppress the *visible cover* effect in a *spectral window* reflectogram.

For similar tasks source separation methods are commonly used [29,33]. Often mentioned methods are *independent component analysis* from the group of blind source separation (BSS) [34–38], *principal component analysis* or other orthogonalizations. Application of source separation algorithms for the described problem is also possible here but has two limitations:

1. Optical model of a behavior of multilayer system is not linear [31]. Mixing model must take this into account. Most of BSS methods expects linear combination represented by mixing matrix, therefore results will not correspond with reality.
2. BSS methods expect that intensities measured in each subband are mixtures of *sources*. This presumption is too general. In our definition of the problem we refine this presumption into terms *visible cover* and *information gain* which we understood in BSS terminology as *sources*.

To conclude, a separation method should reflect the complexity of optical behavior of multilayer system that represent the typical painting structure [39]. For better comparison of our proposed method and BSS see section A.2.

The complexity of the addressed problem is demonstrated in Fig. 1, where the spectral reflectance factors measured in the range $\langle 400, 2250\rangle$ nm for several green colors is presented. The graph illustrates the typical behavior of paint materials: all measured spectral responses are very smooth. In spite of curves similarity in VIS range, in NIR range curves differ much more. Variances are:

$$\max_{\lambda\in\langle 400,700\rangle}(\sigma(I_\lambda)) = 0.1312, \tag{1}$$

$$\max_{\lambda\in\langle 700,2550\rangle}(\sigma(I_\lambda)) = 0.2203, \tag{2}$$

where λ is a *spectral window* central wavelength, I_λ denotes intensity measured in appropriate *spectral window* and $\sigma(I_\lambda)$ denotes standard deviation of intensities measured over all green colors (standard deviation per channel of constructed green phantom shows Fig. 6). VIS and NIR reflectance factors of one paint material correlate but do not relate on each other (both depend on paint material composition). Therefore an intensity relation $f : I(\lambda) \to I(\kappa)$ from *spectral window* λ to *spectral window* κ can be ambiguous if used paint material is impossible to be determined from the acquired dataset.

3.2. Proposed approach

A relevant estimation of the *visible cover* contribution in NIR reflectogram based on the visible spectral response is possible if and only if the set of materials is separable. Therefore existence of a transfer function $f : I(VIS) \to I(NIR)$, where I denotes the reflectance intensity is assumed.[1] To construct the best approximation f_T of this function f according to the collected pixels and their spectral responses, the pixels containing only the *visible cover* with no *information gain* were employed. Only this way extrapolated values containing minimum of *information gain* and maximum information pertinent to *visible cover* are obtained. Such set of pixels T belonging to K classes (according to *layer* content, i.e. optical properties) was used for the development of a f_T robust to noise:

$$T = \{C_1 \cup C_2 \cup \cdots \cup C_K\}, \tag{3}$$

$$C_i = \left\{p_{i,1}, \cdots, p_{i,|C_i|}\right\}, \tag{4}$$

$$I(p_{i,k}, NIR) = I(c_i, NIR) + n(c_i, NIR, k), \tag{5}$$

$$f : I\left(p_{i,k}, VIS\right) + n\left(c_i, VIS, k\right) \to I\left(p_{i,k}, NIR\right) + n\left(c_i, NIR, k\right), \tag{6}$$

where C_i is a set of pixels representing a material i. $p_{i,k}$ represents a pixel of the class C_i. c_i is a mean representation of the class C_i and $n(C_i, NIR, k)$ is a deviation of a pixel $p_{i,k}$ from this mean. Finally $I(p_{i,k}, NIR)$ is a reflectance intensity measured for a pixel $p_{i,k}$ in NIR range and n is a noise of C.

Being $f_T \sim f$, by using f_T spectral responses in the NIR *spectral windows* for all the pixels in the image can be extrapolated, creating a hypothetical image in the NIR *spectral window*, $\hat{I}_{NIR}$, containing only *visible cover*, which can be subtracted[2] from the measured data:

$$f_T(I_{VIS}) = \hat{I}_{NIR}, \tag{7}$$

$$\Delta = \left|I_{NIR} - \hat{I}_{NIR}\right|. \tag{8}$$

With suitable scaling of *information gain* Δ, an enhancement of hidden details is obtained.

3.3. f_T construction by feed forward ANN

For purpose of method demonstration, feed forward artificial neural network (ANN) for f_T construction was selected. An ANN

[1] This assumption is not valid but will be discussed in section 4.3.
[2] Subtraction is one possibility. We plan to focus on this problem in future.

All problems according to Preflight profile
Convert to PDF/A-2u



Fig. 2. Example of virtual phantom. A simulation of image in spectral window with central wavelength $\lambda = 1750$ nm. Left: a phantom with additive noise; middle: phantom without noise – mean values for each paint material or paint material with underdrawing (right border); right: generated noise (variance used according to variance of real samples). Each horizontal line represents one paint material. On the right border is a simulated underdrawing. Noise image shows that the variance of each paint material differs and also that variance of combination of paint material with underdrawing is higher than that of poor paint material.

provides sufficient performance and ability to show the limitations of the method. Moreover:

1. No classification is needed. We do not want to work directly with C.
2. Produced f_T will be robust with respect to noise and to outliers, and has sufficient performance for separable sets of material.

There are several alternatives for f_T construction such as: Associative Memories Networks with various architectures [40,41], Support Vector Machines [42], Regression tools [43]. More can be found in [39].

Proposed feed forward ANN is based on the model of associative memory returning $c_i(NIR)$ for $c_i(VIS)$. The used associative memory divides space into polygons, where each polygon represents one pattern. This memory type is especially suitable for a high number of outliers included in data set and an a priori unknown number of classes K (number of used pigments and their mixtures).

A standard feed–forward ANN working with sum square error[3] was used. The proposed ANN has an input layer with 16 neurons accepting the reflectance in 16 sub-bands of the visible part of the spectrum and output layer has also 16 neurons corresponding to 16 sub-bands of near infrared spectrum. Various numbers of layers (from 1 up to 10) with various width (from 5 up to 1000 perceptrons) were examined in the testing phase. Each layer has sigmoid transfer function except for the last one where each neuron produces only linear combination of its inputs. For training the scaled conjugate gradient algorithm included in Matlab™ train function *trainscg* was employed, where 70% of samples were used for training, 15% for testing and 15% for validation of learning progress. Learning process was stopped when number of iterations exceeds 10000 or when 6 validations failed or the performance of ANN decreased[4] under 10^{-8}.

4. Calculations and method limitations

For testing the limits of proposed method several parameters were considered:

1. The size of scanned artwork
2. The number of used materials
3. VIS based separability of used materials
4. Pixel with non-zero *Information gain* coverage ratio

For each variable, several ANNs (20–25) were trained to result in the best performance; the training being performed on fully controlled virtual phantoms (Fig. 2). They were created in compliance with measured paint materials mean reflectance μ and variance σ^2 that were acquired from samples simulating a real painting (mentioned in section 2.1), used in the previous research [30,31].

$$\mu(\lambda, m) \sim avg\,(I(\lambda, m)) \tag{9}$$

$$\sigma(\lambda, m)^2 \sim var\,(I(\lambda, m))\,. \tag{10}$$

The virtual phantom was then created as follows:

1. A width S in pixels, a number of materials used $N < |M|$ and an underdrawings *coverage* $q \in \langle 0; 1 |$ were defined.
2. A height of the phantom was set as $|S/N| \cdot N$, where each $|S/N|$ line corresponds to one material
3. Finally, pixels were set as follows:
   (a) From the spectral database specified number of materials were randomly selected and both versions, without and with underdrawings ($m_C, m_D \in M$) were used.
   (b) Pixels in a row were set with the normal distribution corresponding to the material database records. Last $|S \cdot q|$ columns have distribution $\sim \mathcal{N}(\mu(\lambda, m_D), \sigma(\lambda, m_D)^2)$ and first $|S \cdot (1-q)|$ columns $\sim \mathcal{N}(\mu(\lambda, m_C), \sigma(\lambda, m_C)^2)$

The created phantom a has matrix size $(|S/N| * N, S, 32)$. Constructed virtual phantoms, reflecting the parameters of multispectral dataset of a real painting, had the following properties: $N = 12$, size $10k - 4M$, $q = 0.02$.

4.1. Effect of phantom size

Tests of the algorithm on real paintings revealed that size of the region on which ANN is trained influence the output quality demanded. The quality of extrapolation decreases as a function of the increasing size and hidden information disappears from an output image. Thus the first experiment is testing the hypothesis.

Hypothesis 1. The size of the processed area (used for the training and the estimation) affects the quality of an approximation.

[3] Improvements here are possible – sub-bands near to VIS spectral band should be estimated better than further sub-bands moreover another metric can be used or architecture can be changed to recurrent network.

[4] Performance stop case never happened.

All problems according to Preflight profile
Convert to PDF/A-2u

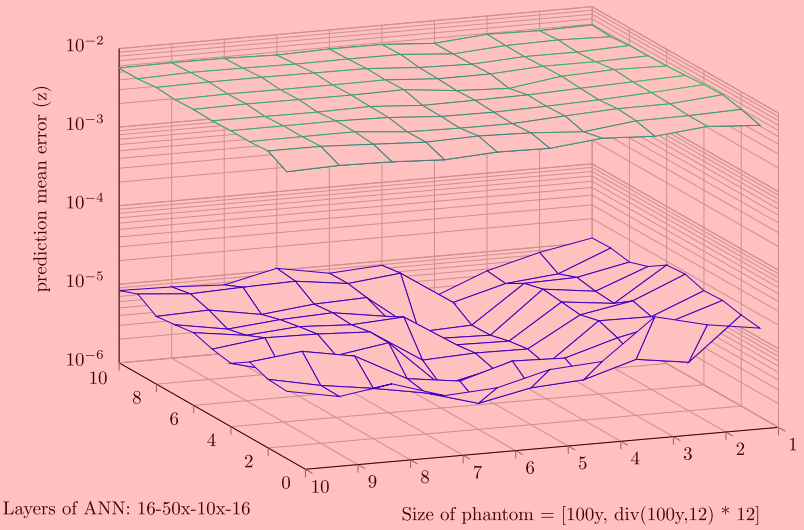


Fig. 3. Error in extrapolation as a function of the phantom size. Green upper mesh shows the error in the case of underdrawing present, blue bottom mesh is error between estimated and real reflectance values. Both graphs have similar shape (z-axis is logarithmic) with local minima for phantom size of 400×400 pixels due to the limitation of training samples to $50k$. The error behavior along the layer width axis shows that ANN performance does not increase as a function of growing network. (For interpretation of the references to color in this figure legend, the reader is referred to the web version of this article.)

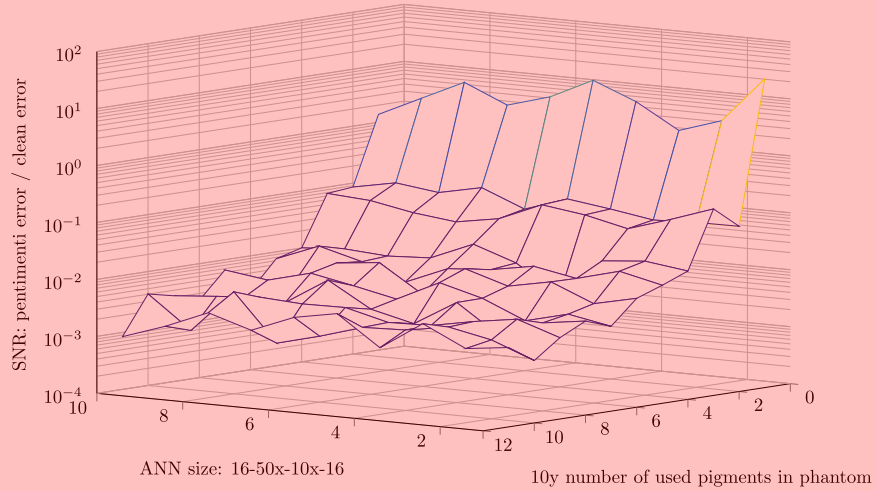


Fig. 4. Extrapolation error according to number of used pigments and ANN width. Mean error of the extrapolation "from VIS to NIR" per material and NIR sub-band. Error is computed according to the number of materials used (y axis) and ANN layer width (x axis). Graph shows that separability of materials used is limited – more materials cause cross-talks in the network and the overall performance decreases. More neurons in the layers cannot fix this problem.

We developed phantoms with size $S = k \cdot 100$, where $k \in 1, 2, \cdots, 20$, *coverage* $q = 0.02$ and number of used materials $N = 12$. Fig. 3 shows resulting graphs, which disapproves the Hypothesis 1. The performance of ANN does not decrease as a function of the growing processed area, however the minimal network size (> 250 neurons for 12 materials) should be kept.

4.2. Effect of used materials

The second experiment ($S = 500$, $q = 0.02$ and $N = 10k$, where $k \in 1, \cdots 11$)[5] was performed to clarify whether or not the ANN efficiency decrease is caused by greater variability of reflectance intensity values (due to increasing number of materials in analysis) in the processed area.

Hypothesis 2. The number of materials present in the processed area affects the performance of ANN.

Results of this experiment (Fig. 4) show that performance of ANN with two inner layers (four in total) is negatively affected by increasing number of materials. Performance improvement by using ANN architecture with more layers was tested as well (see Fig. 5) (with $S = 500$, $q = 0.02$, $N = 10k$ for $k \in 1, \cdots 12$ and the number of layers goes from 1 to 10, each layer has 20 neurons). Increasing the layers amount shows a partial improvement of ANN performance, however is not applicable in practice. The curve representing the performance dependence on ANN depth and the number of materials is hyperbolic like (see Fig. 5) thus the same performance for more materials requires extra hundreds of layers which are hardly trainable in real-time.

The presented graphs show that the paint material variability in the processed area is the most limiting factor for the method

[5] Materials was randomly selected for each training.

All problems according to Preflight profile
Convert to PDF/A-2u

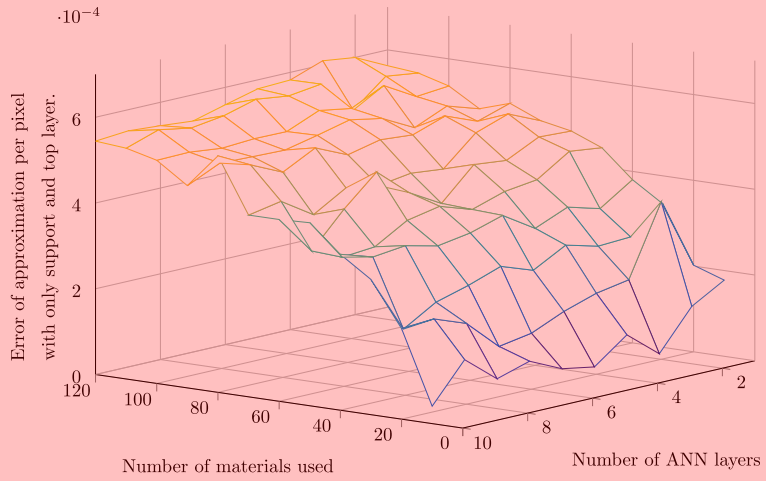


Fig. 5. Error in extrapolation according to pigments used and ANN depth. Error in extrapolation VIS to NIR, mean per material and NIR sub-band, according to the number of materials and the number of ANN layers. Graph shows that separability of materials used can be improved by more layers in ANN on the other hand the number of layers and neurons grows much faster than the number of separable materials.

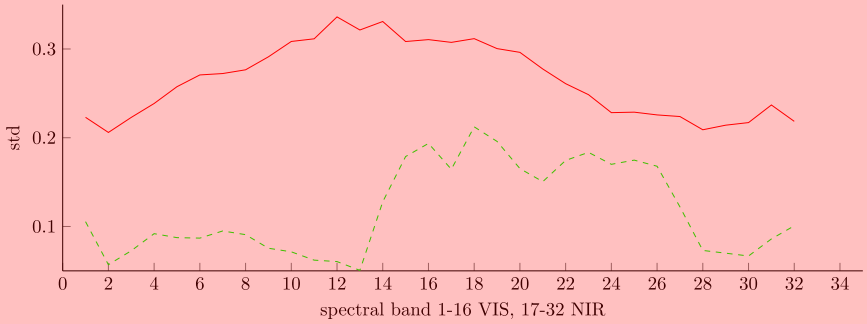


Fig. 6. Standard deviation of pixels on the whole phantom, all pigments together. Green dashed line correspond to inseparable green phantom and red solid line to rainbow phantom. Bands from 1 to 16 represent VIS part of spectra, 17–32 NIR part of spectra. Difference between phantoms is clearly visible. (For interpretation of the references to color in this figure legend, the reader is referred to the web version of this article.)

performance. If the difference of the estimated values and measured intensities is similar for pixels used for training as well as for analyzed pixels with pentimenti the increase of the painting comprehensibility is negligible. On the other hand, as long as the variability of area does not affect separability (Fig. 4, 5), useful results can be achieved with relatively small number of neurons in ANN. Training of such small ANN is fast and easily applicable in practice.

4.3. Separability

It was demonstrated that the increasing number of used materials negatively affects the performance of ANN in spite of the growing size of ANN. One possible explanation is the separability of materials in VIS. When two materials have the same spectral response in the VIS (same color), ANN is not able to distinguish between them and a prediction for NIR will be the same for both materials. During the learning phase, the estimation of ANN can either converge to some weighted mean value or completely diverge. In both cases (convergence or divergence) the final estimation will not be correct. Following hypothesis should be verified:

Hypothesis 3. When materials in VIS behave similarly, they will be inseparable for ANN. The growing size of ANN does not increase the performance.

For testing Hypothesis 3, two phantoms were prepared, both with fixed number of colors $N = 12$. Green colors from Fig. 1 and rainbow colors with varying VIS spectral response were used for the first and second phantom, respectively. Standard deviation of green and rainbow phantom intensity values is depicted in equations (1), (2). (The variations of intensity values per spectral sub-band for both phantoms are in Fig. 6.) The *coverage* was set to $q = 0.02$ and ANN layers width spans from $[16 \to 5 \to 1 \to 16]$ neurons to $[16 \to 100 \to 20 \to 16]$ neurons in individual ANN layers. An approximation for the rainbow phantom improves with an increase of ANN size, whereas for the green one the best approximation is reached with $[16 \to 25 \to 5 \to 16]$ neurons (see Fig. 7).

It is apparent that a key parameter, determining the size of the area to be processed by our algorithm, is the separability of materials in VIS. (However, this parameter is difficult to define or to estimate.)

For real paintings, the problem of the material separability is of minor issue. In fact, limited number of separable materials, of different visible spectral response, is usually used. The separability can decrease for the mixtures of materials that may have the spectral characteristics different from those of the pure colorants. A proposed workaround for such situation consists in processing areas not larger than 15×15 cm. It follows that small ANN, fast in the learning process, can provide satisfactory output. The optimal size of the processed area should depend then on the separability of used materials and on their mixtures.

All problems according to Preflight profile
Convert to PDF/A-2u

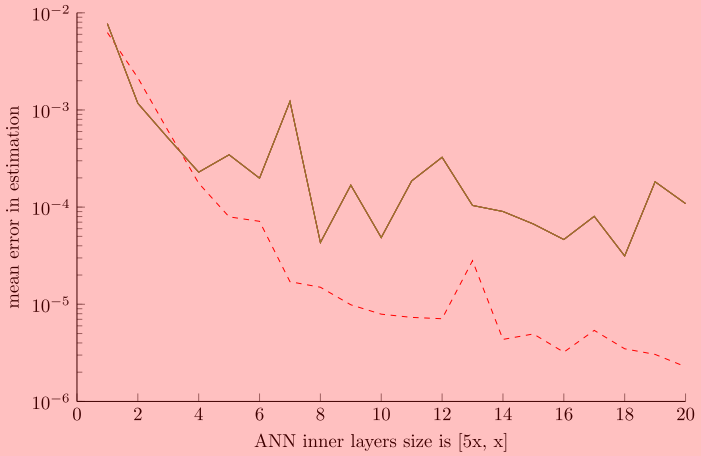


Fig. 7. ANN performance for 12 materials. Performance of ANN on rainbow phantom representing well separable set of materials (red dashed line) and green phantom representing inseparable set of green materials (green solid line) 1. (For interpretation of the references to color in this figure legend, the reader is referred to the web version of this article.)

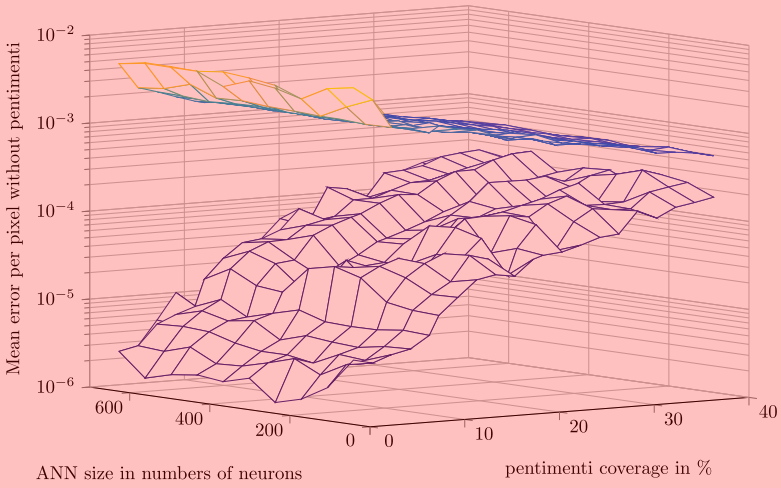


Fig. 8. Error in extrapolation when the coverage grows. Bottom mesh describes the mean error per coverage and ANN size for pixels without underdrawings – this should be minimized. Upper mesh describes mean error for pixels with pentimenti – this should be maximized. When the coverage grows, both errors are closer and as a result, pentimenti are less distinguishable.

4.4. Coverage effect

This work is focused on sparse areas like pentimenti, retouches, etc. which cover no more than 2% of a scanned area. Our last experiment describes what happen if all the pixels of the reflectogram (with non-trivial *information gain* included) are used for the training of ANN. By using of all the pixels necessary expert user interaction for sample selection is eliminated and the processing will be fully automatic.

A set of phantoms ($S = 500$, $N = 12$, and $q = 0.02k + 0.01$, where $k \in 0, \cdots, 19$) were created and all the pixels of the phantom were used for training of ANN. The ability of the extrapolator to distinguish between pixels with and without *information gain* is presented in Fig. 8. This ability corresponds to the distance between the node of the top and the bottom mesh in the figure. Indeed, the growing *coverage* q increases the necessity of purposefully selected training samples. In Fig. 8 pixels with non-zero *information gain* are represented by upper the surface and pixels containing only *visible cover* by the bottom surface. When coverage grows ANN recognition decreases, as both surfaces are closer. The growing size of the neural network does not compensate the ANN recognition ability.

5. The results obtained on artworks

This section presents three illustrative examples of real paintings on which our method was tested.

In the first experiment, a standard DLSR camera without infrared filter was used to capture RGB and $[700, 1050]$ nm NIR images of a Gothic painting. The estimator was a feed forward ANN with $3 \to 50 \to 10 \to 1$ neurons. The processed image had 800×800 pixels and all the pixels were used for training. The results (Fig. 9) show that the most emphasized areas (black and white parts) are caused by spatial registration misalignment of RGB and NIR images. On the other hand, required demanded *information gain* enhancement was achieved: a contour on the top of the head (highlighted in the blue square) is not apparent either in VIS or in NIR image.

In the second experiment, a 32 band multispectral data set of a modern canvas painting measured by VIS-NIR scanner [5,32] was analyzed. The selected input had 16 bands in VIS $[400, 700]$ nm with a 25 nm step. Estimating ANN has four layers with $16 \to 25 \to 25 \to 1$ neurons, the chosen processed area had 312×394 pixels size that were also used for training. The extrapolated and enhanced output band was a *NIR spectral window* centered at

All problems according to Preflight profile
Convert to PDF/A-2u



Fig. 9. A Gothic painting as captured by DLSR camera. Left: RGB image, middle: NIR image, right: output of our algorithm. The images were processed all at once (original size $800 \times 800px$). In the blue squares are details scaled for better visibility. (For interpretation of the references to color in this figure legend, the reader is referred to the web version of this article.)

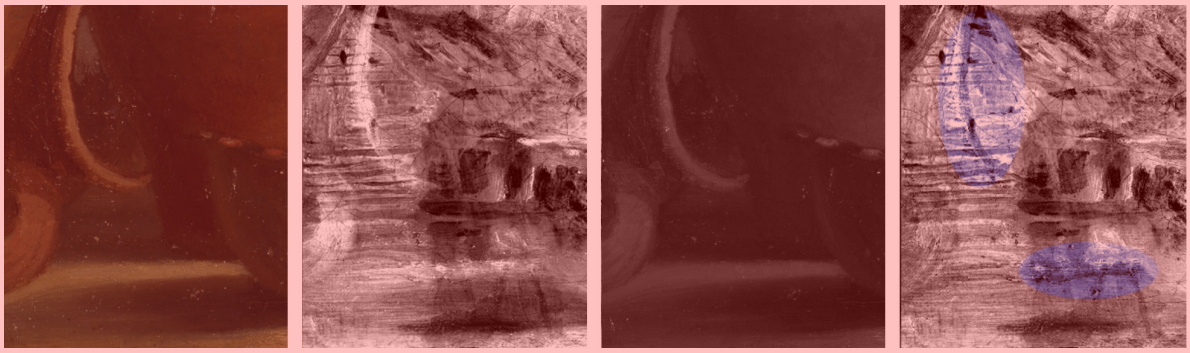


Fig. 10. Experiment with an early 20th century anonymous canvas painting. Left: RGB image, middle left: reflectogram measured at central wavelength $\lambda = 1200$ nm, middle right: output of ANN extrapolation, right: a difference between middle left and right images (*information gain*). Blue areas highlights uncovered areas with significant *information gain*. Note: Contrast of the second and the fourth images was expanded for better visibility and comparison. (For interpretation of the references to color in this figure legend, the reader is referred to the web version of this article.)



Fig. 11. Experiment with the 16th century wooden desk painting attributed to Leonardo da Vinci. Left: RGB image, middle left: a reflectogram centered at wavelength $\lambda = 1050$ nm, middle right: output of ANN extrapolation, right: difference between the measured and the extrapolated outputs; the *information gain*. (For interpretation of the references to color in this figure legend, the reader is referred to the web version of this article.)

1200 nm as shown in Fig. 10. Information uncovered by the algorithm is evidenced with blue color. The unveiled contours are invisible in the NIR reflectograms because concealed by an NIR low transparent *visible cover*.

In the third experiment, another multispectral dataset of a painting on wood with date inscripted on the 15th century was addressed. In agreement with the previous experiment, a selected input for ANN consisted of 16 VIS bands and all 16 IR [750, 2550] nm bands were extrapolated and *information gain* computed and enhanced.

Estimating ANN had four layers with $16 \rightarrow 25 \rightarrow 25 \rightarrow 16$ neurons. The processed area had a size of 300×300 pixels and all of them were involved in training. This experiment (Fig. 11) shows that the highest efficiency of extrapolation is achieved with the highest variability in reflectance intensity values in VIS. The structures masked by *visible cover* in right part of the image were successfully uncovered.

Recommendations for the data processing based on the experimental evidence can be summarized as follows:

- The *visible cover* of the painting should not be homogeneous. Higher variance of the *visible cover* increases the separability of the classes (see Fig. 11).
- Studied infrared reflectogram should contain at least some visible structures. The method cannot achieve results behind the

All problems according to Preflight profile
Convert to PDF/A-2u

scope of reality, it can only accentuate present information and improves its comprehension.
- Analyzed images must be spatially registered. On the misalignment, black and white lines appear on edges in the painting (see Fig. 9).

6. Discussion

In general, the proposed algorithm is well suited for the enhancement of individual detail of painting (from 100*k* pixels up to 1 *Mpx*). However, it is not meant for processing full size images. Using smaller size of processed area leads to emphasizing the noise, due to the worse ANN generalization; larger patches approach is not time-effective. Therefore, the selected size of the area to be processed (as well as ANN number of layers and their width) defined by user should reflect the material separability. For similar colors in VIS smaller areas should be processed whereas for the well separable colors larger areas can be used (code for testing [44]).

Possible improvement can be achieved by other choice than subtraction for the construction of the *visible cover* estimation (equation (8)). The more complex model should be based on the optical behavior of individual *layers*, better reflecting properties of the used materials. This approach will be subject of our future research.

There exist possible generalization of the method for other spectral ranges combining *visible cover* and non-trivial *information gain* acquired in modalities like X-ray, ultra-violet fluorescence or terahertz imaging. The method workflow remains the same and quality of results will be related to the correlation of target modality and VIS modality. Higher correlation means worse visibility of hidden features on a modal image but with good ANN based estimation more distinct visualization will be achieved. ANN estimation performance depends mostly on coverage factor q in training set of pixels.

7. Conclusion

We have presented a new algorithm for information enhancement on multispectral data sets. Spectral imaging technology has recently gained importance in the analysis of ancient paintings. In particular, multispectral imaging in the near-infrared (NIR) and visible (VIS) region has proved useful for studying underlying features and for pigment identification, respectively. Because of the transparency of most pigments to IR radiation, NIR reflectograms can shed light onto the artist's original idea by the visualization of either the underdrawing or the so-called pentimenti. Depending on pigment transparency in the NIR spectral range, the acquired infrared images may partially contain information pertinent to the visible spectrum, decreasing, thus, their readability.

The new methodology consisted in suppressing VIS from NIR information content by extrapolating the reflectograms in the VIS to those recorded in NIR range and subtracting the extrapolated image from the measured IR one. As a result, separated information of the NIR is achieved.

The feed forward artificial neural network (ANN) algorithm for extrapolation was successfully tested on real paintings and a few examples were reported. The results of fully controlled experiments with virtual phantoms were also described to demonstrate the methodology limitations. In the ANN design, the effect of the number and width of the network layers was analyzed, as well as its effectiveness with respect to the number of neurons. The optimum was reached for two inner layers, which outperformed the three layers setting.

The implemented method in Matlab for processing of registered multimodal data sets is open access [44].

In the future we plan to focus on more profound analysis of the ANN setting and on a more accurate model of the optical behavior of multilayer systems.

Acknowledgments

We would like to thank to Janka Hradilová and Blanka Valchářová for the possibility capture photos presented in Fig. 9.

Access to computing and storage facilities owned by parties and projects contributing to the National Grid Infrastructure MetaCentrum, provided under the programme "Projects of Large Infrastructure for Research, Development, and Innovations" (LM2010005), is greatly appreciated. Without them this research cannot be possible.

The authors of INO would like to acknowledge the INSIDDE project (INtegration of cost-effective Solutions for Imaging, Detection, and Digitisation of hidden Elements in paintings), FP7-ICT-2011.8.2 ICT for access to cultural resources. Moreover, we thank Dr. Marta Florez Igual from the Museo de Bellas Artes de Asturias for providing us with the painting shown in Fig. 10.

The authors of IITA CAS would like to acknowledge the Czech Science Foundation, which has supported this work (project no. P103/12/2211).

Appendix A

A.1. Noise enhancement

One not yet mentioned problem of the proposed method is noise. The noise in the multispectral dataset can be independent for each spectral window (according to scanning technique). In such case the estimator f could not suppress it. When a feed forward ANN is used the noise is propagated through the network:

$$f_T\left(n(x_i)\right) = \hat{n}(y_i). \tag{11}$$

This give us in output image:

$$\Delta = \left(n(y_i) - \hat{n}(y_i)\right). \tag{12}$$

If the noise contains regular patterns (is dependent on a signal or correlates through different spectral windows), these patterns will be learned and suppressed. But in most cases the noise will be independent and e.g. randomly distributed according to a normal distribution:

$$n(y) \sim N(0, \sigma_{n_y}^2), \hat{n}(y) \sim N(0, \sigma_{n_x}^2). \tag{13}$$

In such case we obtain the noise level in the output image equal to

$$n(y_i) - \hat{n}(y) \sim N(0, \sigma_{n_y}^2 + \sigma_{n_x}^2). \tag{14}$$

It means that in the output image the noise will be enhanced too. The variance of the noise in the enhanced image will be the sum of variances of input data sets. The choice of suitable noise reduction algorithm is out of the scope of our article. The development of such algorithm should start with the noise distribution measurement. There are big problems in collection of measured samples and their connection with real paintings (aging effect, pigment mixtures, etc.). Moreover the normal distribution assumption can be violated.

A.2. Blind source separation

Common practice for information enhancement from IRR is usage of blind source separation (BSS) algorithms: PCA, ICA, orthogonalization [29,33], morphological component analysis (MCA) [38],

All problems according to Preflight profile
Convert to PDF/A-2u

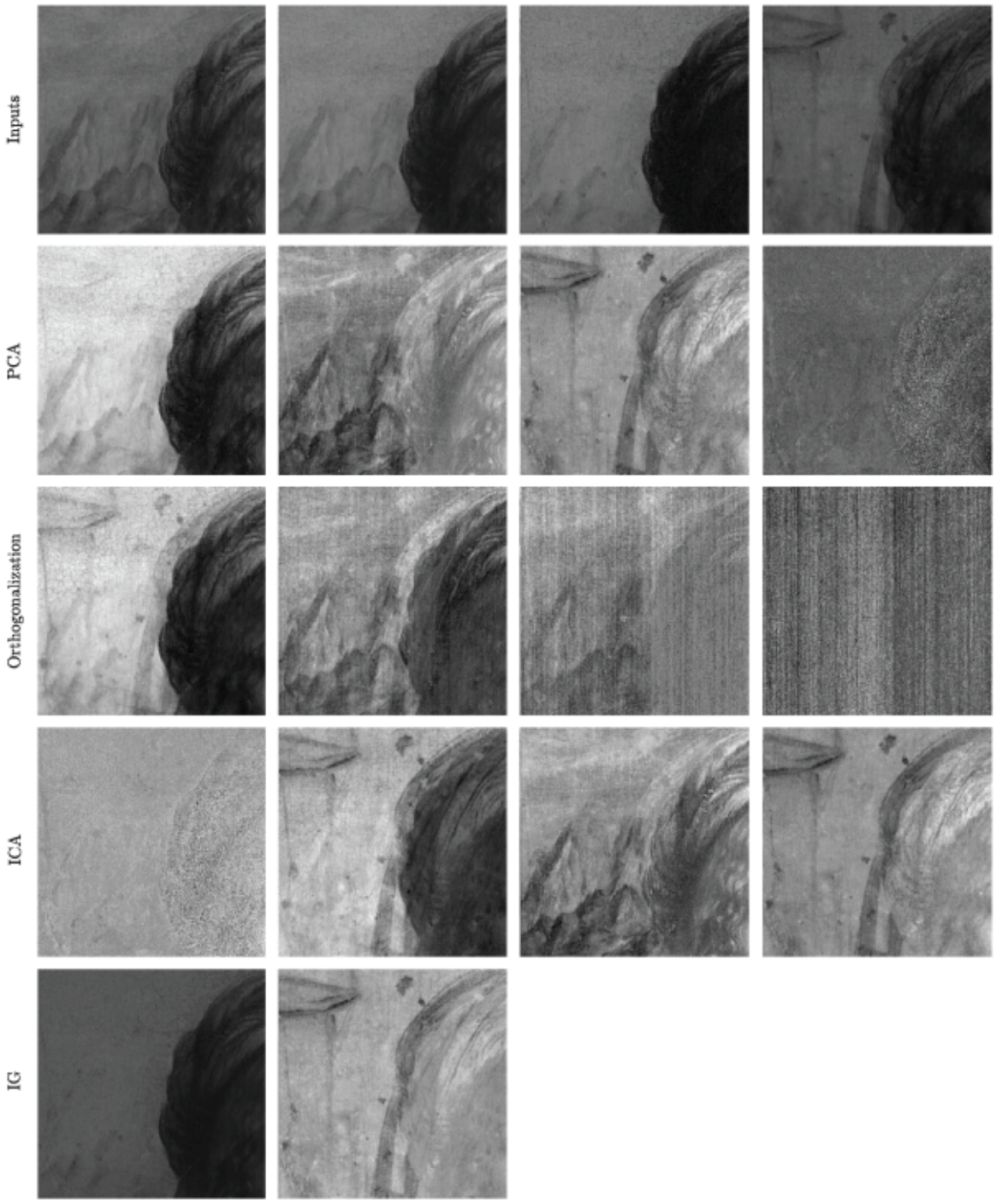


Fig. 12. Visual comparison of various source separation algorithms. First row presents reduced dataset to red, green and blue channel and spectral subband $\lambda = 1050$ nm. Second row shows PCA decomposition according to eigenvectors (Matlab function *pca* with *Algorithm* set to *eig*). Third row is orthogonalization by Matlab function *qr* and for the fourth row EFICA algorithm [45] was used. In the last row the same dataset was processed by our proposed method – left image shows extrapolation of RGB channels into NIR spectral subband, right image shows *information gain* i.e. difference between measured intensities of pixels and extrapolated values.

non-negative matrix factorization (NMF). Therefore we feel a necessity to put our method into this existing context. Following paragraphs describe how the proposed method and BSS relate and their pros and cons.

In the case of estimation of *information gain* in BSS terminology we have one known source signal $I(VIS)$ and one mixture $I(NIR) = \hat{I}(NIR) + \Delta$. Therefore there is no source separation just fitting of $\hat{I}(NIR)$, see equation (7). If we would like to use BSS algorithm for information enhancement we can state the problem as having two mixed signals $I(VIS)$ and $I(NIR)$ and set of unknown sources (typically number of sources is the same as input mixtures). Separation algorithm then creates, according to *contrast function* (for the definition see [37]), independent components.

All problems according to Preflight profile
Convert to PDF/A-2u

Proposed algorithm has therefore these advantages:

- Interpretability. The resulting output image contains just the information gain of the specified modality and a noise. This minimizes possible misinterpretation. In the case of BSS methods the content range of a particular output image is set based on the statistical characteristic of the input data, not taking into account their physical interpretability.
- Enhancement. The information gain from selected modality is enhanced.
- Stability. Our proposed method converges to visually similar results through multiple runs and independently on the input content variation. The BSS methods generate a lot of noisy images (which are useless and can be dropped), often not ordered (for some methods orthogonal vectors can be produced in different order) and with badly set sign of the result (which is caused by the undefined orthogonal vector orientation). The stability of the BSS depends on selected *contrast function* [37].

There are the disadvantages of our proposed method:

- Noise enhancement. In BSS methods, noise and information are concentrated in different channels, whereas our proposed method do not remove noise into any specific channel, moreover its level can increase (see section A.1).

From these qualities we derive following guidelines for choosing the correct tool:

- BSS methods can be useful when:
  - The covered layer is partially visible in VIS. In such case measured $I(VIS)$ is also a mixture of unknown *sources*.
  - Input signals are relatively noisy. Noise can be separated as a source.
- The computation of *information gain* by our proposed method is useful when:
  - Studied layer content is invisible in VIS reflectogram. VIS can be classified as a source.
  - Misinterpretation is critical. BSS methods generates sources blindly and information from various modalities can be mixed, e.g. an edge split into VIS and NIR can be joined in one of BSS output source but not in *information gain* image.
  - Input signals have low level of noise.

Finally Fig. 12 contains an example of output of orthogonalization, PCA and ICA for comparison (as in [29] on reduced dataset from Fig. 11). We present, according to our decision, the best example where these methods generates comparable results as our proposed method.

References

[1] J.R.J. Van Asperen De Boer, Reflectography of paintings using an infrared vidicon television system, Stud. Conserv. 14 (3) (1969) 96–118.
[2] Kirk Martinez, John Cupitt, David Saunders, Ruven Pillay, Ten years of art imaging research, Proc. IEEE 90 (1) (2002) 28–41.
[3] Costas Balas, Vassilis Papadakis, Nicolas Papadakis, Antonis Papadakis, Eleftheria Vazgiouraki, George Themelis, A novel hyper-spectral imaging apparatus for the non-destructive analysis of objects of artistic and historic value, J. Cult. Heritage 4 (Jan 2003) 330–337.
[4] John K. Delaney, Elizabeth Walmsley, Barbara H. Berrie, Colin F. Fletcher, Multispectral imaging of paintings in the infrared to detect and map blue pigments, in: (Sackler NAS Colloquium) Scientific Examination of Art: Modern Techniques in Conservation and Analysis, Front Cover Proceedings of the National Academy of Sciences, Aug 16, 2005, National Academies Press, 2005, pp. 120–136.
[5] C. Bonifazzi, P. Carcagnì, R. Fontana, M. Greco, M. Mastroianni, M. Materazzi, E. Pampaloni, L. Pezzati, D. Bencini, A scanning device for VIS–NIR multispectral imaging of paintings, J. Opt. A, Pure Appl. Opt. 10 (6) (June 2008) 064011.
[6] Yonghui Zhao, Image segmentation and pigment mapping of cultural heritage based on spectral imaging, PhD thesis, Rochester Institute of Technology, 2008.
[7] Claudia Daffara, Enrico Pampaloni, Luca Pezzati, Marco Barucci, Raffaella Fontana, Scanning multispectral IR reflectography SMIRR: an advanced tool for art diagnostics, Acc. Chem. Res. 43 (6) (June 2010) 847–856.
[8] Claudia Daffara, Raffaella Fontana, Multispectral infrared reflectography to differentiate features in paintings, Microsc. Microanal. 17 (05) (Sep 2011) 691–695.
[9] Linda Cséfalvayová, Matija Strlič, Harri Karjalainen, Quantitative NIR chemical imaging in heritage science, Anal. Chem. 83 (13) (Jul 2011) 5101–5106.
[10] Haida Liang, Advances in multispectral and hyperspectral imaging for archaeology and art conservation, Appl. Phys. A, Mater. Sci. Process. 106 (2) (2012) 309–323.
[11] Paola Ricciardi, John K. Delaney, Michelle Facini, Jason G. Zeibel, Marcello Picollo, Suzanne Lomax, Murray Loew, Near infrared reflectance imaging spectroscopy to map paint binders in situ on illuminated manuscripts, Angew. Chem., Int. Ed. 51 (23) (June 2012) 5607–5610.
[12] Camille Simon Chane, Alamin Mansouri, Franck S. Marzani, Frank Boochs, Integration of 3D and multispectral data for cultural heritage applications: survey and perspectives, Image Vis. Comput. 31 (1) (2013) 91–102.
[13] M. Alfeld, J.C. Broekaert, Mobile depth profiling and sub-surface imaging techniques for historical paintings – a review, Spectrochim. Acta, Part B, At. Spectrosc. 88 (2013) 211–230.
[14] Francesca Rosi, Costanza Miliani, René Braun, Roland Harig, Diego Sali, Brunetto G. Brunetti, Antonio Sgamellotti, Noninvasive analysis of paintings by mid-infrared hyperspectral imaging, Angew. Chem., Int. Ed. 52 (20) (May 2013) 5258–5261.
[15] Alejandro Ribés, in: Advanced Color Image Processing and Analysis, Springer Science + Business Media, New York, NY, 2013, pp. 449–483, chapter 14.
[16] Kathryn A. Dooley, Damon M. Conover, Lisha Deming Glinsman, John K. Delaney, Complementary standoff chemical imaging to map and identify artist materials in an early Italian renaissance panel painting, Angew. Chem., Int. Ed. 53 (50) (December 2014) 13775–13779.
[17] Antonino Cosentino Panoramic, Macro and micro multispectral imaging: an affordable system for mapping pigments on artworks, J. Conserv. Mus. Stud. 13 (1) (Jul 2015) 1–17.
[18] John K. Delaney, Mathieu Thoury, Jason G. Zeibel, Paola Ricciardi, Kathryn M. Morales, Kathryn A. Dooley, Visible and infrared imaging spectroscopy of paintings and improved reflectography, Heritage Sci. 4 (1) (2016) 1.
[19] A. Gooch, J. Tumblin, Visualizing pentimenti: revealing the hidden history of paintings, J. Math. Arts 1 (June 2007) 133–142.
[20] Anila Anitha, Andrei Brasoveanu, Marco F. Duarte, Shannon M. Hughes, Ingrid Daubechies, Joris Dik, Koen Janssens, Matthias Alfeld, Virtual underpainting reconstruction from X-ray fluorescence imaging data, in: 19th European Signal Processing Conference, EUSIPCO, Barcelona, 2011, pp. 1239–1243.
[21] A. Del Mastio, A. Pelagotti, V. Cappellini, Multispectral and multi-modal imaging data processing for the identification of painting materials, in: Lasers in the Conservation of Artworks, CRC Press, August 2008, pp. 453–458.
[22] A. Pelagotti, A.D. Mastio, A.D. Rosa, A. Piva, Multispectral imaging of paintings, IEEE Signal Process. Mag. 25 (4) (2008) 27–36.
[23] Kathryn A. Dooley, Suzanne Lomax, Jason G. Zeibel, Costanza Miliani, Paola Ricciardi, Ann Hoenigswald, Murray Loew, John K. Delaney, Mapping of egg yolk and animal skin glue paint binders in early renaissance paintings using near infrared reflectance imaging spectroscopy, Analyst 138 (2013) 4838–4848.
[24] Alicia Jurado-López, María Dolores Luque de Castro, Use of near infrared spectroscopy in a study of binding media used in paintings, Anal. Bioanal. Chem. 380 (4) (2004) 706–711.
[25] V. Kokla, A. Psarrou, V. Konstantinou, Computational models for pigments analysis, Appl. Phys. A 90 (1) (2007) 15–22.
[26] R. Hedjam, M. Cheriet, Historical document image restoration using multispectral imaging system, Pattern Recognit. 46 (8) (2013) 2297–2312.
[27] J. Dik, K. Janssens, G. Van Der Snickt, L. van der Loeff, K. Rickers, M. Cotte, Visualization of a lost painting by Vincent van Gogh using synchrotron radiation based X-ray fluorescence elemental mapping, Anal. Chem. 80 (16) (2008) 6436–6442. PMID: 18662021.
[28] É. Baudrier, A. Riffaud, A method for image local-difference visualization, in: Ninth International Conference on Document Analysis and Recognition, vol. 2, ICDAR 2007, IEEE, 2007, pp. 949–953.
[29] S. Legnaioli, E. Grifoni, G. Lorenzetti, L. Marras, L. Pardini, V. Palleschi, E. Salerno, A. Tonazzini, Enhancement of hidden patterns in paintings using statistical analysis, J. Cult. Heritage 14 (3, Supplement) (2013) S66–S70, Science and Technology for the Safeguard of Cultural Heritage in the Mediterranean Basin.
[30] A. Aldrovandi, M.L. Altamura, M.T. Cianfanelli, P. Riitano, I materiali pittorici: tavolette campione per la caratterizzazione mediante analisi multispettrale, OPD, Restauro 8 (1996) 191–210, 101–103.
[31] J. Blažek, J. Soukup, B. Zitová, J. Flusser, J. Hradilová, D. Hradil, T. Tichý, M3art: a database of models of canvas paintings, in: Marinos Ioannides, Nadia Magnenat-Thalmann, Eleanor Fink, Roko Žarnić, Alex-Yianing Yen, Ewald Quak (Eds.), Digital Heritage. Progress in Cultural Heritage: Documentation, Preservation, and Protection, in: Lecture Notes in Computer Science, vol. 8740, Springer International Publishing, 2014, pp. 176–185.

All problems according to Preflight profile
Convert to PDF/A-2u

[32] R. Fontana, M. Barucci, E. Pampaloni, J. Striova, L. Pezzati, From Leonardo to Raffaello: insights by Vis-IR reflectography, in: Interpretation of Fine Art's Analyses in Diverse Contexts, 2014, Acta Artis Academica, 2014, pp. 15–26.
[33] Gianfranco Bianco, Fabio Bruno, Anna Tonazzini, Emanuele Salerno, Pasquale Savino, Barbara Zitová, Filip Sroubek, Elena Console, A framework for virtual restoration of ancient documents by combination of multispectral and 3D imaging, in: Italian Chapter Conference 2010, Eurographics, pp. 1–7.
[34] A. Hyvärinen, J. Karhunen, E. Oja, Independent Component Analysis, vol. 46, John Wiley & Sons, 2004.
[35] P. Comon, Ch. Jutten, Handbook of Blind Source Separation: Independent Component Analysis and Applications, 1st edition, Academic Press, 2010.
[36] G. Chabriel, M. Kleinsteuber, E. Moreau, Hao Shen, P. Tichavsky, A. Yeredor, Joint matrices decompositions and blind source separation: a survey of methods, identification, and applications, IEEE Signal Process. Mag. 31 (3) (May 2014) 34–43.
[37] J-F. Cardoso, Blind signal separation: statistical principles, Proc. IEEE 86 (10) (1998) 2009–2025.
[38] J. Bobin, Y. Moudden, J.L. Starck, M. Elad, Morphological diversity and source separation, IEEE Signal Process. Lett. 13 (7) (July 2006) 409–412.
[39] Luis B. Almeida, Nonlinear source separation, Synthesis Lectures on Signal Processing 1 (1) (Jan 2006) 1–114.
[40] T. Kohonen, Self-organization and Associative Memory, 3rd edition, Springer-Verlag, Inc., New York, NY, USA, 1989.
[41] G.A. Carpenter, Neural network models for pattern recognition and associative memory, Neural Netw. 2 (4) (January 1989) 243–257.
[42] Y.W. Chang, Ch.J. Hsieh, K.W. Chang, M. Ringgaard, Ch.J. Lin, Training and testing low-degree polynomial data mappings via linear SVM, J. Mach. Learn. Res. 11 (August 2010) 1471–1490.
[43] G.A.F. Seber, A.J. Lee, Polynomial Regression, John Wiley & Sons, Inc., 2003, pp. 165–185.
[44] J. Blažek, Algorithm for invisible information separation in multimodal datasets, http://github.com/gimlidc/matlab/dip-toolbox.git, October 2015, An algorithm for multimodal artwork investigation, enhances the visibility of information hidden in various modalities.
[45] Zbynek Koldovsky, Petr Tichavsky, Erkki Oja, Efficient variant of algorithm fastICA for independent component analysis attaining the CramÉ r-Rao lower bound, IEEE Trans. Neural Netw. 17 (5) (2006) 1265–1277.

Jan Blazek is a Ph.D. student at Charles University, Prague, Czech Republic. He obtained the M.Sc. degree, in 2009, at the same university at the faculty of Mathematics and Physics. Since 2010, he develops algorithms for digital image processing at Institute of Information Theory and Automation, Czech Academy of Sciences. During his Ph.D. studies he focus on application of visualization techniques, artificial intelligence and statistics in field of art investigation to support art conservators and restorers.

Jana Striova was born in Jicin, 1977, Czech Republic. She graduated, in 2002, at the Institute of Chemical Technology in Prague in Chemical Technology for the Conservation of Historical Monuments (M.Sc.) and, in 2004, at Kansas State University, USA, in Analytical Chemistry (M.Sc.). She obtained her Ph.D. (2009) in Science for the Conservation of Cultural Heritage (CH) at University of Florence, Italy, as a Marie-Curie Fellow. She has been a researcher at the National Institute of Optics CNR-INO in Florence, since 2012, after 2 years of postdoctoral fellowship at the Institute for the Conservation and Valorization of CH. Her research interest spans from the development and application of new spectroscopic and imaging techniques for examinations of artworks to the studies of novel cleaning systems applied in the field of cultural heritage. More generally, she focuses on setting-up of multianalytical protocols to probe non-invasively materials constituting artworks.

Raffaella Fontana was born in Pavia, Italy, in 1964. She graduated in Physics at the University of Florence, in 1992; she obtained the Ph.D. in Non Destructive Techniques, in 1997, at the Department of Electronic Engineering in Florence and the Post-graduation in Medical and Environmental Physics at the University of Florence, in 2000.

Since 2004, she has been working at INO-CNR (National Institute of Optics of the National Research Council) where she is Researcher. Since 2010, she is the Responsible for the Cultural Heritage Group of INO.

She is involved in many research projects in the field of optical technologies applied to Cultural Heritage. She is the scientific responsible for INO of the EU-project IPERION CH (Integrated Platform for the European Research Infrastructure ON Cultural Heritage, H2020-INFRAIA-1-2014/2015) and the EU-project INSIDDE (Integration of technological Solutions for Imaging, Detection, and Digitization of hidden Elements in artworks, FP7-ICT-2001-9). Her research activity concerns the study of methodologies, the development of optical techniques and instruments for the diagnostics of artworks, and the processing of both 2D and 3D data.

Barbara Zitova received the M.Sc. degree in computer science and the Ph.D. degree in software systems from Charles University, Prague, Czech Republic, in 1995 and 2000, respectively. Since 1995, she has been with the Institute of Information Theory and Automation, Czech Academy of Sciences. Since 2008, she has been the Head of the Department of Image Processing. She gives undergraduate and graduate courses on digital image processing and wavelets in image processing with the Czech Technical University and Charles University. Her research interests include geometric invariants, image enhancement, image registration and image fusion, and image processing applications in cultural heritage and medical imaging. She has authored/coauthored over 60 research publications in these areas, including monographs Moments and Moment Invariants in Pattern Recognition (Wiley, 2009) and 2D and 3D Image Analysis by Moments (Wiley, 2016).

All problems according to Preflight profile
Convert to PDF/A-2u

12.1 IMPROVED VISUALIZATION OF CONCEALED FEATURES - THE CONTEXT OF THE STATE OF THE ART

This supplementary material of the paper was created after publication. I am incorporating here a wider context of the state of the art from the perspective of mutual information. In the current section I would like to compare the approaches of recent papers [73, 48, 72, 49].

In the mentioned papers the authors present algorithms for the separation of VIS information content from an X-ray transmissiongram. The algorithms used are based on correlation, mutual information and machine learning algorithms. The target in all cases is a function that is able to estimate the information content common to all studied modalities. In our research we identify how important careful preparation of the dataset is for function construction. The training dataset must contain minimum of the extra information in a more penetrating modality, because its content in the training set behaves as an increased noise level. The visibility of concealed features is increased more when common information is higher, i.e. the penetrative ability of modalities is close to each other (see equation 25). In general, the more layers affect the modal image, the higher is the divergence between the information content of this modality and VIS.

In Section 6.2 we address the problem of blind source separation. In the case of layers we would like to obtain sources corresponding to painting layer(s). In the case of our paper we reduce the number of layers to 2:

1. Layers affecting a VIS reflectogram.
2. Layers not affecting a VIS reflectogram.

In all mentioned studies [73, 48, 72, 49] the second modality is an X-ray transmissiongram, which, unlike the NIR reflectogram used in our research, goes through all layers present in a painting. Despite the different modality used, all these studies deserve a closer look.

In [73], Gooch and Tumblin separated X-ray-specific information from the X-ray transmissiongram: *"... we would like to separate the parts of the X-ray image that do and do not correspond to the visible light image."* The authors used the observation that the intensity of pixels in an X-ray transmissiongram is similar to the intensities in VIS, and proposed an algorithm that is based on inconsistency detection.

First of all, a VIS reflectogram was segmented by the Mean Shift Segmentation algorithm [207], which determines areas with homogeneous intensity R_k. The second step worked with these areas in an X-ray transmissiongram. According to the main assumption, these areas should be homogeneous in X-rays as well. Therefore, the authors looked for pixels breaking this assumption, as they are the regions of expert interest. The pixels are separated into two classes:

All problems according to Preflight profile
Convert to PDF/A-2u

$$p \in C_1 \Leftrightarrow p \in R, p - \mu_R < k \cdot std\ R \tag{39}$$
$$p \in C_2 \Leftrightarrow p \in R, p - \mu_R \geq k \cdot std\ R \tag{40}$$

where p is the pixel from segmented area R, C_1 is the class of corresponding intensities and C_2 is the class of pixels we are interested in. $\mu\ R$ and $std\ R$ is the mean intensity of R in an X-ray transmissiongram and standard deviation, respectively. Finally, k is a parameter tunable by an expert.

The correspondence of intensities is approximated here by a piecewise constant function based on mean shift segmentation. Mutual information of the VIS and X-ray modalities is simplified by expert-based assumptions to some "correlation-like" measure.

Six years later (2013), Anitha et al. [48] resolved the separation problem on XRF modality and VIS. The assumption that allows the usage of correlation instead of mutual information was not fulfilled here, and therefore the correspondence between modalities had to be defined by mutual information. The authors minimize:

$$\min_{C_s, C_u} \frac{H\ C_s|I_{VIS}}{H\ C_s} - \frac{H\ C_u|I_{VIS}}{H\ C_u} \quad \zeta TV\ C_s \quad \zeta TV\ C_u \tag{41}$$

with constraints:

$$I_{XRF} \quad C_s \quad C_u \tag{42}$$
$$\forall x, y : C_s\ x, y\ \geq 0, C_u\ x, y\ \geq 0, \tag{43}$$

where I_{VIS}, I_{XRF} are source images, C_s,C_u are separated signals, s denotes a surface signal and u a signal from underlying layers. $H\ A$ and $H\ A|B$ denote the entropy of image A and the conditional entropy of $A|B$, respectively. $TV\ A$ is the total variance of an image A; x and y are coordinates of a pixel and ζ is the coefficient for regularization.

The minimized equation 41 has four parts:

$$\frac{H\ C_s|I_{VIS}}{H\ C_s}, \tag{44}$$

which minimizes conditional entropy between separated surface signal C_s and VIS input image I_{VIS}, but also prevents a trivial solution by maximizing C_s entropy. The second element:

$$-\frac{H\ C_u|I_{VIS}}{H\ C_u}, \tag{45}$$

maximizes the conditional entropy of the signal from underlying layers C_u and the VIS input image, with the same constraint for a non-trivial

All problems according to Preflight profile
Convert to PDF/A-2u

solution as in the first element of the equation. The third and fourth elements:

$$\zeta TV\ C_s \qquad \zeta TV\ C_u \tag{46}$$

serve here as a regularization by keeping continuity over the output. Continuity is a common property of images. Let's point out that the mixing function (see Section 6.2.2 and equation 27) is represented here by a sum (see equation 42).

Usage of mutual information precisely reflects the target of the processing, but runs into problems in a discrete case and low frequencies (e.g. in [208]). Performance of the above-mentioned minimization greatly depends on the number of intensity levels in I_{VIS}, I_{XRF}, C_s and C_u. While a high number of gray levels indicates a problem with convergence, a low number of gray levels leads to blurred and rough results.

In the third article [72], Deligiannis et al. resolves the low frequency problem by using coupled dictionaries trained on a huge set of images. The basic idea is to represent each patch in the image by a linear combination of a limited number of words from a dictionary of patch words. The problem resolved in this paper is little bit different, because the input dataset contains two-side VIS reflectograms and an X-ray transmissiongram of an altar panel. But the core problem remains the same: to separate information content of high penetrating modality (X-ray) according to the panel layer to which it belongs. Let

$v,\ x$ - be our coupled dictionaries for VIS and X-ray modality, respectively

w - be a dictionary of information content hidden in X-ray modality

$q_{v,1}, q_{v,2}, q_x$ - be linearized corresponding image patches for the left and right side of the panel and X-ray transmissiongram, respectively.

Representation of a patch by dictionary words means:

$$\begin{aligned} q_{v,1} &\quad {}_v z_1 \\ q_{v,2} &\quad {}_v z_2 \\ q_x &\quad {}_x z_1 \quad {}_x z_2 \quad {}_w w \end{aligned} \tag{47}$$

where z_1, z_2, w are sparse vectors with low l_0 norm. The authors minimize:

$$\min_{z_1,z_2} \|z_1\|_0 \quad \|z_2\|_0 , \tag{48}$$

for the given dictionaries $_v,\ _x$. A detailed view of information separation based on mutual information needs a closer look at the building and coupling of dictionaries.

All problems according to Preflight profile
Convert to PDF/A-2u

"Let $V, X \in \mathbb{R}^{n \times t}$ represent a set of t co-located vectorized visual and X-ray patches, each containing $\sqrt{n} \times \sqrt{n}$ pixels. We assume that the columns of V and X can be decomposed as in equation 47, and we collect their common components into the columns of the matrix $Z \in \mathbb{R}^{\gamma \times t}$ and their innovation components into the columns of $W \in \mathbb{R}^{d \times t}$. We formulate the coupled dictionary learning problem as

The notation of the cited paragraph was adapted to be coherent with this thesis. γ and d denote the number of words in the dictionary.

$$\begin{aligned} &\min_{\substack{v, \\ w,}} \frac{1}{2}\|V - {}_{v}Z\|^2 \quad \frac{1}{2}\|X - {}_{x}Z - {}_{w}W\|^2 \\ &\text{subject to } \|z_\tau\|_0 \leq s_z, \\ &\qquad \|w_\tau\|_0 \leq s_w, \forall \tau \quad 1, 2, \cdots, t, \end{aligned} \tag{49}$$

where z_τ, w_τ are sparse vector-columns of matrix Z and W, τ runs over the columns of Z and W, and s_z, s_w are thresholds on the sparsity level. Given initial estimates for the dictionaries, the problem in equation 49 is solved by iterating between a sparse-coding step, where the dictionaries are fixed, and a dictionary update step, in which the coefficients are fixed, ..." [72].

According to equation 49, the square error is taken for learning. Square error minimization generates a Gaussian distribution of corresponding pixel intensities, with different means but variance as low as possible. Contrary to the conditional probability of a single pixel, the conditional probability of two patches eliminates single pixel outliers, whose weight decreases with growing patch size. This explains why this approach is more robust and stable than [48]. Training of coupled dictionaries on a big dataset eliminates outliers as well, but separability and thus reversibility of the mixing function decreases due to more blurry bins of pixel ICM. To demonstrate this effect we need to look more closely at ICM.

The ICM contains the frequency of correspondent pixel intensities in two different modalities (it is relevant to compare X-ray and VIS, as well as the intensities of separated sources C_x and C_y). The number of rows and columns corresponds to the intensity levels recognized in each modality, and highly affects the estimated separation. If we use a correspondence matrix as a visualization of mutual information (or entropy), we recognize two patterns:

1. The highest entropy/the lowest mutual information is reached when the correspondence matrix is uniform with zero total variance.

2. The lowest entropy/the highest mutual information is reached when there is only one non-zero column for each row, and vice versa.

The total variation in the matrix affects separation performance. When local discrete derivations are high, separation according to this matrix

All problems according to Preflight profile
Convert to PDF/A-2u

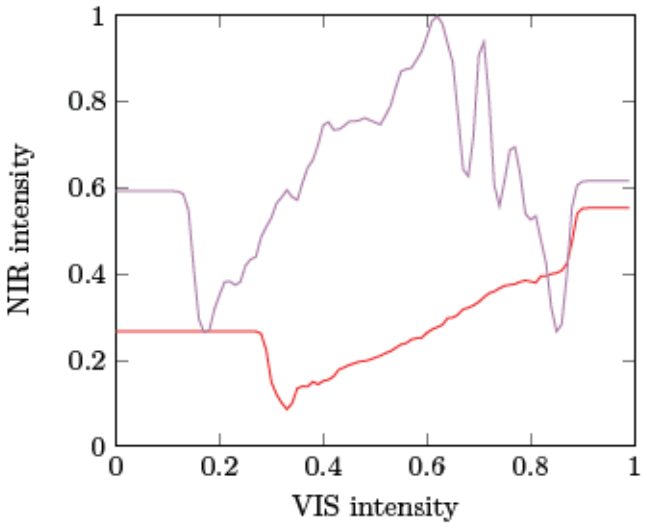


Figure 28: Two successfuly trained transfer functions from intensity in VIS to intensity in NIR. Purple line demonstrates how non-trivial such function can be. On the contrary the red one is example of identity like function. Both lines was trained on the dataset presented in [74], purple on dataset in figure 10, red line on the dataset in figure 9. VIS input were reduced to one dimensional intensity gray values.

converges to a local minima by using a gradient descent method. Otherwise, a uniform matrix with low total variance corresponds to inseparable clusters (caused, e.g. by a growing number of used paint materials and their mixtures). ICM with high total variance has better separability, but separated correspondence clusters are not stable by means of outliers. It is possible to partially solve this problem by reducing the number of columns or rows in a correspondence matrix (a histogram bin size estimation is exactly the same problem). With a low number of possible intensity values and clusters merged together, poor results will be achieved.

The correspondence matrix forms described above were distinguished in our paper [74], where we searched for conditions under which a correspondence matrix is obtained. We tested several hypotheses on real phantoms:

- **Number of samples** does not affect separability and distribution values in ICM remains
- **Number of paint materials** greatly affects the thresholds for classification, because classes are closer to their neighbors. Classification is more problematic with an increasing number of paint materials.
- **Types of paint materials** separability is worse for materials with a similar response in VIS, because classes are closer to each other in the sense of ICM bins

All problems according to Preflight profile
Convert to PDF/A-2u

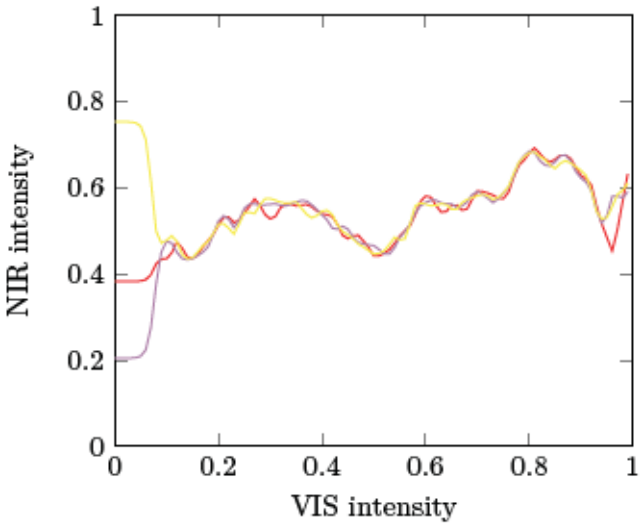


Figure 29: All three lines represent three approximations learned by ANN from VIS to X-ray in the case when result is really poor. This dataset was taken from [127], figure 6a, 6b.

- The number of samples with nontrivial *information gain* in the penetrating modality in a training set. This number must be reduced to a minimum; usable separability is obtained for up to 10 percent of samples with underdrawing. The reason for this is that the learning set is significantly affected by the separated signal.

Our results highlight the problem of the number of materials and their mixtures to be separated in the dataset. We recommend doing a general approximation from VIS to penetrating modality and interpreting the residua as an *information gain* of this modality. Our tests on real paintings demonstrate the usability of this approach.

Here, I amend our paper with two graphs with complementary results, illustrating transfer function approximations. The first graph (see Figure 28) visualizes two approximations generated for two well-separable datasets; the other (see Figure 29) does so for a problematic one. We reduce input and output intensities into the range $\langle 0, 1 \rangle$ and use our approximation schema (with ANN) for generating these approximations.

All problems according to Preflight profile
Convert to PDF/A-2u

All problems according to Preflight profile
Convert to PDF/A-2u

COLOPHON

This document was typeset using the typographical look-and-feel `classicthesis` developed by André Miede. The style was inspired by Robert Bringhurst's seminal book on typography "*The Elements of Typographic Style*". `classicthesis` is available for both LaTeX and LyX:

https://bitbucket.org/amiede/classicthesis/

Custom modifications were made in selected math font, where the AMS font family was used. Literature was printed according to ISO 690. The implementation used can be found at:

https://github.com/michal-h21/biblatex-iso690

Final Version as of June 30, 2018.